



# Circulation de saumures à la discordance socle / couverture sédimentaire et formation des concentrations uranifères protérozoïques (Bassin de l'Athabasca, Canada)

Antonin Richard

## ► To cite this version:

Antonin Richard. Circulation de saumures à la discordance socle / couverture sédimentaire et formation des concentrations uranifères protérozoïques (Bassin de l'Athabasca, Canada). Autre. Institut National Polytechnique de Lorraine, 2009. Français. NNT : 2009INPL092N . tel-01749588

HAL Id: tel-01749588

<https://hal.univ-lorraine.fr/tel-01749588>

Submitted on 29 Mar 2018

**HAL** is a multi-disciplinary open access archive for the deposit and dissemination of scientific research documents, whether they are published or not. The documents may come from teaching and research institutions in France or abroad, or from public or private research centers.

L'archive ouverte pluridisciplinaire **HAL**, est destinée au dépôt et à la diffusion de documents scientifiques de niveau recherche, publiés ou non, émanant des établissements d'enseignement et de recherche français ou étrangers, des laboratoires publics ou privés.



## AVERTISSEMENT

Ce document est le fruit d'un long travail approuvé par le jury de soutenance et mis à disposition de l'ensemble de la communauté universitaire élargie.

Il est soumis à la propriété intellectuelle de l'auteur. Ceci implique une obligation de citation et de référencement lors de l'utilisation de ce document.

D'autre part, toute contrefaçon, plagiat, reproduction illicite encourt une poursuite pénale.

Contact : [ddoc-theses-contact@univ-lorraine.fr](mailto:ddoc-theses-contact@univ-lorraine.fr)

## LIENS

Code de la Propriété Intellectuelle. articles L 122. 4

Code de la Propriété Intellectuelle. articles L 335.2- L 335.10

[http://www.cfcopies.com/V2/leg/leg\\_droi.php](http://www.cfcopies.com/V2/leg/leg_droi.php)

<http://www.culture.gouv.fr/culture/infos-pratiques/droits/protection.htm>

INSTITUT NATIONAL POLYTECHNIQUE DE LORRAINE  
ÉCOLE DOCTORALE RESSOURCES, PRODUITS,  
PROCEDES ET ENVIRONNEMENT (RP2E)

Laboratoire de Géologie et Gestion des Ressources minérales et énergétiques (G2R)

**THÈSE**

Présentée et soutenue publiquement le 04/12/2009  
pour l'obtention du grade de Docteur de l'INPL  
(Spécialité : Géosciences )

Par

Antonin RICHARD

Circulation de saumures à la discordance socle / couverture  
sédimentaire et formation des concentrations uranifères  
protérozoïques (Bassin de l'Athabasca, Canada)

**Directeur de thèse :** Michel CATHELINÉAU DR CNRS, UHP, Nancy 1

**Composition du jury :**

<i>Président du jury :</i>	Michel CUNÉY	DR CNRS, UHP, Nancy 1
<i>Rapporteurs :</i>	Bruce W.D. YARDLEY	Professeur, Université de Leeds
	Philippe MUCHEZ	Professeur, Université Catholique de Louvain
<i>Examinateurs :</i>	Marie-Christine BOIRON	CR CNRS, UHP, Nancy 1
	Philippe BOULVAIS	MDC, Université de Rennes 1
	Anthony FALICK	Professeur, SUERC - Université de Glasgow
	Jean-Pierre MILESI	Ingénieur, AREVA, Paris La Défense



## Remerciements

Au terme de ce travail, je tiens à remercier Michel Cathelineau et Marie-Christine Boiron pour m'avoir proposé ce sujet de thèse. Leur implication et leur soutien ont été une aide précieuse à la réalisation de ce travail. La confiance et la liberté de travail qu'ils m'ont accordé, ont été une grande source de motivation, et je les en remercie. J'associe à ces remerciements Michel Cuney, qui sans être un encadrant officiel, s'est beaucoup investi dans ce projet, et m'a permis de faire mes premiers pas au G2R en 2005.

Je remercie vivement Claude Caillat (AREVA) pour avoir accepté de co-financer ce projet avec le CNRS, et le CNRS pour m'avoir attribué une bourse de docteur ingénieur (BDI). Je remercie particulièrement Pierre Schuhmacher (CREGU) pour la gestion du financement de la thèse et la grande liberté qu'il m'a accordée pour l'utilisation des fonds.

Je suis particulièrement reconnaissant à Bruce Yardley et à Philippe Muchez, pour avoir accepté de juger ce travail en tant que rapporteurs. Merci également à Anthony Fallick, Philippe Boulvais et Jean-Pierre Milési, pour avoir accepté d'être les examinateurs de cette thèse.

Dans le désordre, je remercie chaleureusement toutes les personnes qui ont collaboré de près, ou de moins près, à ce travail :

A Rennes : Merci à Philippe Boulvais (pour ton accueil, tes encouragements, ton enthousiasme à l'épreuve des fuites de BrF<sub>5</sub>, les pizzas, les bières etc...), Martin Gaboriau (merci pour ton accueil chez toi et pour les bons moments passés à pomper l'hydrogène et regarder le foot...bonne chance pour la suite), David Vilbert pour les analyses isotopiques, et tous les habitués du RU pour m'avoir passé le sel.

A Leeds : Merci à David Banks pour son accueil, sa philosophie du judo, et son hyperactivité contagieuse, et merci à Bruce Yardley pour son intérêt porté à ce travail et à son goût pour les réceptions « at home »...

A CRPG : Merci à Christian France-Lanord pour m'avoir accordé un peu de son temps et ouvert les portes de son labo. Un grand merci à Caroline Guilmette pour son aide de tous les jours, et à Maarten Lupker pour les nombreux coups de mains.

A Zürich : Merci à Thomas Pettke pour ses corrections et pour avoir grandement contribué à dé poussiérer des données en perdition !

A AREVA : Merci à Claude Caillat et Jean-Pierre Milési encore une fois, Marc Brouand, Jean-Luc Lescuyer, Jean-Louis Feybesse, Joseph Roux pour leur intérêt porté à ce projet.

Enfin au G2R : Merci d'abord à Marie-Camille et à Stéphane pour la cohabitation joyeuse dans quelques mètres carrés pendant trois ans (ça rapproche), à Julien pour tout le boulot à deux (tu me dois toujours une bière au quinoa, et je t'en dois bien une au stollen), à Jérémy (le quatrième homme du bureau), aux « anciens » (Lucho et Gringo), et à tous les habitués du RU et de la cafét' (comme ça je n'oublie personne mais c'est sincère) qui ont rendus ces trois années plus intenses, plus marrantes, plus délirantes...Merci beaucoup à Cédric, Roland, Patrick, Laurence, Marie-Odile et Christine pour leur aide précieuse au quotidien !

Merci à toute la famille et à la belle famille, votre soutien et votre amour ont été une source de motivation à toute épreuve...enfin merci à Julie, là je n'ai plus les mots...

## **Notice to the reader**

This PhD thesis is divided into nine parts. The general introduction ([Part 1](#)) and general conclusion ([Part 9](#)) are written in French due to INPL administrative recommendations. The other parts are written in English. [Parts 3 to 8](#) are articles in preparation for various journals. In order to avoid repetitions along the manuscript, the geological setting, sampling, and fluid inclusion petrography, initially included in each article, were summarized in [Part 2](#). All references cited, are put together at the end of the manuscript. Analytical techniques are presented in detail in each part where results obtained from these techniques are discussed. An abridged version in French, with no references cited, was added at the end of each part from [Part 2 to 8](#).

## **Avertissement au lecteur**

Ce mémoire de thèse est divisé en neuf parties. L'introduction générale ([Partie 1](#)) et la conclusion générale ([Partie 9](#)) sont rédigées en français, comme recommandé par l'administration de l'INPL. Les autres parties sont rédigées en anglais. Les [Parties 3 à 8](#) sont des articles en préparation pour différentes revues. Afin d'éviter les répétitions le long du manuscrit, le contexte géologique, l'échantillonnage et la pétrographie des inclusions fluides, initialement intégrés dans chaque article, sont résumés dans la [Partie 2](#). Toutes les références citées dans le texte sont regroupées en fin de manuscrit. Les techniques analytiques sont présentées en détail dans chaque partie dans lesquelles les résultats obtenus par ces techniques sont discutés. Une version abrégée en français, sans référence bibliographique, a été ajoutée à la fin des [Parties 2 à 8](#).



## Table des matières

<i>Remerciements.....</i>	<b>3</b>
<i>Notice to the reader.....</i>	<b>5</b>
<i>Avertissement au lecteur.....</i>	<b>5</b>
<i>Table des matières .....</i>	<b>7</b>
<b>1. Introduction générale.....</b>	<b>11</b>
1.1. Circulation des fluides entre socles et bassins sédimentaires.....	12
1.2. Concentrations de métaux dans les fluides géologiques.....	14
1.3. Origine de la salinité des fluides .....	15
1.4. Gisements d'uranium de type discordance .....	16
1.5. Objectifs de la thèse .....	18
1.6. Moyens et méthodes .....	19
<b>2. Geology, sampling and fluid inclusion petrography.....</b>	<b>23</b>
2.1. The Athabasca Basin and Basement.....	23
2.2. McArthur River deposit .....	26
2.3. Rabbit Lake deposit.....	27
2.4. Eagle Point deposit.....	28
2.5. P-Patch deposit .....	29
2.6. Millennium deposit.....	30
2.7. Shea Creek deposit .....	31
2.8. Quartz and carbonate veins.....	32
2.9. Petrography of fluid inclusions .....	34
Version abrégée .....	36
<b>3. Mixing of diagenetic-hydrothermal brines at McArthur River U deposit, Canada: LA-ICP-MS investigation of fluid inclusions.....</b>	<b>39</b>
Abstract .....	39
3.1. Introduction.....	40
3.2. Geology and fluid inclusions .....	41
3.3. LA-ICP-MS analysis.....	42
3.4. Na-Ca-Mg-K-Sr-Ba relations .....	43
3.5. Minor and trace elements .....	48
3.6. Genetic implications.....	49
Version abrégée .....	50
<b>4. Large scale percolation and mixing of basinal brines in the Athabasca Basement, Canada: PTX conditions from fluid inclusions.....</b>	<b>53</b>
Abstract .....	53
4.1. Introduction.....	54
4.2. Analytical methods .....	57
4.2.1. Microthermometry .....	57
4.2.2. LA-ICP-MS analysis.....	58
4.3. Results .....	59
4.3.1. Microthermometry results .....	59
4.3.1.1. Te - Tm ice pairs .....	59
4.3.1.2. NaCl-rich brine inclusions.....	61
4.3.1.3. CaCl <sub>2</sub> -rich brine inclusions .....	64
4.3.1.4. Low-salinity fluid inclusions .....	65
4.3.1.5. Tm ice - Th pairs and Th distributions among brines .....	65
4.3.1.6. Quartz vs. carbonate samples.....	66
4.3.1.7. Intra- and inter-sample variability .....	66
4.3.2. LA-ICP-MS results .....	75

4.4. Discussion .....	80
4.4.1. Fluid mixing .....	80
4.4.2. P-T estimations .....	80
4.4.2.1. Reconsidering the McArthur River model .....	80
4.4.2.2. Pressure fluctuations .....	81
4.4.2.3. Saturation with respect to halite .....	83
4.4.2.4. H <sub>2</sub> contamination.....	84
4.4.2.5. Post-trapping processes: stretching and necking down.....	84
4.4.2.6. An alternative P-T model.....	85
4.4.3. Conditions for uranium deposition.....	86
4.4.4. Comparison between unconformity and basement-hosted deposits.....	87
4.4.5. Basin-scale circulation .....	88
4.5. Conclusion.....	89
Version abrégée .....	90
<b>5. Uranium concentration in ore fluids: A LA-ICP-MS study of fluid inclusions in unconformity-related U deposits.....</b>	<b>93</b>
Abstract .....	93
5.1. Introduction.....	94
5.2. Analytical methods .....	95
5.3. Results .....	96
5.3.1. Data quality.....	96
5.3.2. U in fluid inclusions.....	98
5.3.3. NaCl-rich vs. CaCl <sub>2</sub> -rich brine .....	99
5.4. Discussion .....	101
5.4.1. Comparison with crustal fluids .....	101
5.4.2. Spent-ore, pre-ore, or remobilization fluids? .....	104
5.4.3. Significance for uranium source(s).....	104
5.5. Conclusion.....	106
Version abrégée .....	107
<b>6. Multiple origins of chlorine in diagenetic brines from the Athabasca Basin and Basement, Canada: Cl/Br and δ<sup>37</sup>Cl analysis of fluid inclusions.....</b>	<b>109</b>
Abstract .....	109
6.1. Introduction.....	110
6.2. Analytical methods .....	113
6.2.1. Crush-leach analysis.....	113
6.2.2. Stable chlorine isotope analysis .....	113
6.2.3. Cl concentration in rocks and minerals.....	114
6.3. Results .....	115
6.3.1. Two brines with contrasted chlorinities.....	115
6.3.2. Cl-Br-F-SO <sub>4</sub> concentrations .....	115
6.3.3. Chlorine isotopes .....	116
6.3.4. Cl from basement rocks and minerals .....	116
6.4. Discussion .....	120
6.4.1. Cl-Cl/Br-δ <sup>37</sup> Cl relationships in the Athabasca Basin .....	120
6.4.1.1. Primary brine component .....	120
6.4.1.2. Secondary brine component .....	122
6.4.2. Cl-Cl/Br-δ <sup>37</sup> Cl changes during percolation in the Athabasca Basement.....	126
6.4.2.1. The Athabasca Basement as a source of chlorine .....	126
6.4.2.2. Diffusion, ion filtration, hydration reactions .....	129
6.4.3. Brine flows from surface to basement .....	130
6.4.3.1. Evaporitic environments in the Athabasca Basin .....	130
6.4.3.2. Migration paths for brines.....	132
6.5. Conclusion.....	133
Version abrégée .....	134

<b>7. Conversion of NaCl-rich basinal brines to CaCl<sub>2</sub>-rich brines through fluid-rock interaction in the Athabasca Basement, Canada .....</b>	<b>137</b>
Abstract .....	137
7.1. Introduction .....	138
7.2. Basinal fluid database .....	140
7.3. Crush-leach analysis .....	141
7.4. Comparison of brine compositions with basinal fluids .....	144
7.4.1. Cation concentrations .....	144
7.4.2. Anion concentrations .....	153
7.5. Discussion .....	155
7.5.1. Origin of solutes in the NaCl-rich brine .....	155
7.5.2. Origin of solutes in the CaCl <sub>2</sub> -rich brine .....	156
7.5.3. Metal transport .....	159
7.5.4. Integration to geochemical budgets and fluid circulation models .....	162
7.6. Conclusion .....	164
Version abrégée .....	165
<b>8. Stable isotope composition (O, H, C) of diagenetic brines in the Athabasca Basement, Canada .....</b>	<b>167</b>
8.1. Introduction .....	168
8.2. Analytical methods .....	170
8.2.1. δ <sup>18</sup> O of quartz .....	170
8.2.2. δ <sup>18</sup> O and δ <sup>13</sup> C of carbonates .....	170
8.2.3. δD of brines and δ <sup>13</sup> C of CO <sub>2</sub> .....	171
8.3. Results .....	172
8.3.1. Oxygen isotopes .....	172
8.3.2. Hydrogen isotopes .....	173
8.3.3. Carbon isotopes .....	174
8.4. Discussion .....	178
8.4.1. δ <sup>18</sup> O (H <sub>2</sub> O) shift during basement alteration .....	178
8.4.2. Production of CO <sub>2</sub> during fluid-graphite interaction .....	182
8.4.3. Production of low δD H <sub>2</sub> during water radiolysis .....	185
8.4.4. Production of low δD water during abiogenic bitumen synthesis .....	186
8.4.5. Implication for interpretation of low δD of alteration minerals .....	187
8.5. Conclusion .....	189
Version abrégée .....	190
<b>9. Conclusion générale .....</b>	<b>193</b>
9.1. Synthèse des résultats et apports au modèle de circulations de fluides .....	193
9.1.1. Homogénéité des fluides à l'échelle du bassin .....	193
9.1.2. Identification des processus de mélange de saumures .....	194
9.1.3. Conditions de température et de pression .....	195
9.1.4. Source et transport de l'uranium .....	196
9.1.5. Lessivage du socle .....	197
9.1.6. Conversion saumure sodique – saumure calcique .....	198
9.1.7. Origine du chlore .....	199
9.1.8. Origine du CO <sub>2</sub> dissous .....	200
9.1.9. Composition isotopique de l'hydrogène des saumures .....	201
9.1.10. Echelles des migrations de fluides .....	202
9.1.11. Comparaison gisements type socle et type discordance .....	203
9.1.12. Dépôt de l'uranium .....	204
9.2. Perspectives .....	205
9.2.1. La phase fluide .....	205
9.2.1.1. Spéciation de l'uranium .....	205
9.2.1.2. Concentrations des saumures en éléments des terres rares .....	206
9.2.1.3. Analyse des gaz et de l'uranium par spectroscopie Raman .....	206

9.2.2. Les interactions fluides-roches.....	207
9.2.2.1. Origine du bore dans les dravites.....	207
9.2.2.2. Analyse des gaz rares et des halogènes.....	208
9.2.2.3. Isotopie du strontium et du néodyme sur les carbonates.....	208
9.2.2.4. Altération des monazites et sources de l'uranium .....	209
9.2.3. La modélisation.....	209
9.2.3.1. Modélisation thermodynamique des interactions fluides-roches.....	209
9.2.3.2. Moteurs des circulations de fluides .....	210
<b>Références.....</b>	<b>211</b>
<b>Liste des figures.....</b>	<b>227</b>
<b>Liste des tableaux .....</b>	<b>233</b>

## **1. Introduction générale**

La découverte de minéralisations uranifères à des teneurs exceptionnelles, localisées à la discordance entre le Bassin de l'Athabasca, d'âge mésoprotérozoïque, et son socle cristallin, d'âge paléoprotérozoïque à archéen, dans la province de la Saskatchewan (Canada), a encouragé de nombreux travaux depuis les années 1970, dans le but de comprendre les mécanismes de concentration de l'uranium dans ces environnements. La genèse de ces gisements a nécessité l'implication, à l'interface socle - couverture sédimentaire, de phases fluides pour le lessivage, le transport et le dépôt de l'uranium. Si la composition des phases fluides, ainsi que les conditions de température et de pression dans lesquelles elles ont circulé, ont été étudiées grâce aux inclusions fluides depuis les premiers travaux de [Pagel \(1975\)](#) jusqu'aux travaux récents de [Derome et al., \(2005\)](#), de nombreuses questions restaient en suspens, et sont l'objet de ce mémoire de thèse.

Les concepts généraux utilisés dans ce mémoire, l'état des connaissances sur les circulations de fluides associées à ces gisements, les objectifs de ce travail de thèse, ainsi que les moyens et méthodes engagés, sont présentés ci-après.

## 1.1. Circulation des fluides entre socles et bassins sédimentaires

Les bassins sédimentaires et les socles cristallins sur lesquels ils reposent sont des réservoirs hydrogéologiques majeurs. En revanche, ces réservoirs sont souvent considérés comme des systèmes distincts du fait des forts contrastes de perméabilité ([Figure 1.1](#) ; [Garven, 1995](#)).

Parallèlement, l'analyse de fluides actuels ou des paléofluides (inclusions fluides), ou de minéraux authigènes dans les bassins laissent penser que des fluides de bassin interagissent avec le socle ([Shelton et al., 1995](#) ; [Davisson and Criss, 1996](#)). A l'inverse, de nombreux fluides échantillonnés à plusieurs kilomètres de profondeur dans les socles ont des compositions qui tendent à montrer qu'ils proviennent d'un bassin sédimentaire sus-jacent ([Möller et al., 2000](#)). De plus, ces fluides ont pour origine soit l'eau météorique, soit l'eau de mer. Il semble donc que des fluides de surface soient capables de circuler à grande échelle entre les bassins et les socles ([Glesson et al., 2000](#)).

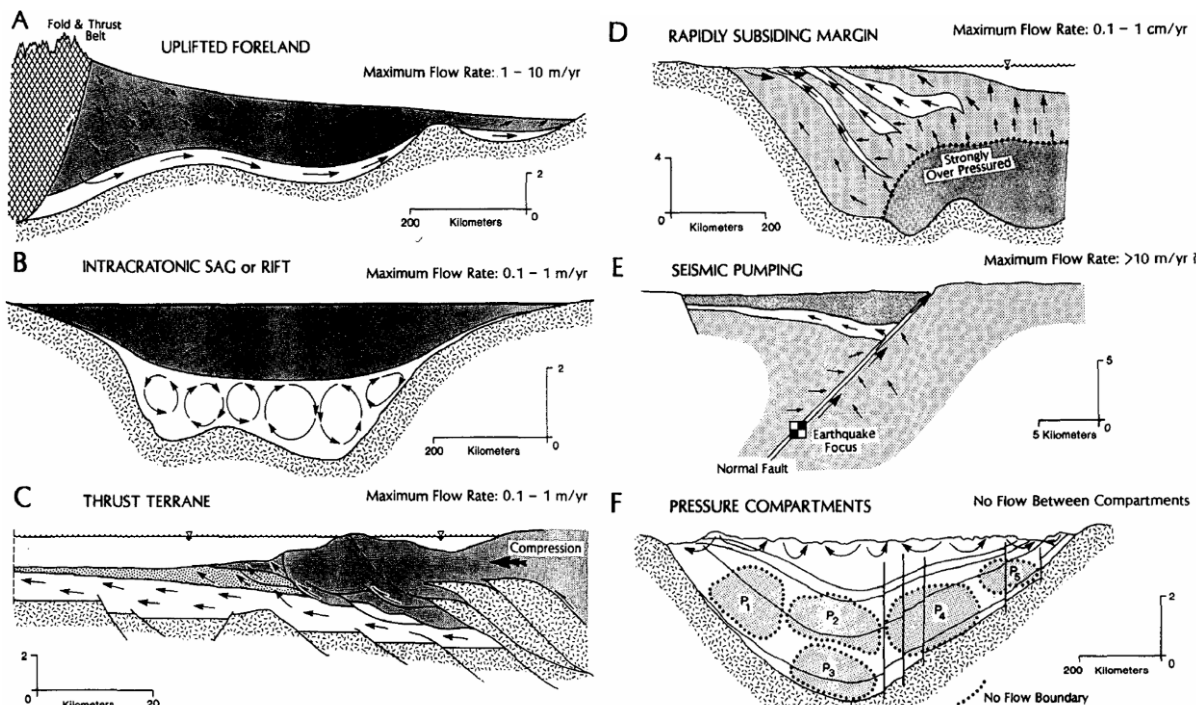


**Figure 1.1 : Régimes hydrogéologiques et tectoniques pour les circulations de fluides de bassin à grandes échelles, d'après [Garven, \(1995\)](#).** (A) Circulations induites par la topographie ou la gravité. (B) Convection thermique libre. (C) Circulations induites par la tectonique dans des ceintures de plis et chevauchements. (D) Surpression pendant la compaction d'une marge continentale. (E) Pompe sismique de fluides profonds dans un rift. (F) Compartimentation d'un bassin sans circulation de fluides à grande échelle.

De nombreux types de gisements sont connus pour l'implication de circulation de fluides à l'interface socle-couverture parmi lesquels : Pb-Zn de type MVT (Shelton et al., 1995), Ag-Co de Bou Azzer (Maroc) (Essaraj et al., 2005), talc de Trimouns (Boulvais et al., 2006), Pb-Zn type « Irish type » (Banks et al., 2002 ; Blakeman et al., 2002), Cu-Co de la Copperbelt (Zambie) (McGowan et al., 2006 ; Heijlen et al., 2008), Au-Pd liés à discordance Permien-Trias (Shepherd et al., 2005), F-Ba-Pb-Zn du Massif Central, (Munoz et al., 1999 ; Boiron et al., 2002), ou encore U de type discordance (Derome et al., 2005) l'objet de ce travail. Les mécanismes possibles de transferts de fluides à l'interface socle-couverture en contextes minéralisés sont divers, et sont résumés dans la Figure 1.2 (Oliver et al., 2006). Les principaux moteurs de ces circulations sont les flux de chaleur, la déformation, la topographie et la densité des fluides.

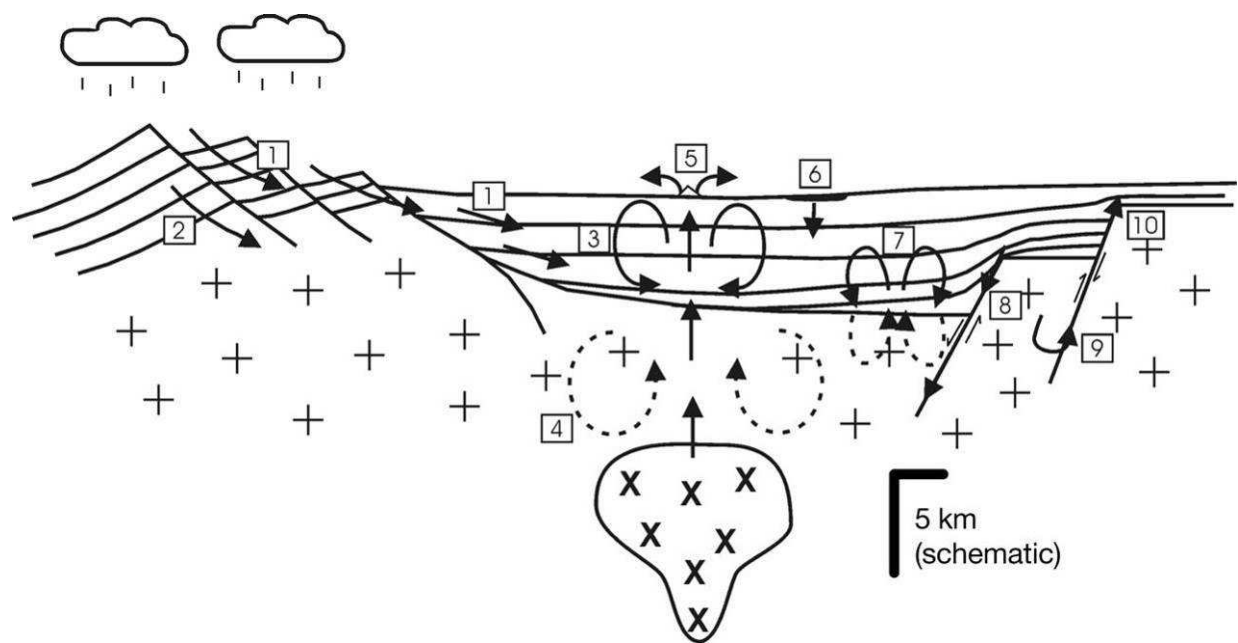


**Figure 1.2 : Schéma résumant la diversité des types de circulations de fluides impliqués dans des minéralisations dans les bassins sédimentaires, d'après Oliver et al., (2006).** (1) Circulations induites par la topographie dans le bassin. (2) Circulations induites par la topographie dans le socle. (3) Convection dans le bassin. (4) Convection dans le socle. (5) Exhalation à l'aplomb de panaches convectifs. (6) Percolation de saumures par densité. (7) Convection localisée à l'interface socle-bassin. (8) Circulations induites par la déformation le long de failles extensives actives ou réactivées. (9) Convection autour des failles dans le socle. (10) Circulations induites par l'inversion d'anciennes failles extensives.

## 1.2. Concentrations de métaux dans les fluides géologiques

Les fluides crustaux sont les principaux transporteurs de métaux et sont à l'origine de la majeure partie des concentrations métalliques. Les fluides minéralisateurs sont par nature difficilement échantillonables directement, et leurs concentrations en métaux sont donc mal connues. Les développements analytiques récents sur les inclusions fluides (« écrasement-lessivage », PIXE, LA-ICP-MS, SXRF) ont permis de mesurer ces concentrations en métaux dans les fluides minéralisateurs. Ces avancées ont rendu possible une meilleure compréhension des paramètres qui contrôlent la solubilité des métaux dans les fluides crustaux. Il apparaît que la température et la concentration en chlore sont les deux variables indépendantes principales qui régissent la teneur en métaux des fluides profonds ([Yardley, 2005](#) ; Figure 1.3).

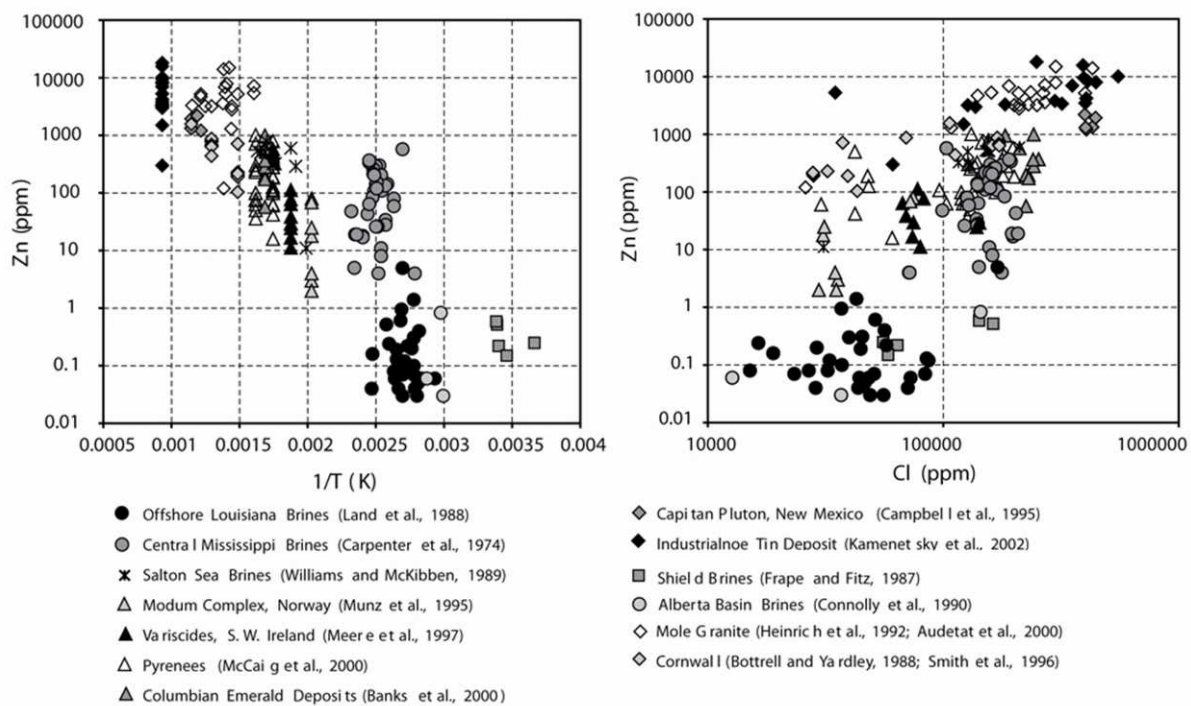


**Figure 1.3 : Concentrations en zinc dans les fluides crustaux en fonction de la température (g.) et de la concentration en chlore (dr.), d'après [Yardley \(2005\)](#). La température et la concentration en chlore sont les deux variables majeures contrôlant la concentration en métaux dans les fluides crustaux.**

### 1.3. Origine de la salinité des fluides

Le chlore est un élément essentiel pour le transport de métaux dans les fluides géologiques, et l'origine des concentrations en chlore est une donnée importante pour la construction de modèles métallogéniques. Les traceurs dits conservatifs (Cl-Br-I) ainsi que la composition isotopique du chlore sont couramment utilisés pour déterminer les mécanismes d'acquisition de la salinité des fluides (Banks et al., 2000a ; Worden, 1996). Dans le contexte de minéralisations dans les bassins sédimentaires, il apparaît que les fortes salinités des fluides minéralisateurs sont acquises par évaporation de l'eau de mer en surface (saumure primaire), ou par dissolution de formations évaporitiques en profondeur (saumures secondaires). Ces deux mécanismes ne sont pas mutuellement exclusifs et le mélange de ces deux types de saumures est couramment observé (Chi and Savard, 1997). L'exemple des gisements de Pb-Zn des bassins sédimentaires européens est frappant par l'homogénéité du caractère primaire dominant des saumures minéralisatrices (Muchez et al., 2005 ; Figure 1.4).

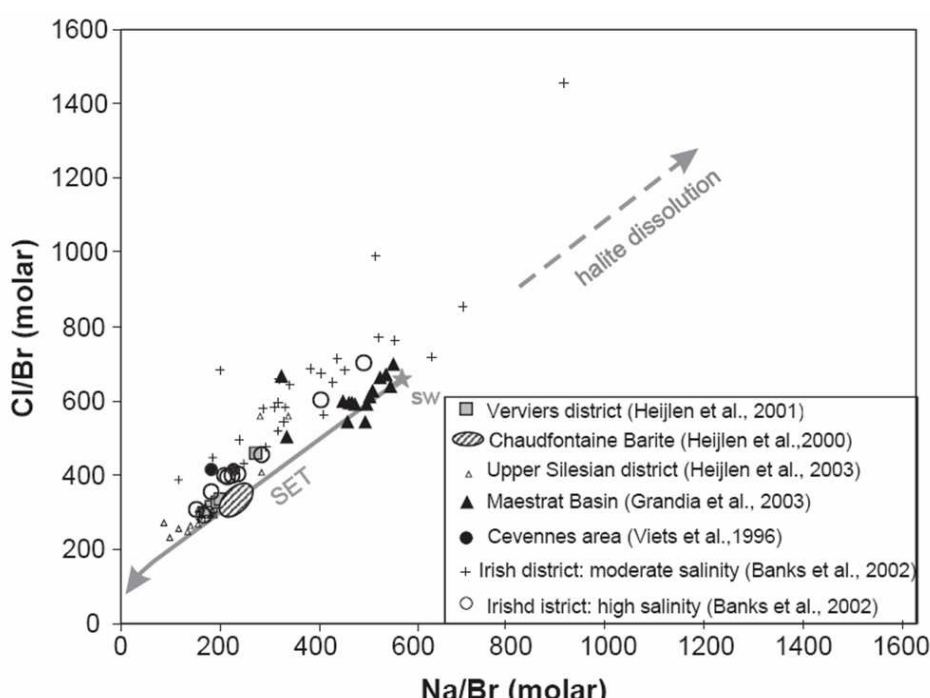


Figure 1.4 : Composition en Na-Cl-Br des fluides minéralisateurs en Pb-Zn dans les bassins sédimentaires européens, en contexte de tectonique extensive, d'après Muchez et al., (2005). Dans tous les districts, l'évaporation de l'eau de mer est la source principale des fortes salinités des saumures minéralisatrices. SW: eau de mer. SET: courbe d'évaporation de l'eau de mer.

#### **1.4. Gisements d'uranium de type discordance**

Les gisements d'uranium de type discordance sont localisés dans deux grands bassins intracratoniques d'âge protérozoïque : le Bassin de l'Athabasca (Saskatchewan, Canada) et le Bassin de McArthur (Northern Territory, Australie). Dans ces deux bassins, les gisements d'uranium sont associés spatialement à la discordance entre le socle magmatique et métamorphique, et les grès qui constituent la base de la couverture sédimentaire. Les études minéralogiques, géochimiques et d'inclusions fluides ont montré que ces gisements se sont formés dans les conditions de la diagenèse profonde (environ 200°C). Le socle et les grès présentent des halos d'altérations argileuses importantes autour des minéralisations. Les gisements de type discordance sont les témoins essentiels des circulations de fluides entre le bassin et le socle, et sont des objets modèles pour étudier les mécanismes et les implications de tels transferts.

Le modèle de circulations de fluides le plus abouti jusqu'à présent pour la formation des gisements canadiens est basé sur l'étude des inclusions fluides du gisement de McArthur River, et implique deux saumures, de salinité équivalente à dix fois celle de l'eau de mer, et de compositions chimiques contrastées ([Derome et al., 2005 ; Figure 1.5](#)). Une saumure à dominante sodique circule à la base des grès à environ  $220 \pm 30^\circ\text{C}$  et peut interagir avec les lithologies du toit du socle, dans les zones de forte porosité, anciennement altérées lors de l'émergence. L'infiltration de cette saumure sodique dans des niveaux structuraux plus élevés du socle, et l'interaction entre cette saumure sodique et les lithologies du socle, provoquent une conversion du rapport Na/Ca de la saumure, qui devient alors une saumure à dominante calcique, à environ  $110 \pm 30^\circ\text{C}$ . Ces deux saumures se mélangent, à la faveur de réactivation de failles enracinées dans le socle, en même temps que se forment les minéralisations uranifères. Dans les deux bassins, l'origine des fortes salinités de ces saumures est connue par l'utilisation des rapports Cl/Br, qui indiquent qu'elles se sont formées par évaporation de l'eau de mer ([Derome et al., 2005 ; 2007](#)).

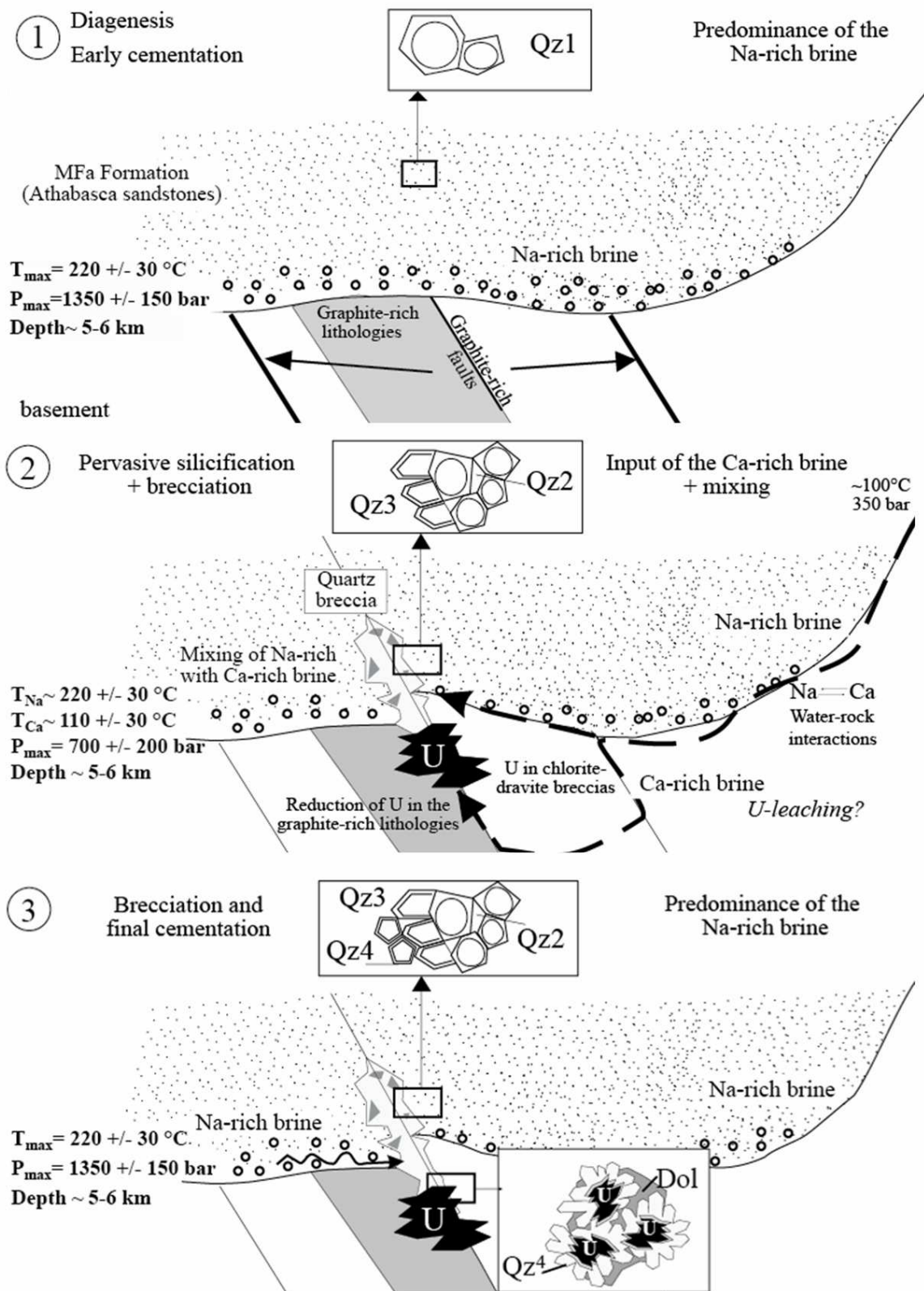


Figure 1.5 : Représentation schématique des circulations de fluides et des conditions P-T à la base du Bassin de l'Athabasca, à chaque étape des cimentations de quartz dans le gisement de McArthur River, et leur lien possible avec la genèse des minéralisations en uranium, d'après Derome et al., (2005). Qz : quartz. Dol : dolomite (1) Cimentation précoce à la base des grès. (B) Interactions entre la saumure sodique et les lithologies du socle, formation de la saumure calcique, et mélange entre ces deux saumures le long des failles pendant le dépôt de l'uranium. (C) Cimentation finale des brèches par la saumure sodique.

## **1.5. Objectifs de la thèse**

Les modèles récents de circulations de fluides à l'interface socle-couverture dans le Bassin de l'Athabasca constituent une avancée significative dans la mise en évidence de la diversité des compositions chimiques des fluides ainsi que des phénomènes de mélange. Ces travaux ont permis de soulever de nouvelles questions qui sont à l'origine de ce travail de thèse :

(1) Le modèle établi pour le gisement de McArthur River par Derome et al., (2005) est-il généralisable à l'ensemble des gisements d'uranium du Bassin de l'Athabasca ? Les deux saumures sont-elles présentes dans tous les gisements ? Les conditions de température et de pression pour leur circulation sont-elles les mêmes dans tout le bassin ? Y a-t-il mélange entre ces deux saumures dans tous les gisements ? Y a-t-il des différences entre les conditions de formation des gisements localisés à la discordance, et de ceux localisés dans le socle ?

(2) Quel est le rôle des saumures sodiques et calciques dans le lessivage, le transport, et le dépôt de l'uranium ? Ces saumures sont-elles enrichies en autres métaux qui sont associés dans ces gisements à l'uranium (Fe, Ni, Co, Cu, Pb, Zn, As, Mo) ? Quelle sont les importances relatives du bassin et du socle comme source de l'uranium dans les saumures et les gisements ?

(3) Peut-on affiner les modèles d'acquisition des fortes salinités de ces saumures ? L'évaporation de l'eau de mer est-elle le seul facteur d'enrichissement en chlore dans les saumures ? Le socle peut-il fournir du chlore par l'altération de porteurs spécifiques ? Les saumures sodiques et calciques ont-elles la même origine ?

(4) Quels changements dans la composition des fluides sont associés à la percolation des saumures dans le socle ? Quelle est l'origine des fortes concentrations en Ca dans la saumure calcique ? Quels sont les liens entre altérations, mobilités élémentaires autour des gisements, et composition des saumures ?

(5) Quelles sont les échelles verticales et horizontales des circulations dans le bassin et le socle ? Les saumures ont-elles circulé dans des zones non-altérées du socle, ou à distance des gisements ?

## 1.6. Moyens et méthodes

Pour répondre aux questions posées ci-dessus, six gisements ont été sélectionnés. Trois d'entre eux sont localisés exclusivement dans le socle (Eagle Point, P-Patch, Millennium) et les trois autres présentent des minéralisations à la discordance mais aussi dans le socle (Rabbit Lake, McArthur), voire également dans les grès (Shea Creek). Ceci permettra de comparer les résultats en terme de localisation de la minéralisation par rapport à la discordance et vérifier si cette localisation est fonction de la composition des fluides mis en jeu, ou des conditions de pression et de température. Le gisement de Shea Creek est situé à l'ouest du bassin, au sud de la structure Carswell. Les cinq autres gisements se trouvent à l'est du bassin, et répartis du Nord au Sud sur la « Wollaston Mudjatik transition zone » qui renferme la majorité des gisements économiques d'uranium du bassin. Cet échantillonnage à l'échelle du Bassin de l'Athabasca permet d'appréhender les échelles de circulation des fluides.

Les inclusions fluides, ainsi que leurs minéraux hôtes, sont les principaux objets d'études de ce travail. Les inclusions fluides ont été sélectionnées dans les veines de quartz et de carbonates qui sont liées spatialement et génétiquement à la formation des gisements d'uranium. Les techniques utilisées, ainsi que le nombre d'échantillons ou d'inclusions fluides analysés pour chaque gisement étudié, sont résumés dans la [Table 1.1](#). Les techniques analytiques utilisées seront décrites brièvement ci-dessous, et plus en détail au fur et à mesure du manuscrit, avant présentation et discussion des résultats acquis par ces techniques.

	McArthur River	Rabbit Lake	Shea Creek	Eagle Point	Millennium	P-Patch
Microthermométrie	-	21 éch.	6 éch.	18 éch.	5 éch.	22 éch.
LA-ICPMS	45 Ifs	86 Ifs	-	39 Ifs	42 Ifs	90 Ifs
Ecrasement lessivage	5 éch.	19 éch.	-	10 éch.	4 éch.	9 éch.
$\delta^{18}\text{O}$ Qz	5 éch.	12 éch.	6 éch.	12 éch.	5 éch.	9 éch.
$\delta^{13}\text{C} + \delta^{18}\text{O}$ Carb	1 éch.	9 éch.	-	6 éch.	-	13 éch.
$\delta\text{D}$	5 éch.	15 éch.	2 éch.	6 éch.	3 éch.	12 éch.
$\delta^{13}\text{C CO}_2$	1 éch.	8 éch.	-	2 éch.	-	3 éch.
$\delta^{37}\text{Cl}$	4 éch.	12 éch.	-	5 éch.	4 éch.	9 éch.

**Table 1.1 : Résumé des techniques d'analyse d'inclusions fluides et de minéraux hôtes utilisées dans ce travail, classées par gisements étudiés. ifs : inclusions fluides. éch : échantillons. Qz : quartz. Carb : carbonates. Les analyses en microthermométrie pour le gisement de McArthur River ont été réalisées par [Derome et al., \(2005\)](#).**

Les conditions de pression et de température des fluides ainsi que leur salinité et leur composition dans des systèmes simples comme  $\text{H}_2\text{O-NaCl}$ ,  $\text{H}_2\text{O-CaCl}_2$  ou  $\text{H}_2\text{O-NaCl-CaCl}_2$  ont été reconstituées par la technique de microthermométrie. Cette technique consiste à observer les transitions de phases à basse et haute températures dans les inclusions fluides. Des analyses microthermométriques ont été réalisées de manière systématique sur tous les échantillons. Sur la base des travaux de [Derome et al., \(2005\)](#), la microthermométrie permet de discriminer les inclusions fluides ayant piégé la saumure sodique de celles ayant piégé la saumure calcique. Cette technique permet donc de déterminer si les veines de quartz ou de carbonates ont précipité à partir d'une saumure ou de deux saumures. Elle permet également d'identifier les phénomènes de mélange des fluides, et sert de base pour la reconstitution des concentrations absolues des éléments majeurs et traces par les techniques « d'écrasement-lessivage » et de LA-ICP-MS (voir ci-dessous).

L'identification du mélange des saumures, du transport de l'uranium, ainsi que des interactions fluides-roches passe par la reconstitution de la composition chimique détaillée en éléments majeurs et traces des saumures. Ces compositions ont été déterminées par deux techniques complémentaires. L'ablation laser couplée à la spectrométrie de masse (LA-ICP-MS) consiste à atteindre les inclusions fluides à l'aide d'un laser, à ioniser la solution sous forme de plasma et à l'analyser par spectrométrie de masse. Ceci permet l'analyse, inclusion par inclusion, de la composition détaillée des saumures. Entre autre, les

limites de détection sont suffisamment basses pour déterminer les concentrations en éléments traces, dont les métaux (limite de détection de l'ordre du ppm). Ces analyses ont été réalisées sur des échantillons sélectionnés en collaboration avec Thomas Pettke (ETH, Zürich, Suisse) et David A. Banks (Université de Leeds, Angleterre). L'analyse par « écrasement lessivage » consiste à écraser mécaniquement un échantillon pour en récupérer le lixiviat d'inclusions fluides. Les anions (Cl, Br, SO<sub>4</sub>, F) sont analysés par chromatographie ionique et les cations sont analysés par spectroscopie à émission de flamme (Na, K, Li) et ICP-MS. La technique d'« écrasement-lessivage » permet de reconstituer la composition détaillée de populations d'inclusions fluides à l'échelle de l'échantillon. Elle présente le désavantage de mélanger les différentes populations d'inclusions fluides (par exemple les deux types de saumures) mais reste le seul moyen de déterminer les concentrations en anions, et d'en déduire les rapports Cl/Br qui sont des traceurs de l'origine de la salinité des fluides. Ces analyses ont été réalisées de manière la plus systématique que possible, lorsque la masse d'échantillon le permettait (collaboration avec David A. Banks, Université de Leeds, Angleterre).

La question de l'acquisition des fortes salinités des saumures sodiques et calciques, et par conséquent de l'origine du chlore dans ces saumures, est abordée par l'analyse des rapports Cl/Br par « écrasement-lessivage » mais également par l'analyse de la composition isotopique du chlore ( $\delta^{37}\text{Cl}$ ). L'analyse du  $\delta^{37}\text{Cl}$  procède également de la technique d'« écrasement-lessivage ». Le chlore récupéré dans les lixiviats d'inclusions fluides est isolé chimiquement sous forme d'AgCl pour être analysé isotopiquement par spectrométrie de masse. Ces analyses ont été réalisées sur les mêmes échantillons que ceux analysés par « écrasement-lessivage » lorsque la quantité de chlore récupérée était suffisamment importante (collaboration avec David A. Banks, Université de Leeds, Angleterre, et avec le laboratoire Environment Canada, Saskatoon, Saskatchewan, Canada).

Les interactions fluides-roches peuvent être tracées par l'analyse de la composition isotopique de l'oxygène ( $\delta^{18}\text{O}$ ), du carbone ( $\delta^{13}\text{C}$ ) et de l'hydrogène ( $\delta\text{D}$ ) des saumures et des minéraux hôtes des inclusions fluides. L'analyse du  $\delta^{18}\text{O}$  des quartz est réalisée par

l'attaque chimique de poudres de quartz au BrF<sub>5</sub>, et permet de déterminer le δ<sup>18</sup>O des saumures à partir desquelles ils ont précipité, si leur température de formation est connue. L'oxygène récupéré sous vide est ensuite converti en CO<sub>2</sub> par combustion avec du graphite. Le CO<sub>2</sub> est alors analysé isotopiquement par spectrométrie de masse. Tous les échantillons de quartz présentés dans ce travail ont été analysés en collaboration avec Philippe Boulvais (Géosciences Rennes). L'analyse du δ<sup>13</sup>C des carbonates est réalisée par attaque chimique des poudres de carbonates au H<sub>3</sub>PO<sub>4</sub>, et permet également de déterminer le δ<sup>13</sup>C du CO<sub>2</sub> dissous dans les saumures, et donc son origine, si la température est connue. Le CO<sub>2</sub> récupéré sous vide est ensuite analysé isotopiquement par spectrométrie de masse. Tous les échantillons de carbonates présentés dans ce travail ont été analysés en collaboration avec Philippe Boulvais (Géosciences Rennes). L'analyse du δD de l'eau se fait par écrasement d'échantillons sous vide, à 110°C pour dégazer les inclusions fluides, et permet de déterminer l'origine de l'eau des saumures. L'eau récupérée est transférée dans un four à uranium, et radiolysée en O<sub>2</sub> + H<sub>2</sub>. L'hydrogène est ensuite analysé isotopiquement par spectrométrie de masse. Ces analyses ont été effectuées de manière systématique, lorsque la masse d'échantillon nécessaire (environ 5g) pour extraire une quantité d'eau analysable était disponible (collaboration avec Christian France-Lanord et Caroline Guilmette, CRPG, Nancy). L'analyse directe du δ<sup>13</sup>C du CO<sub>2</sub> dissous dans les saumures peut se faire conjointement à celle du δD de l'eau, si la quantité de CO<sub>2</sub> dissous est suffisante, ce qui était le cas pour les inclusions fluides dans les veines de carbonates. Cette mesure permet de déterminer l'origine du CO<sub>2</sub> si la température est connue. Le CO<sub>2</sub> est séparé de l'eau sous vide et est analysé isotopiquement par spectrométrie de masse (Collaboration avec Christian France-Lanord et Caroline Guilmette, CRPG, Nancy).

## 2. Geology, sampling and fluid inclusion petrography

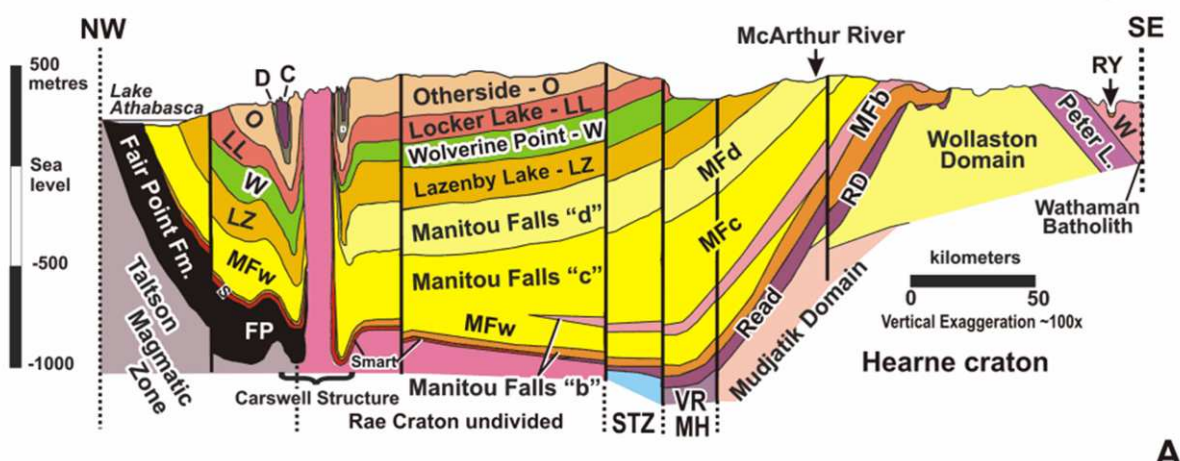
### 2.1. The Athabasca Basin and Basement

The Athabasca Basin lies on an Archean to Paleoproterozoic basement complex separated by the Northeast-trending Snowbird tectonic zone into two provinces, the Rae Province in the west and the Hearne Province in the east (Hoffman, 1990; Card et al., 2007) (Figure 2.1, 2.2). These two provinces consist of Archean gneisses, Paleoproterozoic metapelites and mafic to felsic intrusions, and were affected respectively by the ca. 2.0 to 1.9 Ga Thelon-Talston and the ca. 1.9 to 1.8 Ga Trans-Hudson orogenies (Card, 2002; Card et al., 2003; Chiarenzelli et al., 1998; Annesley et al., 2005). Most of the unconformity-related uranium deposits of the Athabasca Basin, including those presented in this paper (except for Shea Creek) are located in the vicinity of the transition between two lithostructural domains of the Hearne Province, known as the Wollaston-Mudjatic transition zone (WMTZ) that consists of a Northeast-trending, anastomosing structure of Precambrian age (Annesley et al., 2005). A regolith profile up to several tens of meters thick, develops at the top of the basement and is interpreted alternatively as the result of lateritization processes during emersion (Macdonald, 1985; Pagel, 1991) or percolation of oxidizing diagenetic brines in the basement (Cuney et al., 2003).

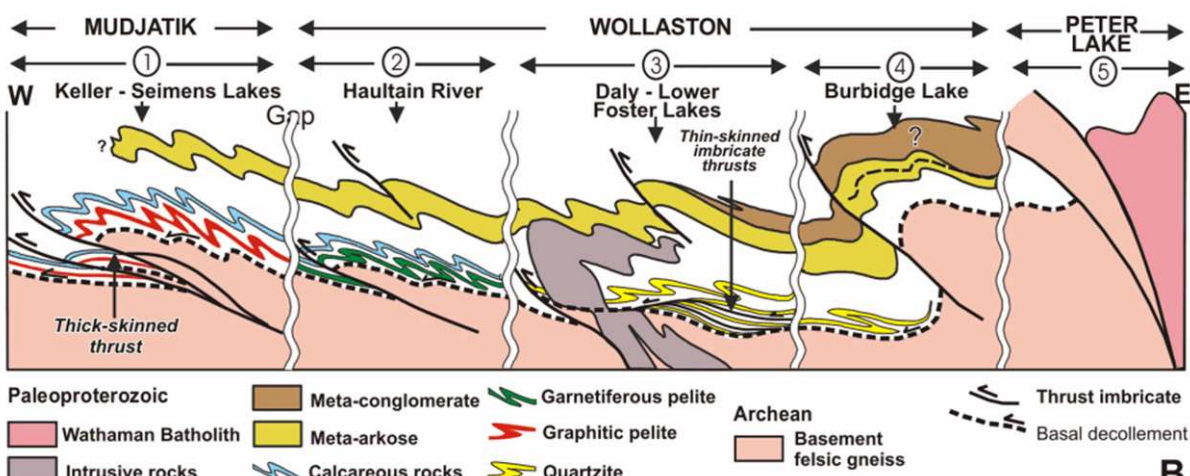
The sedimentary sequence of the Athabasca Basin, known as the Athabasca Group, unconformably overlies the crystalline basement and was deposited between 1.75 and 1.65 Ga (Rainbird et al., 2007) (Figure 2.1, 2.2.). Current maximum thickness of the sedimentary cover is of 1500m (Rumple Lake) and is thought to have reached ca. 5 km based on pressure/temperature estimations from fluid inclusion studies (Pagel, 1975; Derome et al., 2005). Chronologically, the Athabasca Group is composed of fluvial to marine quartz-rich sandstones of the Fair Point and Manitou Falls Formations, marine sandstones, phosphatic siltstones, and phosphatic mudstones of the Lazenby Lake and Wolverine Point Formations,

sandstones of the Locker Lake and Otherside Formations, shales of the Douglas Formation and finally stromatolitic carbonates of the Carswell Formation (Ramaekers et al., 2007). The Douglas and Carswell formations are only preserved around the Carswell structure, which is thought to be the result of a meteorite impact (Pagel et al., 1985).

Both basement and sedimentary cover are cut by Northwest-trending mafic dykes dated at ca.  $1227 \pm 11$  Ma by the Rb-Sr method (Armstrong and Ramaekers, 1985), well after tectonic activity linked with the formation of the Athabasca Basin and most probably related to the McKenzie dike swarms, but not considered as heat source for secondary U mineralizations (Cumming and Krstic, 1992).



A



B

**Figure 2.1 : (A) Lithostratigraphic cross-section of the Athabasca Basin (Jefferson et al., 2007). MF: Manitou Falls Formation. D: Douglas Formation. C: Carswell Formation. (B) Diagrammatic structural cross-section south of Key Lake, illustrates structural geometry of Wollaston-Mudjatik transition zone that underlies the most economically productive area of the Eastern Athabasca Basin (Jefferson et al., 2007).**

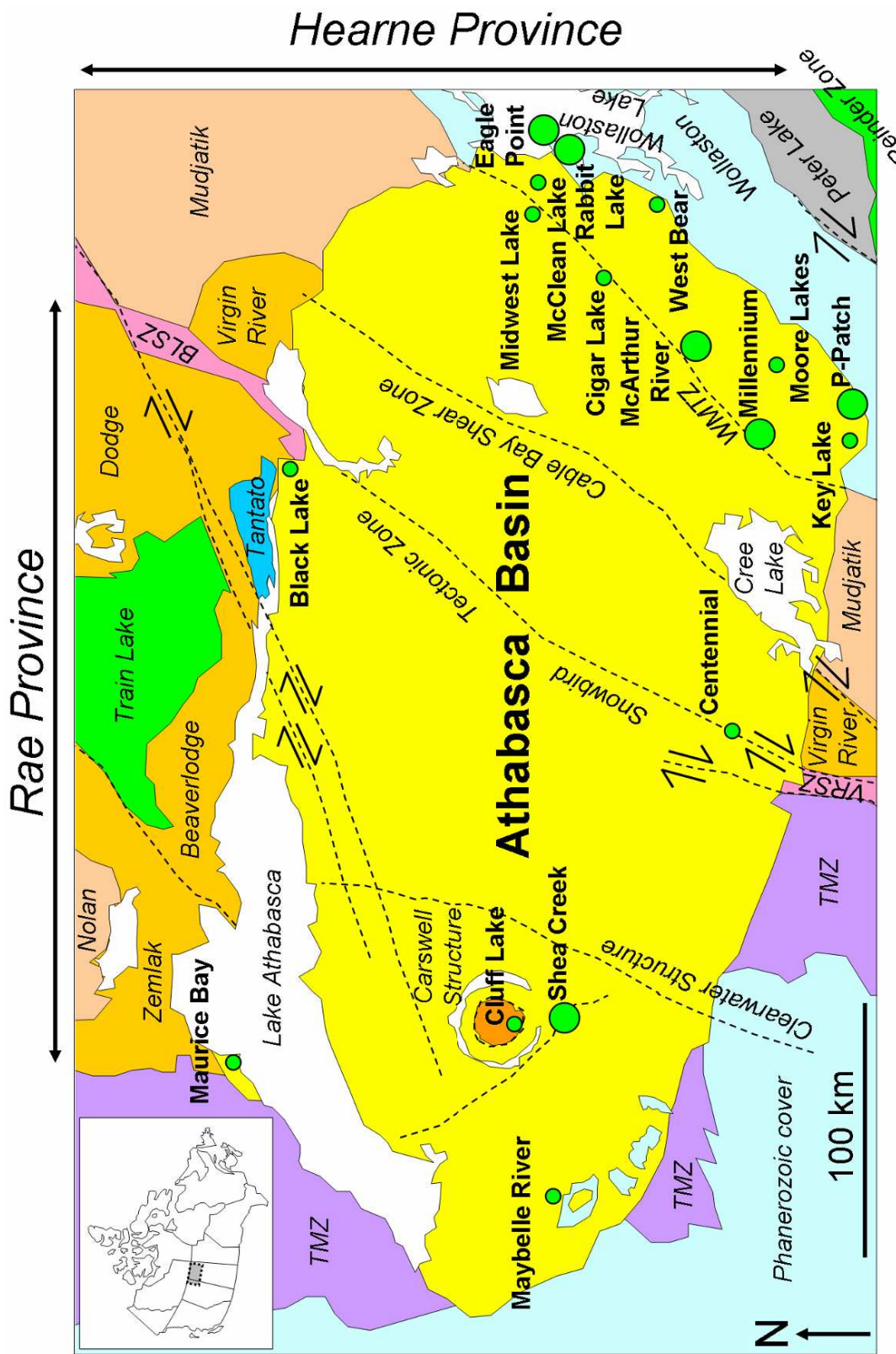
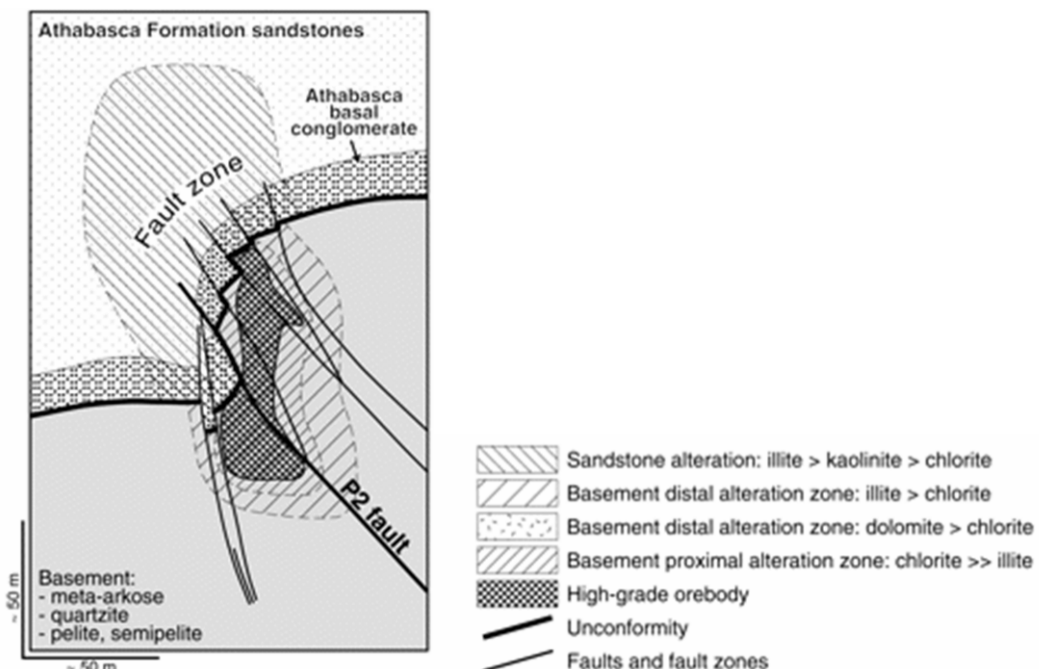


Figure 2.2 : Simplified geological map of the Athabasca Basin and Basement, Canada. Basement domains are individualized. Modified from Jefferson et al., (2007). Circles indicate main uranium deposits. Large circles indicate main uranium deposits studied in this work. TMZ: Thelon magmatic zone. WMZ: Wollaston Mudjatik transition zone. VRSZ: Virgin River shear zone. BLSZ: Black Lake shear zone.

## 2.2. McArthur River deposit

The McArthur River deposit (P2 North orebody, this study), discovered in 1988, is mostly basement-hosted and located in the footwall of the P2 Northeast-trending, Southwest dipping reverse fault ([Figure 2.3.](#)). Hangingwall lithologies comprise mainly graphitic biotite-quartz-garnet metapelitic gneisses. Footwall lithologies consist of arkosic semipelitic gneisses and feldspathic metaquartzite ([McGill et al., 1993; Matthews et al., 1997; Thomas et al., 2000](#)). The overlaying Athabasca sandstones display diagenetic quartz overgrowths and postdiagenetic, premineralization, pervasive silicifications associated with drusy quartz veins. Alteration minerals around the mineralization include silicification, Mg-chlorite (sudoite), Mg tourmaline (dravite), and kaolinite. Mineralization is predominantly monometallic with pitchblende occurring mainly in chlorite-rich breccias. Minimum proposed U/Pb age for mineralization has been estimated at  $1514 \pm 18$  Ma ([Cummings and Krstic, 1992](#)),  $1519 \pm 22$  ([Fayek et al., 2002](#)) and  $1540 \pm 19$  Ma ([Alexandre et al., 2009a](#)). Recrystallisation or new deposition is thought to have occurred at  $1327 \pm 8$  Ma ([Cummings and Krstic, 1992](#)),  $1247 \pm 19$  and  $971 \pm 27$  Ma ([Alexandre et al., 2009a](#)).



**Figure 2.3 : Simplified schematic representation of lithology, structure, clay mineral alteration halos, and orebodies of the McArthur River deposit ([Alexandre et al., 2005](#)).**

### 2.3. Rabbit Lake deposit

The Rabbit Lake Deposit was the first unconformity-related uranium deposit to be discovered (1968) and exploited in the Athabasca Basin ([Figure 2.4.](#)). Basement lithologies belong to the Paleoproterozoic Wollaston Group and are divided into two blocks separated by the Northeast-trending reverse Rabbit Lake Fault. Footwall lithologies comprise sediments of the Athabasca Group, regolithic altered rocks, sulphide-rich albited plagioclase and granitic intrusives. Hangingwall lithologies consist of plagioclase similar to that of the footwall, diopside-bearing dolomitic marbles, highly altered and fractured pyrite-rich graphitic granulite, gneisses (Upper Gneisses) composed of green diopside-amphibole-chlorite bands, interlayered with red feldspar-scapolite-quartz layers, granitic intrusives, microcline-rich granitic sills and a microgranite localized within a breccia zone ([Hoeve and Sibbald 1978](#); [Heine, 1986](#)). Alteration is intense in and around the orebody and is characterised by Mg-chlorite (sudoite), quartz, dolomite, dravite, and hematite assemblage ([Alexandre et al., 2005](#)). The mineralization is essentially monometallic and located close to the microgranite-breccia zone. Minimum age for mineralization ranges from  $1570 \pm 38$  Ma ([Alexandre et al., 2009a](#)) to  $1342 \pm 11$  Ma ([Cumming and Krstic, 1992](#)). However U suffered several episodes of redistribution in the basement until recent times ([Cumming and Rimsaite, 1979](#)).

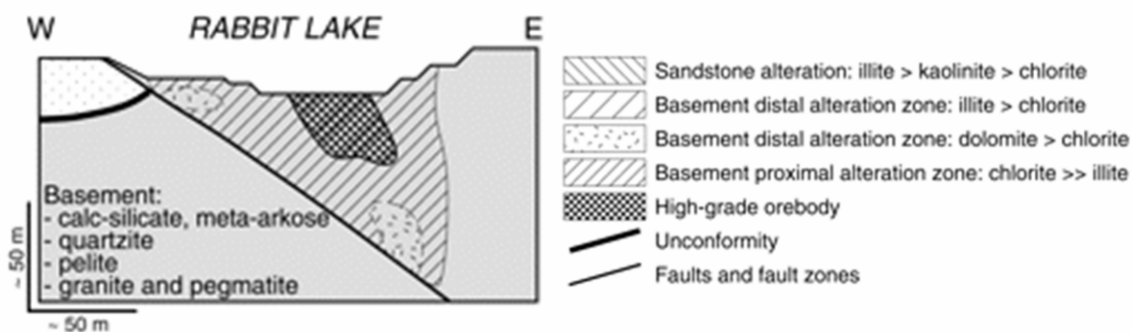


**Figure 2.4 : Simplified schematic representation of lithology, structure, clay mineral alteration halos, and orebodies of the McArthur River deposit ([Alexandre et al., 2005](#)).**

## 2.4. Eagle Point deposit

The Eagle Point deposit was discovered in 1980 ([Figure 2.5](#)). Basement rocks comprise Archean granodioritic to tonalitic gneisses (Collins Bay Dome), graphitic pelites and their anatetic derivatives; quartzofeldspathic and biotite-quartz-feldspar gneisses, and pegmatite. Alteration assemblages consist of illite, pyrite, hematite, carbonate ± quartz veins, quartz veins, sericite and chlorite. Mineralization is entirely basement-hosted and monometallic ([Quirt, 1989](#); [Thomas, 2003](#)). No dating on mineralization are available due to the impossibility to obtain suitable samples, nevertheless indicating that late remobilization and redeposition of uranium occurred ([Cumming and Krstic, 1992](#); [Kotzer and Kyser, 1993](#); [Fayek and Kyser, 1997](#); [Mercadier et al., in prep](#)).

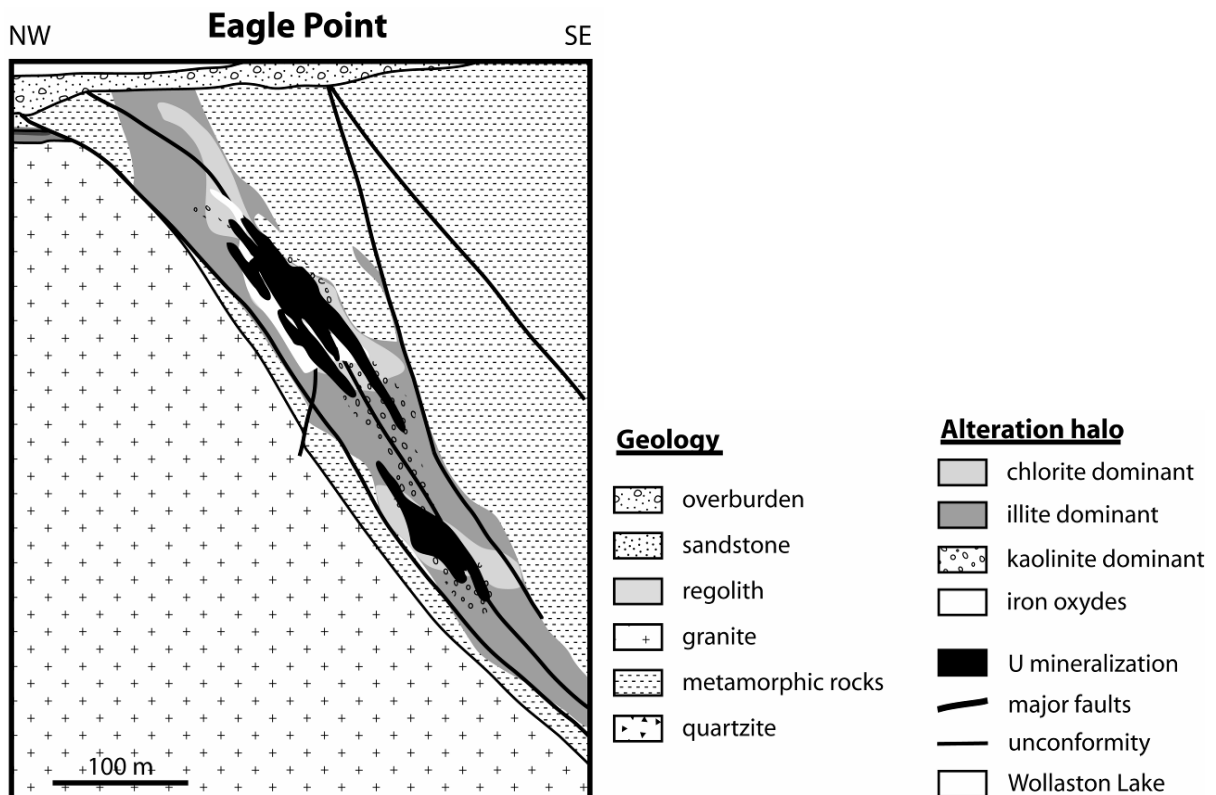


**Figure 2.5 : Simplified schematic representation of lithology, structure, clay mineral alteration halos, and orebodies of the Eagle Point deposit ([Mercadier, 2008](#)).**

## 2.5. P-Patch deposit

The P-Patch deposit was discovered in 1997, 3 km east of the Key Lake deposit and is almost entirely hosted in Paleoproterozoic metasediments, pegmatoids and granitoids, of the Wollaston Domain, unconformably overlain by 70m thick sandstones of the Athabasca Group ([Figure 2.6](#)). Mineralization occurs mostly in the pegmatoids, and is structurally controlled by N70°E dravite-quartz breccia, with direction similar to that of the Key Lake Fault which hosts other U deposits (e.g. GAX Zone and BV) and results from reactivation of Hudsonian structures ([Mercadier et al., in press](#)). Ore mineralogy consists of pitchblende with lesser amount of coffinite. The alteration halo almost entirely restricted to the basement and consists of a complex illite-chlorite-dravite assemblage (bleaching alteration) with quartz and dolomite veins developed up to several meters around U mineralizations. Very discrete bleaching alteration is present in various parts of the sandstones. ([Wheatley and Tan, 1998](#); [Mercadier et al., in prep](#)). No geochronological data are currently available for the P-Patch deposit.

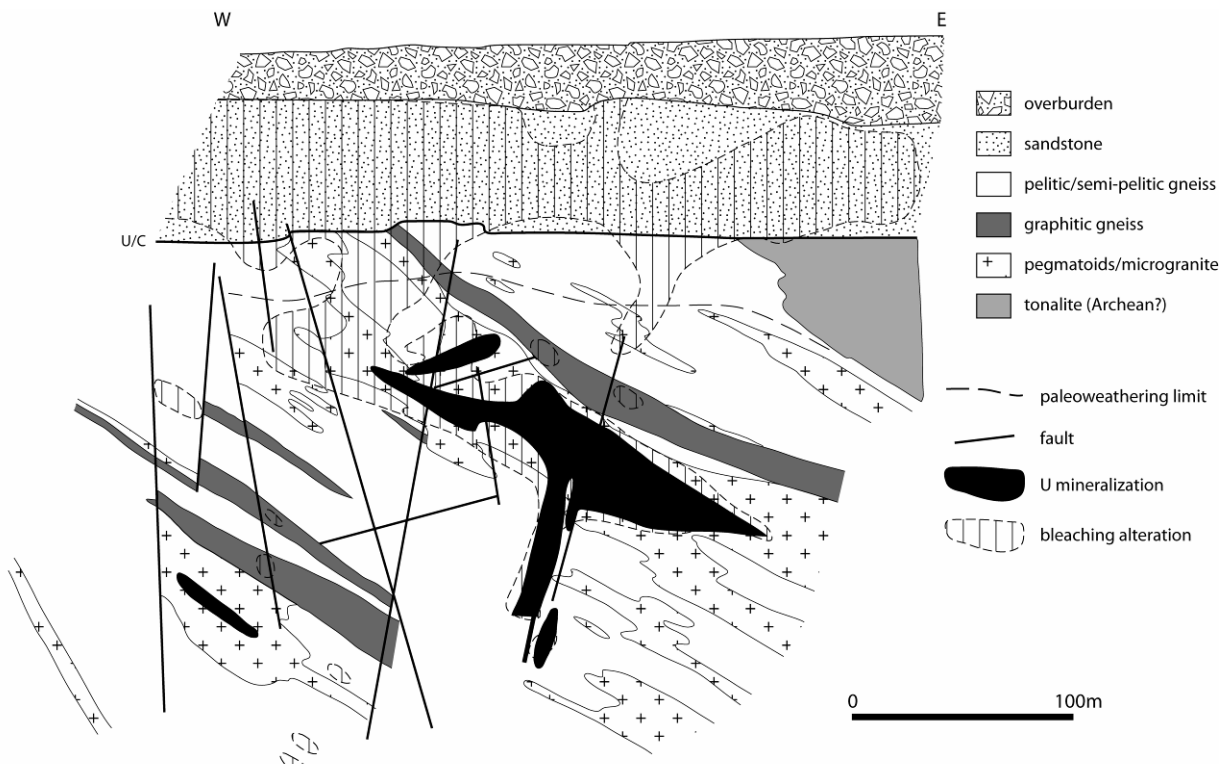


**Figure 2.6 : Simplified schematic representation of lithology, structure, clay mineral alteration halos, and orebodies of the P-Patch deposit ([Mercadier et al., in prep](#)).**

## 2.6. Millennium deposit

The Millennium deposit was discovered in 2000, 35 km North of the P-Patch deposit, and is entirely hosted in Paleoproterozoic Wollaston Group metasedimentary rocks, unconformably overlain by the 500m thick sandstones of the Athabasca Group ([Figure 2.7](#)). Mineralization is essentially stratabound and monometallic and is situated in the hangingwall of a major reverse fault. Ore mineralogy consists of pitchblende with a lesser amount of coffinite. Hydrothermal alteration minerals around U ore include illite, chlorite and dravite ([Roy et al., 2005](#)). U-Th-Pb chemical dating of mineralization yielded age clusters of 1350-1250 Ma for primary mineralization and 1200-900 Ma and 750-550 Ma for secondary remobilizations ([Annesley et al., 2007](#)). U/Pb datings on uraninites yielded ages of 1590, 1430, 1350, 1275, 1090 and 825 Ma ([Cloutier et al., 2008](#)).

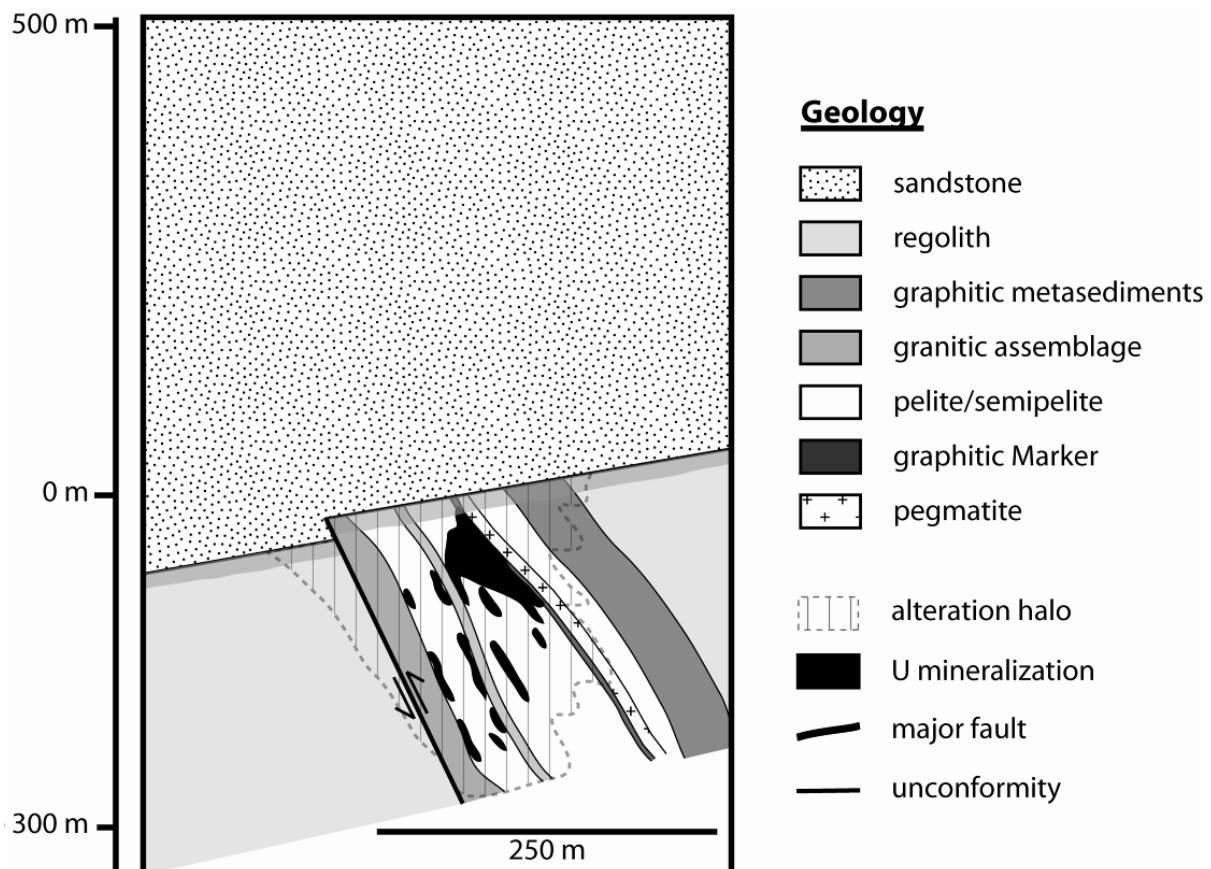


**Figure 2.7 : Simplified schematic representation of lithology, structure, clay mineral alteration halos, and orebodies of the Millennium deposit ([Mercadier, 2008](#)).**

## 2.7. Shea Creek deposit

The Shea Creek prospect is located in the Western part of the Athabasca Basin, 20km south of the Carswell impact structure (Figure 2.8). The mineralized body is divided into three zones along the Saskatoon Lake electromagnetic Conductor (SLC), the Colette area to the North, Anne area to the South and Kyana area in between. The present-day sandstone cover is up to 750m thick. Basement rocks consist of more or less albitized gneiss and aluminous metapelites and garnetites. Mineralization mainly consists of pitchblende and/or coffinite, and is located at the unconformity, in the basement and in the sandstones. The mineralization is polymetallic and uranium is associated with Ni, As, Cu, Co, Mo, Au (Rippert et al., 2000). Main alteration minerals include hematite, kaolinite, illite, Mg-chlorite (sudoite) and dravite (Kister et al., 2005; Laverret et al., 2006, Kister et al., 2006). Massive fluid flows along breccias in both sandstones and basement led to intense quartz dissolution close to the unconformity and silicification of immediately overlying sandstones (Lorilieux et al., 2002; Le Carlier de Veslud et al., 2009). Early mineralizing events are dated with the U/Pb method at  $1362 \pm 71$  and successive remobilizations were identified until recent times (Cuney et al., 2002). No fluid inclusion data were published so far.

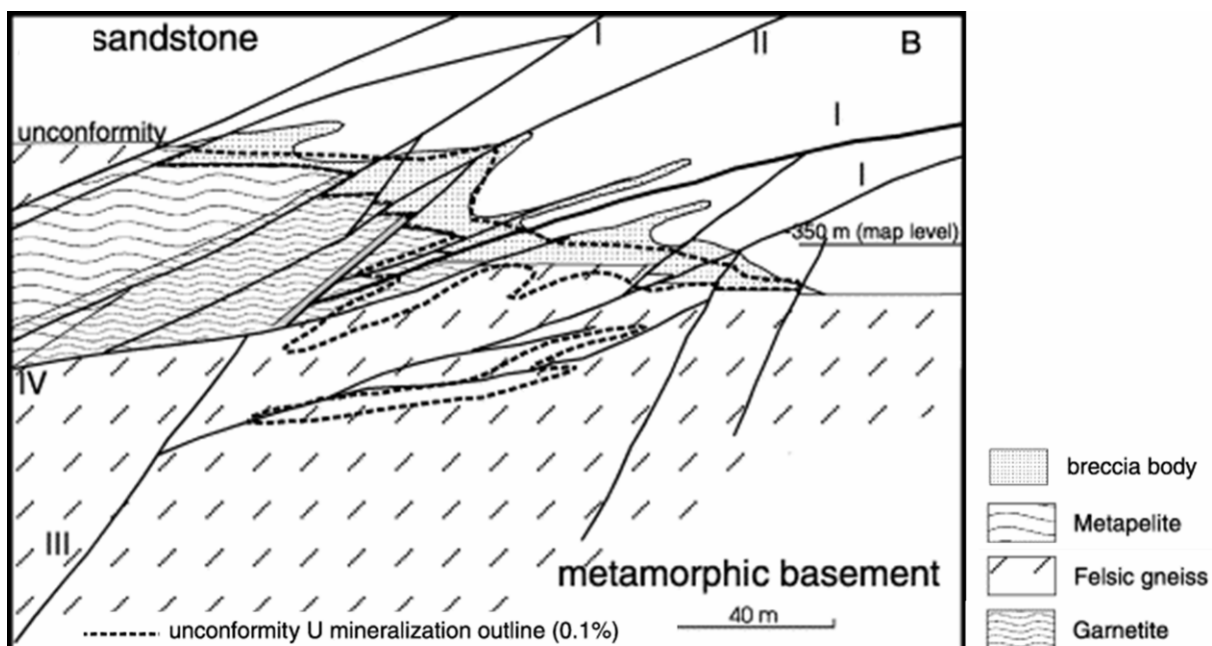


Figure 2.8 : Cross-section displaying the relationship between faults, the breccia body, the unconformity and the mineralization at the Shea Creek deposit (Lorilieux et al., 2002).

## 2.8. Quartz and carbonate veins

At McArthur River, [Derome et al., \(2005\)](#) have shown that quartz veins immediately pre-date and post-date U mineralization. [Kotzer and Kyser \(1995\)](#) and [Alexandre et al., \(2005\)](#) have also described quartz veins immediately pre-dating pitchblende, although [Alexandre et al., \(2005\)](#) have interpreted this association as recrystallization event. A single quartz veining event immediately preceding U deposition is described at Eagle Point ([Kotzer and Kyser, 1995; Mercadier, 2008](#)), P-Patch ([Mercadier et al., in prep](#)), Shea Creek ([Lorilleux et al., 2002](#)) and Millennium ([Beshears et al., 2008; Mercadier, 2008](#)). Carbonate veins are associated to late-ore stages at McArthur River ([Derome et al., 2005; Alexandre et al., 2005, 2009a](#)), Eagle Point, P-Patch and Millennium ([Mercadier, 2008](#)); Shea Creek ([Lorilleux et al., 2002](#)). Thus, quartz and carbonate veins are unambiguously genetically associated to the formation of the deposits and are likely to host fluid inclusions that are relicts of fluids responsible for major alteration and mineralization events.

Most of the studied veins were sampled in the basement. For the Rabbit Lake, Eagle Point, and P-Patch deposits, quartz and carbonate veins were all sampled in the basement. Lack of sedimentary cover at Rabbit Lake and Eagle Point precludes sampling of quartz veins in sandstones. At P-Patch, no quartz or carbonate veins are present in the sandstones. For the Shea Creek, and McArthur River deposits four quartz veins were sampled at the base of silicified sandstones (MAC13Qz, MAC8Qz from McArthur River, SHE03externe, IF74 from Shea Creek). For basement-hosted samples, depth below unconformity ranges from 21.6 m (DDH197.2, Rabbit Lake) to 360.7 m (EPE44.4, Eagle Point).

[Figure 2.9](#) shows some typical quartz and carbonate veins studied in this work. The veins cross-cut various lithologies such as gneisses ([Figure 2.9A, 2.9E-F](#)) or pegmatoids ([Figure 2.9C](#)). Veins were sampled in relatively unaltered ([Figure 2.9.A, 2.9E](#)) to fully altered (bleached) lithologies ([Figure 2.9C, 2.9F](#)). Veins are filled by the different possible following assemblages: dravite + quartz ([Figure 2.9.A](#)), quartz + dolomite  $\pm$  bitumen  $\pm$  pyrite ([Figure 2.9B, 2.9F](#)); quartz only ([Figure 2.9C](#)); dolomite  $\pm$  hematite ([Figure 2.9E; 2.9D](#)).

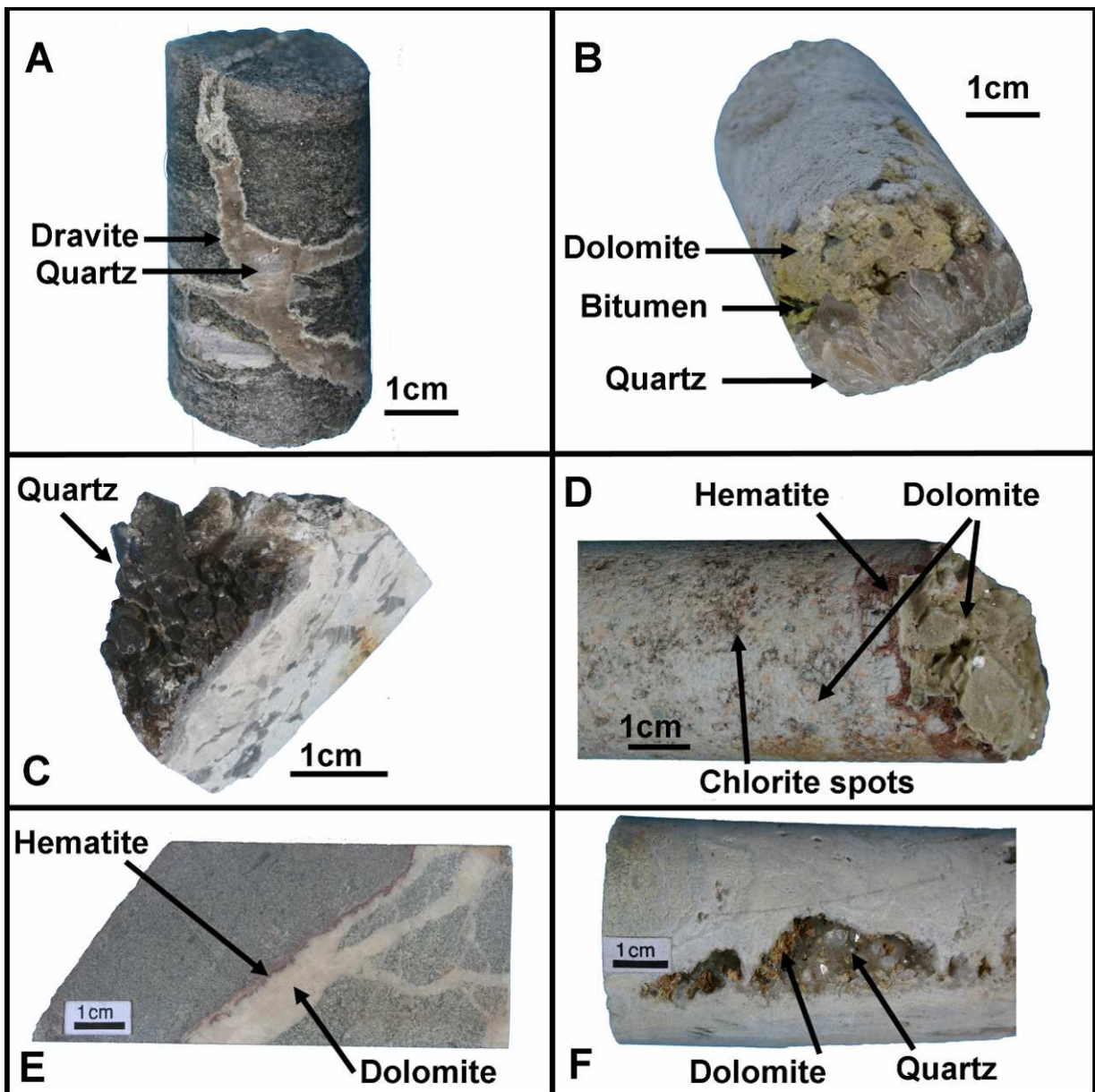


Figure 2.9 : Example of quartz and carbonate veins, hosting fluid inclusions studied in this work. (A) dravite+quartz vein cross-cutting graphite-rich pelitic gneiss (sample H3042-1, Eagle Point). (B) Quartz+dolomite vein, with small bitumen balls and pyrite (not shown) (sample P48-3, P-Patch). (C) Smoky quartz in open fracture cross-cutting illitized pegmatoid (sample P53-6, P-Patch). (D) Massive dolomite intercept, intergrown with hematite and chlorite (sample P63-6, P-Patch). (E) Hematite+dolomite vein in relatively unaltered fine grained gneiss (sample H-1935-8, Eagle Point). (F) Quartz+dolomite in open fracture cross-cutting bleached gneiss (sample CX52-1, Millennium).

## 2.9. Petrography of fluid inclusions

In quartz and carbonate veins, 5 to 25 µm two phase (liquid-vapor) or three phase (liquid-vapour-halite) fluid inclusions were observed ([Figure 2.10](#)). The volumetric fraction of vapour phase is comprised between 5 and 15% with maximum frequency around 10%. Inclusions show alternatively negative crystal, or more irregular shapes. There is little evidence for post-trapping deformation (stretching and necking down), that do not visibly affect liquid/vapour ratio. Fluid inclusions with anomalously high volumetric fraction of vapour phase and showing no apparent post-trapping deformations are contaminated by H<sub>2</sub>, as shown in [Derome et al., \(2005\)](#) ([Figure 2.10F](#)). H<sub>2</sub> is the product of radiolytic processes ([Derome et al., 2003b](#)). H<sub>2</sub>-rich inclusions were discarded for microthermometry.

Fluid inclusions are distributed either along host minerals growths bands (rare), or as clusters of fluid inclusions, or isolated. Supposed occurrences of secondary fluid inclusions planes were discarded for this study. Thus, we considered that all the fluid inclusions presented in this study are primary or pseudosecondary and coeval with the formation of their host minerals.

Fluid inclusions contain randomly distributed solids. Occurrences of hematite and phyllosilicates are frequent. These solids are interpreted as daughter minerals due to their relatively constant volume compared to the fluid inclusions volume. However, accidental trapping of phyllosilicates cannot be ruled out.

Finally, fluid inclusions found in the Rabbit Lake, Eagle Point, Shea Creek, P-Patch and Millennium quartz and dolomite veins share common petrographic features to those described in quartz veins and sandstone silicifications at McArthur River ([Derome et al., 2005](#)).

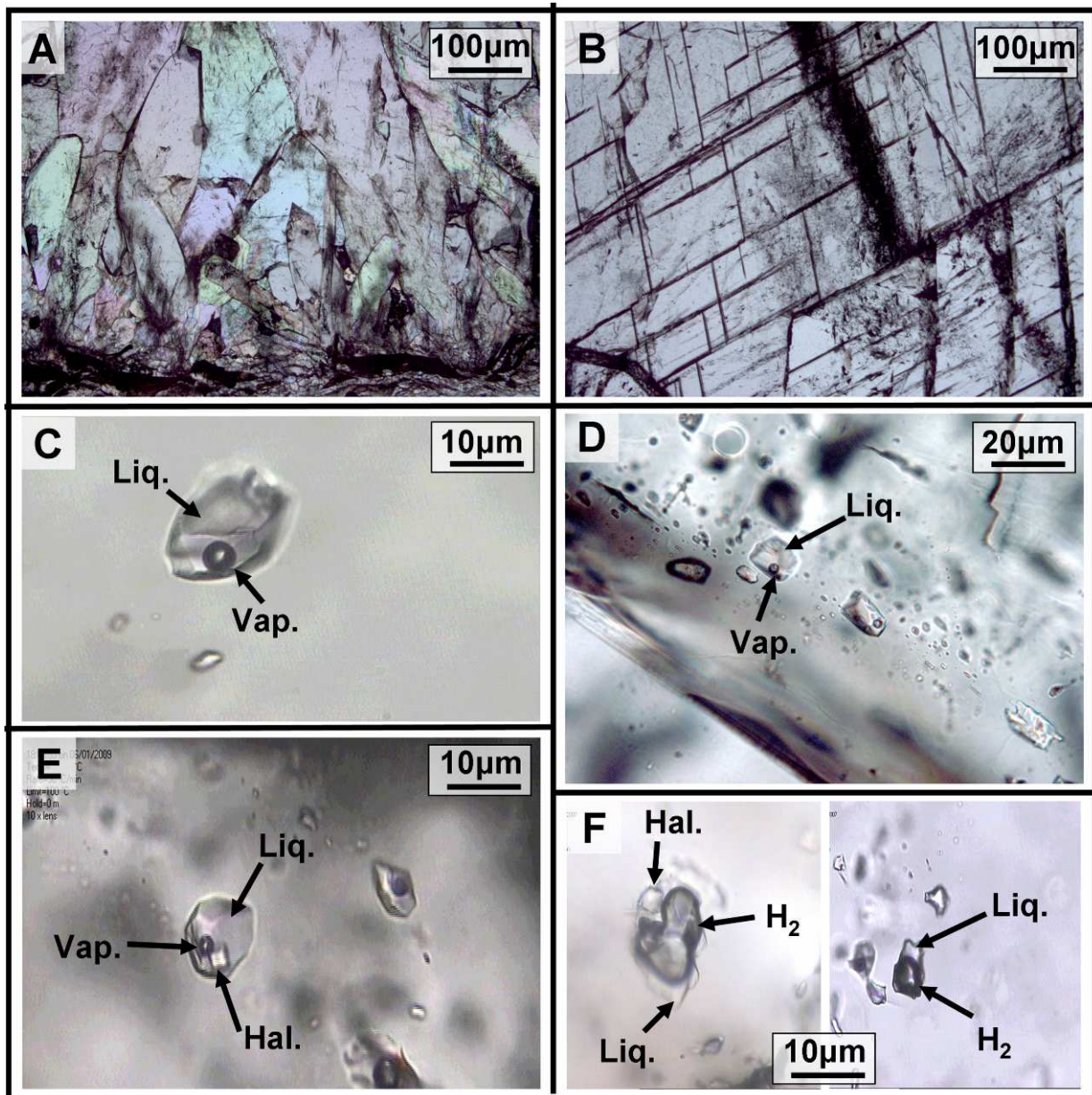


**Figure 2.10 :** Example of fluid inclusions and host minerals studied in this work. *Liq.*: liquid phase. *Vap.*: vapor phase. *Hal.*: halite solid. (A) Druzy quartz (sample RBL2Qz, Rabbit Lake), thick section, transmitted light. (B) Dolomite vein (sample RBL1Carb, Rabbit Lake) thick section, transmitted light. (C) Typical primary liquid-vapor fluid inclusion in quartz. (D) (C) Typical primary liquid-vapor fluid inclusion in dolomite. (F) Typical primary liquid-vapor-halite fluid inclusion in dolomite. (F) Typical fluid inclusions with anomalously large vapor phase, indicating contamination by H<sub>2</sub>.

## Version abrégée

Le Bassin de l'Athabasca, d'âge mésoprotérozoïque, repose sur un socle archéen à paléoprotérozoïque séparé en deux provinces par la Snowbird tectonic zone ([Figure 2.1, 2.2](#)). La plupart des gisements d'uranium de type discordance du Bassin de l'Athabasca sont situés à proximité de la zone de transition entre les domaines de Wollaston et Mudjatik du socle (WMTZ, [Figure 2.2](#)). Un profil régolithique de plusieurs mètres à plusieurs dizaines de mètres de profondeur est développé au toit du socle.

La séquence sédimentaire du Bassin de l'Athabasca s'est déposée entre 1.75 et 1.65 ma. Son épaisseur maximale actuelle est de 1.5 km et a pu atteindre environ 5 km d'après les études d'inclusions fluides. Le remplissage sédimentaire est composé principalement de grès quartzeux marins à fluviatiles à la base, et de silts et de formations carbonatées au sommet ([Figure 2.1](#)).

Le socle et la couverture sédimentaire sont recoupés par des dykes mafiques datés à  $1227 \pm 11$  ma, associés aux essaims de dykes de type « McKenzie ».

Les gisements étudiés sont les suivants : McArthur River, Rabbit Lake, Shea Creek, Eagle Point, P-Patch et Millennium ([Figure 2.2](#)). Les gisements d'Eagle Point, P-Patch et Millennium sont exclusivement encaissés dans le socle, alors que les gisements de McArthur River, Rabbit Lake et Shea Creek présentent des minéralisations dans le socle et à la discordance ([Figures 2.3-2.8](#)).

Plusieurs épisodes successifs de dépôt et/ou remobilisation de l'uranium sont proposés pour ces gisements. Les âges proposés les plus vieux pour le dépôt de l'uranium sont aux alentours de 1500 ma et les plus jeunes, autour de 800 ma.

L'altération autour des gisements est principalement constituée d'un assemblage complexe de minéraux argileux (illite, chlorite, sudoite et dravite).

Des sulfures et arsénures de Ni, As, Cu, Co, Mo et autres métaux sont fréquemment associés aux minéralisations uranifères.

Les veines de quartz et de carbonates sont spatialement et temporellement associées à la formation des gisements, et contiennent des inclusions fluides qui sont les reliques des fluides liés aux épisodes majeurs d'altération et de minéralisation.

La plupart des veines a été échantillonnée dans le socle à des profondeurs sous discordance comprises entre 21.6 et 360.7 m.

Les veines de quartz et carbonates recoupent différentes lithologies (gneiss, pegmatoïdes...) ([Figure 2.9](#)). Les veines ont été échantillonnées dans des zones dans lesquelles l'intensité de l'altération est variable.

Les différents remplissages de veines observés sont les suivants : dravite + quartz ([Figure 2.9.A](#)); quartz + dolomite  $\pm$  bitumes  $\pm$  pyrite ([Figure 2.9B, 2.9F](#)); quartz seul ([Figure 2.9C](#)); dolomite  $\pm$  hématite ([Figure 2.9E; 2.9D](#)).

Des inclusions fluides biphasées (liquide + vapeur) et triphasées (liquide + vapeur + gaz) sont observées dans tous les types de veines ([Figure 2.10](#)). Les inclusions fluides montrent peu de trace de déformation post-piégeage. Les inclusions fluides dont le volume de la phase vapeur est anormalement élevé sont contaminées par l'hydrogène issu de la radiolyse de l'eau. Ces inclusions contaminées n'ont pas été analysées en microthermométrie.

Les inclusions fluides étudiées dans les gisements de Rabbit Lake, Eagle Point, Shea Creek, P-Patch and Millennium ont les mêmes caractéristiques pétrographiques que celles précédemment étudiées dans le gisement de McArthur River, et sont considérées comme primaires, ou pseudo-secondaires, c'est-à-dire contemporaines de la formation des veines.



### **3. Mixing of diagenetic-hydrothermal brines at McArthur River U deposit, Canada: LA-ICP-MS investigation of fluid inclusions**

Antonin Richard<sup>1</sup>, Thomas Pettke<sup>2</sup>, Michel Cathelineau<sup>1</sup>, Marie-Christine Boiron<sup>1</sup>, Julien Mercadier<sup>1</sup>, Michel Cuney<sup>1</sup>, Donatienee Derome<sup>1</sup>

Article in preparation for *Geology*

<sup>1</sup>G2R, Nancy-Université, CNRS, CREGU, Boulevard des Aiguillettes B.P. 239, F-54506,  
Vandoeuvre-lès-Nancy, France

<sup>2</sup>Institute of Geological Sciences, University of Bern, Baltzerstrasse 1+3, CH-3012 Bern,  
Switzerland

#### **Abstract**

Fluid inclusions in close relation to uranium ore from the world class McArthur River unconformity-related U deposit, were analyzed by microthermometry and LA-ICP-MS. Two brines are distinguished: A NaCl-rich brine, which is a Na-Ca-Mg-K-Sr-Ba brine with  $\text{Na} > (\text{Ca} + \text{Mg})$ , and a CaCl<sub>2</sub>-rich brine, which is a Ca-Mg-Na-K-Sr-Ba brine with  $(\text{Ca} + \text{Mg}) > \text{Na}$ . A strong anticorrelation is observed between Na and Ca-Mg-K-Sr-Ba, which suggests mixing of two brine end-members. Despite analytical difficulties, a wide range of U concentrations (<0.2 to 560 ppm) is strongly suspected, which infers that these brines are involved in U leaching of source rocks and U transport. Both brines are thought to share a common basinal origin. The chemical differentiation between the NaCl-rich brine and the CaCl<sub>2</sub>-rich brine is likely to have occurred in the Athabasca Basement during fluid-rock interaction and subsequent U extraction.

### 3.1. Introduction

The McArthur River deposit is one of the largest U deposits in the world (ca. 200.000 t  $\text{U}_3\text{O}_8$  at 25% average), and belongs to the unconformity-related type (Kotzer and Kyser, 1995; Derome et al., 2005). Diagenetic-hydrothermal brines are thought to be involved in the alteration and mineralizing processes that occurs at the interface between the Mesoproterozoic Athabasca Basin and the Archean to Paleoproterozoic basement (Hoeve and Sibbald, 1978). These brines are believed to have circulated at the basement – cover interface and strongly interacted with various lithologies, leading to the formation of large illite-sudoite-dravite alteration haloes around U ores (Wilson and Kyser, 1987; Kotzer and Kyser, 1995; Fayek and Kyser, 1997; Alexandre et al., 2005). The chemical composition of these brines was investigated by Pagel and Jaffrezik, (1977) from atomic absorption, colorimetry and neutron activation techniques, and estimated in the  $\text{H}_2\text{O}-\text{NaCl}-\text{CaCl}_2\pm\text{MgCl}_2$  system by Derome et al., (2005) from microthermometry, Raman spectroscopy and Laser Induced Breakdown Spectroscopy (LIBS). The latter study clearly pointed out the mixing of two NaCl-rich and CaCl<sub>2</sub>-rich brine end-members immediately preceding ore deposition. However, in order to better identify mixing and fluid-rock interaction processes, more detailed characterization of brines chemistry is needed.

Laser Ablation – Inductively Coupled Plasma – Mass Spectrometry (LA-ICP-MS) analysis is presently one of the best techniques for the determination of major and trace element concentrations in individual fluid inclusions (Günther et al., 1998; Heinrich et al., 2003). To add, this technique has permitted to successfully determine the U content of fluid inclusions related to the magmatic-hydrothermal activity of various granitic plutons (e.g. Audétat et al., 2000; Audétat and Pettke, 2003; Zajacz et al., 2008) and showed that the analyzed high temperature - high chlorinity brines are able to carry up to 15 ppm U.

The results of the first LA-ICP-MS analyses of fluid inclusions from the richest U deposit in the world are reported in this paper. The McArthur River U deposit was targeted because a detailed fluid inclusion study by Derome et al., (2005) provides a full description of

the fluid events associated to high grade U mineralization. A wide spectrum of major and trace elements was analyzed in order to establish the detailed chemistry of U mineralizing brines and to better constrain the genesis of unconformity-related U deposits.

### **3.2. Geology and fluid inclusions**

The McArthur River deposit is located in the Eastern part of the Athabasca Basin, Saskatchewan, Canada. U mineralization is mostly basement-hosted, but straddles the unconformity, and is structurally controlled by a major reverse fault. The main alteration minerals comprise coarse grained illite synchronous with massive pitchblende in Mg-chlorite (sudoite) – alkali-deficient Mg-tourmaline (dravite) breccias with minor amounts of pyrite, chalcopyrite, quartz and hematite ([McGill et al., 1993](#); [Kotzer and Kyser, 1995](#); [Derome et al., 2005](#); [Alexandre et al., 2005](#)). U-Pb geochronology on the oldest U oxide generation, has yielded  $1514 \pm 18$  Ma ([Cummings and Krstic, 1992](#)),  $1519 \pm 22$  Ma ([Fayek et al., 2002](#)) and  $1540 \pm 19$  Ma ([Alexandre et al., 2009a](#)) respectively.

Studies of fluid inclusions in quartz cements and euhedral quartz veins in the McArthur River basinal sandstones revealed the presence of a diagenetic 30-35 eq. wt.% NaCl brine which would have circulated at temperatures of about 200°C ([Kotzer and Kyser, 1995](#)). More recently, [Derome et al., \(2005\)](#) have distinguished the following successive generations of authigenic quartz: i) diagenetic quartz overgrowths Qz1 in sandstones, ii) post-diagenetic pervasive silicification Qz2 in sandstones, iii) pre-ore euhedral quartz Qz3 in sandstones, iv) late-ore euhedral quartz Qz4 in sandstones and gneissic and quartzitic basement. These authors identified a NaCl-rich brine (25 wt.% NaCl, up to 14 wt.% CaCl<sub>2</sub>, and up to 1 wt.% MgCl<sub>2</sub>) and a CaCl<sub>2</sub>-rich brine (5-8 wt.% NaCl, 20 wt.% CaCl<sub>2</sub>, and up to 11 wt.% MgCl<sub>2</sub>), and evidenced mixing between the two end-members in Qz3 and Qz4.

According to [Derome et al., \(2005\)](#), the NaCl-rich brine is typically represented by the fluid inclusions showing temperature of hydrohalite melting higher than temperature of final ice melting (Lw2 type). The CaCl<sub>2</sub>-rich brine is best represented by inclusions with

temperature of final ice melting below -30°C or showing failure in freezing even down to -190°C (Lw' type), and inclusions similar to Lw' inclusions showing a halite cube at room temperature (Lwh' type). Their main characteristics are given in [Table 3.1](#). In order to establish the typical detailed compositions of the NaCl-rich and CaCl<sub>2</sub>-rich brines, Lw2, Lw' and Lwh' inclusions in Qz3 and Qz4 were the best candidates for LA-ICP-MS analysis.

	<b>NaCl-rich brine</b>	<b>CaCl<sub>2</sub>-rich brine</b>	
Type	Lw2	Lw'	Lwh'
Te (°C)	-75 to -50	-75 to -60	-75 to -60
Tm ice (°C)	-28.8 to -21	-58.8 to -30	-58 to -36
Tm hyd (°C)	-7 to 21.9	-	-
Ts NaCl	-	-	115 to 235
Th (°C)	71.3 to 196	58 to 148	63 to 175
Cl (molal)	5.5 to 6.5	6	6.5
Na/Ca (mole)	3 to 7.7	0.5	0.8
Ca/Mg (mole)	1 to 17.9	1.5	1.7
wt.% NaCl	22 to 24	5	8
wt.% CaCl <sub>2</sub>	6 to 12	20	19
wt.% MgCl <sub>2</sub>	0 to 0.9	11.5	9.5
T <sub>trapping</sub> (°C)	220 ± 30	110 ± 30	
P <sub>trapping</sub> (bar)	1350 ± 150	700 ± 200	

**Table 3.1 : Characteristics the Lw2, Lw' and Lwh' type fluid inclusions at McArthur River. All data are based on microthermometry, LIBS and Raman spectroscopy from [Derome et al., \(2005\)](#). Te: eutectic melting. Tm ice: final ice melting. Tm hyd: hydrohalite melting. Ts NaCl: halite dissolution. Th: total homogenization. Lw' and Lwh' frequently fail to nucleate any ice upon cooling and only observed Tm ice ranges are reported. Inclusions selected for LA-ICP-MS analyses were attributed to the Lw2, Lw' or Lwh' type, based on microthermometry.**

### 3.3. LA-ICP-MS analysis

Prior to LA-ICP-MS analyses, fluid inclusions were studied by microthermometry, and inclusions representing the Lw2, Lw' or Lwh' microthermometric types as defined by [Derome et al., \(2005\)](#) were carefully selected. The estimated bulk salinities range from 26.9 to 29.2 eq. wt.% NaCl for Lw2 inclusions and from 28 to 35 eq. wt.% NaCl for Lw' and Lwh' inclusions.

45 fluid inclusions were ablated, using a 193 nm ArF excimer laser (Lambda Physik, Germany), and analyzed with an ELAN 6100 DRC ICP-MS (Perkin Elmer, Canada), at ETH

Zürich, Switzerland, at instrument conditions similar to those reported in [Pettke et al., \(2004\)](#).

The procedure for the reconstitution of the fluid inclusions absolute element concentrations is detailed in [Heinrich et al., \(2003\)](#). Briefly,  $^7\text{Li}$ ,  $^{11}\text{B}$ ,  $^{23}\text{Na}$ ,  $^{24}\text{Mg}$ ,  $^{31}\text{P}$ ,  $^{39}\text{K}$ ,  $^{40}\text{Ca}$ ,  $^{55}\text{Mn}$ ,  $^{56}\text{Fe}$ ,  $^{59}\text{Co}$ ,  $^{65}\text{Cu}$ ,  $^{66}\text{Zn}$ ,  $^{85}\text{Rb}$ ,  $^{88}\text{Sr}$ ,  $^{133}\text{Cs}$ ,  $^{137}\text{Ba}$ ,  $^{208}\text{Pb}$ , and  $^{238}\text{U}$  were recorded. After correction for the host quartz signal contribution, resulting fluid element count rates were converted into element concentration ratios using calibrations with SRM610 glass from NIST. Absolute element concentrations were then calculated based on Na as the internal standard using microthermometric equivalent NaCl data corrected for the presence of other major salts (e.g.  $\text{MgCl}_2$ ,  $(\text{Ca}-\text{Mg})\text{Cl}_2$ ). Limits of detection (LODs) were calculated using the  $3\sigma$  criterion ([Longerich et al., 1996](#)).

### 3.4. Na-Ca-Mg-K-Sr-Ba relations

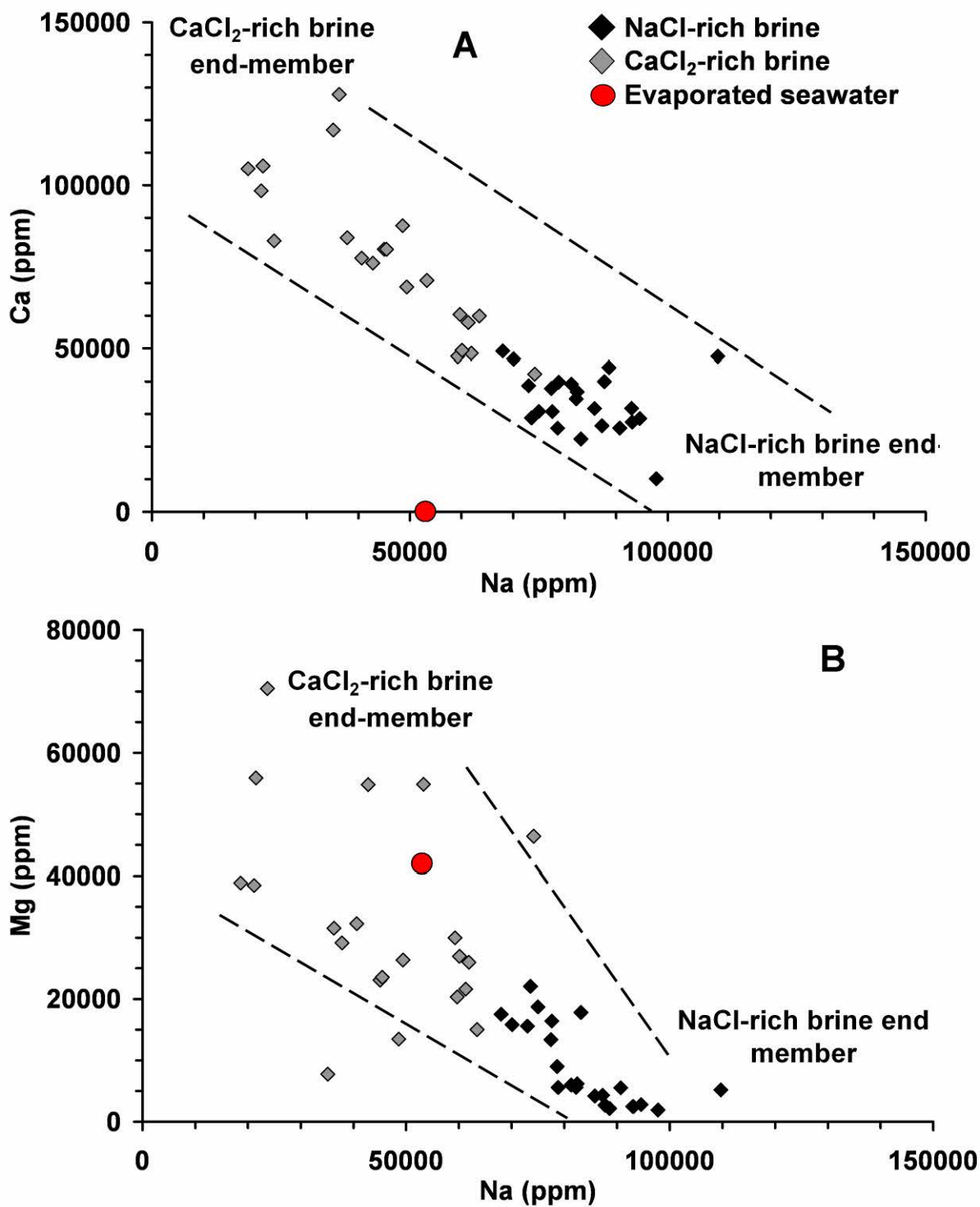
Microthermometric data with corresponding Na-Ca-Mg-K-Sr-Ba compositions of selected well-defined Lw2, Lw' and Lwh' fluid inclusions, are given in [Table 3.2](#). Lw2 inclusions have a Na-dominated composition and Lw' and Lwh' inclusions, although rich in Na, have a Ca-Mg-dominated composition. The compositions of the three fluid inclusion types are efficiently discriminated using the  $(\text{Ca} + \text{Mg} - \text{Na})$  number (concentrations in ppm). This number is consistently negative for Lw2 inclusions and positive for Lw' and Lwh' inclusions. Therefore, Lw2 and Lw'-Lwh' inclusions can reliably be considered as representative of the NaCl-rich brine and  $\text{CaCl}_2$ -rich brine respectively as defined by [Derome et al., \(2005\)](#) and previously inferred from microthermometry.

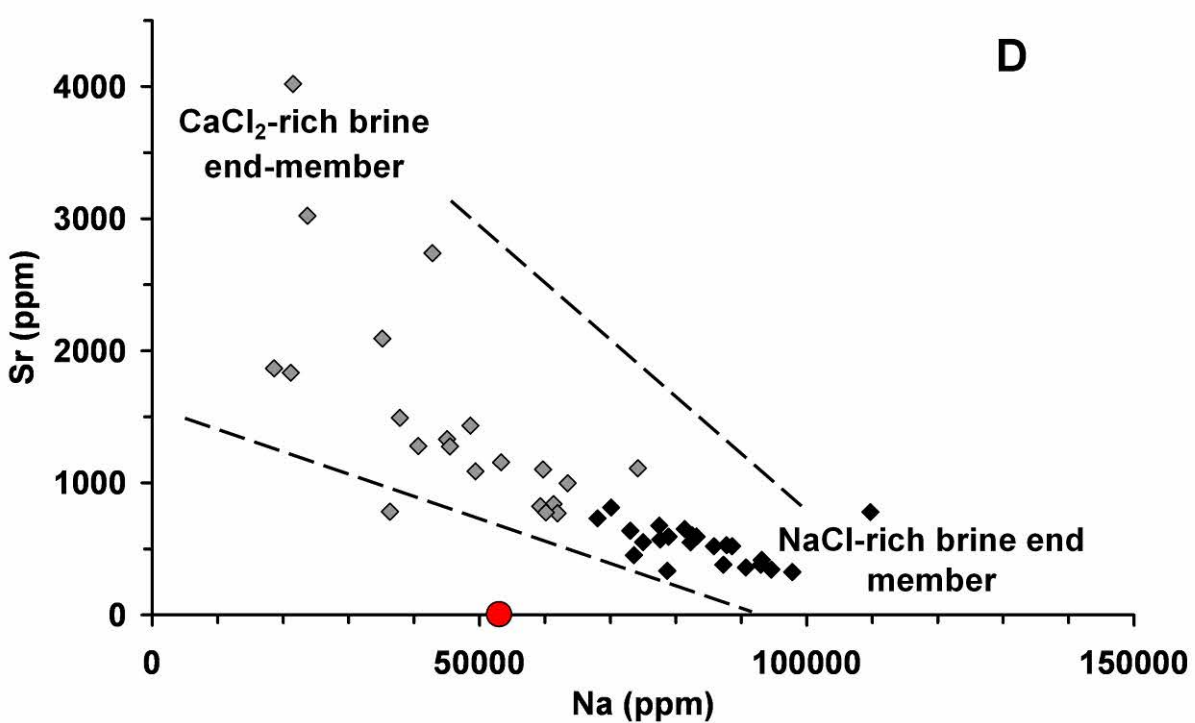
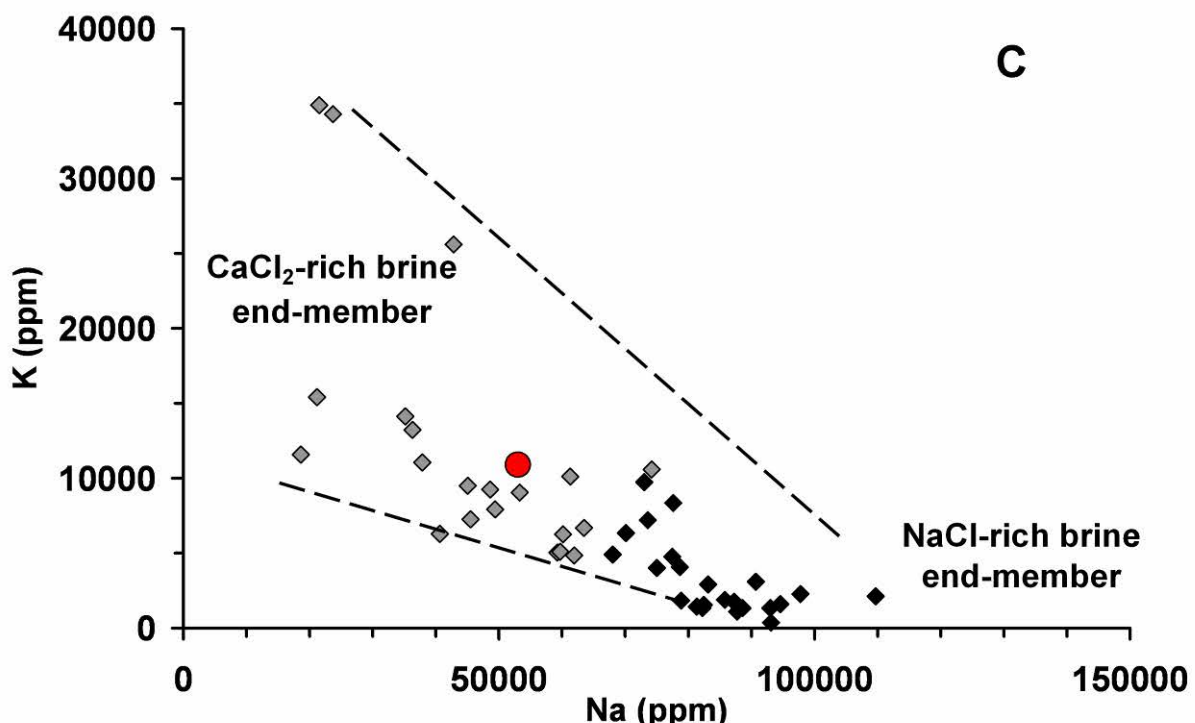
Fluid type type	Size $\mu\text{m}$	F. I. type	$T_e$ (°C)	$T_{\text{m ice}}$ (°C)	$T_{\text{m hyd}}$ (°C)	$T_{\text{s NaCl}}$ (°C)	$T_h$ (°C)	eq. NaCl wt%	Na ppm	Ca ppm	Mg ppm	K ppm	Sr ppm	Ba ppm	Ca+Mg-Na
NaCl-rich brine	45	Lw2	-60	-25.3	4	-	151.5	26.9	87249	26426	4295	1750	381	96	-56529
	23	Lw2	-60	-27.5	6.3	-	127.8	27.2	85800	31700	4190	1880	520	130	-49910
	40	Lw2	-60	-25.4	3.9	-	155.9	26.9	78854	39760	5572	1828	592	141	-33522
	35	Lw2	-60	-27.8	6.8	-	141.7	27.3	75000	30800	18700	4010	550	16	-25500
$\text{CaCl}_2$ -rich brine	14	Lw'	n.f.	n.f.	n.f.	-	77.5	35.0	42800	76100	54800	25600	2740	45	88100
	12	Lw'	n.f.	n.f.	n.f.	-	75	35.0	23691	82962	70468	34300	3022	<84	129740
	-	Lwh'	n.f.	n.f.	n.f.	183	114	28.0	45492	80367	23555	7259	1276	504	58430
	-	Lwh'	n.f.	n.f.	n.f.	135	106.5	28.0	37840	83917	29137	11044	1492	476	75215

**Table 3.2 : Representative microthermometric and LA-ICP-MS analyses of selected fluid inclusions. n.f.: no freezing. F.I.: fluid inclusion. Value preceded by a < symbol stand for limit of detection (LOD).**

Together with Ca and Mg, the  $\text{CaCl}_2$ -rich brine appears to be significantly enriched in K-Sr-Ba, compared to the NaCl-rich brine ([Table 3.2](#), [Figure 3.1](#)). The NaCl-rich brine has a relatively homogeneous Na-Ca-Mg-K-Sr-Ba composition while the  $\text{CaCl}_2$ -rich brine displays a much greater variability. One of the most striking features is the anticorrelation between Na and Ca-Mg-K-Sr-Ba ([Figure 3.1](#)). Low Cl/Br ratios provided by crush-leach analysis in both brines from the McArthur River deposit ([Derome et al., 2005](#)) but also from Australian unconformity-related U deposits ([Derome et al., 2003, 2007](#)) are compatible with surface evaporation of seawater beyond halite saturation as the dominant mechanism for the acquisition of high salinities. By comparison with the chemical composition of a primary halite-saturated evaporitic brine ([Fontes and Matray, 1993](#)), the NaCl-rich brine appears to be enriched Na-Ca-Sr-Ba and depleted in Mg-K, while the  $\text{CaCl}_2$ -rich brine is depleted in Na and enriched in Ca-Sr-Ba. The composition of both brines is thus significantly shifted from that of the primary evaporitic brine ([Figure 3.1](#)).

There is no evidence of alteration process in the basin itself which could account for such compositional changes of the brines. The lack of significant dolomitization or albitization process in sandstones do not favour Na/Ca ratio shifts ([McGill et al., 1993](#)). This is the reason why we suggest that the  $\text{CaCl}_2$ -rich brine results from the interaction between the NaCl-rich brine and Ca-Mg-rich basement lithologies. Significant changes in the Na-Ca-Mg-K-Sr-Ba concentrations from a common parent fluid can result from the alteration processes which affect feldspars and Fe-Mg silicates (biotite, chlorite) and are developed over large volumes of the basement. The contrasted chemical evolution of the two brines through fluid-rock interactions probably attests for distinct pathways in the Athabasca Basin and Basement, as suggested by [Derome et al., \(2005\)](#).





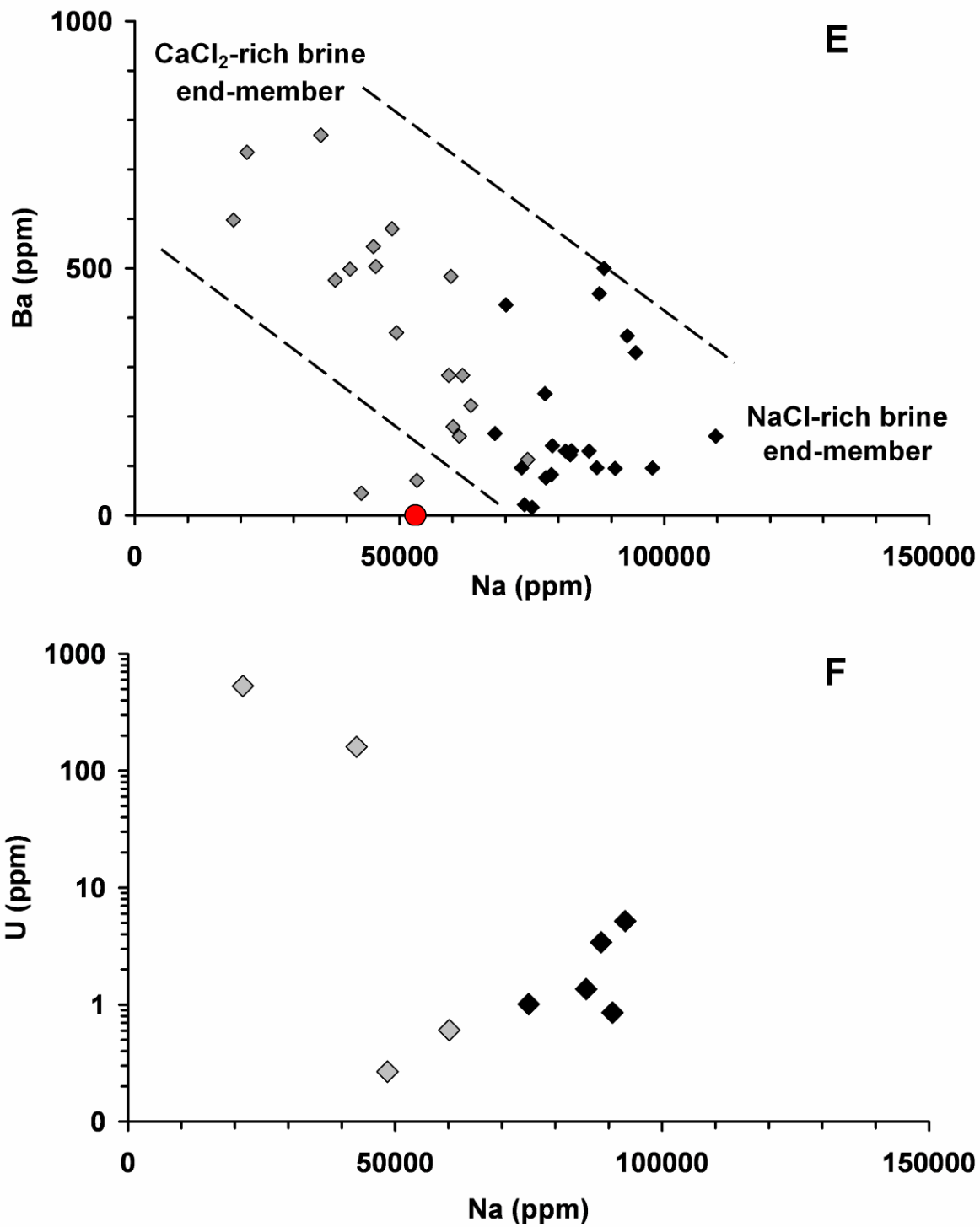


**Figure 3.1 : Na-Ca-Mg-K-Sr-Ba-U relations in analyzed fluid inclusions. Black diamonds stand for NaCl-rich brine inclusions and grey diamonds stand for CaCl<sub>2</sub>-rich brine inclusions. Full circles represent the hypothetical composition of the common parent fluid for the NaCl and CaCl<sub>2</sub>-rich brines (halite-saturated evaporated seawater, data from [Fontes and Matray, 1993](#)). Dashed lines symbolize possible envelopes for mixing trends.**

### 3.5. Minor and trace elements

The determination of U concentration in fluid inclusions was frequently complicated by surface contamination and the presence of U-rich domains in the matrix (up to 1 ppm U in the quartz). Fortunately, 9 inclusions showed reliable U signals with concentrations above LODs ranging from ca. 0.3 to 530 ppm ([Figure 3.1F](#)). Although the two highest U concentrations are measured in  $\text{CaCl}_2$ -rich brine inclusions, it is difficult to assess that one brine is richer than another. However, the fact that some of the fluid inclusions have U concentration above LODs demonstrates that these brines can be exceptionally U-rich, as the highest recorded U concentration determined in basinal brines is of ca. 10 ppb ([Hodge et al., 1996](#)). Matrix contamination has also affected other trace elements such like Cu, B, Li, and P and their concentrations should be considered with caution. There is no clear difference between the Li (100-1500 ppm), B (30-900 ppm), Mn (30-600 ppm), Fe (200-2000 ppm), Rb (5-60 ppm) content of the two brines. P, Co, Cu, Zn, Cs, Pb concentrations can hardly be compared for the two brines due to the few measured concentrations above LODs ([Figure 3.2](#)).

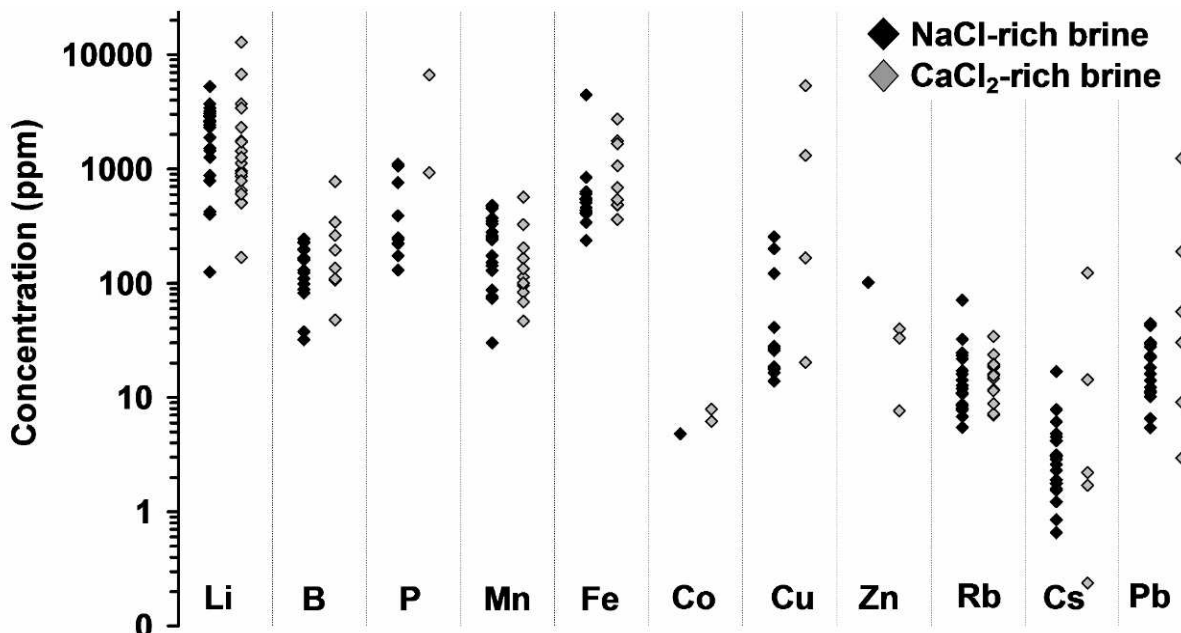


**Figure 3.2 : Range of minor and trace elements compositions for the  $\text{NaCl}$ -rich brine and for the  $\text{CaCl}_2$ -rich brine fluid inclusions.**

### 3.6. Genetic implications

The U source of unconformity-related deposits is still widely debated. [Fayek and Kyser, \(1997\)](#) proposed that U was leached from accessory minerals the basin. Other authors state that basement alteration is one of the key factors for the genesis of such deposits, as basement contains several potential U sources such like magmatic uraninite ([Annesley and Madore, 1999; Madore et al., 2000](#)), pre-Athabasca U mineralizations ([Parslow and Thomas, 1982](#)) and monazites ([Hecht and Cuney, 2000](#)). Our very preliminary results do not permit to reasonably discuss the source of U on the basis of the few measured U concentrations. However, fluid-rock interactions, particularly within basement rocks appear to have largely affected the brines chemistry, especially for the  $\text{CaCl}_2$ -rich brine, which could be consistent with a basement U source.

Brine mixing appears to be coeval with U deposition and was probably favoured by reactivation of Hudsonian basement structures ([Mercadier et al., in press](#)). Again, the mechanism for U mineralization is debated and the exact role of fluid mixing for U deposition has to be compared with that of fluid-rock interactions ([Fayek et al., 1997](#)). Based on isotopic analyses of alteration minerals, [Wilson and Kyser, \(1987a\)](#), [Kotzer and Kyser, \(1995\)](#), [Fayek and Kyser, \(1997\)](#) and [Alexandre et al., \(2009b\)](#) proposed that U deposition occurred during mixing of a basin-derived and a basement-derived fluid. Here, we suggest that the  $\text{NaCl}$ -rich brine and the  $\text{CaCl}_2$ -rich brine could respectively be the basin-derived and basement-derived fluids. However, we support the hypothesis of a common basinal origin for the two brines, which implies that large-scale percolation of basinal brines and equilibration within basement rocks occurred.

## Version abrégée

Les inclusions fluides dans des veines de quartz du gisement de McArthur River ont été analysées par ablation laser couplée à la spectrométrie de masse (LA-ICP-MS). Cette technique permet de reconstituer la composition détaillée des inclusions fluides et a déjà permis de mesurer les concentrations en uranium dans les inclusions fluides liées à l'activité magmatique-hydrothermale d'intrusions granitiques.

45 inclusions ont été analysées pour les éléments suivants :  $^7\text{Li}$ ,  $^{11}\text{B}$ ,  $^{23}\text{Na}$ ,  $^{24}\text{Mg}$ ,  $^{31}\text{P}$ ,  $^{39}\text{K}$ ,  $^{40}\text{Ca}$ ,  $^{55}\text{Mn}$ ,  $^{56}\text{Fe}$ ,  $^{59}\text{Co}$ ,  $^{65}\text{Cu}$ ,  $^{66}\text{Zn}$ ,  $^{85}\text{Rb}$ ,  $^{88}\text{Sr}$ ,  $^{133}\text{Cs}$ ,  $^{137}\text{Ba}$ ,  $^{208}\text{Pb}$ , et  $^{238}\text{U}$ .

Les inclusions de type Lw2 (représentatives de la saumure sodique) ont une composition dominée par le Na (Na > Ca + Mg), alors que les inclusions de type Lw' et Lwh' (représentatives de la saumure calcique) ont une composition dominée par Ca et Mg (Ca + Mg > Na). Les données microthermométriques et LA-ICP-MS sont donc cohérentes ([Tables 3.1, 3.2](#)).

La saumure sodique présente des concentrations en Na, Ca, Mg, K, Sr, Ba relativement homogènes, alors que la saumure calcique présente une variabilité plus importante.

On note une anticorrélation entre les concentrations en Na et les concentrations en Ca, Mg, K, Sr, et Ba ([Figure 3.1](#)). Cette anticorrélation est interprétée en termes de mélange entre un pôle riche en Na (saumure sodique) et un pôle riche en Ca, Mg, K, Sr, Ba (saumure calcique).

La détermination des concentrations en U des inclusions fluides est compliquée par des problèmes de contamination de surface et par la présence de domaines de quartz riches en U (jusqu'à 1 ppm). Neuf inclusions, cinq sodiques et quatre calciques, montrent un signal de l'U exploitable et des concentrations comprises entre 0.3 et 530 ppm ([Figure 3.1F](#)). Ces résultats ne permettent pas d'identifier clairement des différences de concentrations en U dans les deux saumures. Les concentrations en Li (100-1500 ppm), B (30-900 ppm), Mn (30-

600 ppm), Fe (200-2000 ppm), Rb (5-60 ppm) semblent comparables pour les deux saumures. Les concentrations en P, Co, Cu, Zn, Cs, Pb sont très hétérogènes et ne permettent pas une comparaison pertinente de part le nombre limité de données ([Figure 3.2](#)).

Les deux saumures sont donc porteuses d'uranium. La différenciation chimique entre les deux saumures s'est probablement produite dans le socle. Le mélange des deux saumures a lieu pendant la minéralisation en uranium.



## **4. Large scale percolation and mixing of basinal brines in the Athabasca Basement, Canada: PTX conditions from fluid inclusions**

Antonin Richard<sup>1</sup>, Michel Cathelineau<sup>1</sup>, Marie-Christine Boiron<sup>1</sup>, David A. Banks<sup>2</sup>, Michel Cuney<sup>1</sup>, Julien Mercadier<sup>1</sup>, Donatienee Derome<sup>1</sup>

Article in preparation for *Chemical Geology*

<sup>1</sup>G2R, Nancy-Université, CNRS, CREGU, Boulevard des Aiguillettes B.P. 239, F-54506,  
Vandoeuvre-lès-Nancy, France

<sup>2</sup>School of Earth and Environment, University of Leeds, Woodhouse Lane, Leeds, LS2 9JT,  
UK

### **Abstract**

The Mesoproterozoic Athabasca Basin, Canada, hosts numerous giant unconformity-related uranium deposits. These deposits are important witnesses of circulations of diagenetic fluids at the basement-cover interface. The scope of this study is to establish the PTX conditions of diagenetic fluids that have circulated at the base of the Athabasca Basin and in its crystalline basement, and which were responsible for U leaching, transport and deposition. Fluid inclusions in quartz and carbonate veins, closely linked to alteration of the Athabasca Basement and U mineralization were studied by microthermometry and LA-ICP-MS. In all studied deposits, a NaCl-rich and a CaCl<sub>2</sub>-rich brine are described. The CaCl<sub>2</sub>-rich brine is enriched in Ca-Mg-K and depleted in Na compared to the NaCl-rich brine. Both brines carry up to hundreds of ppm of Cu, Pb, Zn and U. These brines show evidence of isothermal mixing at 150 ± 30°C with pressure having fluctuated between lithostatic (800 to 1500 bars) and hydrostatic (300 to 500 bars) conditions. Mixing process appears to be

coeval with the formation of uranium deposits, and  $150 \pm 30^\circ\text{C}$  is thought to be the range of temperatures that have prevailed during the formation of U deposits. Basin-hosted and basement-hosted deposits have formed under similar P-T conditions in the presence of both brines. The basal sandstones as well as the top of the basement have formed a single giant aquifer, which has favoured percolation and mixing of basinal brines in the crystalline basement, a critical factor for the formation of giant unconformity-related uranium deposits.

#### 4.1. Introduction

Percolation of diagenetic brines in crystalline basements is thought to have occurred in numerous settings (e.g. Munz et al., 1995; Davisson and Criss, 1996; Boiron et al., 2002; Oliver et al., 2006). This phenomenon is frequently accompanied by metal extraction by sedimentary brines in the basement, sometimes leading to ore deposition (Gleeson et al., 2001; Feltrin et al., 2003; Essaraj et al., 2005; Kendrick et al., 2005; Muchez et al., 2005; McGowan et al., 2006; Piqué et al., 2008).

Here, we examine the case of the Mesoproterozoic Athabasca Basin, Saskatchewan, Canada and its underlying Archean to Paleoproterozoic basement. The Athabasca Basin and Basement host numerous unconformity-related uranium deposits that are indicators of extensive fluid circulation at the basement-cover interface.

The most commonly accepted models for the formation of unconformity-related uranium deposits, involve the interaction between an oxidizing diagenetic brine and a basement-derived reducing fluid or reduced basement lithologies (Pagel and Jaffrezic, 1977; Hoeve and Sibbald, 1978; Pagel et al., 1980; Hoeve and Quirt, 1984; Wilson and Kyser, 1987a; Kotzer and Kyser, 1995; Komninou and Sverjensky, 1996; Fayek and Kyser, 1997; Derome et al., 2005). Uranium is thought to be leached by the oxidizing diagenetic brine from accessory minerals either in the basin (Fayek and Kyser, 1997, Kyser et al., 2000) or in the basement (Pagel et al., 1980; Annesley and Madore, 1999; Hecht and Cuney, 2000; Madore et al., 2000).

Numerous fluid inclusion studies have been performed in the vicinity of unconformity-related uranium deposits during the last thirty years in the Athabasca Basin ([Table 4.1](#)). The only well-constraint deposit from the fluid inclusion point of view (PTX conditions) is the McArthur River deposit ([Pagel and Ahamdach, 1995](#); [Kotzer and Kyser, 1995](#); [Derome et al., 2005](#); [Part 3](#)). [Derome et al., \(2005\)](#) showed that a NaCl-rich brine has circulated at P-T conditions of  $220 \pm 30^\circ\text{C}$  and  $1350 \pm 150$  bars, and a CaCl<sub>2</sub>-rich brine has circulated at P-T conditions of  $110 \pm 30^\circ\text{C}$  and  $700 \pm 200$  bars. Mixing between the two brines occurred during the pre-ore stage at  $700 \pm 200$  bars after a pressure decrease from lithostatic to near hydrostatic conditions. Compositions of individual NaCl-rich and CaCl<sub>2</sub>-rich brine fluid inclusions in the H<sub>2</sub>O-NaCl-CaCl<sub>2</sub>-MgCl<sub>2</sub> system have been obtained in individual fluid inclusions using microthermometry, Raman spectroscopy and Laser Induced Breakdown Spectroscopy (LIBS) ([Derome et al., 2005](#)). More detailed Na-Ca-Mg-K-Sr-Ba compositions were obtained from LA-ICP-MS analyses, showing mixing trends between the NaCl-rich brine and the CaCl<sub>2</sub>-rich brine end-members at McArthur River ([Part 3](#)). These studies provided crucial information on diagenetic brines that appear to have evolved from a Na-dominated to a Ca-dominated composition during progressive interaction with basement lithologies.

In order to establish what characteristics of the McArthur River deposits could be or not generalized to the entire Athabasca Basin, a systematic microthermometric study of five deposits (Rabbit Lake, Shea Creek, Eagle Point, P-Patch and Millennium) was carried out as well as LA-ICP-MS analysis of fluid inclusions in selected samples.

Locality	Reference	Sample	Sandstones	Basement	Fluid inclusion types			
					Lw1	Lw2	Lwh	Lwh'
McArthur River	Derome et al., (2005)	Quartz overgrowths Qz1	X		X			
		Pervasive silification Qz2	X		X	X	X	X
		Quartz veins Qz3	X		X	X	X	X
P-Patch	Mercadier et al., (in press)	Drusy Quartz veins Qz4	X		X	X	X	X
		Primary quartz		X	X	X	X	X
					Reinterpreted data			
McArthur River	Kotzer & Kyser (1995)	Pre-Quartz overgrowths	X		X			
		Quartz veins (Q2)	X		X?		X	X
		Late-ore siderite	X					
Rabbit Lake	Pagel & Ahamndach (1985)	Quartz overgrowths	X		X?		X?	X?
		Quartz veins	X		X		X	X
					X?		X?	X?
Shea Creek	Freiburger et al., (2003)	Quartz veins						
		Dolomite veins						
		Calcite veins						
Midwest	Lawer & Crawford (1982)	Primary quartz	X		X?		X?	X?
		???		X				
					X?		X?	X?
Eagle Point	Kotzer & Kyser (1995)	Quartz veins (Q2)	X		X?		X	X?
		Pre-Quartz overgrowths	X		X?	X	X	X?
		Quartz overgrowths	X		X			
Cluff Lake	Pagel (1975)	Quartz veins	X		X			
		Calcite veins	X					
Sue C - McClean	Pagel & Ahamndach (1995)	Quartz veins	X		X?		X	X?
		Quartz veins	X		X?	X	X	X?
					X?		X?	X?
Rumple Lake	Pagel (1975)	Pre-Quartz overgrowths	X		X?		X	X?
		Quartz veins	X		X			
Millennium	Beshears et al., (2008)	Quartz veins	X		X			X
		Quartz overgrowths	X		X?		X	X?
					X?		X?	X?
Key Lake	Poty & Pagel (1988)	Quartz overgrowths	X					

Table 4.1 : Reinterpretation of literature data on the basis of recent fluid inclusion studies (Derome et al., 2005; Mercadier et al., in press) of unconformity-related uranium deposits from the Athabasca Basin. Other authors did not distinguish NaCl-rich brine from CaCl<sub>2</sub>-rich brine inclusions. Reinterpreted data show that both brines are probably present in a majority of previously studied deposits.

## 4.2. Analytical methods

### 4.2.1. Microthermometry

Microthermometry was performed on fluid inclusions using a <sup>®</sup>Linkam MDS600 heating-cooling stage adapted to an <sup>®</sup>Olympus optical microscope. The observed temperatures of phase changes are the following: eutectic melting (Te), ice melting (Tm ice), hydrohalite melting (Tm hyd), halite dissolution (Ts NaCl), and total homogenization (Th). According to the calibration curves, temperatures of phase changes are given with an accuracy of about  $\pm 5^\circ\text{C}$  for Te,  $\pm 0.1^\circ\text{C}$  for Tm ice and Tm hyd, and  $\pm 1^\circ\text{C}$  for Ts NaCl and Th.

Fluid inclusions do not contain any gas phase detectable by microthermometry, and only traces of low-density CH<sub>4</sub>, CO<sub>2</sub>, C<sub>2</sub>H<sub>6</sub>, H<sub>2</sub> and O<sub>2</sub> were detected from Raman spectroscopy at McArthur River ([Derome et al., 2003b](#)). For this study, all fluid inclusions are considered as purely aqueous fluids.

Aqueous fluid inclusions, with typical volumetric fraction of vapour phase of 10% were classified using the nomenclature of [Derome et al., \(2005\)](#) based on low temperature microthermometric behaviours. Inclusions showing a halite cube at room temperature are noted Lwh' or Lwh according to the nature of their last phase to melt (ice or hydrohalite respectively). Inclusions with no halite cube whose last phase to melt is hydrohalite are noted Lw2. Inclusions without halite cube whose last phase to melt is ice are noted Lw' ( $-45^\circ\text{C} < \text{Tm ice} < -30^\circ\text{C}$ ), Lw1 ( $-30^\circ\text{C} < \text{Tm ice} < -15^\circ\text{C}$ ) or Lw " ( $-15^\circ\text{C} < \text{Tm ice} < -1^\circ\text{C}$ ).

The bulk composition of aqueous inclusions was reconstructed in the H<sub>2</sub>O-NaCl-CaCl<sub>2</sub> or H<sub>2</sub>O-NaCl<sub>2</sub> or H<sub>2</sub>O-CaCl<sub>2</sub> systems using the AqSo2e program (Package *FLUIDS* 1, [Bakker et al., 2003](#)) based on purely empirical best-fits from [Naden \(1996\)](#) on experimental data ([Vanko et al., 1988; Oakes et al., 1990](#)). Isochores were calculated using BULK and ISOC programs ([Bakker et al., 2003](#)) based on the [Zhang and Frantz \(1987\)](#) equation of state for aqueous fluid inclusions.

#### 4.2.2. LA-ICP-MS analysis

LA-ICP-MS analysis of fluid inclusions was carried out at the School of Earth and Environment, University of Leeds for selected Rabbit Lake, Eagle Point, P-Patch and Millennium deposits samples at experimental conditions described in [Allan et al., \(2005\)](#).

Individual quartz-hosted fluid inclusions were ablated with a 193 nm Geolas Q Plus excimer laser (ArF, 193 nm, Microlas, Göttingen, Germany). Ablation occurred in an He atmosphere and the ablated material was transported by a 0.68-ml/min He flow to a mixing device where 1-l/min Ar was added. Ablated samples were subsequently analyzed in an Agilent 7500c Quadrupole ICP-MS equipped with an Octopole Reaction System. The analyses were run with the reaction cell pressurized with 2.5 ml/min H<sub>2</sub> in order to eliminate <sup>40</sup>Ar<sup>+</sup> and <sup>40</sup>Ar<sup>16</sup>O<sup>+</sup> interferences on <sup>40</sup>Ca<sup>+</sup> and <sup>56</sup>Fe<sup>+</sup> and to reduce the high Ar-based backgrounds on <sup>39</sup>K<sup>+</sup>. The recoded elements were <sup>7</sup>Li, <sup>23</sup>Na, <sup>24</sup>Mg, <sup>39</sup>K, <sup>40</sup>Ca, <sup>55</sup>Mn, <sup>56</sup>Fe, <sup>63</sup>Cu, <sup>66</sup>Zn, <sup>88</sup>Sr, <sup>137</sup>Ba, <sup>208</sup>Pb and <sup>238</sup>U. In all cases, <sup>23</sup>Na was used as internal reference standard. Limits of detection (LOD) of the other elements were calculated using the 3σ criterion ([Longerich et al., 1996](#)). Calibration, and signal integration were performed with the Matlab®-based SILLS program ([Guillong et al., 2008](#)). Absolute element concentrations can be calculated from analyzed ratios to Na if this concentration is known. Na concentration can be obtained from the salinity estimated from microthermometry (in wt % NaCl equiv) using the charge-balance relationship ([Allan et al., 2005](#)). This method corrects the modelled amount of Na (from the wt % NaCl equiv) for contributions of other chloride salts using the analyzed element ratios to Na. Based on microthermometric measurements, a chlorinity of 6.5 molal was attributed to all inclusions which should over or underestimate absolute concentrations by a maximum of 30% relative, but more generally around 10%.

To minimize problems of surface contamination and the presence of U-rich quartz domains, as noted [Part 3](#), quartz veins from barren samples were selected. Note that the fluid inclusion content of quartz veins from barren samples is comparable to that of mineralized samples ([Derome et al., 2005](#)). Fluid inclusions assemblages containing both

NaCl-rich and CaCl<sub>2</sub>-rich brine inclusions were selected. Fluid inclusions devoid of any visible solids (except halite) were ablated. No petrographic criteria allow the discrimination of NaCl-rich and CaCl<sub>2</sub>-rich brine inclusions. Thus, the NaCl-rich brine and the CaCl<sub>2</sub>-rich brine inclusions were discriminated from the LA-ICP-MS results using the (Ca+Mg)-(Na) number (concentrations in ppm). This number is negative for NaCl-rich brine inclusions and positive for CaCl<sub>2</sub>-rich brine inclusions as shown for the McArthur River deposit ([Part 3](#)).

## 4.3. Results

### 4.3.1. Microthermometry results

#### 4.3.1.1. *Te - Tm ice pairs*

Temperatures of eutectic melting (Te) – temperatures of ice melting (Tm ice) pairs are plotted in [Figure 4.1](#) for all studied deposit. For Lw" inclusions, Te range from ca. -20°C to ca. -60°C with Tm ice being above -15°C. This could be interpreted as variability of Lw" inclusions composition from NaCl-H<sub>2</sub>O system (eutectic temperature: -21.2°C) towards Na Cl-CaCl<sub>2</sub>-MgCl<sub>2</sub>-H<sub>2</sub>O system (eutectic temperature: -57°C).

For Lw1, Lw2 and Lwh inclusions, Te range from ca. -40°C to ca. -75°C and are centred around -65°C. For Lw' and Lwh' inclusions, Te range from ca. -50°C to ca. -75°C and are centred around -70°C. Te can be interpreted as reflecting complex salt systems. Te well below -21.2°C coupled with Tm ice below -23.2°C exclude the possibility of purely NaCl-H<sub>2</sub>O compositions. For similar reasons, NaCl-KCl-H<sub>2</sub>O and NaCl-MgCl-H<sub>2</sub>O compositions are also ruled out (eutectic temperature: -22.9°C and -35°C respectively). Te of ca -52°C or -57°C would indicate NaCl-CaCl<sub>2</sub>-H<sub>2</sub>O system or NaCl-CaCl<sub>2</sub>-MgCl<sub>2</sub>-H<sub>2</sub>O system respectively. A majority of measured Te are below -60°C for all fluid inclusion types except Lw". Metastable eutectic melting is frequent in NaCl-CaCl<sub>2</sub>-MgCl<sub>2</sub>-KCl-H<sub>2</sub>O systems ([Davis et al., 1990](#)), and the presence in solution of significant amounts of Li, Fe, Sr may lower the stable eutectic

melting temperature. Unusually low Te could thus reflect either metastable eutectic melting in NaCl-CaCl<sub>2</sub>-MgCl<sub>2</sub>-KCl-H<sub>2</sub>O systems or stable eutectic melting in presence of additional salts. Differences in Te modes between Lw1, Lw2, Lwh and Lw', Lwh' inclusions may therefore result from partial-to-complete replacement of monovalent cations Na<sup>+</sup> and K<sup>+</sup> by divalent cations Ca<sup>2+</sup> and Mg<sup>2+</sup>, which is compatible with evolution from Tm ice between -20°C and -30°C to Tm ice below -30°C and with evolution from NaCl-rich brine composition to CaCl<sub>2</sub>-rich brine composition. Finally, the composition of fluid inclusions was calculated in the NaCl-CaCl<sub>2</sub>-H<sub>2</sub>O system, as commonly applied to diagenetic fluids (Goldstein and Reynolds, 1994).

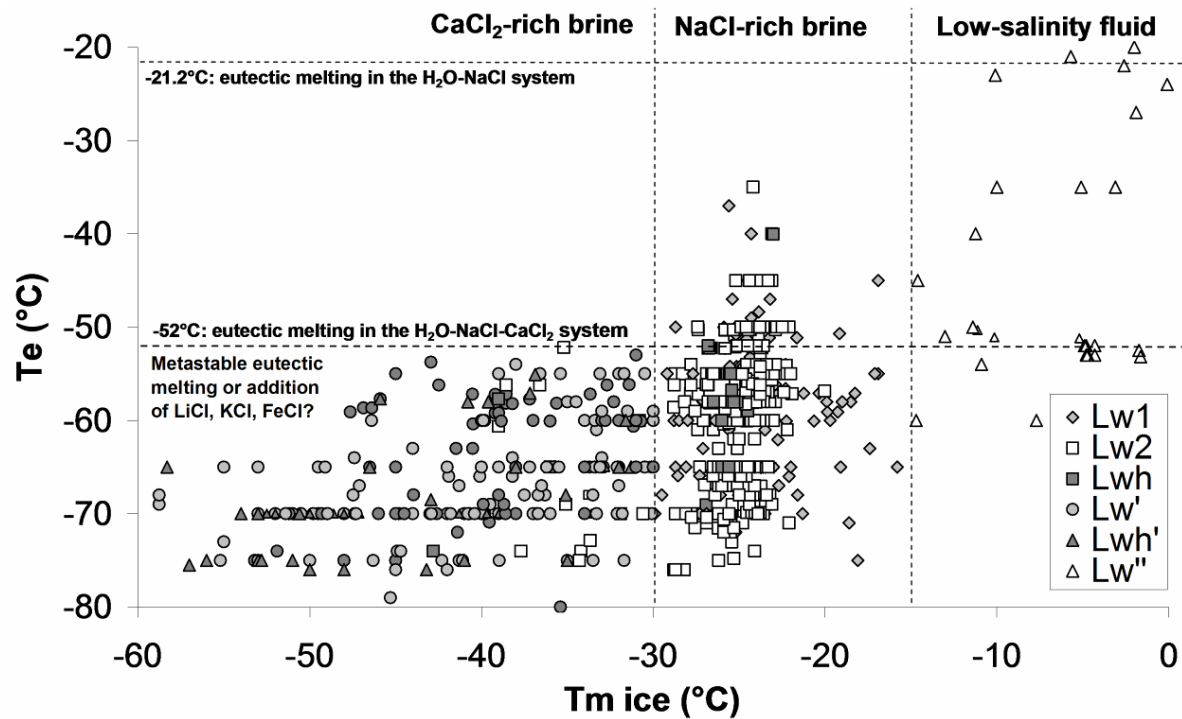


**Figure 4.1 : Te vs. Tm ice diagram for studied fluid inclusions.** Temperatures of phase changes: Te: eutectic melting, Tm ice: ice melting. Te indicate that low-salinity fluid is a nearly pure H<sub>2</sub>O-NaCl or H<sub>2</sub>O-NaCl-CaCl<sub>2</sub> fluid, while NaCl-rich and CaCl<sub>2</sub>-rich brines are either pure H<sub>2</sub>O-NaCl-CaCl<sub>2</sub> fluids or more complex fluids with additional salts.

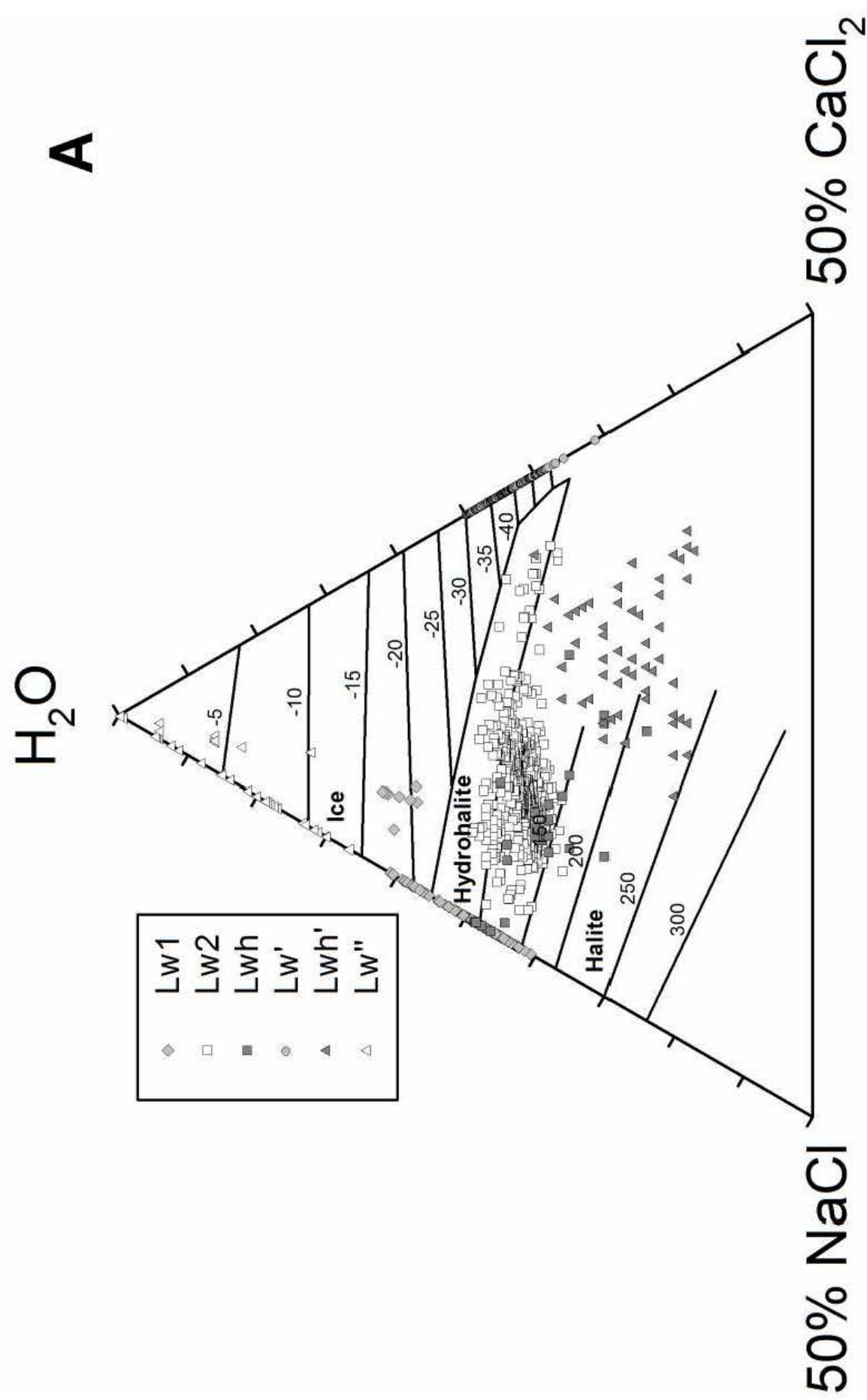
#### 4.3.1.2. NaCl-rich brine inclusions

Lw1 inclusions have Tm ice ranging from ca. -30°C to ca. -15°C with maximum observed values around -25°C ([Table 4.2](#)). Interpretation of microthermometric data for Lw1 inclusions in terms of composition is difficult. Lw1 inclusions could not represent a H<sub>2</sub>O-NaCl brine because of the low Te (predominantly below -52°C) indicating rather more complex chemistry. Alternatively, Lw1 inclusions could be the equivalent of Lw2 inclusions, but failure of hydrohalite nucleation during cooling or difficulties in observing hydrohalite in small fluid inclusions could preclude any Tm hyd measurement. The maximum observed values for Tm ice is centred around -25°C for Lw1 and Lw2 inclusions, coupled with comparable Th distributions, are in favour of this hypothesis. If Lw1 inclusions belong to the H<sub>2</sub>O-NaCl-CaCl<sub>2</sub> system, which is highly probable due to the low Te, hydrohalite melting occurs theoretically before ice melting. This could result in a wide range of Na/Ca ratios and we can not exclude that some of the Lw1 inclusions have a Ca-dominated composition. In practice the observation of hydrohalite melting before ice melting is complicated by the difficulty in distinguishing ice from hydrohalite when the two phases are mixed. Attempts of sequential freezing to coarsen hydrohalite to observable sizes before ice melting were unsuccessful ([Haynes et al., 1985](#)) which could indicate that Lw1 inclusions are metastable Lw2 inclusions that fail to nucleate any hydrohalite during cooling. Thus, according to the latter observations and to the previously established Na-dominated compositions by LIBS ([Derome et al., 2005](#)), Lw1 inclusions were attributed to the NaCl-rich brine, and composition of Lw1 inclusions were calculated in the NaCl-H<sub>2</sub>O system ([Figure 4.2](#)).

In Lw2 inclusions, hydrohalite is the last phase to melt. Tm ice is centred around -25°C and Tm hyd range from -21°C to +21°C ([Table 4.2](#)). In the system H<sub>2</sub>O-NaCl-CaCl<sub>2</sub> hydrohalite melting is limited to the -21.0 to -0.1°C range, and compositions lie into the hydrohalite field ([Figure 4.2](#)). Here, positive Tm hyd indicate either stable hydrohalite melting temperature in a complex solution, or metastable hydrohalite melting ([Zwart and Touret, 1994](#)), although repeated measurements showed that Tm hyd are quite reproducible.

Therefore, we consider that positive Tm hyd are the consequence of complex chemistry of the solutions. Composition of Lw2 inclusions were interpreted in the H<sub>2</sub>O-NaCl-CaCl<sub>2</sub> system using the AqSo2 program ([Bakker, 2003](#)). The poor definition of hydrohalite isotherms as well as difficulties in calculating composition for fluid inclusions with positive Tm hyd may have introduced little errors in the composition of Lw2 inclusions. This can be seen from [Figure 4.2A](#) where a majority of Lw2 inclusions lie out of the hydrohalite field, when it should be only the case for inclusions with positive Tm hyd. If negligible error was introduced on Na/Ca ratios that are mainly controlled by Tm ice, bulk salinity was probably overestimated from a maximum of ca. ± 5% and chlorinity by a maximum of ca. ± 0.5 molal. Although a wide range of molar Na/Ca ratios were calculated in Lw2 inclusions, most values are centred on 3 to 4. Calculated Cl content of Lw2 inclusions is generally close to 6 to 7 molal. A vast majority of Lw2 inclusions lie into the NaCl-rich brine field, as defined by [Derome et al., \(2005\)](#), but some of them with Tm ice below -30°C lie into the CaCl<sub>2</sub>-rich brine field. Nevertheless, these inclusions are very few compared to NaCl-rich Lw2 inclusions and we consider Lw2 inclusions as typical of the NaCl-rich brine ([Figure 4.2](#)).

Lwh inclusions have a halite cube at room temperature. Hydrohalite is generally the last phase to melt. When ice is the last phase to melt, Tm ice is above < -30°C. Calculation of composition in the H<sub>2</sub>O-NaCl-CaCl<sub>2</sub> system is based on coupled Tm hyd - Ts NaCl pairs (AqSo2 program, [Bakker, 2003](#)), or Tm ice - Ts NaCl pairs when ice is the last phase to melt ([Vanko et al., 1988](#)) ([Table 4.2](#)). As for Lw2 inclusions, Lwh inclusion have calculated Na/Ca ratios close to 5, but with slightly higher Cl content between 7 and 8 molal. Composition of Lwh inclusions predominantly fall into the NaCl-rich field and Lwh inclusions were thus attributed to the NaCl-rich brine ([Figure 4.2](#)).



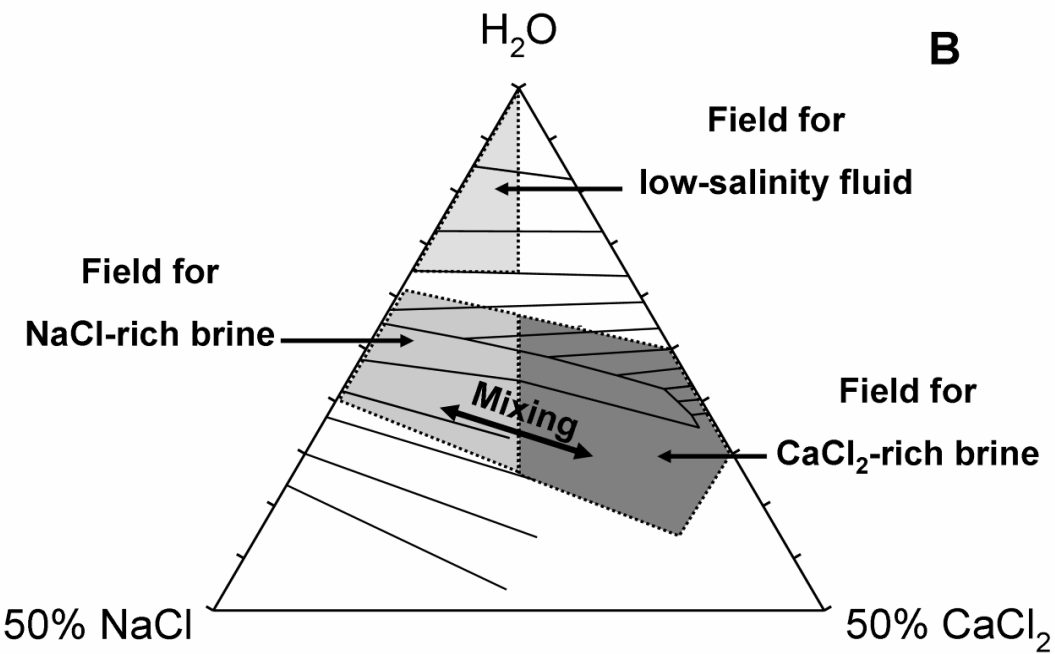


**Figure 4.2:**  $\text{H}_2\text{O}-\text{NaCl}-\text{CaCl}_2$  diagrams for studied fluid inclusions from microthermometry. (A) Data for the studied fluid inclusions. Data for McArthur River deposit are also plotted ([Derome et al., 2005](#)). (B) Interpretation of fluid inclusion data in terms of mixing between a  $\text{NaCl}$ -rich brine and a  $\text{CaCl}_2$ -rich brine. Low-salinity fluid does not show clear evidence for mixing with brines.

#### 4.3.1.3. $\text{CaCl}_2$ -rich brine inclusions

For a majority of  $\text{Lw}'$  inclusions ice melting is frequently not observed as fluid inclusions can fail to nucleate any ice during cooling even down to  $-190^\circ\text{C}$ . When ice melting was observed,  $\text{Tm}$  ice range from  $-55$  to  $-30^\circ\text{C}$ . These low  $\text{Tm}$  ice indicate a Ca-rich composition ([Table 2](#)). As for  $\text{Lw}1$  inclusions, if  $\text{Lw}'$  inclusions belong to the  $\text{H}_2\text{O}-\text{NaCl}-\text{CaCl}_2$  system, which is highly probable due to the observed low  $\text{Te}$ , hydrohalite melting occurs theoretically before ice melting. Attempts of sequential freezing to coarsen hydrohalite to observable sizes before ice melting were unsuccessful ([Haynes et al., 1985](#)) and composition of  $\text{Lw}'$  inclusions were calculated in the  $\text{CaCl}_2-\text{H}_2\text{O}$  system. The field for possible compositions of  $\text{Lw}'$  inclusions in the  $\text{H}_2\text{O}-\text{NaCl}-\text{CaCl}_2$  system, is comprised between the  $\text{H}_2\text{O}-\text{CaCl}_2$  axis and the hydrohalite field ([Figure 4](#)).

$\text{Lwh}'$  inclusions show low temperature behaviour comparable to  $\text{Lw}'$  inclusions. Their composition in the  $\text{H}_2\text{O}-\text{NaCl}-\text{CaCl}_2$  system was estimated graphically using  $\text{Tm}$  ice (when observed) -  $\text{Ts}$   $\text{NaCl}$  pairs ([Vanko et al., 1988](#)) ([Table 2](#)). Calculated molar  $\text{Na}/\text{Ca}$  ratios

mostly range from 0.3 to 1. Cl content can reach ca. 12 molal but are mostly comprised between 8 and 10 molal. Lwh' inclusions fall predominantly in the field for CaCl<sub>2</sub>-rich field and were thus attributed to the CaCl<sub>2</sub>-rich brine ([Figure 4](#)).

#### *4.3.1.4. Low-salinity fluid inclusions*

The low-salinity fluid is represented by Lw'' fluid inclusions. Tm ice is comprised between -15 and -1°C. Low-salinity fluid inclusions are scarce in the studied deposits ([Table 4.2](#)) ([Figure 4.2](#)). Th are highly variable and comprised between 100 and 200°C. At McArthur River, low salinity fluid was contaminated by radiolytic H<sub>2</sub> resulting in low liquid/vapor ratios in fluid inclusions ([Derome et al., 2005](#)) and was interpreted as post-ore fluid. Here, the post-ore nature of the low-salinity fluid is not obvious, as no secondary fluid inclusion planes and no contamination by radiolytic H<sub>2</sub> are clearly identified. Nevertheless, the fact that Lw'' inclusions are always scarce, not homogeneously represented, and nearly absent of some deposits (Eagle Point, Shea Creek) stresses that this is not a critical factor for the mineralization in the Athabasca, contrary to the Kombolgie sub-Basin ([Derome et al., 2003b](#); [Derome et al., 2007](#)).

#### *4.3.1.5. Tm ice - Th pairs and Th distributions among brines*

For NaCl-rich brine inclusions (Lw1, Lw, Lwh) Tm ice are restricted to the -15 to -30°C range and show a mode at -25°C, while Tm ice display much greater variability for CaCl<sub>2</sub>-rich brine inclusions (Lw', Lwh') and range from -30 to ca. -55°C. A continuum of measured Tm ice is observed from -20°C to -55°C ([Figure 4.3](#)). Th are highly variable and range from ca. 70°C to ca. 200°C for all fluid inclusion types, most values being comprised between 100°C and 150°C in all deposits. Th distributions of NaCl-rich brine inclusion types (Lw1, Lw2, Lwh) are pretty similar, as for CaCl<sub>2</sub>-rich brine inclusion types (Lw', Lwh') ([Figure 4.4](#)). This is in agreement with the fact that Lw1, Lw2 and Lwh inclusions represent a single fluid type

(NaCl-rich brine) and Lw' and Lwh' inclusions represent another single fluid type (CaCl<sub>2</sub>-rich brine). CaCl<sub>2</sub>-rich brine inclusions show a mode of Th at 115°C in all deposits while being around 125°C to 135°C for the NaCl-rich brine inclusions, except for the McArthur River deposit where the mode of Th for NaCl-rich brine inclusions is 165°C ([Figure 4.4](#)). Thus, a small but significant difference in minimum trapping temperature is identified between NaCl-rich and CaCl<sub>2</sub>-rich brines in all deposits ([Figure 4.4G-H](#)).

#### *4.3.1.6. Quartz vs. carbonate samples*

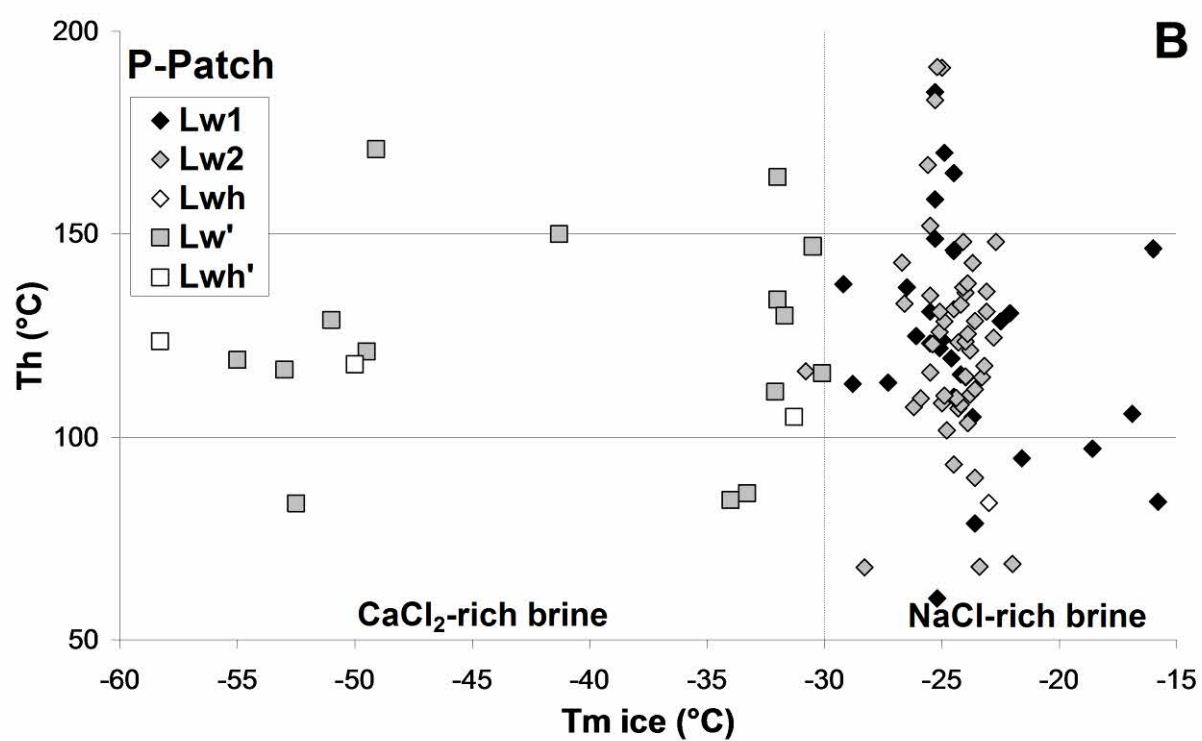
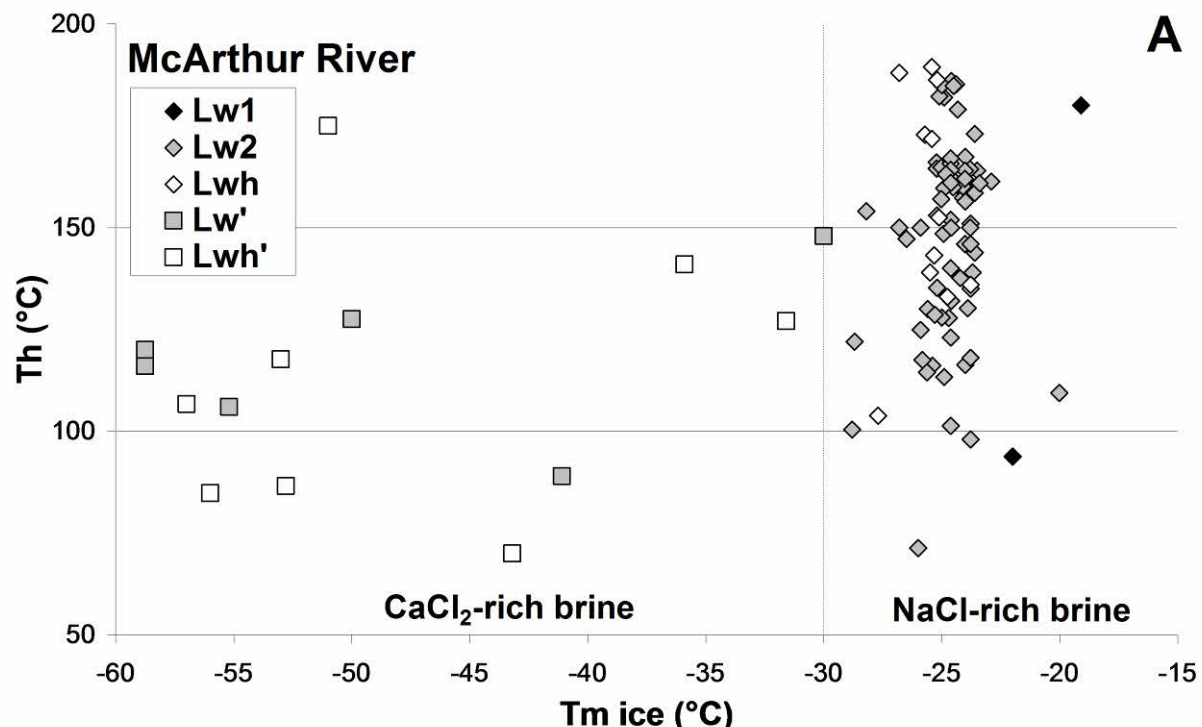
The above mentioned fluid inclusion types were all found in both quartz and carbonate samples for all studied deposits. The only exception is for Lwh' inclusions, which were only found in quartz samples. They are relatively homogeneous for each microthermometric type among quartz and carbonate veins. Thus, quartz and carbonate veins were probably formed from similar fluids at comparable temperatures. As no systematic differences between quartz-hosted and carbonate-hosted fluid inclusions were found, the microthermometric characteristics of fluid inclusions will be further discussed from one fluid inclusion type to another, without distinction between host minerals.

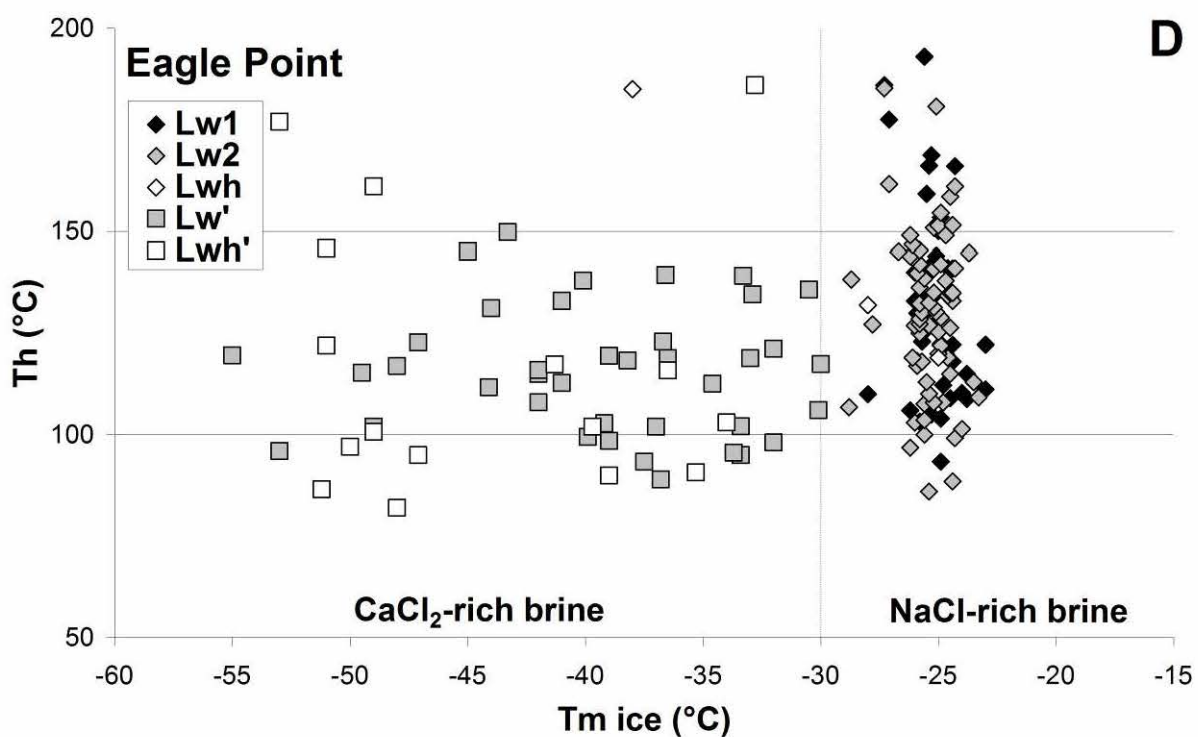
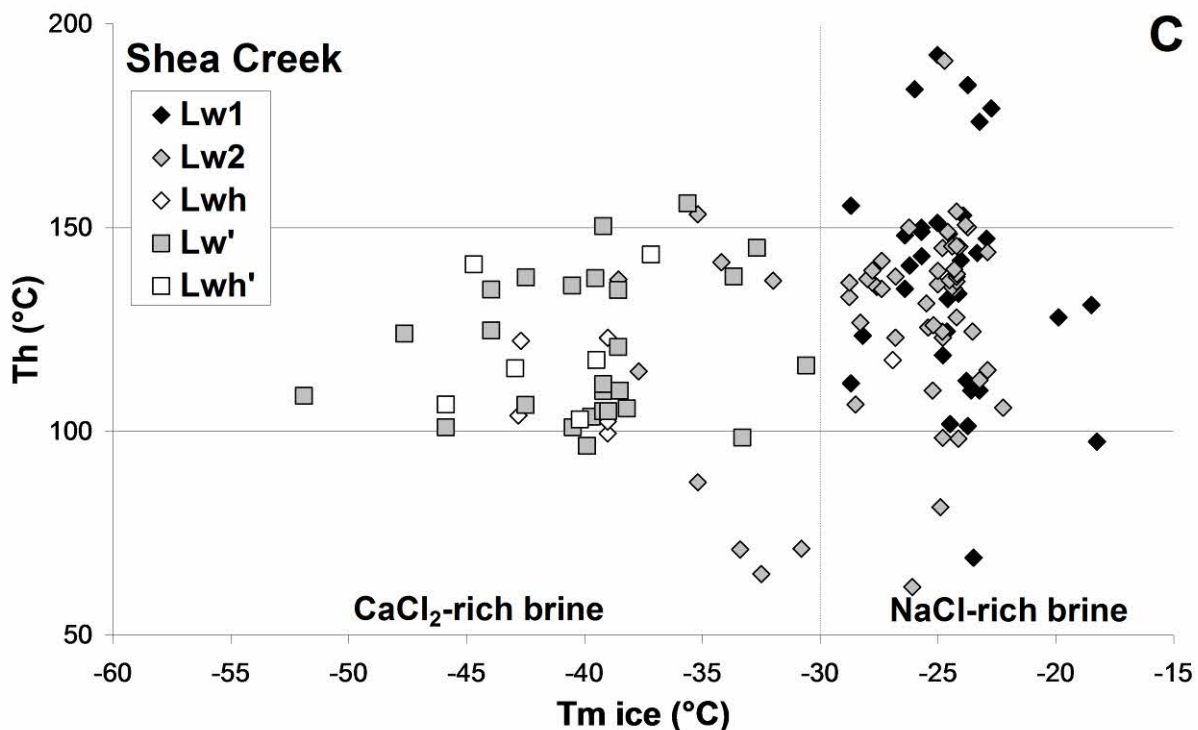
#### *4.3.1.7. Intra- and inter-sample variability*

A majority of quartz and carbonate samples contain variable amounts of NaCl-rich and CaCl<sub>2</sub>-rich brine inclusions. Some quartz and carbonate samples contain only NaCl-rich brine inclusions, and a few carbonate samples contain only CaCl<sub>2</sub>-rich brine inclusions. Samples with different brine content are petrographically and spatially undistinguishable which suggests that the trapping of the two brines was heterogeneous. No evidence of mixing could have been clearly established at the scale of individual samples containing NaCl-rich and CaCl<sub>2</sub>-rich brine inclusions display wide range of Tm ice which could be an evidence for fluid mixing within open fractures or prior entering fractures.

	NaCl-rich brine	Deposit	Te (°C)	Tm ice (°C)	Tm hyd (°C)	Ts NaCl (°C)	Th (°C)	wt% NaCl	wt% CaCl <sub>2</sub>	Na/Ca (molar)	Cl (molar)
Lw1 -30 < Tm ice < -15	McArthur River	-60 to -45 (-50), 17	-25.0 to -16.2 (n.d.), 17	-	-	93.8 to 240.0 (n.d.), 7	15.2 to 26.1 (20), 17	-	-	4.6	3.0 to 4.5 (4), 17
	Rabbit Lake	-75 to -45 (-55), 45	-29.5 to -18.1 (-27), 56	-	-	81.0 to 165.2 (130), 29	21.9 to 29.2 (28), 56	-	-	-	4.7 to 7.1 (7), 56
	Shea Creek	-70 to -50 (-60), 56	-28.7 to -18.3 (-25), 64	-	-	69.0 to 192.4 (145), 34	21.1 to 28.9 (27), 64	-	-	-	4.6 to 7.0 (6), 64
	Eagle Point	-70 to -35 (-60), 39	-29.9 to -20.7 (-26), 48	-	-	93.3 to 193.0 (125), 40	23.8 to 29.7 (27), 48	-	-	-	5.2 to 7.0 (6), 48
	P-Patch	-72 to -55 (-55), 38	-29.2 to -15.8 (-25), 45	-	-	19.0 to 29.4 (26), 45	-	-	-	-	4.1 to 6.7 (6), 42
	Millennium	-70 to -45 (-60), 25	-28.7 to -16.9 (-23), 30	-	-	83.5 to 193.4 (125), 19	20.4 to 28.9 (28), 30	-	-	-	4.3 to 6.9 (7), 30
Lw2 Tm ice < Tm hyd	McArthur River	-76 to -55 (-55), 90	-28.8 to -21.0 (-25), 90	-7.0 to 21.9 (10), 90	-	71.3 to 186.0 (165), 66	12.0 to 25.0 (20), 90	1.0 to 12.0 (3), 90	1.1 to 19.0 (3), 90	5.5 to 6.5 (6), 90	5.5 to 6.5 (6), 90
	Rabbit Lake	-75 to -45 (-80), 187	-35.1 to -21.9 (-24), 199	-16.9 to 21.0 (-3), 199	-	61.9 to 185.3 (130), 163	6.1 to 26.9 (21), 199	2.3 to 23.8 (6), 199	0.4 to 25.4 (4), 199	5.5 to 7.4 (7), 199	5.5 to 7.4 (7), 199
	Shea Creek	-75 to -50 (-55), 67	-39.0 to -22.2 (-24), 78	-20.3 to 15.6 (4), 78	-	61.8 to 154.0 (135), 55	5.0 to 25.0 (21), 78	3.3 to 26.1 (9), 78	0.3 to 18.5 (5), 78	5.4 to 7.3 (6), 78	5.4 to 7.3 (6), 78
	Eagle Point	-70 to -50 (-55), 81	-15.9 to -23.3 (-25), 85	-15.1 to 21.0 (-1), 85	-	86.0 to 185.1 (35), 70	8.5 to 22.8 (17), 85	6.6 to 20.1 (12), 85	0.7 to 7.9 (3), 85	5.4 to 6.8 (6), 85	5.4 to 6.8 (6), 85
	P-Patch	-77 to -50 (-60), 76	-30.8 to -22.0 (-25), 82	-21.6 to 19.7 (-10), 82	-	67.9 to 197.5 (120), 53	9.6 to 25.5 (17), 82	2.9 to 19.4 (11), 82	0.8 to 23.8 (3), 82	5.3 to 7.0 (6), 82	5.3 to 7.0 (6), 82
	Millennium	-68 to -55 (-60), 15	-33.8 to -23.1 (-25), 15	-25.3 to 10.2 (5), 15	-	116.5 to 140.6 (125), 14	5.5 to 22.5 (20), 15	6.1 to 22.5 (10), 15	0.4 to 8.5 (5), 15	6.0 to 6.5 (6), 15	6.0 to 6.5 (6), 15
Lwh Tm ice < Tm hyd Ts NaCl < Th	McArthur River	-60 to -50 (-55), 12	-27.7 to -24.0 (-26), 12	-3.2 to 19.0 (n.d.), 12	99.5 to 208.0 (140), 12	103.4 to 188.0 (135), 9	20.0 to 27.0 (n.d.), 12	1.8 to 4.5 (n.d.), 12	7.4 to 9.2 (8), 12	6.5 to 9.5 (7), 9	6.5 to 9.5 (7), 9
	Rabbit Lake	-65 to -40 (n.d.), 7	-36.0 to -22.8 (n.d.), 9	7.6 to 10.4 (n.d.), 4	81.0 to 149.0 (n.d.), 9	86.0 to 152.0 (n.d.), 8	12.5 to 26.8 (n.d.), 9	1.0 to 20.0 (n.d.), 9	1.2 to 50.1 (5), 9	6.8 to 8.7 (8), 7	6.8 to 8.7 (8), 7
	Shea Creek	-75 to -50 (-50), 5	-42.8 to -25.0 (-39), 7	-1.7 to 13.3 (n.d.), 3	96.9 to 156.2 (n.d.), 7	98.5 to 123.0 (n.d.), 6	8.5 to 27.7 (n.d.), 7	1.4 to 23.5 (n.d.), 7	0.7 to 38.1 (n.d.), 7	6.7 to 10.7 (n.d.), 4	6.7 to 10.7 (n.d.), 4
	Eagle Point	-	-38.0 to -25.0 (n.d.), 4	-8.0 to 21.0 (n.d.), 3	122.2 to 176.0 (n.d.), 4	119.0 to 185.0 (n.d.), 3	17.5 to 22.0 (n.d.), 4	6.0 to 18.0 (n.d.), 4	1.9 to 7.0 (n.d.), 4	4.4 to 4.4 (n.d.), 1	4.4 to 4.4 (n.d.), 1
	P-Patch	-	-23.0 to -23.0 (n.d.), 1	-	80.6 to 80.6 (n.d.), 1	83.8 to 83.8 (n.d.), 1	21.0 to 21.0 (n.d.), 1	9.0 to 9.0 (n.d.), 1	7.4 to 7.4 (n.d.), 1	-	-
	Millennium	-	-	-	-	-	-	-	-	-	-
	CaCl <sub>2</sub> -rich brine	Deposit	Te (°C)	Tm ice (°C)	Tm hyd (°C)	Ts NaCl (°C)	Th (°C)	wt% NaCl	wt% CaCl <sub>2</sub>	Na/Ca (molar)	Cl (molar)
Lw' no freezing or Tm ice < -30	McArthur River	-75 to -80 (-70)	-58.0 to -30 (n.d.)	-	-	58.0 to 148.0 (115), 27	-	25.0 to 35.0 (n.d.)	0.5 to 1.7 (n.d.)	6.0 to 9.7 (n.d.)	6.0 to 9.7 (n.d.)
	Rabbit Lake	-80 to -55 (-70), 40	-55.0 to -30.0 (-45), 63	-	-	78.5 to 188.0 (115), 102	-	24.7 to 31.0 (29), 63	-	5.9 to 8.1 (7), 63	5.9 to 8.1 (7), 63
	Shea Creek	-75 to -55 (-70), 37	-51.9 to -30.6 (-39), 37	-	-	75.0 to 160.0 (125), 57	-	25.0 to 30.7 (28), 57	-	6.0 to 8.0 (7), 57	6.0 to 8.0 (7), 57
	Eagle Point	-75 to -55 (-70), 49	-55.0 to -30.0 (-42), 57	-	-	77.5 to 162.9 (115), 58	-	24.7 to 31.4 (28), 57	-	5.9 to 8.3 (7), 57	5.9 to 8.3 (7), 57
	P-Patch	-70 to -65 (-55), 21	-55.0 to -28.1 (-32), 26	-	-	56.0 to 193.3 (115), 63	-	24.0 to 31.4 (25), 26	-	5.7 to 8.2 (6), 26	5.7 to 8.2 (6), 26
	Millennium	-80 to -55 (-70), 17	-45.3 to -30.7 (-42), 24	-	-	75.0 to 191.9 (115), 36	-	25.0 to 29.3 (27), 24	-	6.0 to 7.5 (7), 24	6.0 to 7.5 (7), 24
Lwh' no freezing or Tm ice < -30 Th < TsNaCl	McArthur River	-75 to -60 (-75)	-58.0 to -36.0 (n.d.)	-	-	115.0 to 235.0 (200), 31	63.0 to 175.0 (110), 18	10.0 to 15.0 (n.d.), 14	17.5 to 27.5 (n.d.), 14	0.3 to 10.9 (10), 14	8.5 to 10.9 (10), 14
	Rabbit Lake	-70 to -60 (-70), 9	-54.0 to -30.8 (-40), 14	-	-	99.4 to 234.2 (200), 25	70.2 to 156.6 (95), 24	12.0 to 19.0 (n.d.), 14	16.0 to 25.0 (n.d.), 14	0.9 to 2.3 (17), 14	6.2 to 12.0 (8), 14
	Shea Creek	-75 to -55 (-75), 5	-45.9 to -36.9 (-42), 7	-	-	102.9 to 143.0 (125), 13	8.5 to 12.0 (n.d.), 7	21.0 to 24.0 (n.d.), 7	0.7 to 1.1 (n.d.), 7	6.2 to 10.2 (8), 14	6.2 to 10.2 (8), 14
	Eagle Point	-70 to -65 (-70), 20	-53.0 to -32.8 (-49), 22	-	-	115.5 to 265.0 (210), 22	82.0 to 186.0 (95), 18	5.0 to 25.0 (n.d.), 22	0.4 to 3.2 (14), 22	6.9 to 12.2 (10), 22	6.9 to 12.2 (10), 22
	P-Patch	-65 to -65 (-65), 2	-58.3 to -31.3 (n.d.), 3	-	-	99.3 to 239.0 (125), 10	12.0 to 20.0 (n.d.), 3	13.5 to 23.0 (n.d.), 3	1.0 to 2.3 (n.d.), 3	6.2 to 11.7 (7), 10	6.2 to 11.7 (7), 10
	Millennium	-	-54.5 to -33.2 (n.d.), 2	-	-	130.6 to 259.6 (n.d.), 10	78.0 to 126.8 (105), 8	11.0 to 15.0 (n.d.), 2	0.8 to 1.7 (n.d.), 2	7.3 to 10.0 (8), 10	7.3 to 10.0 (8), 10
	Low-salinity fluid	Deposit	Te (°C)	Tm ice (°C)	Tm hyd (°C)	Ts NaCl (°C)	Th (°C)	wt% NaCl	wt% CaCl <sub>2</sub>	Na/Ca (molar)	Cl (molar)
Lw" -15 < Tm ice < 0	McArthur River	-55 to -35 (n.d.), 2	-10.6 to -1.6 (n.d.)	-	-	150.0 to 250.0 (n.d.), 4	2.5 to 130.0 (n.d.)	-	3.7 to 5.0 (n.d.)	0.4 to 2.6 (n.d.)	0.4 to 2.6 (n.d.)
	Rabbit Lake	-60 to -20 (n.d.), 3	-10.1 to -1.8 (n.d.), 7	-	-	113.0 to 197.0 (n.d.), 6	2.7 to 13.6 (n.d.), 7	-	-	0.5 to 2.7 (n.d.), 7	0.5 to 2.7 (n.d.), 7
	Shea Creek	-65 to -50 (n.d.), 4	-11.1 to -4.6 (n.d.), 5	-	-	95.0 to 95.0 (n.d.), 1	7.4 to 15.1 (n.d.), 5	-	-	1.4 to 3.0 (n.d.), 5	1.4 to 3.0 (n.d.), 5
	Eagle Point	-60 to -20 (n.d.), 2	-14.7 to -2.6 (n.d.), 6	-	-	142.0 to 142.0 (n.d.), 1	3.8 to 18.5 (n.d.), 6	-	-	0.7 to 3.8 (n.d.), 6	0.7 to 3.8 (n.d.), 6
	P-Patch	-55 to -20 (n.d.), 5	-11.4 to -0.1 (n.d.), 11	-	-	148.0 to 180.0 (n.d.), 2	0.2 to 15.0 (n.d.), 11	-	-	0.1 to 3.0 (n.d.), 11	0.1 to 3.0 (n.d.), 11
	Millennium	-45 to -45 (n.d.), 1	-15.0 to -0.4 (n.d.), 5	-	-	-	0.4 to 18.8 (n.d.), 5	-	-	0.1 to 3.9 (n.d.), 5	0.1 to 3.9 (n.d.), 5

**Table 4.2 : Summary of microthermometric data for the studied deposits. Data for McArthur River are from Derome et al., (2005). Temperatures of phase changes: Te: eutectic melting, Tm ice: ice melting, Tm hyd: hydrohalite melting, Ts NaCl: halite dissolution, Th: total homogenization. Observations are noted as follows: “min” to “max” (mode), “number of measurements”. (n.d.): not determined.**





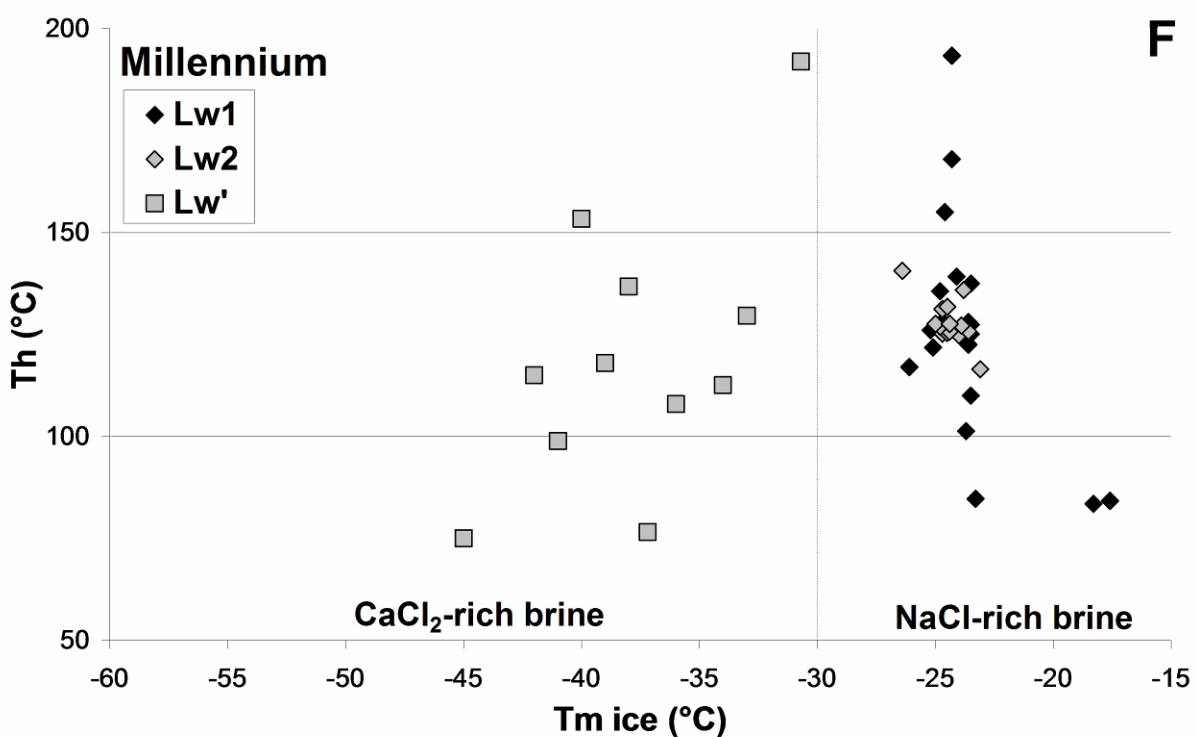
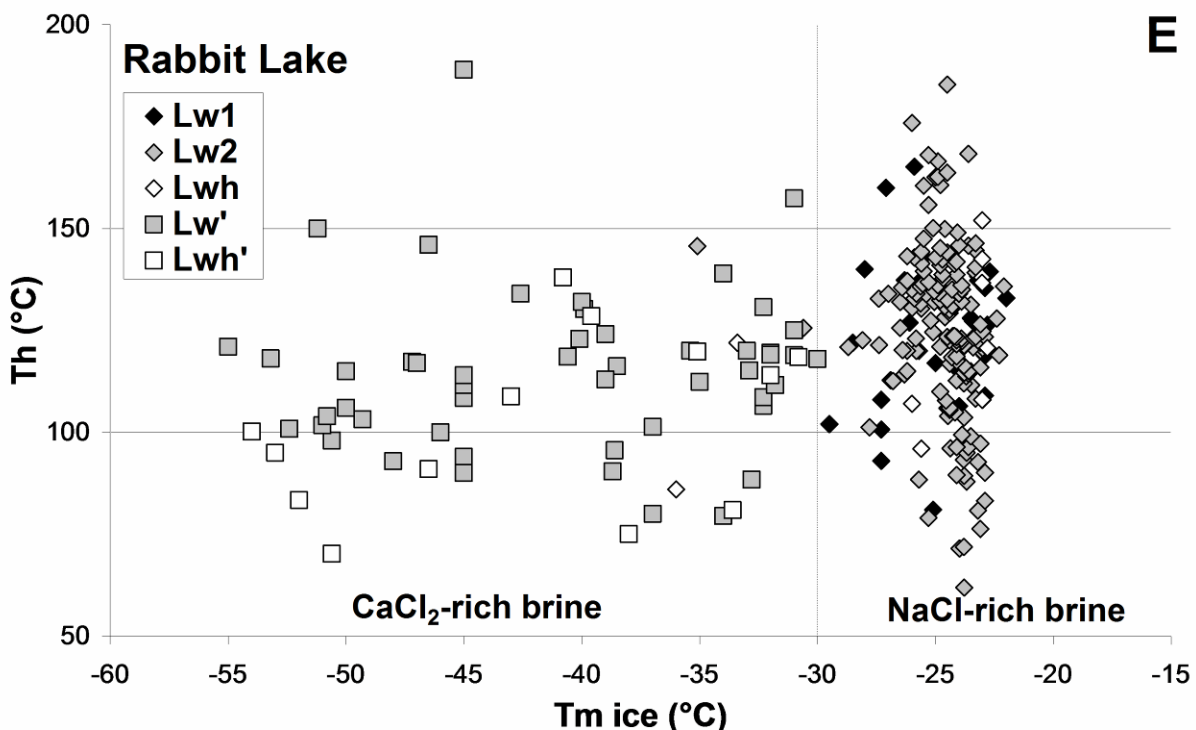
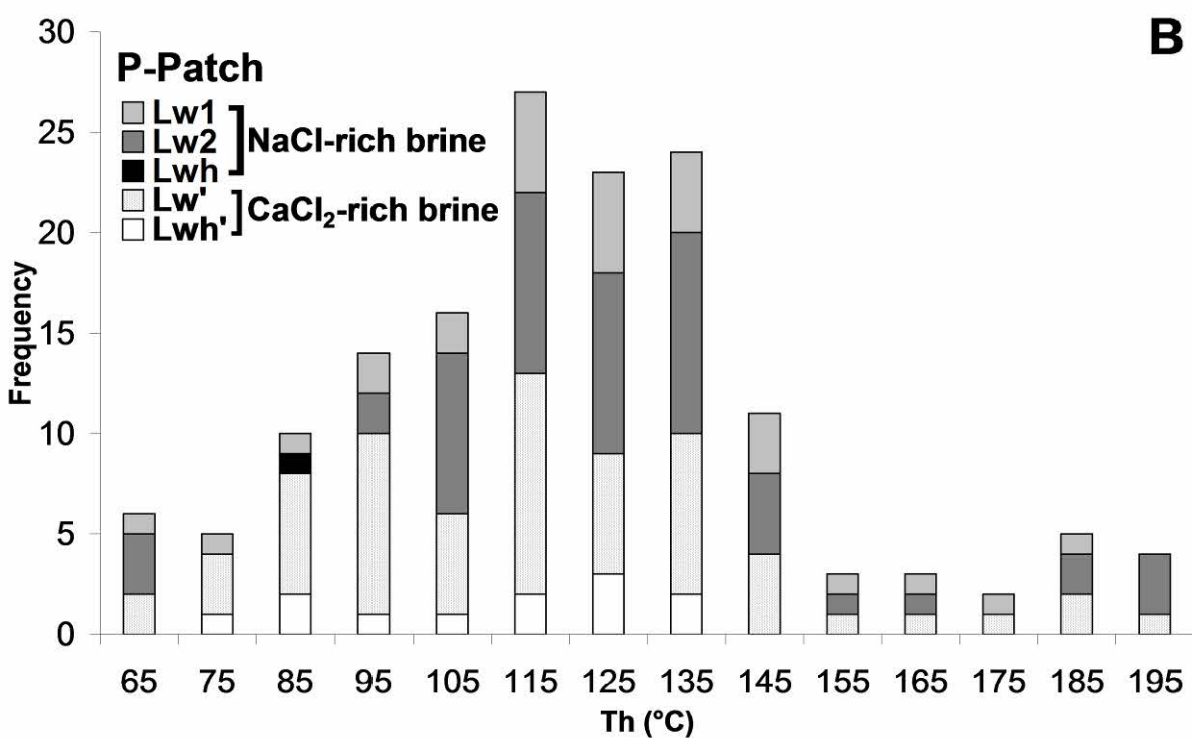
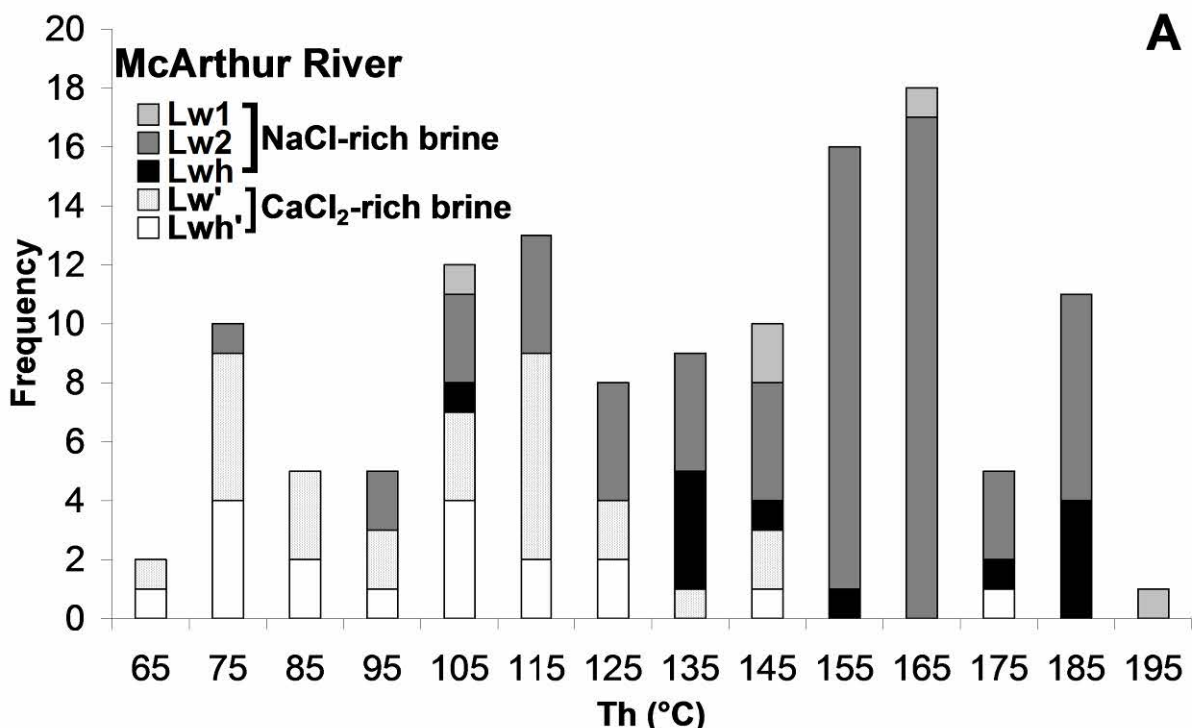
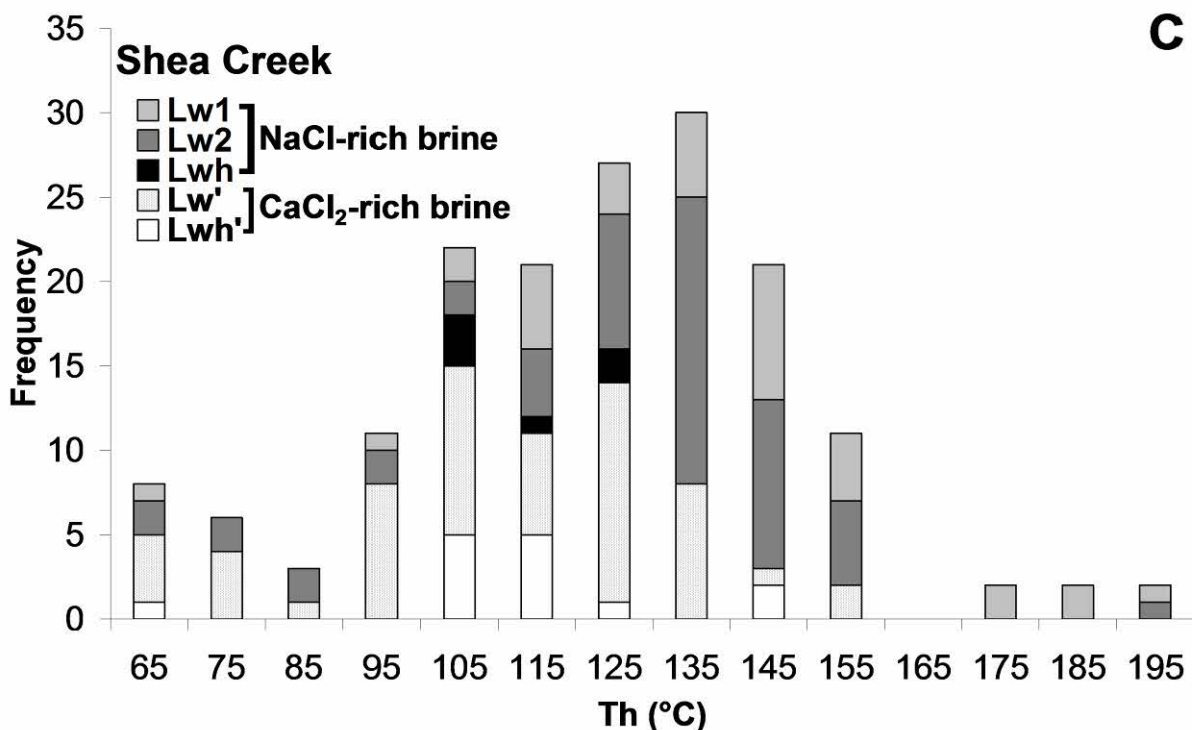
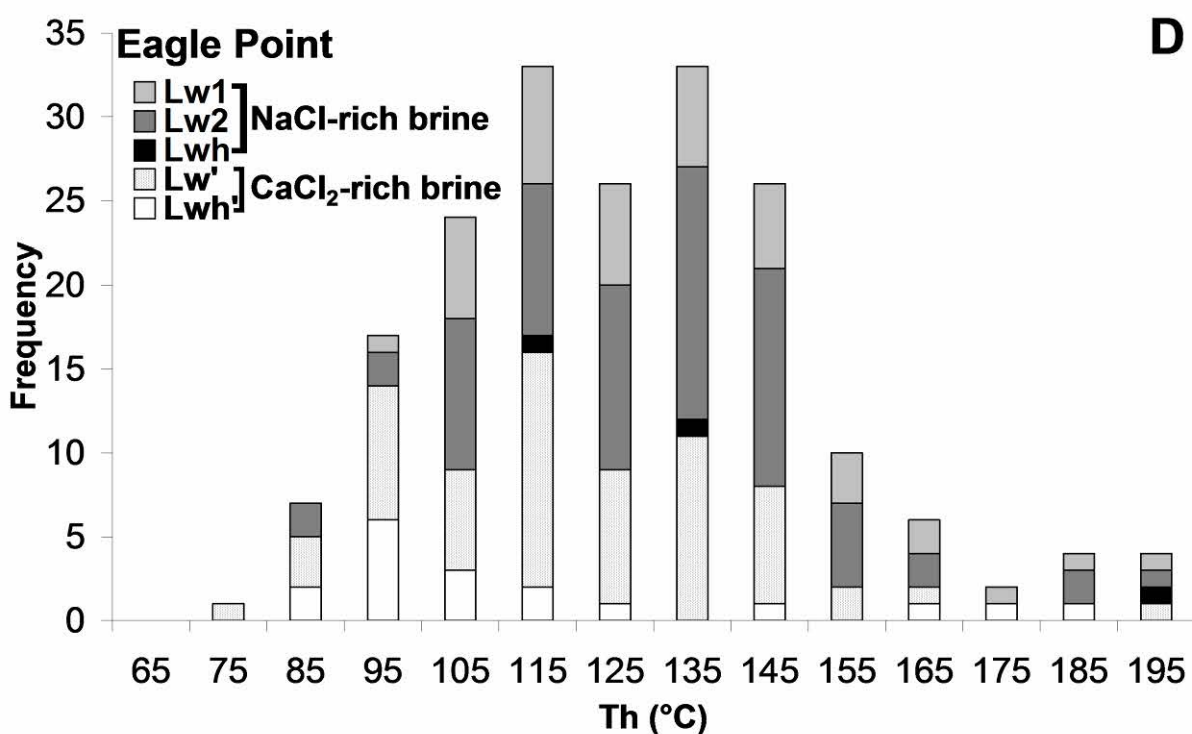
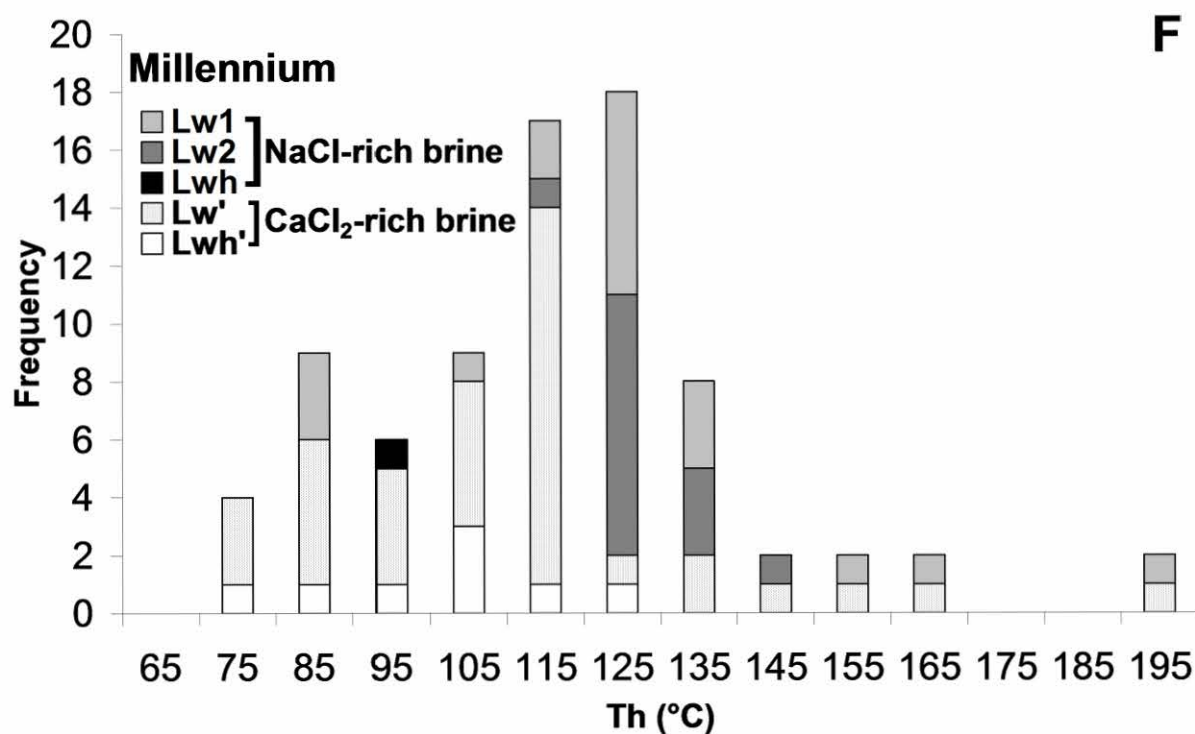
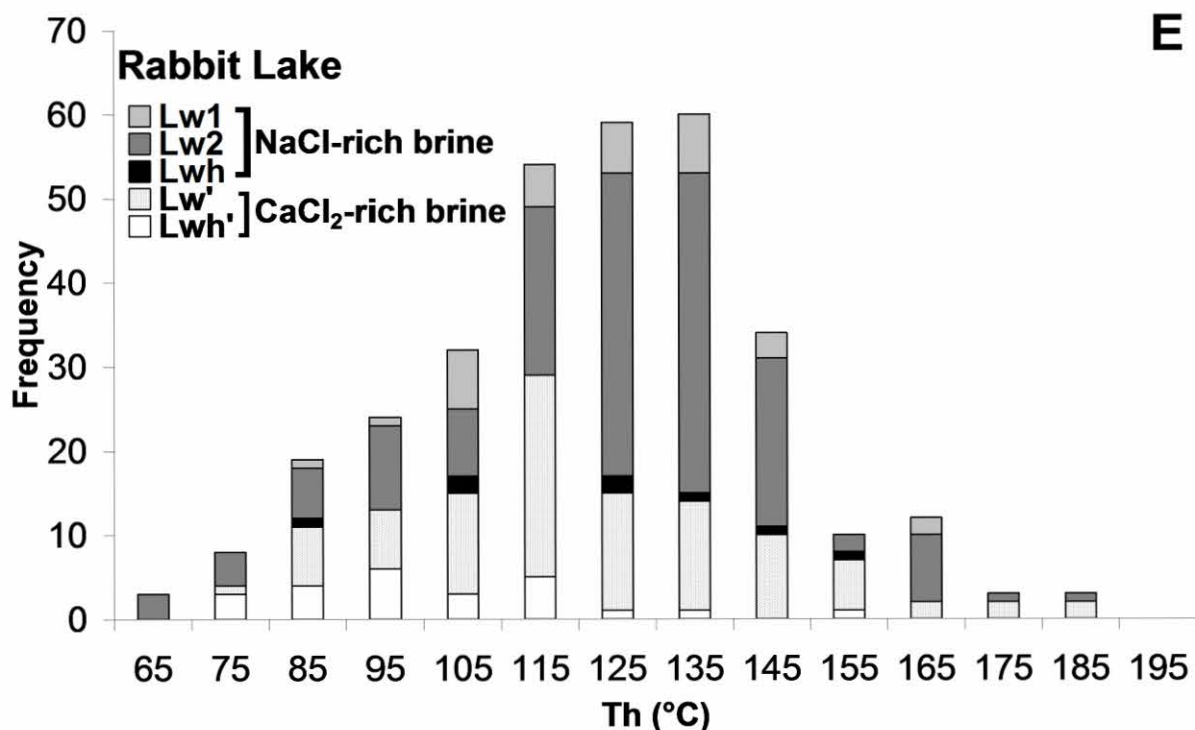
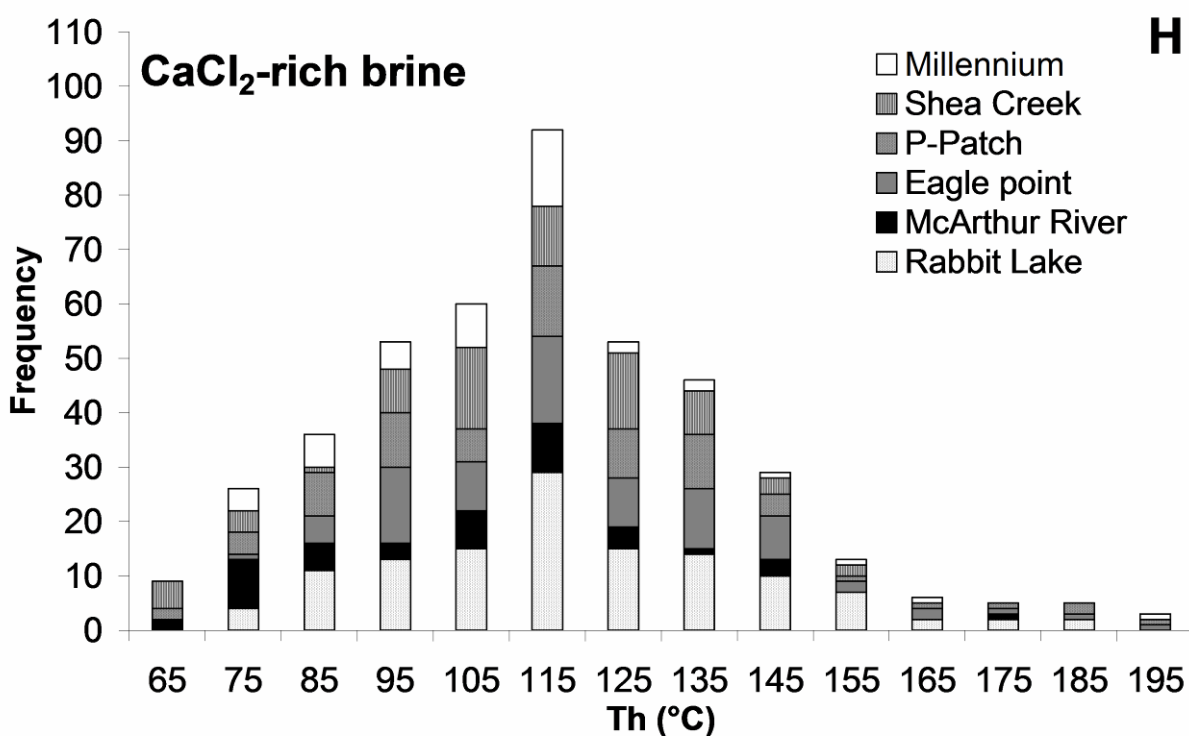
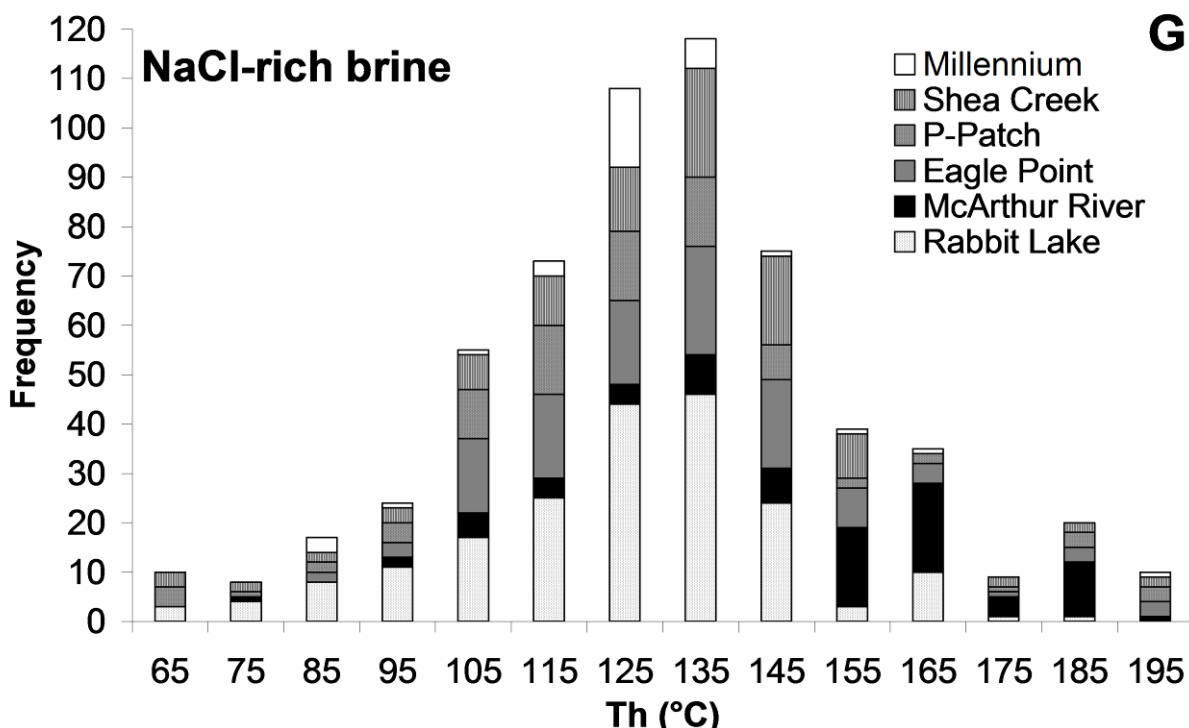


Figure 4.3 : Tm ice vs. Th diagram for studied fluid inclusions. Data for McArthur River are from [Derome et al., \(2005\)](#). Temperatures of phase changes:  $Tm_{ice}$ : ice melting,  $Th$ : total homogenization. Note that a majority of Lw' and Lwh' inclusions failed to nucleate any ice upon cooling and could not be plotted in the CaCl<sub>2</sub>-rich brine field. Large variations of Tm ice suggest mixing between a NaCl-rich brine and a CaCl<sub>2</sub>-rich brine. Th mainly comprised between 100 and 150°C for both brines both brines suggests that mixing is isothermal.



**C****D**



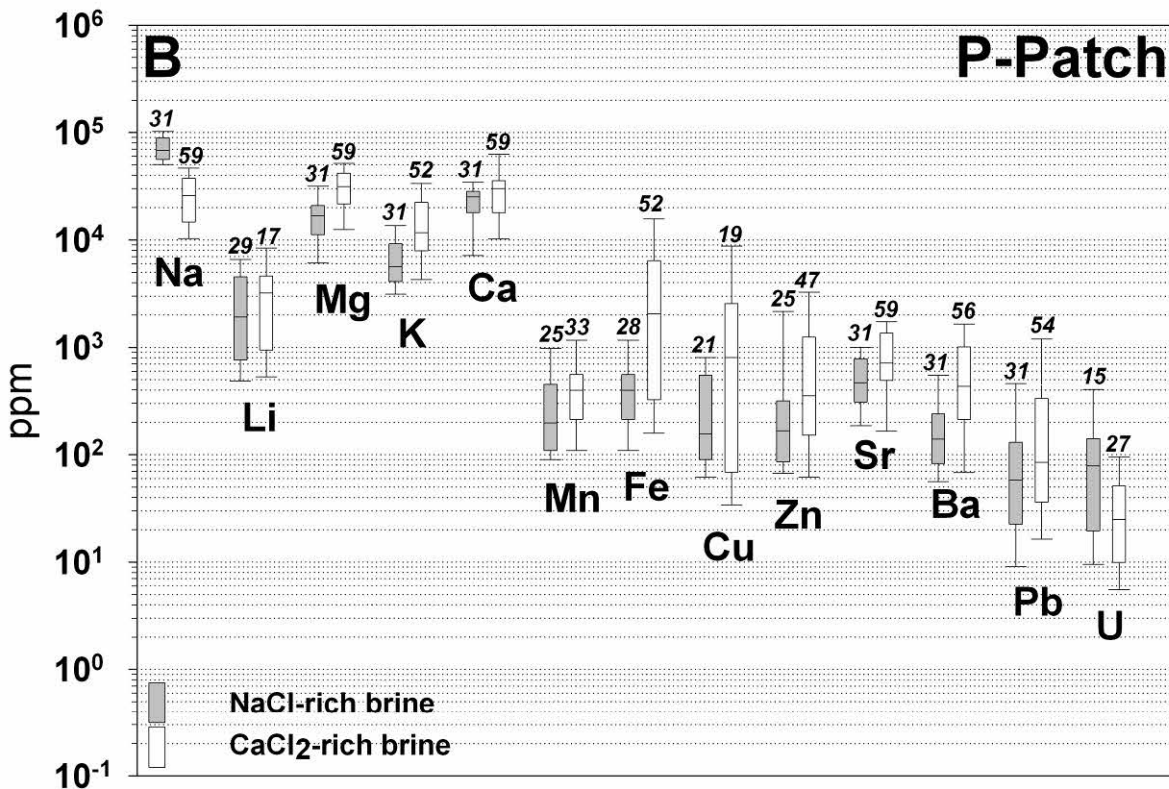
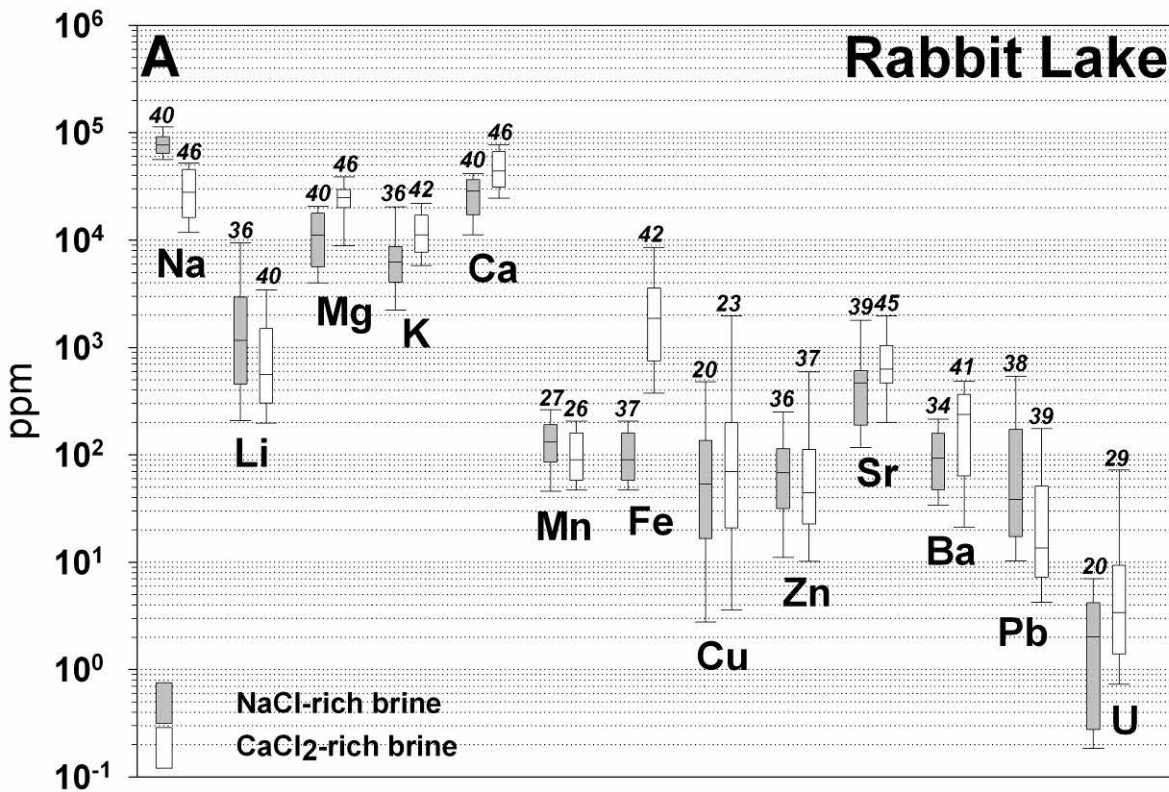


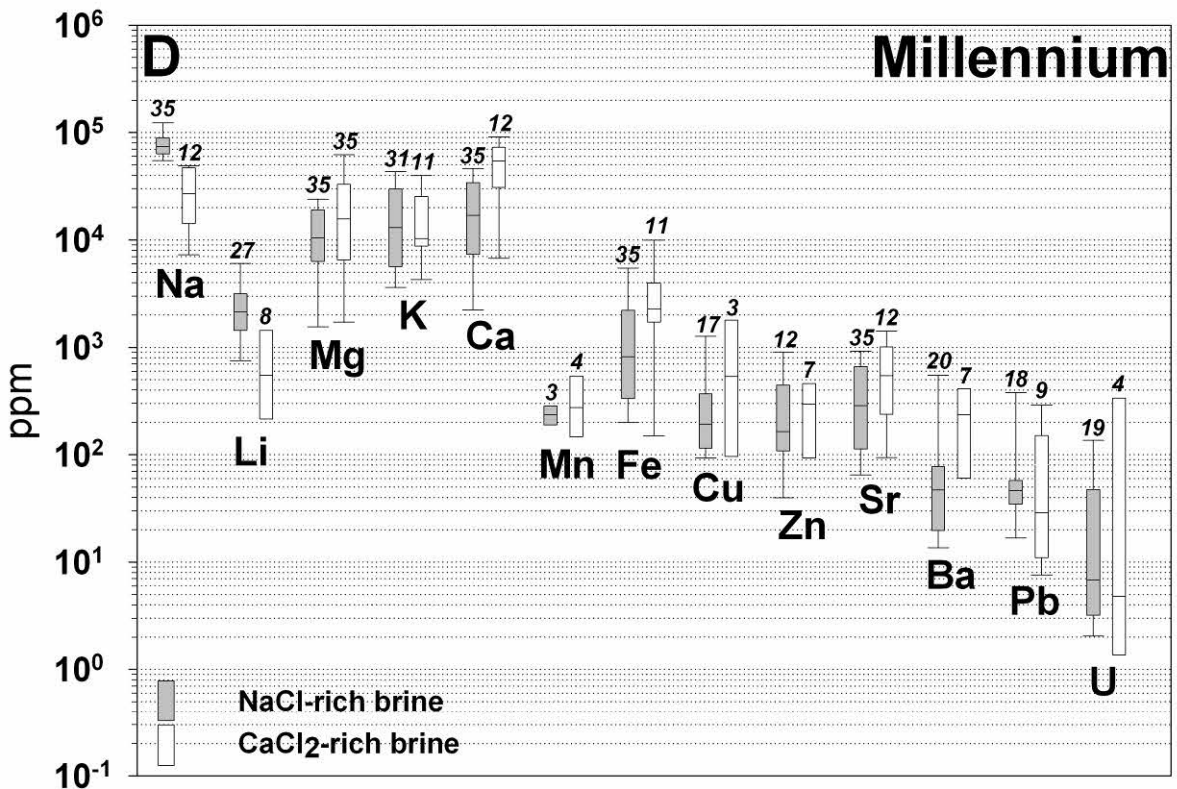
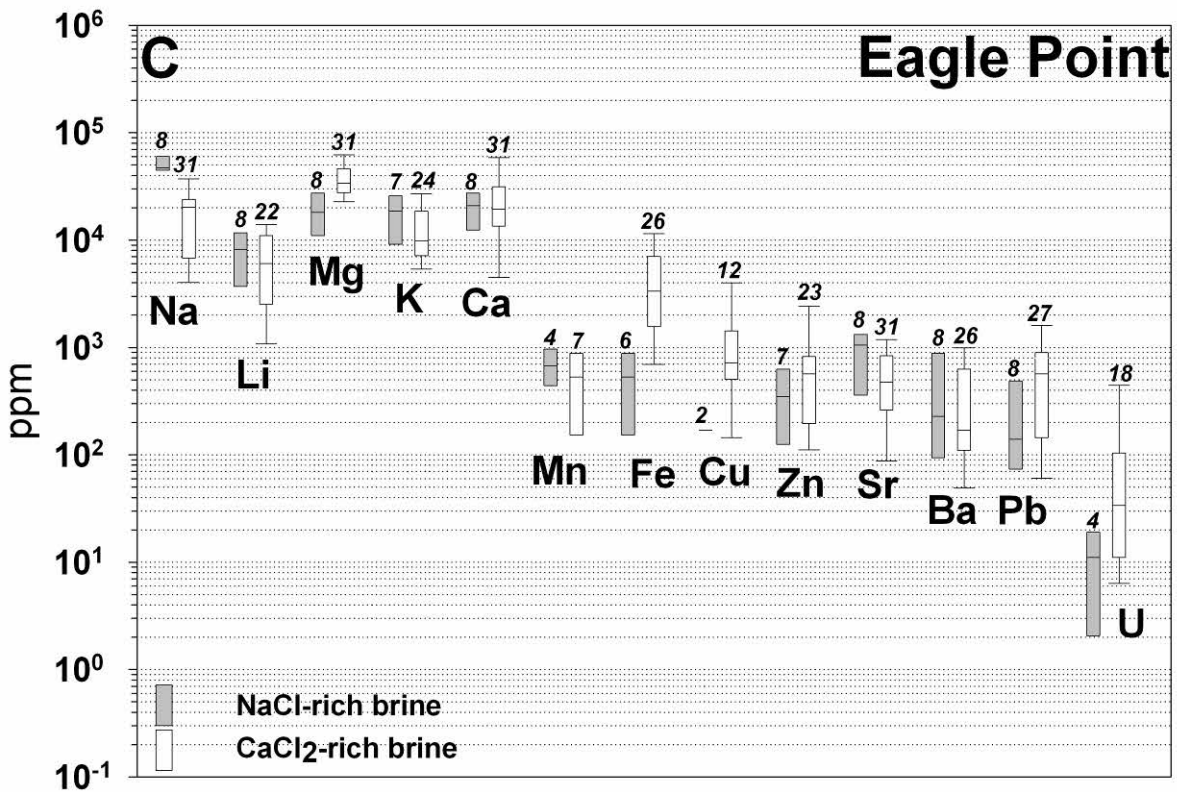
**Figure 4.4 : Th histograms for the studied fluid inclusions. Th: temperature of total homogenization. Data for McArthur River are from [Derome et al., \(2005\)](#). Except for the McArthur River deposit, Th for NaCl-rich brine mostly range from 100 to 150°C with a mode at 135°C, and Th for CaCl<sub>2</sub>-rich brine mostly range from 80 to 130°C with a mode at 115°C.**

#### 4.3.2. LA-ICP-MS results

[Figure 4.5](#) shows LA-ICP-MS data in the form of box and whiskers plots for a better comparison between the element distributions in both brines for each deposit ([Figure 4.5A-D](#)) and for all deposits ([Figure 4.5E](#)). Na, Ca, Mg and K are the dominant cations in solution, and the analyzed inclusions display a wide range of Na-Ca-Mg-K compositions. For the NaCl-rich brine, major elements concentrations are the following: Na (50000-100000 ppm), Ca (5000-40000 ppm), Mg (4000-15000 ppm). For the CaCl<sub>2</sub>-rich brine, major elements concentrations are the following: Na (7000-50000 ppm), Ca (10000-70000 ppm), Mg (10000-50000 ppm). A continuous trend between Na-dominated and Ca-Mg-K-dominated compositions is observed ([Figure 4.6.](#)) similar to that described for the McArthur River deposit ([Part 3](#)).

Comparison of minor and trace element concentration among brines and deposits may be difficult due to the large concentration ranges and sometimes small number of inclusions with element concentration above LODs. As, it seems that the two brines have similar compositions in all deposits, all the LA-ICP-MS data were put together in [Figure 4.5E](#) to get sufficiently large number of analyzed inclusions for both brines. Minor and trace element concentrations are roughly distributed as follows: Li (400-9000 ppm) > Sr (90-1000 ppm) > Fe (60-900 ppm) > Mn (50-800 ppm) > Cu (20-700 ppm) > Zn (30-600 ppm) > Ba (30-500 ppm), Pb (10-500 ppm), U (0.3-100 ppm) for the NaCl-rich brine, and Fe (300-10000 ppm) > Li (200-9000 ppm) > Sr (200-2000 ppm) > Cu (20-5000 ppm) > Ba (40-1000 ppm) > Zn (30-2000 pmm) > Pb (80-1000 ppm) > U (1-1000 ppm) for the CaCl<sub>2</sub>-rich brine. Only small differences are found between minor and trace element concentrations of NaCl-rich and CaCl<sub>2</sub>-rich brine. Fe is significantly enriched (ca. one order of magnitude) in the CaCl<sub>2</sub>-rich brine. Other trace elements are difficult to distinguish among brines. Nevertheless, when considering all data, Mn, Cu, Zn, Ba, Sr, Pb and U can be considered as being slightly enriched in the CaCl<sub>2</sub>-rich brine. U concentrations are discussed in detail in [Part 5](#).





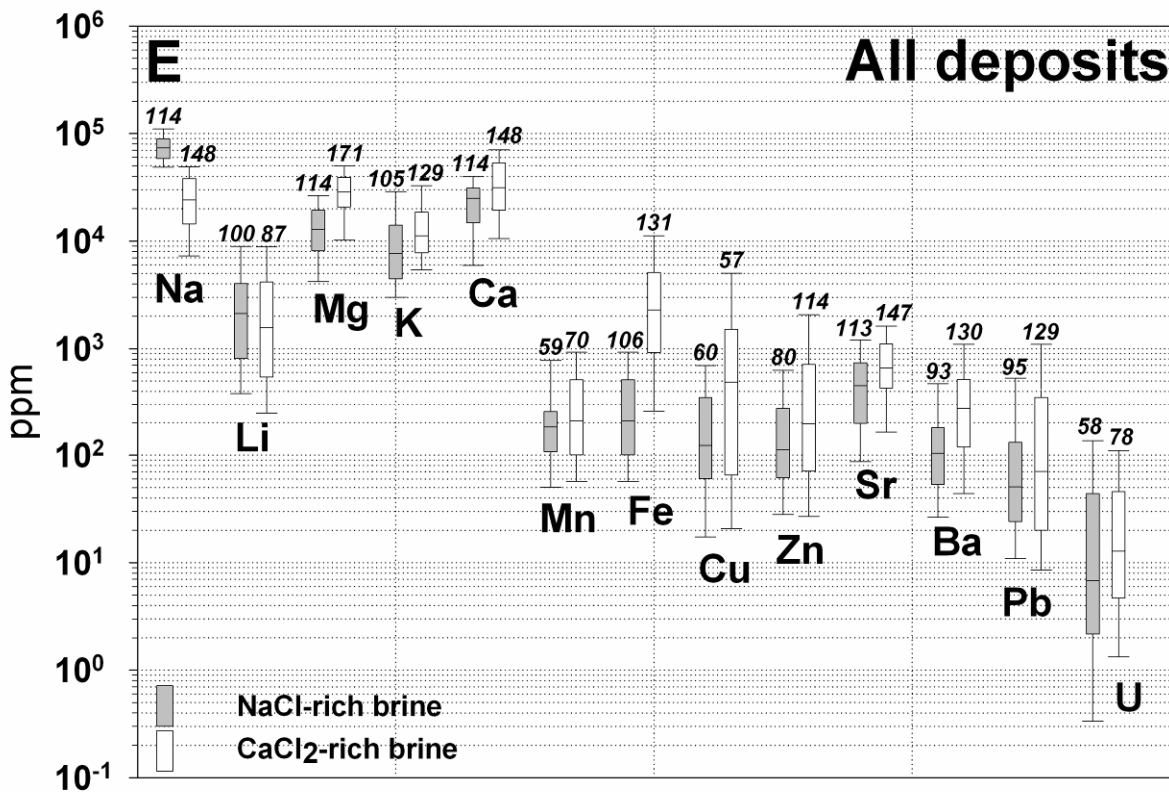


Figure 4.5 : Box and whisker plots for element concentrations in the NaCl-rich and CaCl<sub>2</sub>-rich brines for studied deposits, from LA-ICP-MS analysis of individual fluid inclusions. Numbers of fluid inclusions above limits of detection are shown in italics. Whiskers indicate 10<sup>th</sup> and 90<sup>th</sup> deciles, and box indicate 25<sup>th</sup> deciles, median and, 75<sup>th</sup> deciles. Note that when the amount of data was less than 10 it was not possible to draw whiskers and only median values sometimes associated with 25<sup>th</sup> and 75<sup>th</sup> deciles were calculated. Outliers are not shown.

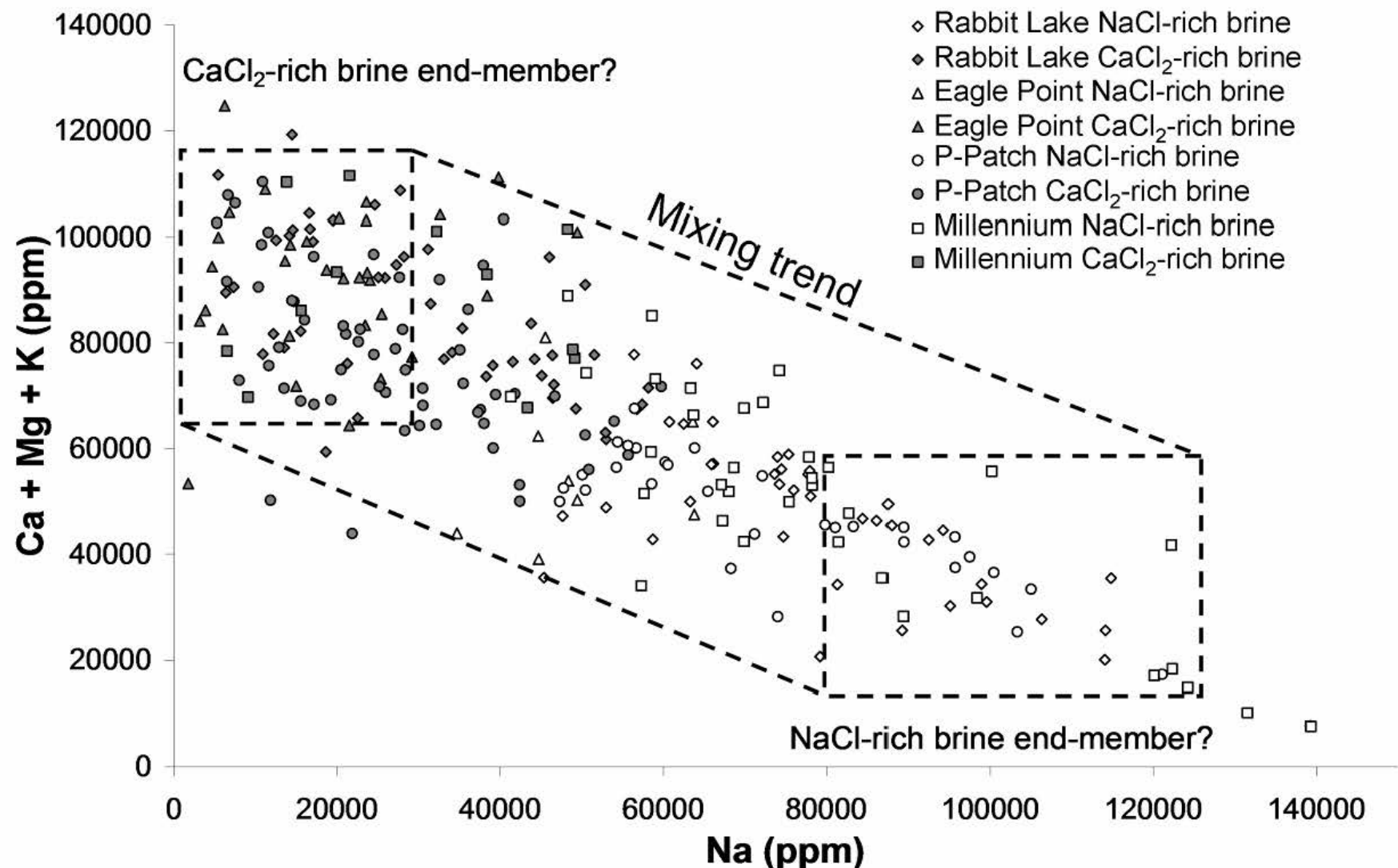


Figure 4.6 : Na vs. Ca + Mg + K plot for the studied fluid inclusions from LA-ICP-MS analysis. A continuum is observed between a Na-rich compositions and Ca-Mg-K-rich compositions, which suggests mixing between a NaCl-rich brine end-member and a CaCl<sub>2</sub>-rich brine end-member.

## **4.4. Discussion**

### **4.4.1. Fluid mixing**

In [Figures 4.3, 4.5 and 4.6](#), an overall continuity between NaCl-rich brine and CaCl<sub>2</sub>-rich brine compositions is observed for all the studied deposits. This observations suggests: either : (i) an evolution of a Na-rich brine towards a CaCl<sub>2</sub>-rich brine composition through interaction with basement lithologies ; (ii) mixing between a Na-rich brine and a CaCl<sub>2</sub>-rich and a CaCl<sub>2</sub>-rich brine; (iii) a combination of both. Based on the previously described mixing trends at McArthur River ([Derome et al., 2005; Part 3](#)) we assume that the second hypothesis is the most probable. Fluid inclusions were attributed either to NaCl-rich or CaCl<sub>2</sub>-rich brine, but most of them may represent mixing terms between the two end-members. In [Figure 4.6](#), NaCl-rich and CaCl<sub>2</sub>-rich brine end-members were tentatively drawn.

### **4.4.2. P-T estimations**

#### *4.4.2.1. Reconsidering the McArthur River model*

[Derome et al., \(2005\)](#) have reconstructed the P-T conditions of the NaCl-rich and CaCl<sub>2</sub>-rich brines and their mixing for the McArthur River deposit. Pressure decrease from lithostatic to near-hydrostatic conditions has been established in close temporal relation to U deposition. The result of this pressure decrease at McArthur River was the mixing of the NaCl-rich brine with the CaCl<sub>2</sub>-rich brine at near hydrostatic conditions with a partial temperature reequilibration between the ca. 140°C CaCl<sub>2</sub>-rich brine and the ca. 200°C NaCl-rich brine. However, in the McArthur River model the deepest and basement-seated fluid (CaCl<sub>2</sub>-rich brine) is relatively cool whereas the shallower basin-seated fluid (NaCl-rich brine) is hotter. According to [Derome et al., \(2005\)](#), this unusual situation is the best way to explain large differences in Th modes between the two brines.

Here, systematic microthermometry on five newly studied deposits shows that Th differences between the two brines, although systematic, are not as high as for the McArthur River deposit ([Figure 4.4](#)). At the basin scale, the  $\text{CaCl}_2$ -rich brine displays nearly constant Th range. It can be postulated that the  $\text{NaCl}$ -rich brine has a Th mode ca. 20°C higher than that of the  $\text{CaCl}_2$ -rich brine ([Figure 3G-H](#)). At McArthur River this difference is close to 50°C because of the high Th measured in the  $\text{NaCl}$ -rich brine. The McArthur River model is potentially applicable to all studied deposits, the only difference being the lower initial temperature difference between the two fluids. However, new microthermometric data on five other deposits, could improve the model or potentially lead to an alternative of P-T model.

#### *4.4.2.2. Pressure fluctuations*

In [Figure 4.3](#), large Th variations in the overall  $T_m$  ice range infer pressure fluctuations between hydrostatic (upper contour) and lithostatic regimes (lower contour), likely to account for ca. 50°C of Th variations. After [Dubessy et al., \(2003\)](#) ([Figure 4.7](#)), if the pressure of every trapped mixed paleofluids represents all the possible values between lithostatic and hydrostatic regimes, data will distribute inside the whole contour. If pressure fluctuations affect only some events in the mixing process, data point will distribute inside a complex contour, with distributions parallel to Th axis, lying inside the contour defined by lithostatic and hydrostatic lines. Despite the numerous data, it is difficult to conclude on that point because of the large range of  $T_m$  ice involved which do not permit to have a significant number of Th measurements for every given restricted  $T_m$  ice range.

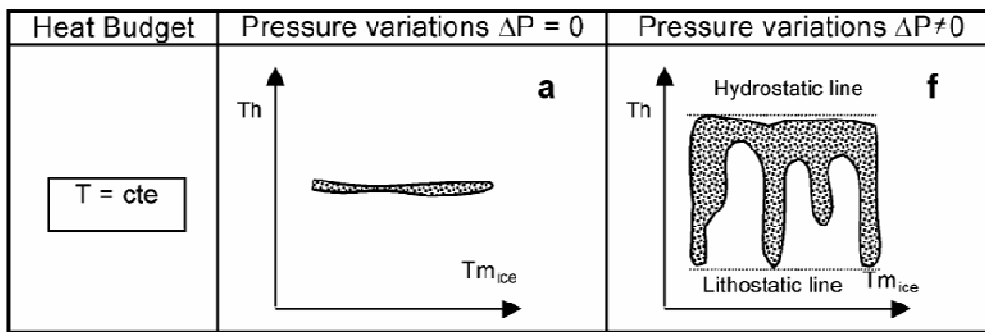


**Figure 4.7 : Plots of microthermometric data in  $\text{Th} - \text{T}_{\text{mice}}$  diagrams for isothermal fluid mixing between a fluid with a low salinity and a saline fluid (Dubessy et al., 2003). (a) Isobaric mixing. (f) Non-isobaric mixing.**

Thus, Th data have potentially recorded non-isobaric mixing of the two brines. However, this would imply that single hydrothermal quartz or carbonate vein would have grown under fluctuating pressure conditions. In this case, one would expect successive growth planes with evidence of mixing between the two brines at a given pressure condition for a given growth plane. Generally, fluid inclusions are randomly distributed within the quartz lattice, rarely along clearly identifiable growth planes. Thus, we have no textural evidence for pressure fluctuation during quartz or carbonate growth and fluid inclusions trapping. Finally, if we consider that mixing was isobaric the sample scale of individual samples, pressure fluctuations at the deposit scale could potentially account for dispersion of Th values. If veins with only NaCl-rich brine inclusions were formed preferentially under lithostatic conditions, while veins showing inclusions typical of both brines were preferentially formed under hydrostatic conditions, and if both brines have the same temperature, Th of CaCl<sub>2</sub>-rich brine inclusions would be statistically lower than Th for NaCl-rich brine inclusions.

Overpressuring is a common phenomenon in sedimentary basins, and periods of overpressuring preceding brecciation and faulting in relation with brine circulation at the basement-cover interface of the Athabasca Basin are suspected. Overpressuring to 130% of lithostatic pressure would lower Th of ca. 15-20°C which could account for the observed Th in the 60-80°C range. However, overpressuring could not account for the overall Th dispersion.

#### 4.4.2.3. Saturation with respect to halite

Lwh' inclusions, typical of the CaCl<sub>2</sub>-rich brine, have Th > TsNaCl which implies that the CaCl<sub>2</sub>-rich brine was saturated with respect to halite at the time of trapping (Figure 4.8). In the McArthur River model, the halite dissolution curve for 30 wt.% NaCl (Bodnar & Vityk, 1994) was plotted in the P-T diagram as a boundary restricting the temperature of the CaCl<sub>2</sub>-rich brine to a maximum of 145°C. However, for 30 wt. % NaCl is a minimal salinity for a NaCl-saturated fluid and most of the analyzed halite-saturated fluid inclusions in the Athabasca Basin have salinities comprised between 35-40 wt.% NaCl (Figure 4.2). Halite dissolution curves for 35 and 40 wt.% NaCl are not anymore a boundary for maximum temperature of the CaCl<sub>2</sub>-rich brine (Bodnar & Vityk, 1994). Thus, this boundary is probably not a strong constrain on the maximal temperature of CaCl<sub>2</sub>-rich brine.

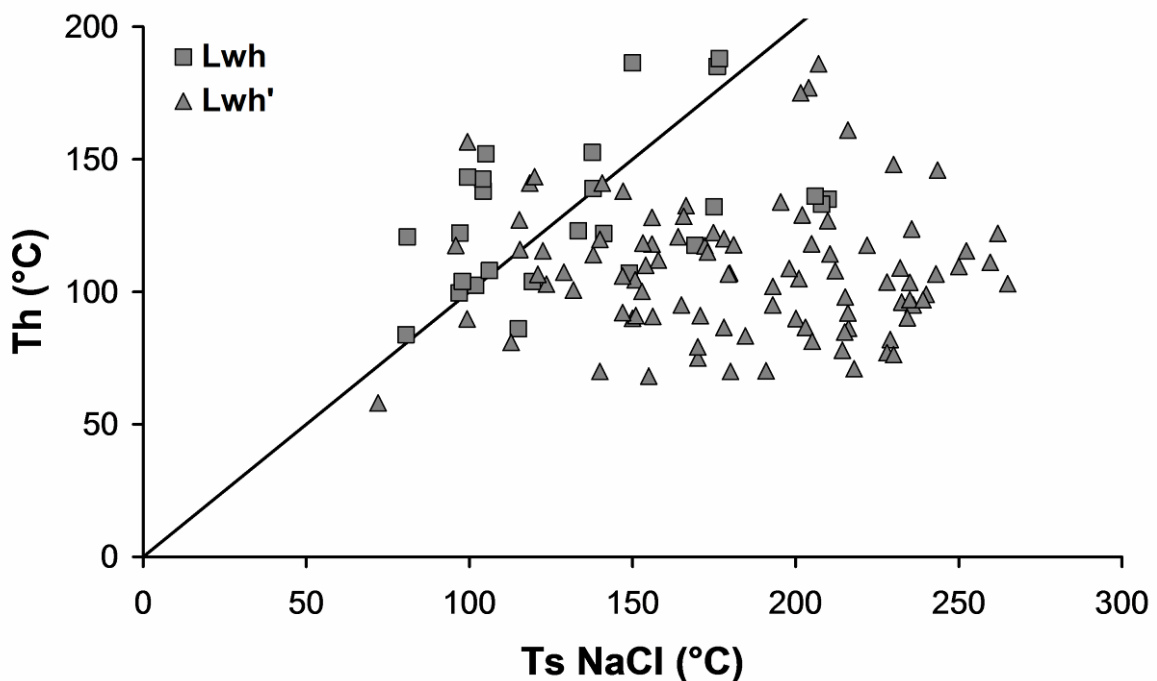


**Figure 4.8 : Th – Ts NaCl diagram for Lwh and Lwh' fluid inclusions. Temperatures of phase changes:  $Ts_{\text{NaCl}}$ : halite dissolution,  $Th$ : total homogenization. A majority of Lwh' inclusions plot below the 1:1 line, indicating that the CaCl<sub>2</sub>-rich brine was saturated with respect to halite at the time of trapping.**

#### *4.4.2.4. H<sub>2</sub> contamination*

Contamination of fluid inclusions by radiolytic H<sub>2</sub> even if not optically visible is likely to lead to anomalously high Th. H<sub>2</sub>-rich inclusions could support the idea that the numerous measured Th higher than 150°C could result from the latter process. This hypothesis was already proposed for high Th values measured in low-salinity fluid inclusions at McArthur River ([Derome et al., 2005](#)). This phenomenon is likely to have been more important at McArthur River because of its exceptional grade compared to the other deposits. In the absence of alternative explanation and in the view of new results on other deposits, we can reasonably assume that the McArthur River deposit was strongly affected by radiolytic H<sub>2</sub> contamination leading to artificially high Th measured in the NaCl-rich brine.

#### *4.4.2.5. Post-trapping processes: stretching and necking down*

Th data were possibly altered by post-trapping stretching and necking down processes, which implies that significant tectonic activity was recurrent in late-ore and post-ore times. However, the analyzed inclusions have pretty constant volumetric fraction of vapor phase <10%, so that there is no obvious optical evidence for post trapping deformation. Inclusions with higher volumetric fraction of vapor phase are systematically contaminated by H<sub>2</sub> and were not analyzed for Th. Thus, post-trapping deformations are unlikely to account for the broad Th range observed in the two brines, but it is not excluded that this phenomenon could have accidentally affected some Th measurements, leading to exceptionally high or low Th.

#### 4.4.2.6. An alternative P-T model

Previously undiscussed phenomena are likely to have affected the brines, leading potentially to alternative P-T estimations. Here, isochores drawn from most likely representative Th ranges for both brines allow the definition of their respective P-T domains during mixing ([Figure 4.9](#)). To built this model, we propose the following assumptions: (i) mixing between NaCl-rich brine and CaCl<sub>2</sub>-rich brine was isobaric at the sample scale, (ii) Pressure conditions have fluctuated from hydrostatic to lithostatic at the deposit scale, (iii) mixing was isothermal, (iv), veins with only NaCl-rich brine inclusions were formed preferentially under lithostatic conditions, while veins showing inclusions typical of both brines were preferentially formed under lithostatic conditions.

In this case, intersection of the lower isochore for CaCl<sub>2</sub>-rich brine with the 30°C/km lithostatic thermal gradient and intersection of higher isochore for NaCl-rich brine with the 40°C hydrostatic thermal gradient would constrain temperature for mixing in the 150 ± 30°C range. Overpressuring, H<sub>2</sub> contamination and post-trapping processes (stretching and necking down) are all likely to have affected the Th data, contributing to the overall Th dispersion and also to extreme Th values. We propose that Th of the NaCl-rich brine at McArthur River were artificially high, probably due to H<sub>2</sub> contamination, and that brine mixing was isothermal at 150 ± 30°C in all deposits including McArthur River. Under purely lithostatic conditions, pressure was comprised between 800 and 1500 bars. Under purely hydrostatic conditions, pressure was comprised between 300 and 500 bars. Considering that depth below unconformity for the studied samples is negligible compared to the thickness of the basin, the deduced past thickness of the Athabasca Basin was comprised between 3 and 6 km, which is consistent results form [Pagel, \(1975\)](#) and [Derome et al., \(2005\)](#) who have estimated the thickness at ca. 5 km.

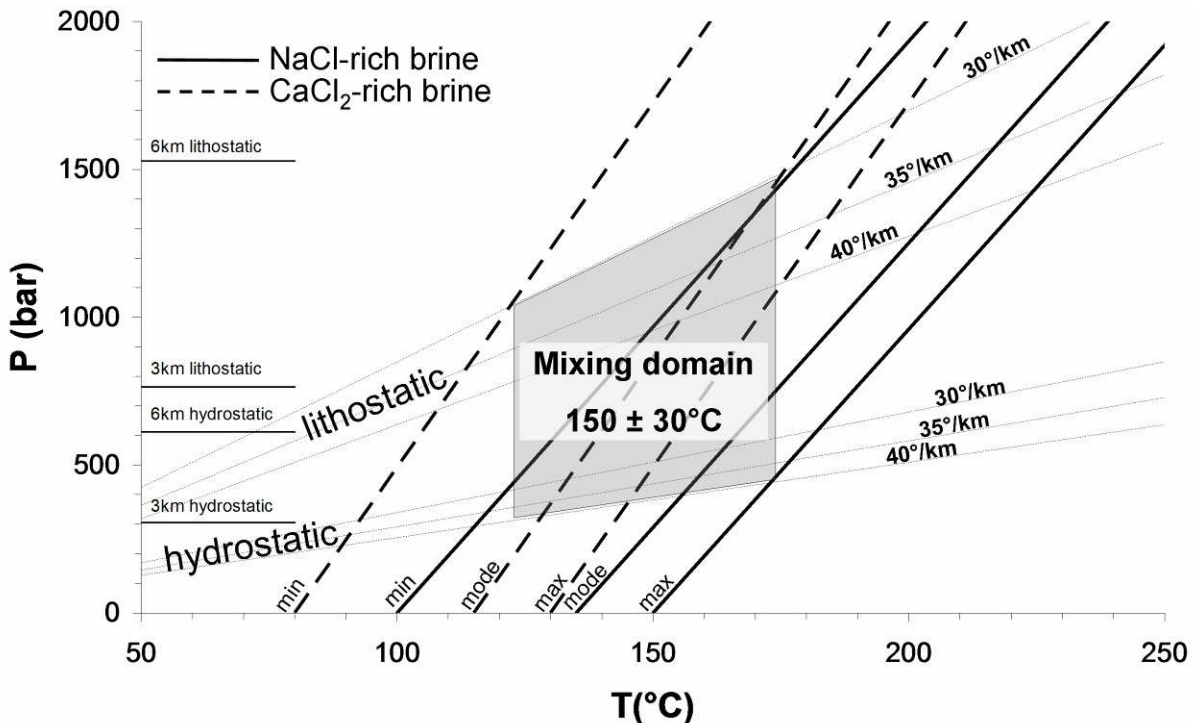


**Figure 4.9 : P-T model for mixing conditions for the NaCl-rich and CaCl<sub>2</sub>-rich brines.** Representative isochores have been drawn from the main range of Th (temperature of total homogenization) for the two brines. The hydrostatic and lithostatic pressures at 3 and 6 km depth are reported as well as the hydrostatic and lithostatic gradients calculated for thermal gradients of 30°, 35°, and 40°C/km.

#### 4.4.3. Conditions for uranium deposition

Mechanisms for reduction of uranium from U<sup>VI</sup> to U<sup>IV</sup> and precipitation of pitchblende are still poorly constraint for unconformity-related U deposits. In Australian unconformity-related deposits, NaCl-rich and CaCl<sub>2</sub>-rich brines are systematically diluted by a CH<sub>4</sub>-bearing low-salinity fluid at the time of mineralization ([Derome et al., 2003b](#); [Derome et al., 2007](#)). However, the role of CH<sub>4</sub> for the reduction of uranium is still unclear. No dilution of brines was observed in the Athabasca Basin. Thus, dilution is not necessary for precipitation of pitchblende in these environments. Lack of dilution and thus failure in destabilization of chloride complexes could also explain the scarcity of Cu, Pb, Zn minerals in these environments despite high concentrations of these metals in brines ([Figure 4.5](#)). In the absence of pH and fO<sub>2</sub> data for brines, speculations on the role of brines mixing on U deposition are highly hazardous.

Despite numerous fluid inclusion studies in the vicinity of Canadian unconformity-related U deposit including this study, no reducing fluid was evidenced ([Table 4.1](#)). Although this hypothesis can not be ruled out, such a fluid is likely to have been recorded as fluid inclusions in quartz and carbonate veins or as secondary fluid inclusions in silicified zones of the sandstones or in primary quartz from basement gneisses and pegmatoids, which is not the case ([Mercadier et al., in press](#)). In the absence of direct fluid inclusion evidence for such fluid in the Athabasca Basin, we support the idea that no reducing fluid was involved in the formation of unconformity-related U deposits. This reinforces the hypothesis that U deposition occurs thanks to redox reactions between U-bearing brines and basin or basement lithologies.

#### **4.4.4. Comparison between unconformity and basement-hosted deposits**

Significant effort has been put over the last ten years to point out genetic differences between unconformity-hosted and basement-hosted deposits ([Quirt, 2003; Alexandre et al., 2005](#)). The frontier is tight between the two types of deposits and especially when a single deposit contains both unconformity-hosted and basement-hosted mineralization (e.g. McArthur River, Shea Creek), with or without spatial connection between the two. Rabbit Lake deposit is considered by [Alexandre et al., \(2005\)](#) as basement hosted, although sandstones were eroded, and alteration is visible on top of the basement and could have been present in the sandstones. Millennium, P-Patch and Eagle Point deposits are generally classified as basement-hosted, as alteration or mineralization are entirely restricted to basement rocks. Thus, the purpose of this classification is questionable.

This study shows that PTX conditions of the fluids are very similar from one deposit type to another. The results suggest that the location of the ore is not controlled by the nature of the fluids involved but rather by other parameters not investigated in this study such as: fluid budgets, structural settings, lithogeochemical heterogeneities in the basement, local hydrology, and emplacement of reducing lithologies.

#### **4.4.5. Basin-scale circulation**

This study shows that fluids responsible for the formation of unconformity-related U deposits with similar P-T-X conditions have circulated at large scale in the Athabasca Basin and are described in both Eastern and Western part of the Basin. [Table 4.1](#) shows that previously published fluid inclusion data could be reinterpreted in terms of NaCl-rich brine and CaCl<sub>2</sub>-rich brines, and that these brines have probably circulated in deposits not investigated here (Midwest, Cluff Lake, SueC-McClean, Key Lake), but also in unmineralized central parts of the basin (Rumple Lake).

A consequence to that is that the basal sandstones of the Athabasca Group as well as the upper part of the Athabasca Basement could be considered as a giant aquifer that was relatively homogenous in terms of P-T conditions for fluids at least at the scale of the present-day Athabasca Basin. The extent of the Athabasca Basin at the time of U mineralizations is unknown. Present-day maximum thickness is of 1.5 km at Rumple Lake and considering a past thickness of ca. 3 to 6 km and a relatively flat lying basement, the past extend of the basin could have been much greater. As some deposits described in this study are located close to the basin margins (Rabbit Lake) and even out of the basin margins (Eagle Point), it can be inferred that the circulations of basinal brines in the basement have occurred remote from the present-day limits of the basin, and that basement-hosted deposits are likely to have formed several tens of kilometers away from the Athabasca Basin as for many Australian deposits.

#### **4.5. Conclusion**

The study of fluid inclusions in close temporal relation with alteration and U mineralization, by microthermometry and LA-ICP-MS, on five unconformity-related U deposits of the Athabasca Basin, Canada, has permitted to draw the following general characteristics of the mineralizing fluids that seem to be shared to all presently and previously studied deposits:

- (1) Diagenetic NaCl-rich and CaCl<sub>2</sub>-rich brine, previously described at McArthur River deposit have been reported for all the newly studied deposits.
- (2) The NaCl-rich brine and the CaCl<sub>2</sub>-rich brine have mixed in all deposits at the time of mineralization. Mixing was isothermal and occurred at 150 ± 30°C in all studied deposits.
- (3) Brines were trapped under pressure conditions fluctuating between lithostatic and hydrostatic conditions.
- (4) No difference in terms of PTX condition is observed between unconformity-hosted and basement-hosted deposits.
- (5) Both brines have comparable metal content, the CaCl<sub>2</sub>-rich brine, being slightly enriched in Cu, Pb, Zn and U.
- (6) The Athabasca Basin has undergone basin-scale percolation of diagenetic brines towards its crystalline basement, interaction with basement lithologies and mixing between end-members. This large-scale fluid event is at the origin of alteration and elements mobility in the Athabasca Basement, a key parameter for the formation of the giant unconformity-related U deposits.

## **Version abrégée**

Les conditions de pression et température de circulation et de mélange des saumures dans les gisements de Rabbit lake, Shea Creek, Eagle Point, Millennium et P-Pach, ont été établies par l'analyse microthermométrique d'inclusions fluides. De plus, la chimie détaillée des inclusions fluides a été reconstituée par ablation laser couplée à la spectrométrie de masse (LA-ICP-MS).

Les inclusions fluides échantillonnées dans les veines de quartz et carbonates présentent des caractéristiques microthermométriques similaires à celles précédemment décrites à McArthur River. Dans tous les nouveaux gisements étudiés, une saumure sodique et une saumure calcique, comparables à celles de McArthur River, sont identifiées.

La saumure calcique est enrichie en Ca, Mg, K et appauvrie en Na par rapport à la saumure sodique. Les deux saumures transportent jusqu'à plusieurs centaines de ppm de Cu, Pb, Zn et U ([Figure 4.5.](#)).

Le continuum des compositions reconstituées dans le système H<sub>2</sub>O-NaCl-CaCl<sub>2</sub> par microthermométrie ([Figures 4.2, 4.3](#)), ainsi que le continuum de compositions reconstituées en LA-ICP-MS entre le pôle riche en Na (saumure sodique) et le pôle riche en Ca, Mg et K (saumure calcique) ([Figure 4.6](#)) atteste de mélanges entre les deux saumures dans tous les gisements étudiés. Ce mélange se produit dans les zones de piégeage des fluides, ce qui atteste d'un manque d'homogénéisation des fluides à l'échelle des gisements.

Les conditions de température et de pression pour le mélange des saumures sont partiellement révisées pour tous les gisements par rapport au modèle de McArthur River. En comparaison des nouveaux gisements étudiés, les inclusions fluides représentatives de la saumure sodique ont des températures d'homogénéisation (Th) anormalement élevées. Ceci est attribué à la contamination possible des saumures de McArthur River par de l'hydrogène issu de la radiolyse de l'eau. Cette contamination est probablement plus importante à McArthur River en raison des teneurs en U exceptionnelles.

Un nouveau modèle de conditions de pression et température pour le mélange des fluides est proposé, dans lequel les deux saumures ont la même température de  $150 \pm 30^\circ\text{C}$  (mélange isotherme). Les conditions de pression pour le mélange fluctuent entre régime lithostatique (800 à 1500 bars) et régime hydrostatique (300 à 500 bars) ce qui explique la grande variabilité des Th pour les deux saumures. Ce mélange est contemporain des minéralisations ([Figure 4.9](#)).

Les gisements strictement encaissés dans les socles (Eagle Point, P-Patch, Millennium) semblent se former dans les mêmes conditions de pression et température, et en présence des mêmes saumures que les autres gisements (McArthur River, Rabbit Lake, Shea Creek).

La base du Bassin de l'Athabasca ainsi que le toit du socle ont probablement constitué un aquifère géant unique, ce qui a favorisé la percolation dans le socle de saumures de bassin et le mélange entre saumures sodiques et calciques dans le socle, un paramètre essentiel dans la formation des gisements d'uranium de type discordance.



## **5. Uranium concentration in ore fluids: A LA-ICP-MS study of fluid inclusions in unconformity-related U deposits**

Antonin Richard<sup>1</sup>, Michel Cathelineau<sup>1</sup>, Marie-Christine Boiron<sup>1</sup>, David A. Banks<sup>2</sup>, Julien Mercadier<sup>1</sup>, Michel Cuney<sup>1</sup>

Article in preparation for *Geochimica et Cosmochimica Acta*

<sup>1</sup>G2R, Nancy-Université, CNRS, CREGU, Boulevard des Aiguillettes B.P. 239, F-54506, Vandoeuvre-lès-Nancy, France

<sup>2</sup>School of Earth and Environment, University of Leeds, Leeds LS2 9JT, UK

### **Abstract**

Uranium concentrations in ore fluids from five unconformity-related U deposits of the Athabasca Basin, Canada, were determined by laser-ablation inductively-coupled-plasma mass-spectrometry analysis of individual fluid inclusions. Two types of diagenetic brines are involved in the mineralizing process: a NaCl-rich brine and a CaCl<sub>2</sub>-rich brine, both close to or at halite saturation, and circulating at temperature of ca. 150 ± 30°C. The two brines exhibit wide range of U concentrations from < 1 ppm to > 100 ppm in all studied deposits. After petrographic considerations and analysis of the distribution of U concentrations, the results are interpreted in terms of spent-ore fluids (U < 1 ppm), pre-ore fluid (1 < U < 100 ppm) and remobilization fluid (U > 100 ppm). The pre-ore NaCl-rich brine appears to have predominantly U concentration between 1 and 10 ppm while the pre-ore CaCl<sub>2</sub>-rich brine is slightly enriched with U concentration ranging from 10 to 100 ppm. This result probably reflects differential flow path and availability or leachability of U-bearing source minerals. The observed heterogeneous U concentrations in ore fluids are considered to result from

leaching of a proximal source, the Athabasca Basement being the best candidate. U concentrations in ore fluids from unconformity-related U deposits are among the highest recorded in the literature so far for crustal fluids. U concentrations reflect the exceptional solubility of U in high salinity chlorinated diagenetic brines and an abundant available U source, which is likely to be the Athabsaca Basement. High grade U deposits of the Athabasca Basin have formed from exceptionally U-rich fluids.

## 5.1. Introduction

The determination of metal concentration in mineralizing fluids is of crucial importance for the understanding of ore-forming processes including source leaching, metal transport and ore deposition (Yardley, 2005). Despite increasing knowledge of metal concentration in crustal fluids and ore fluids in particular, U concentrations in U mineralizing fluids have not been measured directly in individual fluid inclusions so far. The only exception is a pioneer work by Philippot et al., (2000) in which U was detected from synchrotron radiation X-ray fluorescence (SXRF) analysis of fluid inclusions from the Streltsov U deposit, Russia. However, the calculated U concentrations of several wt.% were considered as anomalously high probably due to the presence of a U-bearing solid phase in the inclusions.

Laser microprobe noble gas mass spectrometry (LMNGMS) (Irwin and Reynolds, 1995; Irwin and Roedder, 1995), and SXRF (Bühn and Rankin, 1999) analyses of individual fluid inclusions have permitted to determine U concentrations up to ca. 100 ppm in various magmatic hydrothermal and metamorphic palaeofluids. Recent developments in laser-ablation inductively-coupled-plasma mass-spectrometry (LA-ICP-MS) analysis of individual fluid inclusions have permitted to establish accurate metal concentrations in paleofluids, with limits of detection (LODs) close to 1 ppm for a majority of metals (Heinrich et al., 2003). To date, no LA-ICP-MS studies were devoted to uranium or uranium deposits. However, U concentrations ranging from ca. 0.1 to 100 ppm were determined in magmatic-hydrothermal

fluids from various granitic intrusions ([Audétat et al., 2000; Audétat and Pettke, 2003; Gagnon et al., 2004; Zajacz et al., 2008](#)).

In this paper, we report the first determination of U concentration in U ore fluids, by LA-ICP-MS analyses of individual fluid inclusions. Five unconformity-related uranium deposits, from the Athabasca Basin, Saskatchewan, Canada, were targeted to investigate the U content of the mineralizing fluids responsible for the formation of the richest U deposits in the world. Although an abundant literature exists on thermodynamics of U-bearing solutions (e.g. [Langmuir, 1978; Grenthe et al., 1992; Shock et al., 1997](#)), little is known on the behaviour of U in high salinity and ca. 150-200°C brines such as those thought to be mineralizing fluids in the Athabasca Basin. Thus, analyses of uranium concentration in studied fluid inclusions were compared with data from crustal fluids, including basinal formation waters, spring waters, mid ocean ridge fluids, thermal springs, granite groundwaters, metamorphic and magmatic hydrothermal fluids.

## 5.2. Analytical methods

LA-ICP-MS analysis of fluid inclusions from nine quartz veins samples was carried out at the School of Earth and Environment, University of Leeds at instrumental conditions reported in [Allan et al., \(2005\)](#). Analytical procedures for LA-ICP-MS analysis and data reduction are shown in [Part 4](#).

## 5.3. Results

### 5.3.1. Data quality

The majority of quartz matrix analyses showed no U in the host mineral. Although, some randomly distributed U-rich quartz domains and surface contamination were identified, this problem appears to be considerably reduced compared to McArthur River mineralized samples ([Part 3](#)). Also, because of the heterogeneous distribution of U-rich quartz domains even at the scale of several microns, it was almost impossible to apply a reliable matrix correction when U was suspected. Therefore, analyses of fluid inclusions where U was obviously present in the matrix (i. e. when U signal increases before major element signals or when U signal shows no correlation with major element signal during ablation of fluid inclusions) were systematically discarded. [Figure 5.1](#) shows typical time-resolved LA-ICP-MS signals with no visible U in the quartz matrix, for three inclusions with three orders of magnitudes of calculated U concentrations. When the first increase in the U signal corresponds to the first increase of the major element signals, and when a rather positive relationship between U and major elements signal was observed, as shown in [Figure 5.1](#), the analyses were considered as reliable without matrix correction. However, we cannot exclude that some of the U concentrations presented here may be the result of local contamination. Nevertheless, we consider that the whole of the dataset is representative of the distribution of U concentrations in the investigated ore fluids.

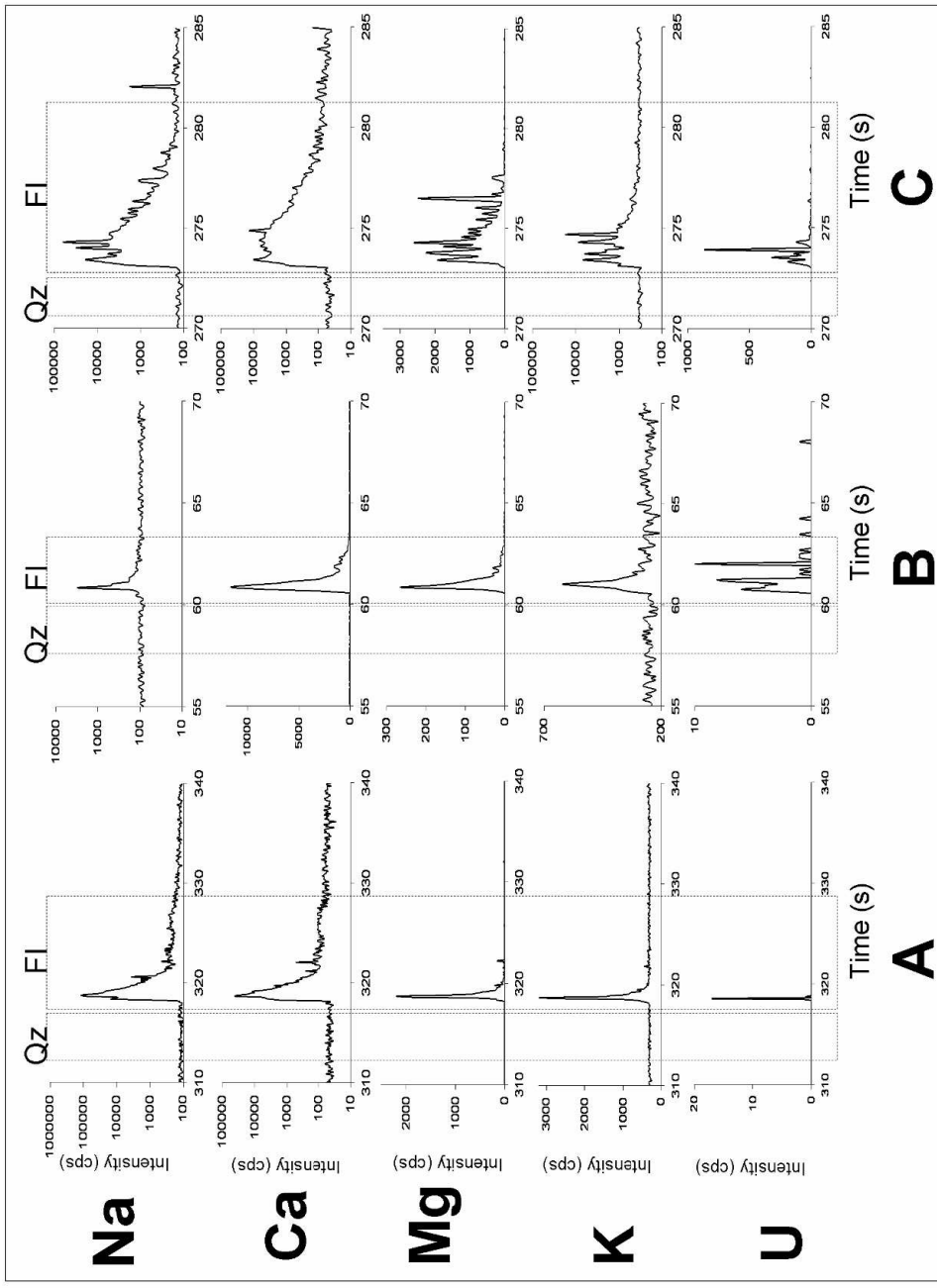


**Figure 5.1 :** Time-resolved LA-ICP-MS response for Na, Ca, Mg, K and U signals. Dashed windows show quartz signal (Qz) during quartz ablation, and fluid inclusion signal (Fl). These spectra suggest that U is nearly absent from quartz and entirely fluid inclusions-hosted, as no U signal is observed during quartz ablation prior Na-Ca-Mg-K shift (i.e. opening of fluid inclusion). Inclusion A returns 3.9 ppm U, inclusion B returns 35 ppm U, inclusions C returns 226 ppm U.

### 5.3.2. U in fluid inclusions.

Among the 205 inclusions with reliable U signal (i.e. no matrix contamination, no problem during ablation), 136 have U concentrations above limit of detection (LOD). LODs vary as a function of inclusion size and therefore of the signal intensity, and are comprised between 0.2 and 50 ppm, most of them being lower than 1 ppm. The calculated U concentrations range from 0.2 to 612 ppm. Large variations in U concentrations in all deposits and in the both NaCl-rich and CaCl<sub>2</sub>-rich brines preclude any relevant calculation of average concentrations and standard deviations. Therefore, distributions of uranium concentrations are presented in frequency histograms ([Figure 4](#)).

The majority of fluid inclusions contain between 10 and 100 ppm of U. U concentrations vary within four orders of magnitudes in all the five studied deposits. The distribution of U concentration in fluid inclusions varies from one deposit to another. Maximum observed values range from 1 to 10 ppm for the Rabbit Lake and Millennium deposits, and from 10 to 100 ppm for the Eagle Point and P-Patch deposits ([Figure 5.2](#)).

There are two possibilities for U distribution in fluid inclusions. Either U is dissolved in the liquid phase or is precipitated as daughter uraninite phase, and forms of a uraninite layer on the walls of the inclusions or uraninite cubes. From analysis of transient LA-ICP-MS signals, the presence a homogeneous uraninite layer on the wall of the inclusions cannot be ruled out ([Figure 5.1](#)). However, this would not affect the calculated U concentrations because a uraninite layer represents dissolved U at the time of trapping. Model calculation from [Phillipot et al., \(2000\)](#) indicate that in the case of complete U precipitation, the diameter of an uraninite solid daughter phase would not be higher than 0.5µm even for a 20µm large inclusion with 100 ppm U. This roughly corresponds to maximum optical microscope resolution. In the case of uraninite precipitation in the wall of the fluid inclusions, the uraninite layer would hardly be thicker than 10<sup>-2</sup> µm. Thus, in both cases there is theoretically almost no chance to see any optically visible uraninite phase in the investigated fluid inclusions.

Further synchrotron X-ray imaging of such fluid inclusions could definitely help understanding U distribution in fluid inclusions.

### **5.3.3. NaCl-rich vs. CaCl<sub>2</sub>-rich brine**

NaCl-rich brine inclusions have maximum observed U concentrations comprised between 1 and 10 ppm for the McArthur River, Rabbit Lake and Millennium deposits, and from 10 to 100 ppm for the P-Patch and Eagle Point deposits. CaCl<sub>2</sub>-rich brine inclusions have maximum observed U concentrations comprised between 1 and 10 ppm for the Rabbit Lake and Millennium deposits, and from 10 to 100 ppm for the P-Patch and Eagle Point deposits. Considering all the deposits, the NaCl-rich brine inclusions have maximum observed U concentrations between 1 and 10 ppm while the CaCl<sub>2</sub>-rich brine have maximum observed U concentrations between 10 and 100 ppm. This could suggest that the CaCl<sub>2</sub>-rich brine is enriched in U compared to the NaCl-rich brine. The difference in the average U concentration between the two brines is below one order of magnitude.

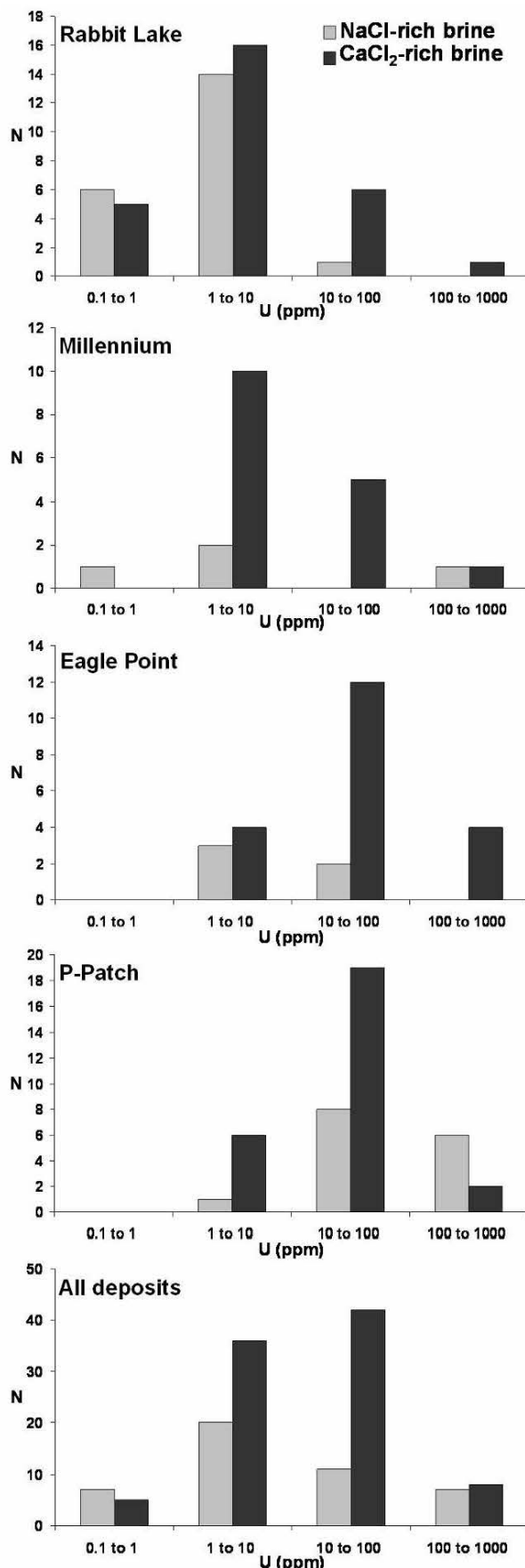


**Figure 5.2: Distribution of uranium concentration in fluid inclusions analyzed by LA-ICP-MS. Only orders of magnitude are indicated due to analytical uncertainties, and heterogeneous distributions.**

## 5.4. Discussion

### 5.4.1. Comparison with crustal fluids

[Figure 5.3](#) shows the range of U concentrations measured in various present-day fluids and palaeofluids sampled as fluid inclusions. U concentrations in the 1 to 100 ppm range are restricted to high temperature and high salinity magmatic-hydrothermal fluids or metamorphic fluids. Low temperature granite groundwaters do not carry more than 1 ppm U. U concentration in thermal springs, mid ocean ridge fluids, basinal formations waters and river waters rarely exceeds 0.01 ppm. In subsurface oxidized waters and in the presence of high U background in the environment, abnormal U concentrations in the 1 to 10 ppm range are reported in some cases (Chardon U mine, [Beaucaire et al., 1999](#), and present-day Athabasca Basin groundwaters, [Earle et al., 1983](#)) which can be explained by the high solubility of U(VI) minerals, although in the absence of ultrafiltration, the presence of U-bearing colloids cannot be ruled out. This means that the U concentrations measured here are anomalously high for relatively low temperature fluids, which suggests an exceptional solubility of pitchblende in these brines.

Evaporation of seawater beyond halite saturation is proposed to be one the dominant mechanism for acquisition of high salinities in the Athabasca and Kombolgie uranium ore fluids ([Derome et al., 2005; Derome et al., 2007, Part 6](#)). U concentration the parent brine is unknown. Simple calculation assuming 3.3 ppb U in the Mesoproterozoic seawater (as for present-day seawater) and an evaporation rate of 65x, which corresponds to the end of halite precipitation ([Knauth and Beeunas, 1986](#)), and negligible incorporation or adsorption of U into evaporitic minerals, leads to a residual brine with ca. 0.2 ppm U. This broadly corresponds to the lowest measured U concentrations in the brines studied here, and lowest LOD for U from LA-ICP-MS analysis. This means the 0.2 ppm U could be considered as a minimum U content of the ore fluids, provided that no U precipitation has occurred before unconformity-related U mineralization.

The high U content in the studied paleofluids may result from combined factors: (1) The high solubility of potential U-bearing source minerals such as uraninite and monazite in presence of high-chlorinity brines, under the oxidizing redox conditions which have prevailed during U transport as shown by the common occurrence of hematite within the brine inclusions. (2) The availability of the U-bearing minerals that could potentially provide U during alteration by the brines (3) The efficiency of uranyl complexation by chlorides under slightly acidic pH as suggested by [Kister et al., \(2005\)](#).

In addition, these results are compatible with results of numerical modelling of groundwater flow, heat transport and hydrogeochemical modelling ([Raffensberger and Garven, 1995a, 1995b](#)), who stated that U mineralizing fluids should contain 20 to 30 ppm U, predominantly in the form of uranyl-chloride complexes, to produce large unconformity-related U deposits within 0.1 to 1 Ma.

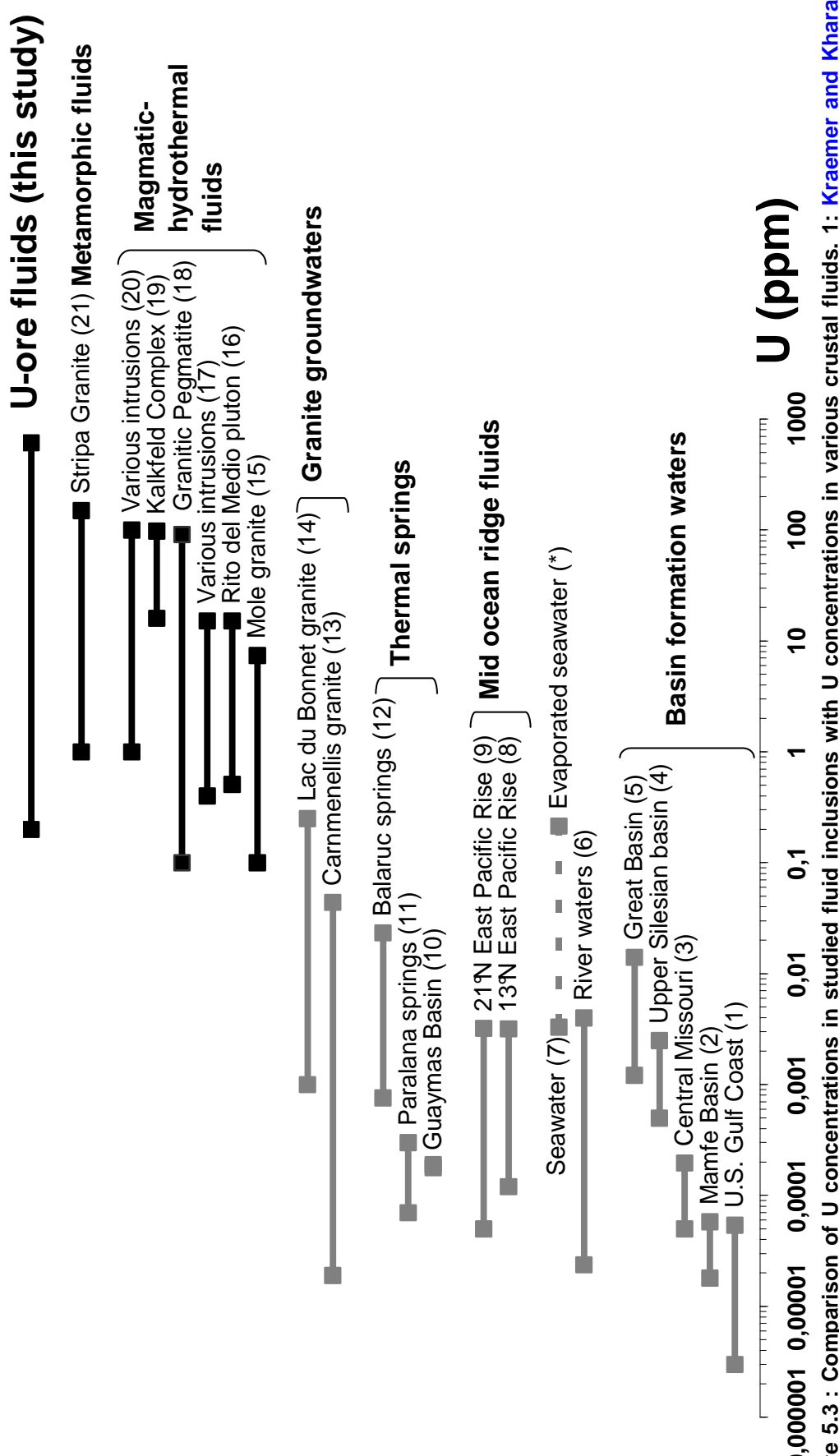


Figure 5.3 : Comparison of U concentrations in studied fluid inclusions with U concentrations in various crustal fluids. 1: Kraemer and Kharaka (1986). 2: Eseme et al., (2006). 3: Banner et al., (1990). 4: Pluta and Zuber (1995). 5: Hodge et al., (1996). 6: Palmer and Edmond (1993). 7: Ku et al., (1977). (\*): Calculated U concentration in evaporated seawater assuming an evaporation ratio of 65x (halite facies, Knauth and Beeunas, 1986) and negligible incorporation of U in evaporitic minerals. Dashed line represents seawater evaporation trend. 8: Michard et al., (1983). 9-10: Chen et al., (1986). 11: Brugger et al., (2005). 12: Aquilina et al., (2002). 13: Edmunds et al., (1987). 14: Gascoyne (2004). 15: Audébat et al., (2000). 16: Audébat and Pettke (2003). 17: Zajacz et al., (2008). 18: Gagnon et al., (2004). 19: Bünn and Rankin (1999). 20: Irwin and Reynolds (1995). Grey bars refer to present-day fluids and black bars refer to paleofluids sampled as fluid inclusions.

#### **5.4.2. Spent-ore, pre-ore, or remobilization fluids?**

The wide distribution of U concentration in fluid inclusions may be attributed to the heterogeneity of U concentration in the pre-ore mineralizing fluids, or alternatively to sampling of pre-ore, spent-ore, and remobilization fluids ([Klemm et al., 2007](#)). At McArthur River, quartz veining occurs before and after the main U mineralization event and some of the inclusions presented here may represent late-ore fluids (i.e. hydrothermal pitchblende was already present in the environment). For the Rabbit Lake, Eagle Point, P-Patch and Millennium deposits, quartz veining is mostly considered as immediately preceding the ore stage ([Alexandre et al., 2005; Mercadier et al., in press](#)), although an older ore stage could have occurred ([Alexandre et al., 2009a](#)). Therefore, potential leaching of previously precipitated pitchblende, and potential trapping of fluids that lost their uranium through uraninite precipitation, have to be considered for further interpretation. Thus, some of the U content of fluid inclusions may not be fully representative of pre-ore fluids and the high U concentrations (ca. > 100 ppm) could be interpreted as the result of U remobilization. If this is the case, although high U content are not attributed to the pre-ore fluids, this would reflect the high solubility of pitchblende in these brines. Conversely the lowest U concentration (0.2 to ca. 1 ppm) could represent spent-ore fluids. However, ca. 80% of the measured U concentrations lies in the 1 to 100 ppm range. A rather preservative interpretation of this is that U concentrations in the 1-100 ppm range are representative of the pre-ore fluids.

#### **5.4.3. Significance for uranium source(s)**

The U source of unconformity-related deposits is still debated. For some authors, U is leached by oxidizing diagenetic brines from accessory minerals in the basin ([Fayek and Kyser, 1997](#)), but the initial U content in oxidized Paleoproterozoic clay-poor continental sandstones and U-bearing accessory minerals is probably very low ([Cuney, 2005](#)). Conversely, the basement contains a large variety of U sources. Uraninite, an easily

leachable U source is found in some pegmatites (Annesley and Madore, 1999; Madore et al., 2000), and as pre-Athabasca U mineralizations (Parslow and Thomas, 1982). In addition, monazite, one of the most refractory U-bearing minerals, is deeply altered up to its complete dissolution and replacement by aluminium phosphates-sulphate minerals or carbonates, this resulting in the U release (Hecht and Cuney, 2000). Basinal formation waters in particular are among the most U-depleted crustal fluids (Figure 5.3). This would mean that the studied brines were probably U-poor before percolation in the basement with a maximum possible value of 0.2 ppm acquired during seawater evaporation. High U concentrations are thus much better explained by fluid-rock interaction with basement lithologies.

Differential flow path between the NaCl-rich and the CaCl<sub>2</sub>-rich brines is necessary to account for the large differences of Na-Ca-Mg-K-Sr-Ba chemistry (Derome et al., 2005; Part 3; Part 4). The CaCl<sub>2</sub>-rich brine is interpreted as the results of deep percolation in the basement whereas the NaCl-rich brine is thought to have less interacted with basement rocks. If the basement is considered as a potential U source, the fact that the CaCl<sub>2</sub>-rich brine has percolated through large volumes of previously unaltered basement rocks would favour high average U concentration.

Finally, the heterogeneity of U concentrations in the ore fluids is better explained by leaching of a proximal source by both brines, incomplete homogenization of U concentration in both brines, and mixing of the two brines before and during U mineralization. Leaching of U in the basin would probably result in a homogeneous U content as the basal sandstones of the Athabasca Basin can be considered as a giant aquifer (Part 4). Thus, we support the hypothesis of the Athabasca Basement as a dominant U source in Canadian unconformity-related deposits.

## 5.5. Conclusion

The main conclusions of this study are the following:

- (1) LA-ICP-MS analyses of individual fluid inclusions from the four studied unconformity-related deposits revealed that dissolved U is present in measurable amounts (0.2 to ca. 600 ppm) in most fluid inclusions.
- (2) The two main fluids investigated, a NaCl-rich brine and a CaCl<sub>2</sub>-rich have comparable U content, the CaCl<sub>2</sub>-rich brine being slightly enriched. Both fluids are involved in the U leaching and transport processes.
- (3) Although we can not exclude that the highest measured U concentrations are the result of remobilization of primary mineralization, and that the lowest observed U concentrations indicate spent-ore fluids, we suggest that the pre-ore mineralizing brines have highly heterogeneous U concentrations (from ca. 0.2 to ca. 100 ppm).
- (4) This heterogeneity is interpreted as the result of leaching of a proximal U source. The Athabasca Basement being probably the dominant U source.
- (5) Comparison with various crustal fluids indicates that the analyzed fluids have exceptionally high U content, well above all recorded basinal fluids. This reveals the exceptional solubility of pitchblende in these NaCl-rich and CaCl<sub>2</sub>-rich diagenetic brines and the availability of an abundant U source, two key parameters for the formation of giant unconformity-related U deposits.
- (6) More generally, these results are compatible with the idea that hydrothermal ore deposits are generated by anomalously metal-rich fluids, as suggested from LA-ICP-MS analysis of fluid inclusions from MVT and Irish-type Pb-Zn deposits ([Wilkinson et al., 2009](#)).

## **Version abrégée**

Les concentrations en uranium dans les inclusions fluides des gisements de Rabbit Lake, Eagle Point, P-Patch et Millennium, ont été mesurées par analyse en ablation laser couplée à la spectrométrie de masse (LA-ICP-MS).

Le choix d'échantillons non minéralisés pour ces analyses a permis de diminuer considérablement les problèmes liés à la contamination de surface en U, et à la présence de domaines de quartz riches en U, par rapport aux analyses réalisées à McArthur River.

Les inclusions fluides représentatives des deux saumures présentent des concentrations qui varient selon quatre ordres de grandeurs (env. 0.2 à env. 600 ppm) ([Figure 5.2](#)).

Après analyse de la distribution des concentrations en uranium dans les saumures, les résultats sont interprétés en termes de fluide minéralisateur, fluide anté-minéralisation (ayant précipité l'U) et fluide de remobilisation (ayant solubilisé de la pechblende déjà existante).

Les saumures minéralisatrices sodiques et calciques avaient des concentrations en U comprises entre 1 et 10 ppm pour la saumure sodique, et entre 10 et 100 ppm pour la saumure calcique. La saumure minéralisatrice calcique est donc en moyenne enrichie en uranium par rapport à la saumure minéralisatrice sodique (un ordre de grandeur d'enrichissement moyen au maximum). Les saumures minéralisatrices ont donc des concentrations en U très hétérogènes.

Par comparaison avec des concentrations en uranium dans divers fluides crustaux échantillonnés par forage ou comme inclusions fluides, les concentrations en uranium mesurées dans les saumures sodiques et calciques sont exceptionnellement élevées. Les seuls fluides connus ayant des concentrations supérieures au ppm sont des saumures de haute température associées à l'activité magmatique-hydrothermale d'intrusions granitiques ([Figure 5.3](#)).

Les fluides de bassins contiennent très rarement plus de 0.01 ppm d'uranium et sont en général les fluides crustaux les moins concentrés. Les saumures sodiques et calciques ont donc des concentrations en uranium totalement anormales pour des fluides de bassin.

Si l'évaporation de l'eau de mer au-delà de la saturation vis-à-vis de la halite est une origine possible pour ces saumures, une saumure évaporitique primaire pourrait contenir jusqu'à 0.2 ppm d'uranium si ce dernier n'est pas incorporé dans les minéraux évaporitiques pendant leur précipitation. Cette valeur correspond aux limites de détection les plus basses pour ces analyses. Il est donc possible que la concentration minimale en uranium des saumures minéralisatrices soit proche de 0.2 ppm.

Les concentrations en uranium très hétérogènes peuvent s'expliquer par le lessivage de sources très proximales par les deux saumures et une homogénéisation incomplète des concentrations en uranium. Les concentrations en uranium des saumures sont donc expliquées par l'interaction des saumures avec les sources potentielles d'uranium du socle (monazite, uraninite magmatique, minéralisations pré-Athabasca).

Les fortes concentrations en uranium dans les inclusions fluides étudiées peuvent résulter de la combinaison des facteurs suivants : (1) la présence de minéraux sources d'uranium, (2) la solubilité élevée des minéraux sources de l'uranium, comme la monazite ou l'uraninite en présence de saumures chlorurées en conditions oxydantes, (3) l'efficacité de la complexation de l'uranyle par les chlorures dans des conditions de pH acides.

L'ensemble des données montre que les gisements d'uranium de type discordance du Bassin de l'Athabasca se sont formés à partir de saumures dont les concentrations en U sont exceptionnelles.

## **6. Multiple origins of chlorine in diagenetic brines from the Athabasca Basin and Basement, Canada: Cl/Br and $\delta^{37}\text{Cl}$ analysis of fluid inclusions.**

Antonin Richard<sup>1</sup>, David. A. Banks<sup>2</sup>, Julien Mercadier<sup>1</sup>, Marie-Christine Boiron<sup>1</sup>, Michel Cathelineau<sup>1</sup>, Michel Cuney<sup>1</sup>

Article in preparation for *Geochimica et Cosmochimica Acta*

<sup>1</sup>G2R, Nancy-Université, CNRS, CREGU, Boulevard des Aiguillettes B.P. 239, F-54506,  
Vandoeuvre-lès-Nancy, France

<sup>2</sup>School of Earth and Environment, University of Leeds, Woodhouse Lane, Leeds, LS2 9JT,  
UK

### **Abstract**

Halogen and stable chlorine isotope analyses of fluid inclusions from quartz and carbonate veins, spatially and temporally associated to giant unconformity-related uranium deposits from the Athabasca Basin (Canada) were performed in order to determine the origin of chlorine in diagenetic brines. Molar Cl/Br ratios of mineralizing diagenetic brines range from ca. 100 to 800 and could have been acquired from two competing processes: (1) Surface evaporation of seawater beyond halite saturation (primary brine). (2) Mixing between a primary brine and a secondary brine derived from dissolution of evaporites. Slight dilution along their flow path is likely to have lowered the chlorinity of the resulting brines, without modifying Cl/Br ratios.  $\delta^{37}\text{Cl}$  values predominantly range between -0.6 and 0‰ and are compatible with evaporated seawater. The overall dispersion of  $\delta^{37}\text{Cl}$  values can be partly attributed to variable degree of mixing with secondary brines and by percolation of brines

through low porosity basement rocks and/or biotite dissolution. The Cl in Athabasca Basin diagenetic brines has thus a dominant marine origin and probably a minor non-marine component resulting from interaction between basinal brines and basement rocks, a key factor for the formation of unconformity-related uranium deposits.

## 6.1. Introduction

Cl/Br ratios and  $\delta^{37}\text{Cl}$  compositions have been widely used as tool for determining the origin of salinity in various present-day and ancient crustal fluids (e.g. Carpenter et al., 1974; Böhlke and Irwin, 1992; Eastoe and Guilbert, 1992; Fontes and Matray, 1993a; Banks et al., 2000a, 2000b; Nahnybida et al., 2009). The main reason for this is that Cl and Br are generally conservative in solution and are rarely incorporated in mineral phases except for Cl in evaporitic minerals. Thus, if Cl is the main anion in solution, Cl/Br and  $\delta^{37}\text{Cl}$  systematics of any given fluid should reflect the mechanism(s) of acquisition of its salinity. In diagenetic environments, Cl is the dominant anion of basinal brines and if multiple mechanisms can potentially fractionate Cl/Br ratios, Cl and Br are considered to be conservative (Fontes and Matray, 1993a; Worden, 1996). Cl from basinal brines has generally a marine origin and chlorinity variations are mostly interpreted in terms of seawater evaporation, dissolution of evaporites and dilution by meteoric waters or seawater (Hanor, 1994).

Chlorine is an important metal-complexing agent in crustal fluids (Yardley, 2005). Numerous basin-hosted mineral deposits are thought to have formed from high chlorinity basinal brines where Cl could have helped to transport metals as for Cu-Co from Zambian Copper Belt deposits (McGowan et al., 2006), Pb-Zn from MVT (Kesler et al., 1995) and extension-related deposits (Muchez et al., 2005), or Ag-Co from Bou-Azzer deposits, Morocco (Essaraj et al., 2005) among other examples. Thus, the origin of Cl in mineralizing fluids is of crucial importance for metallogenetic models.

Here, we present Cl/Br and  $\delta^{37}\text{Cl}$  systematics of diagenetic brines from the Mesoproterozoic Athabasca Basin, Saskatchewan, Canada. These 30-40 wt% eq. NaCl and

$150\pm30^{\circ}\text{C}$  diagenetic brines are thought to have circulated over large distances at the basement-cover interface ([Kyser et al., 2000; Part 4](#)). Along their migration path, brines underwent significant fluid-rock interactions with basin and basement lithologies and have mobilized large quantities of metals and notably U ([Part 5](#)). U was then deposited as giant unconformity-related uranium deposits ([Jefferson et al., 2007](#)). These brines are commonly sampled as fluid inclusions in quartz overgrowths in basin sandstones or in quartz-carbonate veins crosscutting basin sandstones or basement rocks. Microthermometry, LIBS, Raman and LA-ICP-MS analyses of these fluid inclusions showed that the chemistry of the brines range from  $\text{Na} > (\text{Ca} + \text{Mg})$  composition (NaCl-rich brine) to  $\text{Ca} + \text{Mg} > \text{Na}$  composition ( $\text{CaCl}_2$ -rich brine). Large variations in Na-Ca-Mg-K-Sr compositions were interpreted as resulting from mixing process between a NaCl-rich and a  $(\text{Ca}, \text{Mg})\text{Cl}_2$ -rich end-member ([Derome et al., 2005; Part 3](#)). Both brines show important salinity variations in the 20-40 wt% eq. NaCl range, the  $\text{CaCl}_2$ -rich brine being generally more saline than the NaCl-rich brine.

[Pagel and Jaffrezic \(1977\)](#) used atomic absorption to obtain Cl/Br of fluid inclusion leachates from quartz and dolomite veins from the Rabbit Lake deposit. They found molar Cl/Br ratios ranging from 110 to 160. [Pagel and Jaffrezic \(1977\)](#) and [Pagel et al., \(1980\)](#) pointed out the lack of evaporites in the area and interpreted these low Cl/Br ratios as resulting from catagenesis of organic matter, Br being easily substituted to hydrogen in organic compounds. More recently, [Derome et al., \(2005\)](#) used crush-leach techniques to show that fluid inclusions leachates from the McArthur River deposit containing either both NaCl-rich and  $\text{CaCl}_2$ -rich brine inclusions or only NaCl-rich brine inclusions have molar Cl/Br ratios ranging from 120 to 220. These values are comparable with measurements from [Pagel and Jaffrezic \(1977\)](#) but the authors argued that catagenesis of organic matter has not proved to be capable of fractionating Cl/Br ratios. Finally, they interpreted the low Cl/Br ratios as resulting from evaporation of seawater beyond halite saturation, and stated that both brines share a common evaporated seawater origin.

The origin of high chlorinities was discussed on the basis off stable isotope (O, H) composition of alteration minerals. However, O and H isotopes do no behave conservatively

in hydrothermal systems and speculations on the origin of high chlorinities based on O and H isotopes of alterations minerals only are highly questionable. [Bray et al., \(1988\)](#) suggested that  $\delta^{18}\text{O}$  and  $\delta\text{D}$  compositions of the fluids in equilibrium with alteration minerals are incompatible with evaporation of seawater. The authors concluded that high chlorinities were acquired by evaporite dissolution and that diagenesis of organic matter in shales could account for low Cl/Br ratios determined by [Pagel and Jaffrezic \(1977\)](#). Similarly, [Kotzer and Kyser \(1995\)](#) concluded that the brines have a significant meteoric water component and that high chlorinities were achieved by evaporite dissolution and reaction with feldspars. However, based on comparable isotopic analyses, [Alexandre et al., \(2005\)](#) stated that the brines result from mixing between evaporated seawater and low-latitude meteoric waters.

To further test these hypotheses, we have targeted five unconformity-related U deposits (McArthur River, Rabbit Lake, Eagle Point, P-Patch and Millennium) located in various parts of the Athabasca Basin. Sampling was essentially focussed on basement samples because fluid-rock interactions in basement rocks are thought to have drastically affected brines compositions.

It is noteworthy that in their pioneer work on  $\delta^{37}\text{Cl}$  variations of fluids in hydrothermal systems, [Eastoe and Guilbert \(1992\)](#) mentioned the potential usefulness of stable chlorine isotopes to ascertain the origin of high salinity brines in the Athabasca Basin. Since then, no study was undertaken in this direction. Because Cl is by far the most important anion the high salinity Athabasca Basin brines and is suspected to be the main U-complexing agent ([Raffensperger and Garven, 1995a, 1995b](#)), we attempted to answer the following questions:

- (1) What is the process at the origin of high Cl concentrations in the Athabasca brines?
- (2) Is there a difference in the origin of Cl between the NaCl-rich and CaCl<sub>2</sub>-rich brines?
- (3) What can explain the slight but systematic differences of bulk salinities (chlorinities) between the NaCl-rich and CaCl<sub>2</sub>-rich brines?
- (4) Is there any evidence for non-marine Cl input (i.e. Cl from biotites-amphiboles) in the Athabasca brines?

## **6.2. Analytical methods**

### **6.2.1. Crush-leach analysis**

Cl, Br, F and SO<sub>4</sub> concentrations were determined using the bulk crush-leach technique described in Banks and Yardley, (1992); Banks et al., (2000b) and Gleeson (2003) at the School of Earth and Environment, University of Leeds, UK. Quartz and carbonate veins were crushed to a grain size fraction of 1–2mm. Pure mineral separates were then picked under a binocular microscope and placed in a ultrasonic bath for 1 hour. Then samples were cleaned by boiling them twice in double distilled water. Cleaned quartz and carbonate grains (0.5 to 1.5g) were then crushed to a fine powder in an agate pestle and mortar and leached in 5-6ml of double distilled water. Fluid inclusions leachates were analyzed for F, Cl, Br, and SO<sub>4</sub> with a Dionex DX-500 ion chromatograph. The detection limits for the anions in fluid inclusion leachates was ca. 0.003 ppm. Cl/Br ratios are quoted with an error of ± 25%. The average Cl content of fluid inclusions was estimated from the average salinity determined from microthermometry ([Part 4](#)). This Cl concentration from was corrected from F, Br and SO<sub>4</sub> contributions by combining with Cl/Br, Cl/F and Cl/SO<sub>4</sub> ratios to calculate absolute Cl, Br, F, and SO<sub>4</sub><sup>2</sup> concentrations in fluid inclusions following the equation of Banks et al., (2000b). Analyses of cations in fluid inclusion leachates are presented in [Part 7](#).

### **6.2.2. Stable chlorine isotope analysis**

A minimum 0.1mg of Cl is necessary for successful δ<sup>37</sup>Cl determination. Only fluid inclusion leachates containing more than 0.1mg of Cl could have been analyzed for stable chlorine isotopes. Cl was isolated as pure AgCl precipitates by addition of 4ml of 1M AgNO<sub>3</sub> and 2ml of 5% (v/v) HNO<sub>3</sub>, heating to 85°C on a hot plate, and addition of 1 ml 0.5M AgNO<sub>3</sub>. Stable chlorine isotopes analyses, via continuous-flow isotope ratio mass spectrometry, were

carried out at the Stable Isotope Hydrology and Ecology Laboratory of Environment Canada in Saskatoon, Saskatchewan, following the methodology described [Wassenaar and Koehler, \(2004\)](#). The  $\delta^{37}\text{Cl}$  values were obtained using a multicollector GV Instruments Isoprime<sup>TM</sup> IRMS. Values of  $\delta^{37}\text{Cl}$  are reported in standard per mil (‰) notation relative to SMOC (Standard Mean Ocean Chlorine) and are quoted with an error of  $\pm 0.06\text{\textperthousand}$ .

### **6.2.3. Cl concentration in rocks and minerals**

Cl content and loss on ignition (L.O.I.) of fresh and altered pegmatites (P-Patch deposit) and porphyry granites (Eagle Point deposit) were determined from whole-rock geochemical analysis (SARM-CRPG, Nancy, France). In order to take into account the density modifications linked to hydrothermal alterations and to compare the samples at constant volume (i.e. to avoid the cavity volume), a density correction is applied to all the altered samples, using the reference density of the freshest sample for each lithology. If  $d_1$  and  $d_2$  are the densities of the altered and freshest sample respectively, element concentrations of the altered sample are multiplied by  $d_1/d_2$ . These new concentrations allow proper comparison of samples with different alteration degrees ("constant volume" correction).

Cl concentrations in biotites from fresh porphyry granites (Eagle Point deposit) and illite and sudoite from altered porphyry granites (Eagle Point deposit) were measured by electron microprobe CAMECA SX100 (SCMEM laboratory, Nancy, France).

## 6.3. Results

### 6.3.1. Two brines with contrasted chlorinities

Microthermometric observations from [Derome et al., \(2005\)](#) and [Part 4](#) have shown that, samples analyzed here contain variable proportions of both brines ([Table 6.1](#)). These observations must be considered with caution because representativity of microthermometric analyses is always questionable. Cl concentrations in fluid inclusion leachates are controlled by the average concentrations of the fluid inclusions from the related sample. After microthermometric data from [Derome et al., \(2005\)](#) and [Part 4](#), Cl concentrations in NaCl-rich brine inclusions range from 120000 to 180000 ppm and are centred on 150000 ppm which corresponds to the Cl concentration of evaporated seawater from the beginning of halite precipitation to the beginning of epsomite precipitation ([Fontes and Matray, 1993a](#)). CaCl<sub>2</sub>-rich brine inclusions have Cl concentrations ranging from 160000 to 220000 ppm and centred on 190000 ppm which broadly corresponds to evaporating seawater at the beginning of sylvite precipitation stage ([Fontes and Matray, 1993](#)). The majority of calculated Cl concentrations of fluid inclusion leachates which represent various contributions of the two brines fall within the 160000 to 180000 ppm range ([Table 6.1](#)). Further interpretation of Cl/Br and  $\delta^{37}\text{Cl}$  data must take into account the contrasting salinities of the two brines and the fact the analyzed solutions predominantly represent various contributions of the two brines.

### 6.3.2. Cl-Br-F-SO<sub>4</sub> concentrations

[Table 6.1](#) shows average Cl, F, Br and SO<sub>4</sub> concentrations of fluid inclusions in analyzed samples, calculated from microthermometry and crush-leach analyses. Cl ranges from 157000 to 186000 ppm, and is by far the dominant anion. Br ranges from 408 to 7854 ppm. Molar Cl/Br ratios range from 47 to 630 at Eagle Point, 151 to 224 at McArthur River, 333 to 892 at Millennium, 295 to 860 at P-Patch and 127 to 980 at Rabbit Lake. A maximum

of Cl/Br values are centred on 150-350. Cl/Br ratios seem to be heterogeneously distributed in all deposits, and preclude any statistically relevant discrimination of deposits based on Cl/Br ratios. F is frequently below detection limits and, when detected, ranges from 105 to 7400 ppm. SO<sub>4</sub> is also frequently below detection limits and, when detected, ranges from 180 to 8200 ppm. Therefore, the Athabasca brines are nearly pure chloride-salts solutions. Cl, Br, F, and SO<sub>4</sub> concentrations as well as Cl/Br ratios show no relationship with depth below unconformity, host mineral or brine content.

### 6.3.3. Chlorine isotopes

$\delta^{37}\text{Cl}$  values range from -1.08 to +0.79‰ with most values comprised between -0.6 and 0‰ ([Table 6.1](#)). Only 3  $\delta^{37}\text{Cl}$  values are above 0‰. [Figure 6.1](#) shows that all the studied deposits show a mode of  $\delta^{37}\text{Cl}$  values between -0.5 and 0‰. [Figure 6.1B-C](#) shows that  $\delta^{37}\text{Cl}$  values seem to be distributed equally among host minerals and brine contents. A possible positive relation is observed between depth below unconformity and  $\delta^{37}\text{Cl}$  values, and will be discussed below.

### 6.3.4. Cl from basement rocks and minerals

[Table 6.2](#) shows that Cl content of fresh biotites from basement rocks are quite homogeneous and lie in the 3200-4200 ppm range. In altered rocks, biotites are completely altered to illite and sudoite, whose Cl content range from 210 to 340 ppm and 250 to 530 ppm respectively. At the whole rock scale, Cl content of fresh porphyries and pegmatites range from 215 to 343 ppm and from 460 to 1078 ppm respectively. In altered porphyries and pegmatites, Cl ranges from 91 to 207 ppm and from 67 to 298 ppm respectively. The intensity of alteration can be estimated using loss on ignition values (L.O.I.). Fresh rocks have L.O.I. ranging from 1.2 to 1.7wt.% while altered rocks have L.O.I. ranging from 1.5 to 9.4wt.%.

Deposit	Host	Sample	Depth (m)	Brine content	Salinity wt%	Cl (ppm)	Br (ppm)	F (ppm)	SO <sub>4</sub> (ppm)	Cl/Br (molar)	δ <sup>37</sup> Cl (‰)
Eagle Point	Qz	H3042-1	263.5	Na+Ca	30.3	181857	1762	b.d.	b.d.	233	-0.24
		ES287-8	253.2	Na+Ca	28.2	169575	1184	b.d.	n.a.	323	
		ES287-23		n.o.	28.0	165261	592	b.d.	3997	630	
		ES287-10	259.0	Na	28.5	171257	1868	b.d.	b.d.	207	
		EPE44-17	131.2	Na+Ca	28.2	168809	1558	b.d.	696	244	-0.53
		DDH2306-2	135.3	Na+Ca	27.6	159421	627	7436	b.d.	573	
		DDH2306-1	130.0	Na+Ca	29.9	176410	2065	177	2481	193	-0.16
		DDH1733-14	178.5	Na	28.5	163337	7855	729	1204	47	
	Dol	H1935-8	177.9	Na+Ca	31.2	184472	4355	b.d.	373	95	-0.27
		ES287-1	39.9	n.o.	28.0	164165	1259	b.d.	4426	294	-0.41
McArthur River	Qz	MAC5Qz	25	Na+Ca	28.7	170462	2326	b.d.	1368	165	-0.71
		MAC54Qz	50.0	Na	27.5	164142	1655	b.d.	1019	224	
		MAC8Qz		Na+Ca	28.0	166537	1724	b.d.	1589	218	-0.49
		MAC13Qz		Na+Ca	28.0	166250	2479	b.d.	1120	151	-0.4
	Dol	MAC5Carb	25.0	n.o.	28.0	166743	2989	117	n.a.	126	-1.08
Millennium	Qz	CX52-1	99	Na+Ca	29.2	175967	1101	b.d.	n.a.	360	-0.43
		CX48-03	130	Na+Ca	28.1	169552	1147	b.d.	b.d.	333	0.36
		CX44-2	213	Na+Ca	28.0	168807	982	b.d.	b.d.	388	-0.22
		CX48-01-12a	265	Na+Ca	28.0	169421	428	b.d.	b.d.	892	-0.06
P-Patch	Qz	P48-1	59	Na+Ca	26.6	161019	n.a.	b.d.	183	-0.37	
		P48-2	69	Na+Ca	29.9	179582	1273	763	n.a.	318	-0.08
		P48-3Qz	70	Na+Ca	29.4	177390	891	b.d.	b.d.	449	-0.52
		P48-5	82	Na+Ca	27.0	161488	1149	b.d.	1328	317	-0.88
		P54-5	94	Na+Ca	29.8	179844	476	b.d.	206	852	-0.47
		P53-6	96	Na	28.0	169792	n.a.	b.d.	n.a.	-0.06	
		P57-2	134	Na	28.7	166062	n.a.	1076	7018	-0.52	
		P70-1	152	Na	28.4	171440	449	b.d.	326	860	0.79
		P48-3Dol	70	Ca	28.0	168563	1287	b.d.	n.a.	295	-0.45
	Dol	DDH197-2	21.6	Na+Ca	30.2	182094	1343	b.d.	b.d.	306	-0.3
		DDH7-1	125.5	Na+Ca	29.6	178147	409	b.d.	938	981	
		RBL3Qz		Na+Ca	28.1	168901	1491	185	b.d.	255	-0.4
		RBL1Qz		Na+Ca	28.5	170421	n.a.	1330	1047		
		RBL4Qz		Na+Ca	28.7	173114	667	b.d.	375	585	-0.18
		RBL2Qz		Na	29.2	173549	1811	b.d.	2012	216	
		RBL7Qz		Na+Ca	28.9	174080	1350	b.d.	b.d.	291	-0.12
		RBL14Qz		Na	29.0	175455	582	b.d.	b.d.	680	-0.26
		RBL5Qz		Na+Ca	29.7	176942	2620	b.d.	356	152	-0.44
		RBL9Qz		Na+Ca	31.3	186029	2775	b.d.	1003	151	
		RBL2Carb		Na	27.6	157654	1565	b.d.	8204	227	-0.19
		RBL14Carb		Na+Ca	27.2	160609	1162	b.d.	2922	311	
		RBL5Carb		Ca	27.4	161586	2865	105	1653	127	-0.85
	Cal	DDH197-5		Na+Ca	27.3	162410	1682	b.d.	1208	218	0.05
		RBL9Carb		Na+Ca	27.3	162836	1816	b.d.	709	202	
		RBL11Carb		Na+Ca	28.0	167602	749	b.d.	1255	504	-0.24
		RBL7Carb		Na+Ca	28.1	167901	2252	b.d.	n.a.	168	-0.04
		RBL1Carb		Na	28.5	169567	2034	b.d.	1524	188	-0.12
	RBL12Carb			Ca	28.9	172238	2768	b.d.	n.a.	140	

Table 6.1 : Location, host minerals, brine content, depths (available data), and results from crush-leach analyses. n.a.: not analyzed (when ion chromatograph signal do not permit proper quantification). b.d.: below detection limit, n.o.: not observed. Qz: quartz. Dol: dolomite. Cal: calcite. Depth: estimated depth below unconformity. Na: NaCl-rich brine. Ca: CaCl<sub>2</sub>-rich brine.

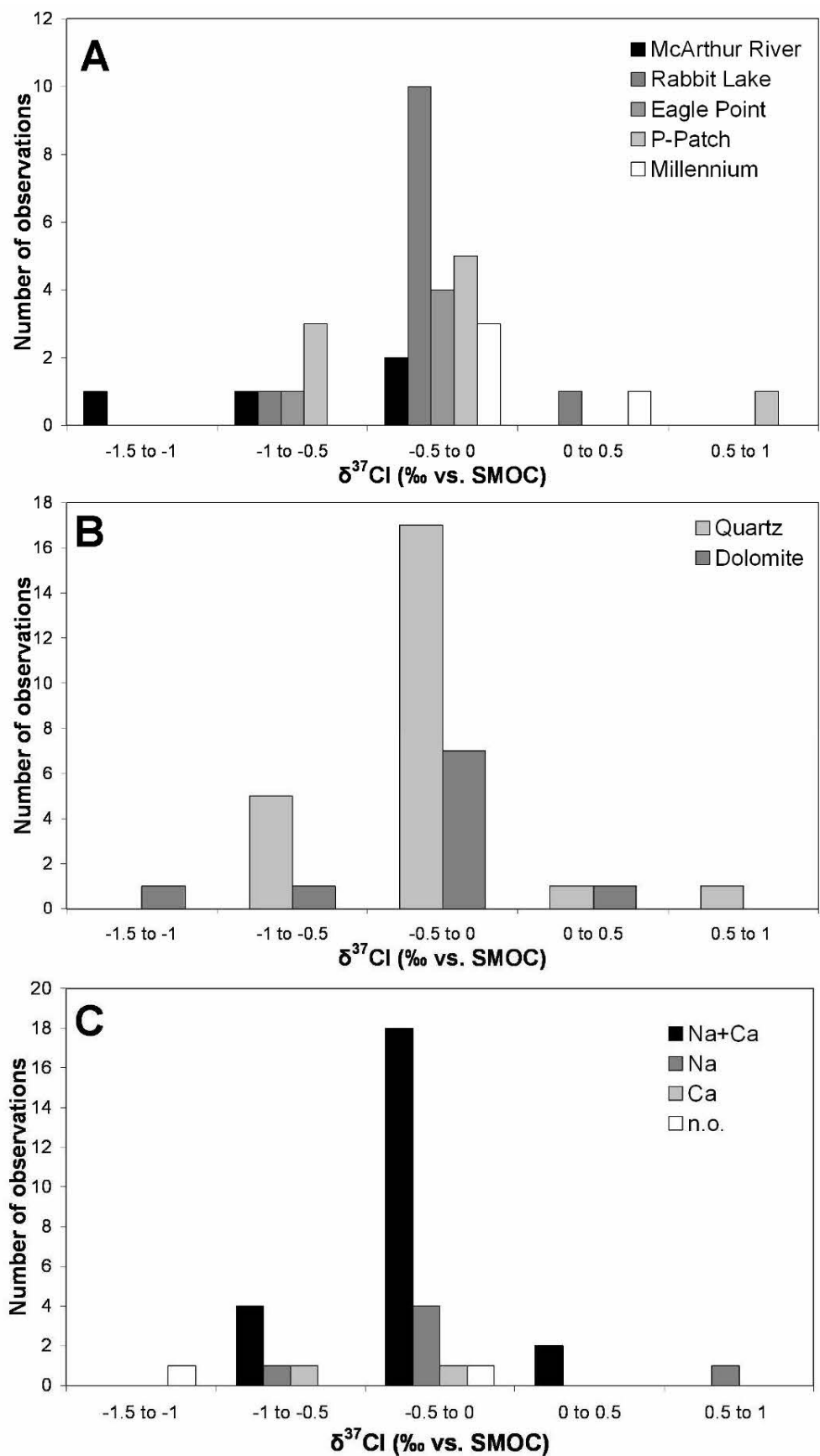


Figure 6.1 : Frequency histogram for δ<sup>37</sup>Cl observations in the Athabasca brines. (A) Data sorted by localities. (B) Data sorted by host minerals. (C) Data sorted by brine content. n.o. Not observed. Na: NaCl-rich brine. Ca: CaCl<sub>2</sub>-rich brine.

Samples	Alteration	Cl (ppm)	L.O.I. wt. %
Biotite	Fresh	3250-4170 (3853) n=18	-
Illite	Altered	210-340 (285) n=4	-
Sudoite	Altered	250-530 (364) n=9	-
<hr/>			
Porphyry	Fresh	215	1.2
		436	1.4
		343	1.7
<hr/>			
Altered	Altered	198	1.5
		106	1.8
		153	2.2
		112	3.0
		106	3.0
		195	3.8
		158	3.9
		127	4.0
		207	4.5
		91	4.6
		271	5.1
		132	5.4
		203	5.5
		118	5.8
<hr/>			
Pegmatite	Fresh	883	1.2
		518	1.2
		1078	1.4
		460	1.7
<hr/>			
Altered	Altered	137	1.9
		185	3.1
		92	3.2
		114	3.3
		298	3.9
		220	3.9
		110	4.1
		282	4.3
		67	5.2
		113	5.9
		73	7.7
		80	9.4
<hr/>			

Table 6.2 : Cl content and loss on ignition (L.O.I.) of Athabasca Basement rocks and minerals. Numbers in parentheses are average Cl contents. *n*: number of measurements.

## 6.4. Discussion

### 6.4.1. Cl-Cl/Br- $\delta^{37}\text{Cl}$ relationships in the Athabasca Basin

#### 6.4.1.1. Primary brine component

Cl/Br ratios below that of seawater unambiguously indicate that the analyzed fluid has undergone surface evaporation (Figure 6.2). If the evaporated fluid was initially seawater, the range of observed Cl/Br ratios indicates evaporation beyond halite precipitation. If Cl/Br ratios of this primary brine component could have been subsequently modified (see below) precluding the identification of the exact evaporation stage, there is no doubt that a significant part of the salinity of the analyzed brines has been acquired by evaporative process.

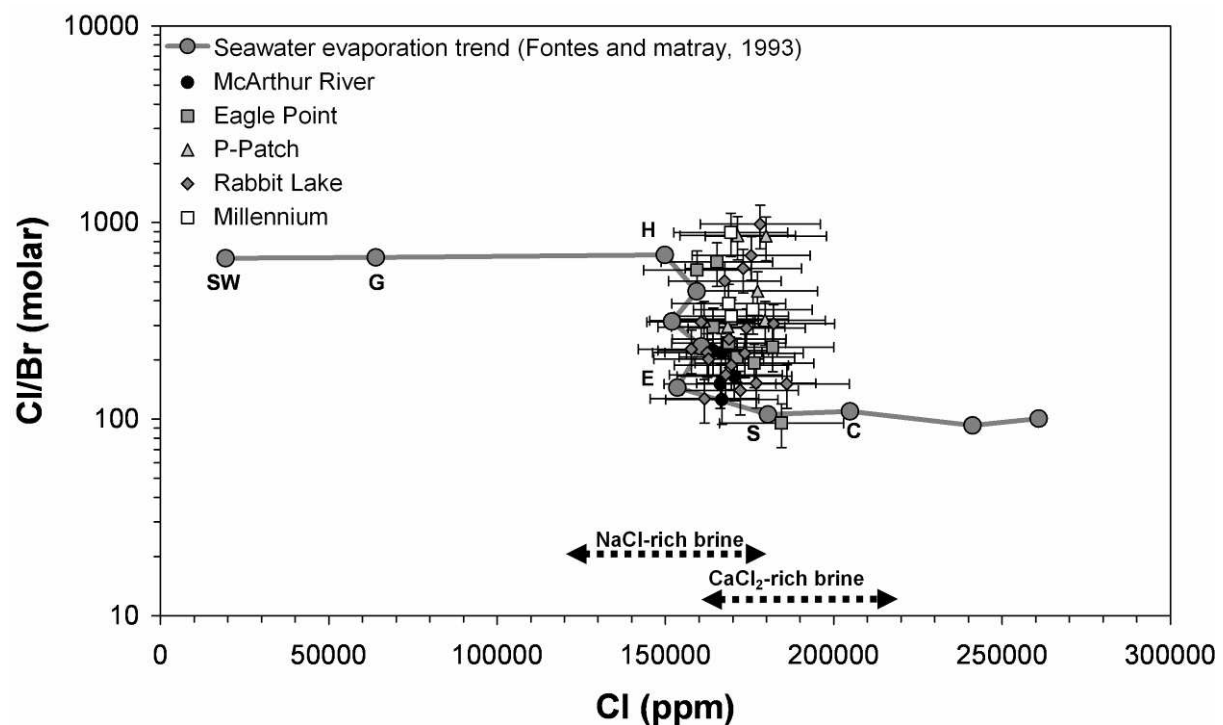


**Figure 6.2 : Cl/Br vs. Cl relationships in the Athabasca Brines. SW: seawater. Minerals precipitating during evaporation of seawater: G: gypsum; H: halite; E: epsomite; S: sylvite; C: carnallite. Also shown the ranges for Cl concentration in NaCl-rich and CaCl<sub>2</sub>-rich brines.**

$\delta^{37}\text{Cl}$  signature of evaporated seawater is known experimentally from [Eggenkamp et al., \(1995\)](#) and [Eastoe et al., \(1999\)](#). Both studies led to comparable results. During evaporation of seawater up to epsomite saturation,  $\delta^{37}\text{Cl}$  decreases in the residual brines from 0‰ (seawater) down to -0.5‰ after [Eggenkamp et al., \(1995\)](#) and down to -0.9‰ after [Eastoe et al., \(1999\)](#).  $\delta^{37}\text{Cl}$  signature of evaporated determined by [Eggenkamp et al., \(1995\)](#) and [Eastoe et al., \(1999\)](#) and Cl/Br ratios of evaporated seawater from [Fontes and Matray \(1993a\)](#) were tentatively matched. The resulting seawater evaporation trend was plotted together with analytical data in a Cl/Br vs.  $\delta^{37}\text{Cl}$  diagram ([Figure 6.3](#)). The great majority of our samples have  $\delta^{37}\text{Cl}$  values compatible with evaporated seawater, most of values being comprised between -0.5 and 0‰. Some of the samples plot below the seawater evaporation trends, but given the difficulties in matching Cl/Br with  $\delta^{37}\text{Cl}$  values of evaporated seawater combined with uncertainties on Cl/Br ratios and  $\delta^{37}\text{Cl}$  values, we suggest that except for the 2 positive  $\delta^{37}\text{Cl}$  values, our  $\delta^{37}\text{Cl}$  data are broadly compatible with evaporated seawater.

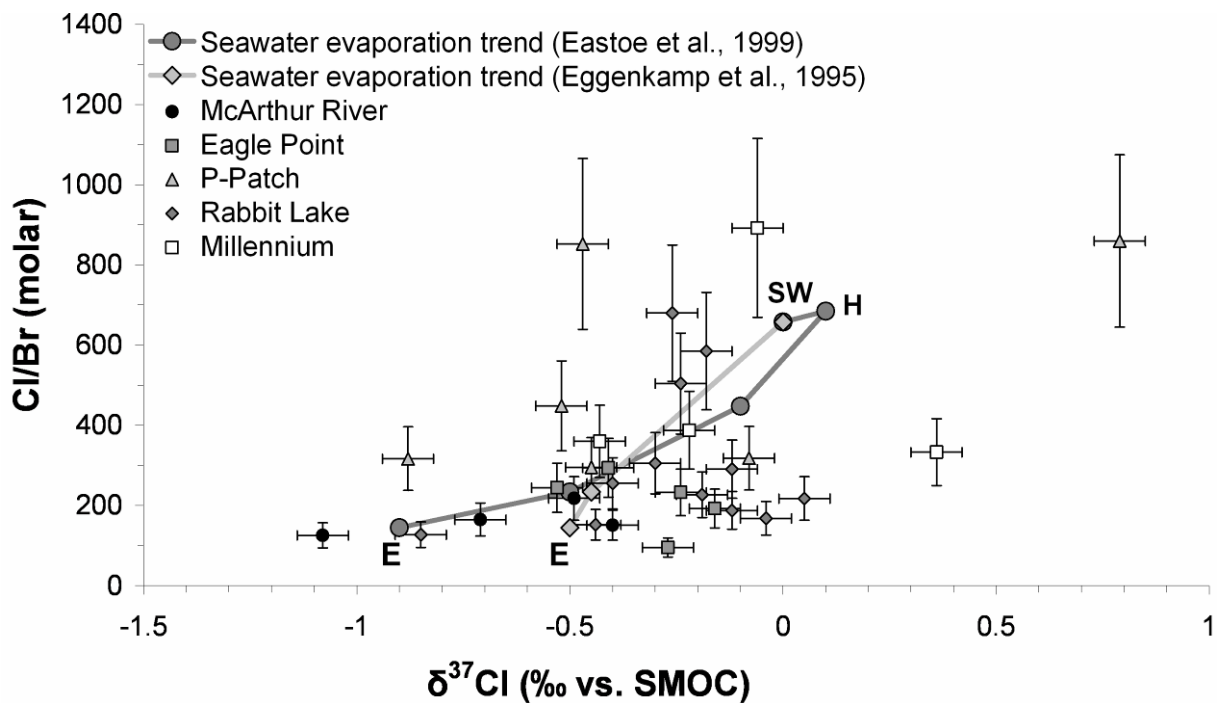


**Figure 6.3 :  $\delta^{37}\text{Cl}$ -Cl/Br relationships in the Athabasca brines. Also shown the ranges for Cl concentration in NaCl-rich and CaCl<sub>2</sub>-rich brines Minerals precipitating during evaporation of seawater: H: halite; E: epsomite.  $\delta^{37}\text{Cl}$ -depth relationships in the Athabasca brines.**

Non-marine (i.e. closed-basin or continental) brines have highly variable compositions due to multiple possible water inputs (mainly rivers waters and groundwaters) ([Risacher et al., 2003](#)). Cl/Br ratio of river waters is comparable to that of seawater but if river water is mixed with groundwater before onset of evaporation, the initial Cl/Br of the evaporating solution may considerably differ from that of seawater. To add, [Risacher et al., \(2006\)](#) have shown that Br can display non-conservative behaviour in surface waters and brines of Central Andes. Indeed, surface waters at salar de Uyuni, Bolivia, are systematically Br-depleted and the authors suggest that the missing Br was transferred into the atmosphere. Stable chlorine isotopic composition of salt lake brines are known from [Liu et al., \(1997\)](#) and range from -2.05 to 1.01‰. Thus, due to their high variability in non-marine environments Cl/Br and  $\delta^{37}\text{Cl}$  signatures could hardly help identifying non-marine origin for the primary brine component. Due to the relative scarcity of non-marine evaporitic environments compared to marine evaporitic environments we strongly favour the hypothesis of evaporated seawater as best candidate for primary brine component.

#### *6.4.1.2. Secondary brine component*

Interpretation of Cl/Br and Cl concentrations data must take into account the possibility of mixing between end-members ([Grandia et al., 2003a](#)). Cl/Br ratios are not correlated to the brine content of samples suggesting that both brines have heterogeneous Cl/Br ratios. Here, we consider the possibility of mixing between halite-to-carnallite-saturated evaporated seawater, and secondary brine resulting from dissolution of halite by meteoric water or seawater or a combination of both. Regardless of the origin of the fluid that dissolves halite, secondary brines are nearly pure NaCl-H<sub>2</sub>O solutions with salinities controlled by halite solubility and temperature ([Bodnar, 1994](#)), and are heavily Br-depleted with molar Cl/Br ratios ranging from ca. 1000 to 10000 ([Banks et al., 2000b](#)). [Figure 6.4](#) shows mixing trend between a hypothetical halite-dissolution fluid, equilibrated with halite at 100°C, with Cl/Br ratio of 4000 and Cl concentration of 170000 ppm, and a halite-to-

carnallite-saturated evaporated seawater. A contribution up to more than 90% from halite-dissolution fluid could account for the measured Cl/Br ratios.

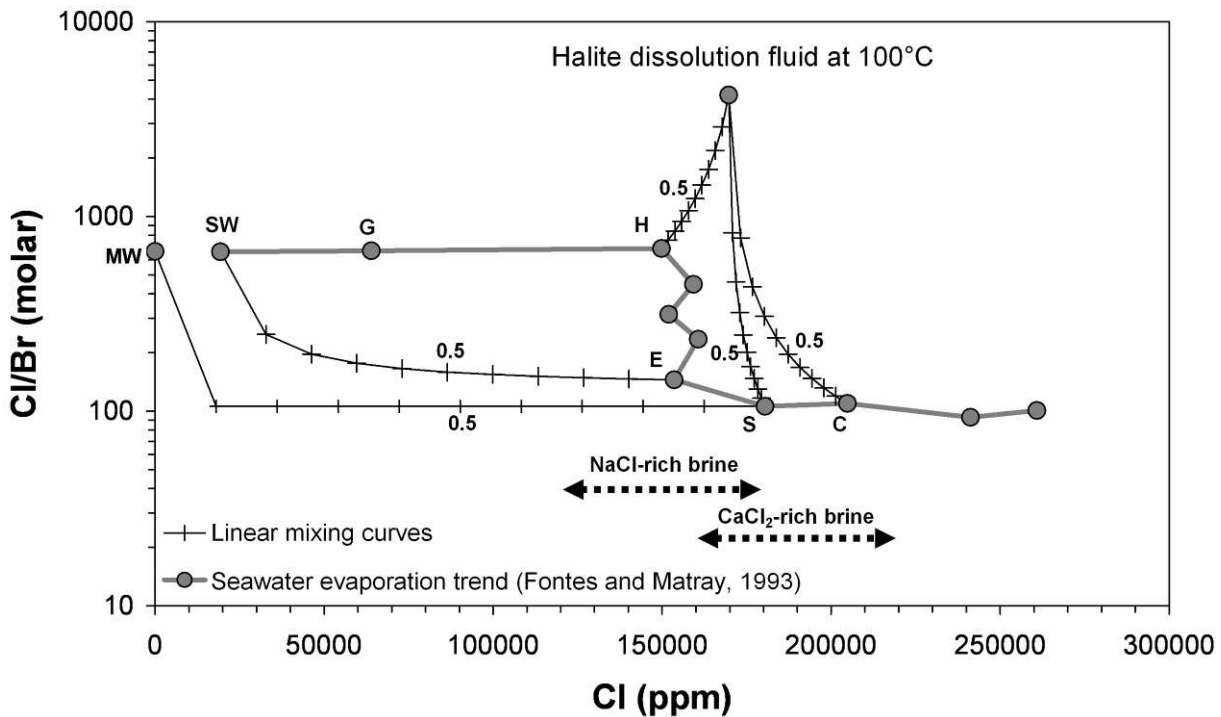


**Figure 6.4 : Mixing scenarios between evaporated seawater and halite dissolution fluid in equilibrium with halite at 100°C, and mixing between evaporated seawater and meteoric water or seawater. 0.5: equal mixing of the two end-members. MW: meteoric water. SW: seawater. Minerals precipitating during evaporation of seawater: G: gypsum; H: halite; E: epsomite; S: sylvite; C: carnallite. Also shown the ranges for Cl concentration in NaCl-rich and CaCl<sub>2</sub>-rich brines.**

Recrystallisation or dissolution do not affect the  $\delta^{37}\text{Cl}$  of halite bodies (Eastoe and Peryt, 1999) and thus the  $\delta^{37}\text{Cl}$  signature of a halite dissolution brines should tend to that of the dissolved halites at the time of its deposition. Phanerozoic marine halites have  $\delta^{37}\text{Cl}$  ranging from -0.5 to +0.5‰ (Eastoe et al., (2007)) and salt lake halites have  $\delta^{37}\text{Cl}$  ranging from -0.6 to +1.2‰ (Liu et al., 1997). Samples with Cl/Br ratios higher than that of seawater (i.e. the most likely to have been influenced by mixing with halite-dissolution fluid) have  $\delta^{37}\text{Cl}$  ranging from -0.5‰ to +0.5‰ with one sample at +0.79‰ (Figure 6.3). Therefore,  $\delta^{37}\text{Cl}$  signatures of the brine may have been influenced by interaction with evaporites but can hardly be quantitatively constrained.

#### *6.4.1.3. A low-salinity fluid component*

NaCl-rich brine inclusions have salinity ranging from ca. 20 to 30 eq. wt% NaCl which corresponds to Cl concentrations ranging from ca. 120000 to 180000 ppm ([Part 4](#)). Cl concentration halite-saturated seawater is close to 150000 ppm ([Fontes and Matry, 1993a](#)) and thus a significant proportion of NaCl-rich brine inclusions have Cl content lower than that of halite-saturated seawater. However, Cl/Br ratios indicate that the NaCl-rich brine has reached the halite precipitation stage. Thus, the NaCl-rich brine may have undergone some dilution during percolation towards the base of the Athabasca sandstones. From mixing scenario between halite-to-sylvite-saturated evaporated seawater and meteoric water or seawater ([Figure 6.4](#)), this dilution would not affect Cl/Br ratios unless the NaCl-rich brine was mixed with more than 80% of diluting fluid. From [Figure 6.4](#), we consider that a maximum of 30% of diluting fluid was added to evaporated seawater to account for the lowest salinities observed in NaCl-rich brine inclusions. As mentioned above, this would not change Cl/Br ratios. [Alexandre et al., \(2005\)](#) suggested that low-latitude meteoric waters have mixed with evaporated seawater. The nature of the diluting fluid is still unclear but stable isotopic (O, H) compositions of fluid inclusions do not support a significant meteoric input and are rather in favour of seawater as diluting fluid ([Part 8](#)).

#### *6.4.1.4. Brine-halite equilibrium?*

Evaporated seawater was introduced in the sedimentary pile either from surface or expelled from evaporitic formations due to compaction during burial (see below). In the latter case, residual evaporitic brines were first trapped at equilibrium within halites basically as fluid inclusions, during halite precipitation. During burial and subsequent heating, significant re-equilibration may have occurred due to increasing halite solubility. In this case, NaCl dissolution may have occurred in the walls of fluid inclusions. In this case, Cl enrichment and increase of Cl/Br ratios are expected in fluid inclusions. Cl concentrations and Cl/Br shifts in

fluid inclusions can be roughly estimated using halite solubility in the H<sub>2</sub>O-NaCl system (Bodnar, 1994). Figure 6.5 shows that Cl concentrations could shift from 150000 ppm (25°C) to 170000 ppm (100°C), 180000 ppm (150°C), and 190000 ppm (200°C). If the primary brine was trapped during beginning of halite precipitation, Cl/Br ratios would shift from 684 (25°C) to 755 (100°C), 822 (150°C), and 883 (200°C). If the primary brine was trapped at the end of halite precipitation, Cl/Br ratios would shift from 234 (25°C) to 247 (100°C), 262 (150°C), and 281 (200°C). Therefore high temperature equilibration of residual brine fluid inclusions with host halites could account for the observed ranges of Cl concentrations and Cl/Br ratios.

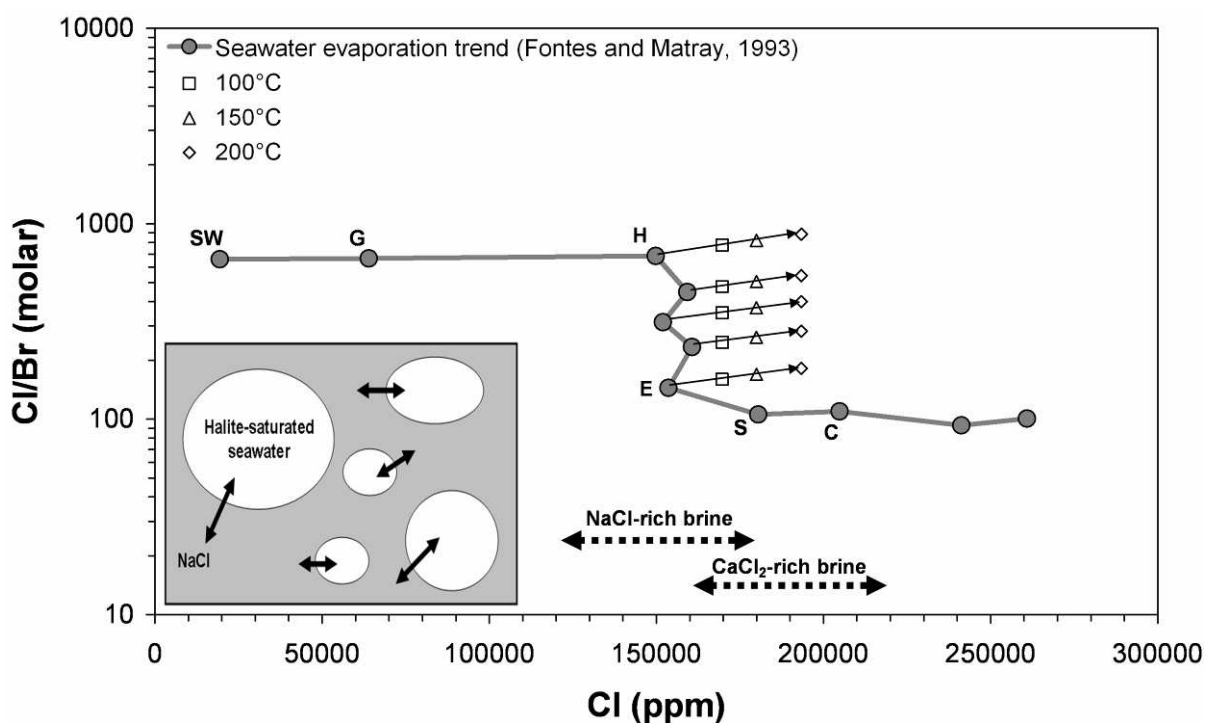


**Figure 6.5 : Scenario for brine-halite reequilibration at 100, 150 and 200°C** SW: seawater. Minerals precipitating during evaporation of seawater: G: gypsum; H: halite; E: epsomite; S: sylvite; C: carnallite. Also shown the ranges for Cl concentration in NaCl-rich and CaCl<sub>2</sub>-rich brines.

However, temperatures of 150-200°C necessary to account for significant Cl enrichment and Cl/Br ratio shifts are comparable to the temperature of the brines sampled at the base of the Athabasca sandstones and in the basement (Derome et al., 2005; Part 4). The evaporitic formation that could have enclosed such brines was located at least 1500m above the unconformity (see below). Thus, we can reasonably assume that the maximum possible temperature of the evaporitic formation before expulsion of enclosed brines was of

150°C. The only possibility for such phenomenon to have significantly affected the composition of the brines would be that brines have been expulsed from the Carswell Formation or from a presently eroded immediately overlying formation. Therefore, we believe that, if primary brines were originally enclosed in halites, their Cl content and Cl/Br ratios could have been significantly shifted, the magnitude of this shift depending on temperature of reequilibration. Reequilibration between 100 and 150°C could account for observed Cl content and Cl/Br ratios.

#### **6.4.2. Cl-Cl/Br- $\delta^{37}\text{Cl}$ changes during percolation in the Athabasca Basement**

##### *6.4.2.1. The Athabasca Basement as a source of chlorine*

The main Cl-bearing minerals in igneous and metamorphic rocks are biotites and amphiboles and can contain from several hundreds to thousands of ppm of Cl ([Kamineni, 1984](#)). [Kamineni \(1984\)](#) has shown that amphibole and biotite breakdown by 100-300°C hydrothermal fluids in the East Bull Lake anorthosite-gabbro complex, was followed by precipitation of Cl-free minerals including various clay minerals. For the authors, this may explain part of the Cl content of the present-day interstitial waters. [Richard \(2000\)](#) has shown that shield brines could contain up to 0.5 molal of Cl inherited from Cl-OH exchange reaction with biotites. In the Athabasca Basement, porphyry granites and pegmatites are, together with pelitic gneisses, the main biotite-bearing rocks. [Table 6.2](#) shows that in porphyry granites and pegmatites, fresh biotites have average Cl concentration of ca. 3800 ppm. In altered samples, illite and sudoite replace biotites and have average Cl content of 280 and 360 ppm respectively. At the whole rock scale, Cl loss from biotites during alteration of Athabasca Basement rocks by diagenetic brines is illustrated in [Figure 6.6](#). With increasing alteration, as shown by increasing L.O.I., Cl content of fresh rock decreases rapidly of ca. one order of magnitude. This is very similar to the scenario described by [Kamineni, \(1984\)](#). Thus, Athabasca Basement rocks may have lost up to 90% of their initial Cl during alteration

by diagenetic brines. The diversity of basement rocks precludes any reasonable mass-balance calculation. However, we suggest that the Athabasca Basement is a potential Cl source for the studied brines, which may partly explain the highest measured Cl concentrations.

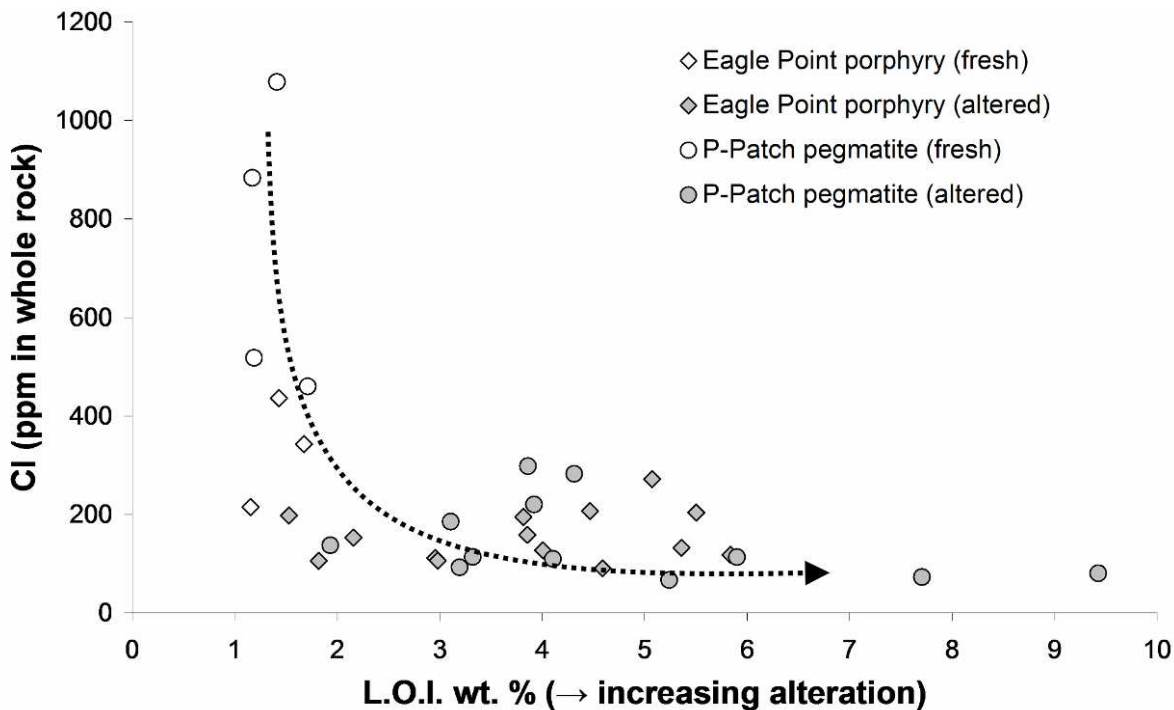


**Figure 6.6 : Loss on ignition (L.O.I.) vs. Cl content in fresh and altered porphyries and pegmatites of the Athabasca Basement.**

The  $\delta^{37}\text{Cl}$  composition of Athabasca Basement biotites is unknown. Biotites from the Bushveld Complex, South Africa, have  $\delta^{37}\text{Cl}$  ranging from -0.6 to +7‰ (Willmore et al., 2002) while biotites from Stillwater Complex, Montana, have  $\delta^{37}\text{Cl}$  ranging from -0.93 to +0.27‰ (Boudreau et al., 1997). Eggenkamp and Schuling (1995) have measured  $\delta^{37}\text{Cl}$  values of metamorphic amphiboles ranging from -0.26 to -0.06‰ and Magenheim et al., (1995) have measured  $\delta^{37}\text{Cl}$  values of hydrothermal amphiboles comprised between +0.4 to 3.4‰. Möller et al., (2005) have estimated that the high  $\delta^{37}\text{Cl}$  values measured in KTB fluids, the highest values for formation waters so far (2-4‰) result from interaction with surrounding amphibolites (Figure 6.7).

In the case of the Athabasca Basin brines, if ca. 10% of the Cl content is provided by biotites with average  $\delta^{37}\text{Cl}$  values of +4‰, one would expect that brines with  $\delta^{37}\text{Cl}$  values of -0.5‰ shift to  $\delta^{37}\text{Cl}$  of -0.05‰ after interaction with biotites. This is a possible explanation for the dispersion of  $\delta^{37}\text{Cl}$  values in the Athabasca brines from -0.5‰ to ca. 0‰ and for the three measured positive  $\delta^{37}\text{Cl}$  values. Therefore, interaction with biotites could potentially shift the  $\delta^{37}\text{Cl}$  values of brines towards heavier compositions although the magnitude of this shift is difficult to estimate.

Such reaction would also necessarily shift the Cl/Br ratios depending of the Cl/Br ratios of the biotites which are highly variable (Fuge, 1974) and unknown for the Athabasca Basement rocks, but may partly account for the dispersion of Cl/Br ratios.

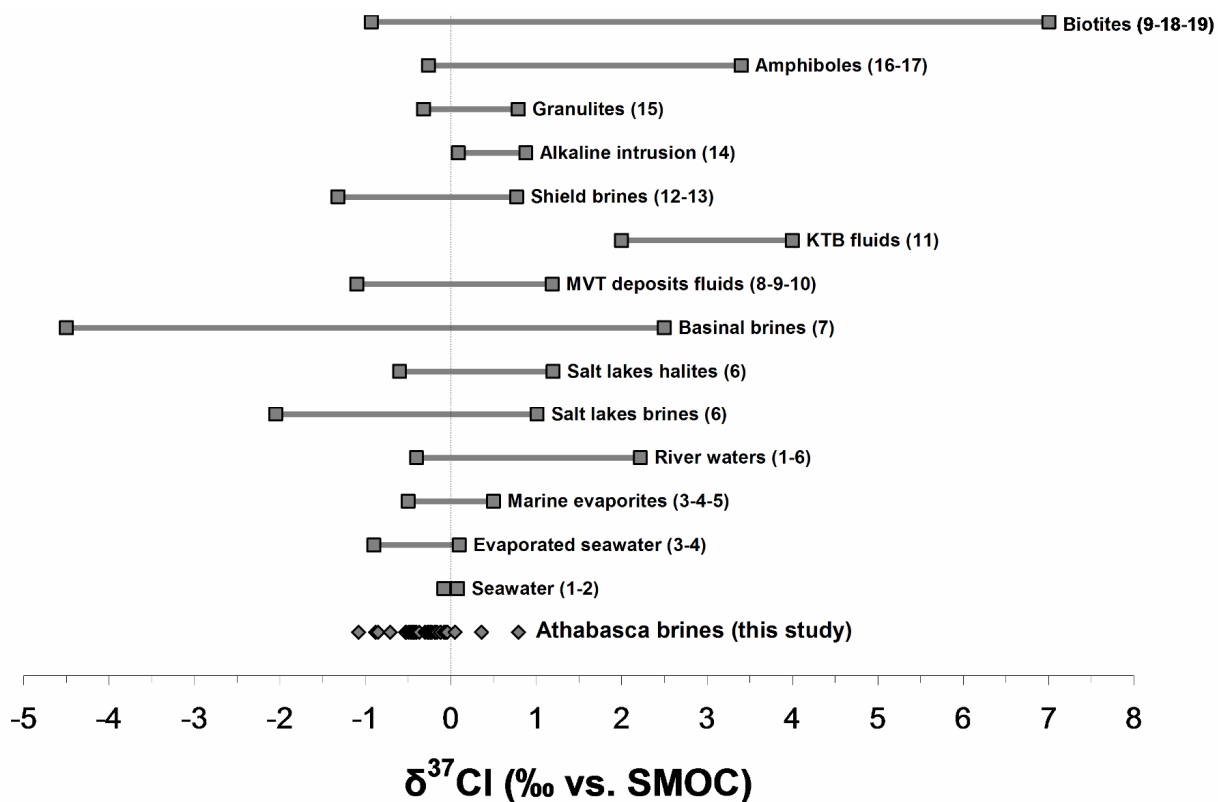


**Figure 6.7 : Ranges of  $\delta^{37}\text{Cl}$  of various fluids, rocks and minerals of interest for interpretation of  $\delta^{37}\text{Cl}$  values of Athabasca brines. Numbers in parentheses indicate references as follows:** (1) Kaufmann et al., (1984a); (2) Godon et al., (2004); (3) Eggenkamp et al., (1995); (4) Eastoe et al., (1999); (5) Eastoe et al., (2007); (6) Liu et al., (1997); (7) Stewart and Spivak (2004) and references therein; (8) Eastoe et al., (1989); (9) Eastoe and Guilbert (1992); (10) Grandia et al., (2003b); (11) Möller et al., (2005); (12) Kaufmann et al., (1984b); (13) Sie & Frape (2002); (14) Musashi et al., (1998); (15) Marlk et al., (2007); (16) Eggenkamp & Schuiling (1995); (17) Magenheim et al., (1995); (18) Boudreau et al., (1997); (19) Willmore et al., (2002).

#### *6.4.2.2. Diffusion, ion filtration, hydration reactions.*

Diffusion of Cl from a high chlorinity reservoir through rocks saturated with lower chlorinity waters leads to  $\delta^{37}\text{Cl}$  depletion in the transported Cl (Kaufman et al., 1988), and is frequently thought to account for negative  $\delta^{37}\text{Cl}$  values in groundwaters (Eggenkamp et al., 1994; Eggenkamp and Coleman, 2009; Desaulniers et al., 1986). Illite-sudoite precipitation may have also contributed to lower the  $\delta^{37}\text{Cl}$  of brines as solids precipitating from seawater are enriched in  $\delta^{37}\text{Cl}$  (Magenheim et al., 1995). Ion membrane filtration produces  $\delta^{37}\text{Cl}$ -enriched fluids (Kaufmann et al., 1988) and is expected in low-porosity basement rocks. Combined with biotite dissolution, the latter three competing processes may all have contributed to the overall dispersion of the  $\delta^{37}\text{Cl}$  values of the Athabasca brines, particularly in basement rocks. Figure 6.8 shows a possible increase of  $\delta^{37}\text{Cl}$  with depth in the basement which would infer that biotite dissolution and membrane ion filtration are the two dominant processes contributing to chlorine isotopes fractionation in basement rocks.

Surface-derived fluids may undergo significant salinity increase during percolation in basement rocks during retrograde hydration reactions (Gleeson et al., 2003). In the Athabasca Basement, altered rocks have L.O.I. up to 10% while fresh rocks have L.O.I. up to 2% (Figure 6.6). Thus, water uptake from brines to alteration minerals (illite, sudoite, dravite) may have enhanced the salinity of brines and could be account for the high salinities observed in the  $\text{CaCl}_2$ -rich brine inclusions, as proposed by Mercadier et al., (in press).

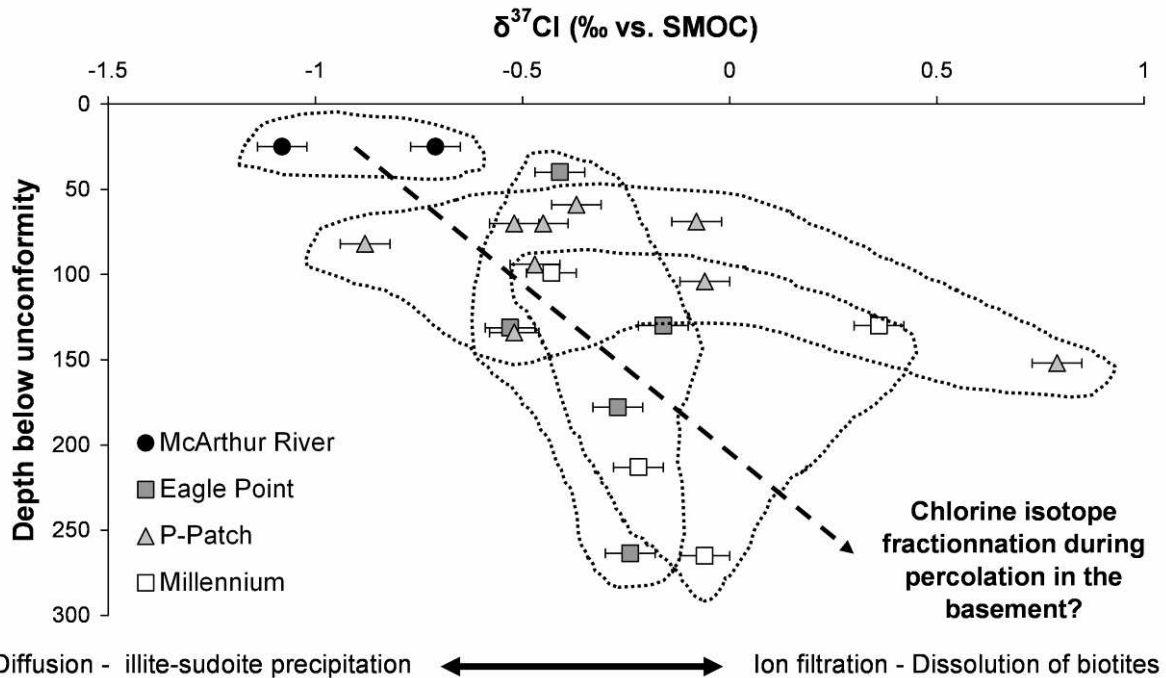


**Figure 6.8 :  $\delta^{37}\text{Cl}$ -depth relationships in the Athabasca brines. Possible  $\delta^{37}\text{Cl}$  fractionation occurs during percolation of brines in the basement.**

#### 6.4.3. Brine flows from surface to basement

##### 6.4.3.1. Evaporitic environments in the Athabasca Basin

The Athabasca Basin brines are thought to have invaded the entire base of the Athabasca sandstones and part of the Athabasca Basement at the time of uranium mineralisation (Kyser et al., 2000; Part 4). Regardless of the origin of high salinities in the Athabasca Basin brines (i.e. evaporite dissolution or seawater evaporation), a relatively large evaporite body must have been present in the sedimentary pile to account for such huge volumes of brines. In the present-day sedimentary succession, there is no evidence for massive evaporite deposit (Ramaekers et al., 2007). Hendry and Weathley (1985) noted that periodic evaporation left gypsum in the Carswell Formation and evidenced solution-collapse breccias following dissolution of evaporites at depth. Sediments of the Carswell Formation are only preserved around the Carswell structure and the original extent of the Carswell Formation was probably much larger (Hendry and Weathley, 1985). Thus, before erosion,

the entire Carswell Formation has potentially hosted large amount of evaporite minerals. Note that the present-day thickness of preserved sedimentary pile is c.a. 1500m ([Ramaekers et al., 2007](#)) and that fluid inclusion data yielded a past thickness of 4-6 km ([Pagel 1975; Derome et al., 2005; Part 4](#)). Thus, most of the sediments potentially containing evaporites have been removed by erosion and/or dissolution.

Paleolatitudes could help to evaluate the possibility of evaporitic environments during sedimentation in the Athabasca Basin. However, timing of sedimentation in the Athabasca Basin is poorly constrained. The onset of sedimentation is thought to have occurred at ca. 1750 Ma ([Ramaekers et al., 2007](#)), but the age of the end of sedimentation is unknown. The age of the Carswell Formation could be considered as a minimum age for possible seawater evaporation processes in the Athabasca Basin. Unfortunately, this age is unknown. Re-Os geochronology on organic-rich shales of the underlying Douglas Formation yielded depositional ages of  $1541 \pm 13$  Ma ([Creaser and Stasiuk, 2007](#)). Thus, in order to evaluate the possibility of evaporitic environments during formation of the Athabasca Basin, paleolatitudes of Northern Saskatchewan must be considered between 1500Ma (approximate age for the Carswell Formation) and 1300Ma (minimum age for primary uranium mineralizations) ([Cummings and Krstic, 1992; Fayek et al., 2002; Alexandre et al., 2009a](#)). Palaeomagnetic reconstructions suggest that Northern Saskatchewan was located within  $30^\circ$  of the equator between 1500 and 1300Ma and possibly within  $5^\circ$  during protracted periods ([Kotzer et al., 1992; Buchan et al., 2000; Meert et al., 2002; Pesonen et al., 2003; Zhao et al., 2004](#)). Thus, low latitudes of the Northern Saskatchewan area during sedimentation of the Athabasca Basin could have favoured evaporitic environments and the production of halite deposits and/or evaporated seawater.

Comparison with Kombolgie sub-Basin (McArthur Basin), NT, Australia, which hosts very similar unconformity-related uranium deposits and where comparable brines were found, could help understanding the origin of high salinity of Athabasca Basin brines ([Wilde et al., 1989; Ypma and Fuzikawa, 1980; Derome et al., 2003, 2007; Polito et al., 2004, 2005](#)). By using crush-leach techniques, [Derome et al., \(2007\)](#) found molar Cl/Br ratios ranging from

151 to 220 in fluid inclusion leachates from quartz veins. They argued that organic matter is nearly absent in the basin and in the basement and interpreted low Cl/Br ratios as resulting from evaporation of seawater beyond halite saturation. Relationship between high salinity brines and evaporite deposits are much more evident in the Kombolgie sub-Basin than in the Athabasca Basin. Evaporites are widely described in the McArthur Basin ([Walker et al., 1977](#); [Warren, 2000](#), [Rawlings, 1999](#)).

#### *6.4.3.2. Migration paths for brines*

Evaporite formations can provide significant amounts of residual brines with low Cl/Br ratios ([Fontes and Matray 1993a](#)). Here, the studied brines have invaded the huge aquifer of basal Athabasca sandstones and part of the Athabasca Basement, and expulsion of brines from evaporitic formations could hardly account for such volumes of fluids. In most sedimentary basins, brines originating from evaporation of seawater are thought to have percolated from the surface down to the sedimentary pile essentially due to their high density if they can percolate in aquifers filled by lower-density fluids, or along extensional faults ([Evans et al., 1991](#); [Munoz et al., 1999](#); [Gleeson et al., 2001](#); [Boiron et al., submitted](#)). Thermally-driven free convection may have been the main force driving brines in the Athabasca sandstones ([Raffensperger and Garven, 1995a, 1995b](#)). Thus, we consider that the Athabasca brines are likely to have percolated from surface to the base of the sandstones and eventually in the basement.

## 6.5. Conclusion

Cl/Br and  $\delta^{37}\text{Cl}$  signatures of Athabasca brines allow us to draw the following conclusions:

- (1) High chlorinities were acquired by surface evaporation of seawater favoured by low-latitudes of the Northern Saskatchewan area between 1.5 and 1.2 Ga.
- (2) During percolation from surface through sedimentary pile, primary evaporitic brines were mixed at various degrees with secondary brines originating from halite dissolution. Brine mixing led to dispersion of Cl/Br ratios.
- (3) The resulting brines were slightly diluted by lower salinity fluids (probably seawater-derived) along their flow path.
- (4) Percolation of brines in the Athabasca Basement is at the origin of significant salinity increase through biotite dissolution and hydration reactions. Extreme salinities reached by the  $\text{CaCl}_2$ -rich brine attest for intense alteration and hydration of basement rocks.
- (5)  $\delta^{37}\text{Cl}$  values of brines were probably affected by biotite dissolution and membrane ion filtration in basement-rocks.

## Version abrégée

La composition en anions ( $\text{Cl}$ ,  $\text{Br}$ ,  $\text{F}$ ,  $\text{SO}_4$ ) et la composition isotopique du chlore ( $\delta^{37}\text{Cl}$ ) des saumures sodiques et calciques des gisements de McArthur River, Rabbit Lake, Eagle Point, P-Patch et Millennium, ont été mesurées sur populations globales d'inclusions fluides à l'échelle de l'échantillon par la méthode d'« écrasement-lessivage ». Les rapports  $\text{Cl}/\text{Br}$  ainsi que le  $\delta^{37}\text{Cl}$  sont considérés comme des traceurs conservatifs, et renseignent sur l'origine des fortes salinités mesurées dans les saumures.

La grande majorité des rapports  $\text{Cl}/\text{Br}$  mesurés sont compris entre 150 et 350, des valeurs typiques d'une saumure évaporitique primaire ayant dépassé la saturation vis-à-vis de la halite ([Figure 6.2](#)). De plus, les valeurs de  $\delta^{37}\text{Cl}$  majoritairement comprises entre -0.5 et 0‰ sont compatibles avec les données expérimentales d'évaporation de l'eau de mer ([Figure 6.3](#)).

En revanche, les gammes de concentrations en chlore déduites des analyses microthermométriques laissent penser que la simple évaporation de l'eau de mer ne permet pas de rendre compte de l'ensemble des données.

Un scénario est proposé impliquant l'évaporation de l'eau de mer au-delà de la saturation vis-à-vis de la halite, et une saumure secondaire dérivée de la dissolution d'évaporites pour expliquer la distribution des rapports  $\text{Cl}/\text{Br}$ . Ces deux saumures, l'une primaire et l'autre secondaire, se sont probablement mélangées à part égale ([Figure 6.4](#)).

Une légère dilution de ce mélange de saumures est également possible.

La localisation géographique du bassin de l'Athabasca sous des basses latitudes entre 1.5 et 1.3 Ma a favorisé les environnements évaporitiques, et ainsi la possibilité de générer des saumures primaires et secondaires dans le bassin.

Les roches et minéraux altérés du socle présentent des concentrations en chlore très faibles par rapport à leurs équivalents non altérés. Le socle a donc pu fournir du chlore aux saumures par dissolution des minéraux porteurs (biotite par exemple) ([Figure 6.6](#)). Pour l'instant cette contribution peut difficilement être estimée.

Les  $\delta^{37}\text{Cl}$  montrent une possible augmentation en fonction de la profondeur sous discordance des échantillons. Ceci pourrait signifier que la filtration ionique dans les roches de faible perméabilité et la dissolution des biotites contrôlent partiellement la composition isotopique du chlore dans le socle.

Les très fortes salinités observées dans les saumures calciques peuvent s'expliquer par l'altération intense et l'hydratation des roches du socle.



# **7. Conversion of NaCl-rich basinal brines to CaCl<sub>2</sub>-rich brines through fluid-rock interaction in the Athabasca Basement, Canada**

Antonin Richard<sup>1</sup>, Julien Mercadier<sup>1</sup>, Marie-Christine Boiron<sup>1</sup>, Michel Cathelineau<sup>1</sup>, David A. Banks<sup>2</sup>, Michel Cuney<sup>1</sup>.

<sup>1</sup>G2R, Nancy-Université, CNRS, CREGU, Boulevard des Aiguillettes B.P. 239, F-54506,  
Vandoeuvre-lès-Nancy, France

<sup>2</sup>School of Earth and Environment, University of Leeds, Woodhouse Lane, Leeds, LS2 9JT,  
UK

Article in preparation for *Geofluids*

## **Abstract**

CaCl<sub>2</sub>-rich formation waters are commonly sampled in sedimentary basins and crystalline shields. The origin of their Ca-rich composition is frequently interpreted as resulting from fluid–rock interaction in basin or basement-rocks, or resulting from evaporation of Ca-rich seawater. Unconformity-related uranium deposits were formed from circulation of NaCl-rich and CaCl<sub>2</sub>-rich brines at the basement-cover interface of the Athabasca Basin (Canada). Both brines share a common basinal origin and their detailed chemistry could help understanding mechanisms and implications of conversion of NaCl-rich brines to CaCl<sub>2</sub>-rich brines. Detailed fluid inclusion chemistry obtained from LA-ICP-MS and crush-leach analyses were compared to 520 analyses of basinal fluids representative of the variability of basinal fluid compositions. The NaCl-rich brine has Na-Ca-Mg-K-Sr composition clearly compatible with commonly sampled basinal fluids. The CaCl<sub>2</sub>-rich brine shows more exotic composition, with high Mg-K-Ca-Sr concentrations coupled with very low Na/K ratios strongly supporting a

dominant basement origin for Mg, Ca, K and Sr. Simple Na/Ca exchange alone, such as albitization of plagioclase, could not account for compositional shift from NaCl-rich brine to CaCl<sub>2</sub>-rich brine. Previously established geochemical budgets show that K, B and Mg were added to alteration haloes around the deposits by fluids having leached basement rocks. Here, high concentrations of K, B and Mg in the CaCl<sub>2</sub>-rich brine are compatible with basement origin for these elements. Interaction of NaCl-rich basinal brines and conversion to CaCl<sub>2</sub>-rich brine was accompanied by metal (U, Ag, Se, As, Ni, Co) and REEs (Ce) leaching in basement rocks, that were further deposited in association to uranium ores. These brines are a remarkable illustration of compositional shift form NaCl-rich basinal brines to CaCl<sub>2</sub>-rich brines by fluid-rock interaction in basement rocks.

## 7.1. Introduction

Hydrothermal fluids are important contributors to mass transfer in the crust (Yardley 2009). In the Mesoproterozoic Athabasca Basin, Canada, diagenetic brines have migrated through basement rocks over large scales and great depths, causing intense element redistribution and alteration at the basement-cover interface (e.g. Hoeve and Sibbald, 1978; Pagel et al., 1980; Hoeve and Quirt, 1984; Kotzer and Kyser, 1995; Derome et al., 2005; Part 4). The ultimate consequence of these fluid circulations is the formation of giant unconformity-related uranium deposits (Jefferson et al., 2007).

Fluid inclusion studies revealed that two types of diagenetic brines are involved in the alteration and mineralizing processes: a NaCl-rich brine (Na>Ca>Mg>K>Sr>Ba) and a CaCl<sub>2</sub>-rich brine (Ca>Mg>Na>K>Sr>Ba) (Derome et al., 2005; Part 3; Part 4). Both brines share a common evaporated seawater origin and show evidence of mixing in close temporal relation to uranium deposition (Part 3; Part 6). Little is known about the origin of major and trace solutes in these brines. On the basis of compositions in the H<sub>2</sub>O-NaCl-CaCl<sub>2</sub>±MgCl<sub>2</sub> system, Derome et al., (2005) proposed that the CaCl<sub>2</sub>-rich brine results from interaction between the basinal NaCl-rich brine and basement rocks, through Na/Ca exchange.

$\text{CaCl}_2$ -rich brines are known in a variety of geological environments, such as sedimentary basins (Wilson and Long, 1993a, 1993b; Davisson and Criss, 1996), and crystalline shields (Frape and Fritz, 1997; Kloppman et al., 2002; Lodemann et al., 1997). Ca-rich compositions are generally attributed to fluid-rock interactions in basin or basement rocks. Alternatively, evaporation of Ca-rich seawater could have produced  $\text{CaCl}_2$ -rich residual brines (Lowenstein, 2001; Lowenstein et al., 2003). However, the hypothesis that chemistry of evaporated seawater is reflected in basinal brines is still debated (Hanor and McIntosh, 2006; Lowenstein and Timofeeff, 2008). In this paper, the origin the  $\text{CaCl}_2$ -rich compositions of brines samples as fluid inclusions in the Athabasca Basement is investigated.

The basin vs. basement origin for major and minor solutes in the studied brines is difficult to ascertain for the following reasons: (1) The present-day maximum thickness of the Athabasca Basin is 1.5 km, while it has reached ca. 5 km at the time of formation of uranium deposits (1.5-1.2Ga) (Pagel, 1975; Derome et al., 2005, Part 4). This means that part of the information on diagenetic reactions was potentially lost. (2) The heterogeneity of basement lithologies among the studied deposits (Card et al., 2007) and more critically the lack of data on basement lithologies that were potentially affected by brine migrations remote from U deposits. (3) The uncertainties on the composition of evaporated seawater which is the common parent fluid to  $\text{NaCl}$ -rich and  $\text{CaCl}_2$ -rich brines, and the degree of mixing with halite-dissolution brines (Part 7). (4) The chemistry of Mesoproterozoic seawater which could have widely influenced the chemistry of evaporated seawater (Lowenstein, 2001; Lowenstein et al., 2003). (5) The relative importance of evaporated seawater chemistry and diagenetic reactions for the control of the chemistry of basinal brines (Hanor and McIntosh, 2006; Lowenstein and Timofeeff, 2008). (7) The debated origin for  $\text{CaCl}_2$ -rich brines in sedimentary basins (Hardie, 1990; Spencer, 1987; Wilson and Long, 1993a, 1993b; Davisson and Criss, 1996; Lowenstein et al., 2003) (8) The lack of knowledge on metal concentration in basinal fluids.

Therefore, we have compared the detailed composition of fluid inclusions with 520 analyses of present-day high salinity deep fluids sampled in 10 sedimentary basins ([Table 7.1](#)). Together with previously established Na, Ca, K, Mg, Li, Sr, Ba, Fe, Mg, Cu, Pb, Zn and U concentrations from LA-ICP-MS analyses of fluid inclusions ([Part 3, Part 4; Part 5](#)), additional data for Na, K, Ca, Mg, Li, B, Cu, Pb, Zn, U, Rb, Ni, Co, Ag, Se, As, and Ce from crush-leach analyses of bulk fluid inclusion populations are presented. Compositions similar to- or different from commonly sampled basinal fluids for a given element could thus be interpreted in terms of basin vs. basement origin. For elements that are not commonly analyzed in basinal fluids (e.g. Ni, Co, As), relations with major elements could help understanding their origin.

Finally, these data could contribute to determine the origin of  $\text{CaCl}_2$ -rich brines in the Athabasca Basement, and their migration path in basement rocks, leading to the formation of giant unconformity-related uranium deposits.

## 7.2. Basinal fluid database

The basinal fluid database includes 520 analyses for major and trace elements from deep fluids in ten sedimentary basins ([Table 7.1](#)). Papers included in the database discuss on the origin and controls on major and trace elements concentrations in these fluids. Chlorine is the dominant ion in these fluids and ranges from ca. 1000 to ca. 250000 ppm. TDS range from 1500 to 290000 mg/l. For comparison, chlorine in the Athabasca brines (this study), ranges from 120000 to 220000 ppm. Fluids from basinal fluid database were all sampled by drilling. Authors presenting analyses of Ca-rich brines are [Carpenter et al., \(1974\)](#) (Central Mississippi, USA) and [Wilson and Long \(1993a, 1993b\)](#) (Michigan Basin, USA). The mineralogical composition of aquifers in which fluids are sampled, and more generally of sedimentary basins filling is highly variable and comprises evaporites, silicoclastics, carbonates and shales. The origin of saline fluids in each basin is matter of debate. Main factors controlling their salinity are seawater evaporation, evaporite dissolution

and dilution by seawater and/or meteoric water ([Hanor, 1994](#)). A lot of papers have been published dealing with chemistry of basinal brines. However, we consider that our restricted basinal fluid database is representative of the variability of composition of basinal fluids.

Location	Reference	TDS range in mg/l
Alberta Basin, Canada	Connoly et al., (1990)	1900-144000
Central Mississippi, USA	Carpenter (1974); Kharaka et al., (1987)	72000-207000
Gulf Coast Basin, USA	Hyeong and Capuano (2001)	31000-132000
Illinois Basin, USA	Stueber and Walter (1991)	2000-137000
Kettleman North Dome, USA	Merino (1975)	1500-42000
Michigan Basin, USA	Wilson and Long (1993a, 1993b)	76000-275000
North German Basin	Kloppmann et al., (2001)	13000-328000
Norwegian shelf	Egeberg and Aaggard (1989)	11000-178000
Palo Duro Basin, USA	Fisher and Kreitler, (1987)	140000-290000
Paris Basin, France	Fontes and Matray (1993b)	1600-140000

**Table 7.1 : Sources of major and trace elements data for basinal fluids used in this study. TDS: total dissolved solids.**

### 7.3. Crush-leach analysis

Crush-leach analyses were carried out on 47 quartz and carbonate veins at the School of Earth and Environment, University of Leeds, UK, following the methodology of [Banks and Yardley, \(1992\)](#); [Banks et al., \(2000\)](#) and [Gleeson \(2003\)](#). Samples preparation and analyses of Cl, Br, F and SO<sub>4</sub> are presented in [Part 6](#) together with discussion on significance of Cl/Br ratios and origin of Cl.

Clean samples powders were leached in double distilled water for Na, K, Li analysis using flame emission spectroscopy and leached in acidified LaCl<sub>3</sub> solution for B, Na, Mg, K, Ca, Mn, Fe, Co, Ni, Cu, Zn, As, Se, Rb, Sr, Ag, Ba, REEs, Pb and U analysis using LA-ICP-MS. Among REEs, only Ce yielded signals above limits of detections. La was not analyzed due to LaCl<sub>3</sub> leaching. Only Na, K and Li could be analyzed in fluid inclusion leachates from carbonate samples, because carbonates potentially contain significant amount of trace elements in their structure. Limits of detections in fluid inclusion leachates are ca. 1-5 ppb for alkalis and alkaline earths and ca. 0.1 ppb for other cations. Atomic ratios relative to Na were combined with Cl, Br, F and SO<sub>4</sub> concentrations and salinity estimates from

Microthermometry, to calculate absolute elements concentrations in fluid inclusions using the equation of Banks et al., (2000).

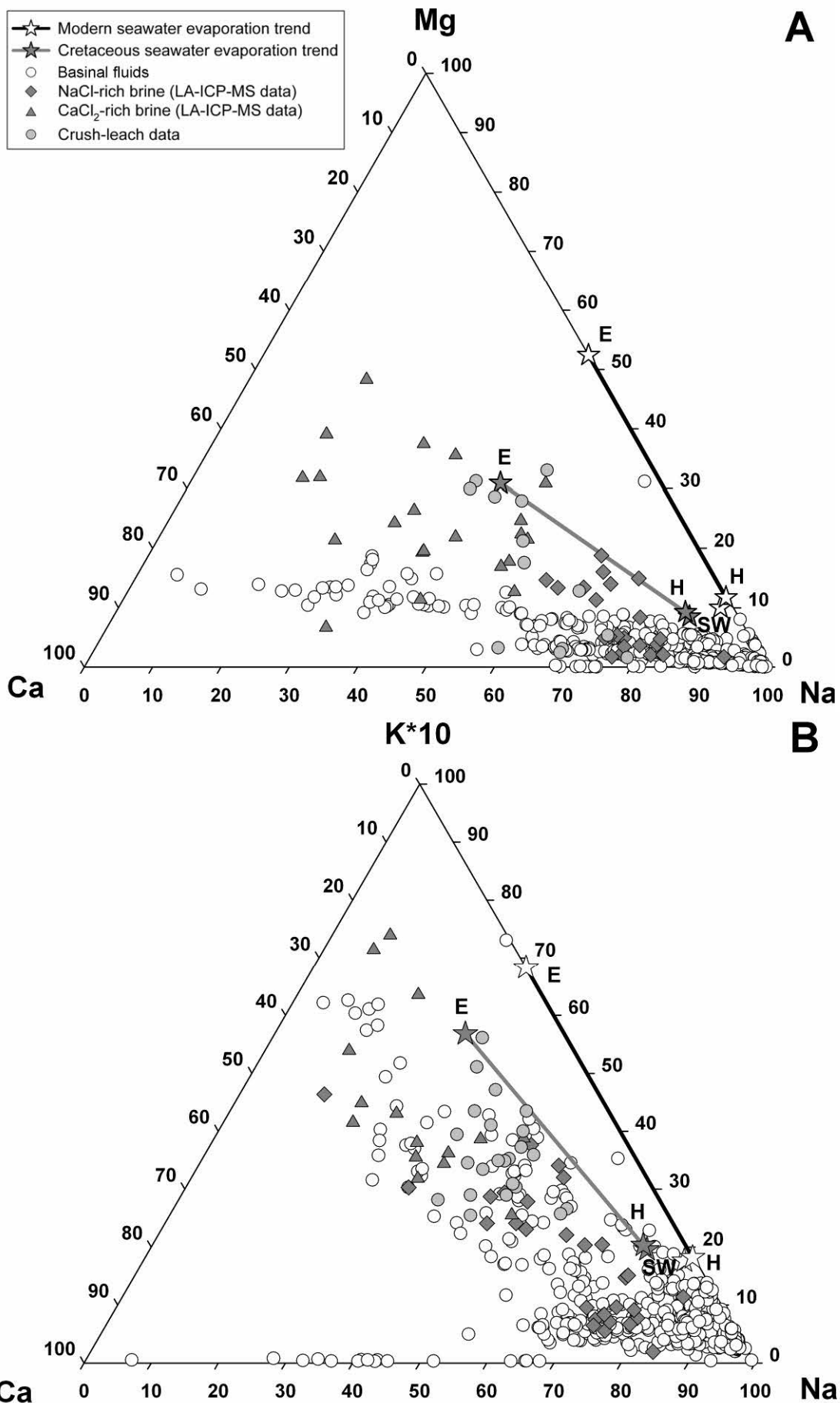
Despite great care in sample separation and cleaning, fluid inclusion leachates from quartz samples show punctually anomalously high concentrations for one or several elements, which is likely to result from contamination by surrounding minerals. Minerals commonly found in the environment of quartz veins and having potentially contaminated fluid inclusion leachates are calcite, dolomite, hematite, pitchblende, illite, sudoite, dravite and pyrite (Part 2). Anomalously high concentrations were removed from dataset and noted as not determined (nd) in Table 7.2. Theoretically, charge balance ( $\Sigma\text{ev+}/\Sigma\text{ev-}$ ) should equal 1 if all species have been determined correctly, and can be used to validate our reconstruction of bulk fluid inclusion chemistry. Charge balance for carbonate samples range from 0.2 to 0.5 which is consistent with the fact that only Na, K, and Li were analyzed, Ca and Mg being potential major cations. For quartz samples, charge balances range from 0.5 to 1.6. When one major element was removed from dataset because of suspicion of contamination, charge balances are consistently generally below 1. Charge balances above 1 could reflect either unsuspected contamination affecting one ore more major cations, or analytical error potentially spread over all solutes. Charge imbalances are frequent in natural water analyses are rarely discussed in crush-leach analyses of fluid inclusions (Banks et al., 2000b; Gleeson et al., 2001; Gleeson and Turner, 2007) Finally, we believe that our crush-leach analyses should not be considered as purely quantitative but rather as semi-quantitative, nevertheless providing valuable information regardless of analytical and contamination issues. Samples contain variable proportions of NaCl-rich and CaCl<sub>2</sub>-rich brine inclusions, and element concentrations reconstructed form crush-leach analyses represent mixtures of the two brines. Crush-leach data are shown in Table 7.2.

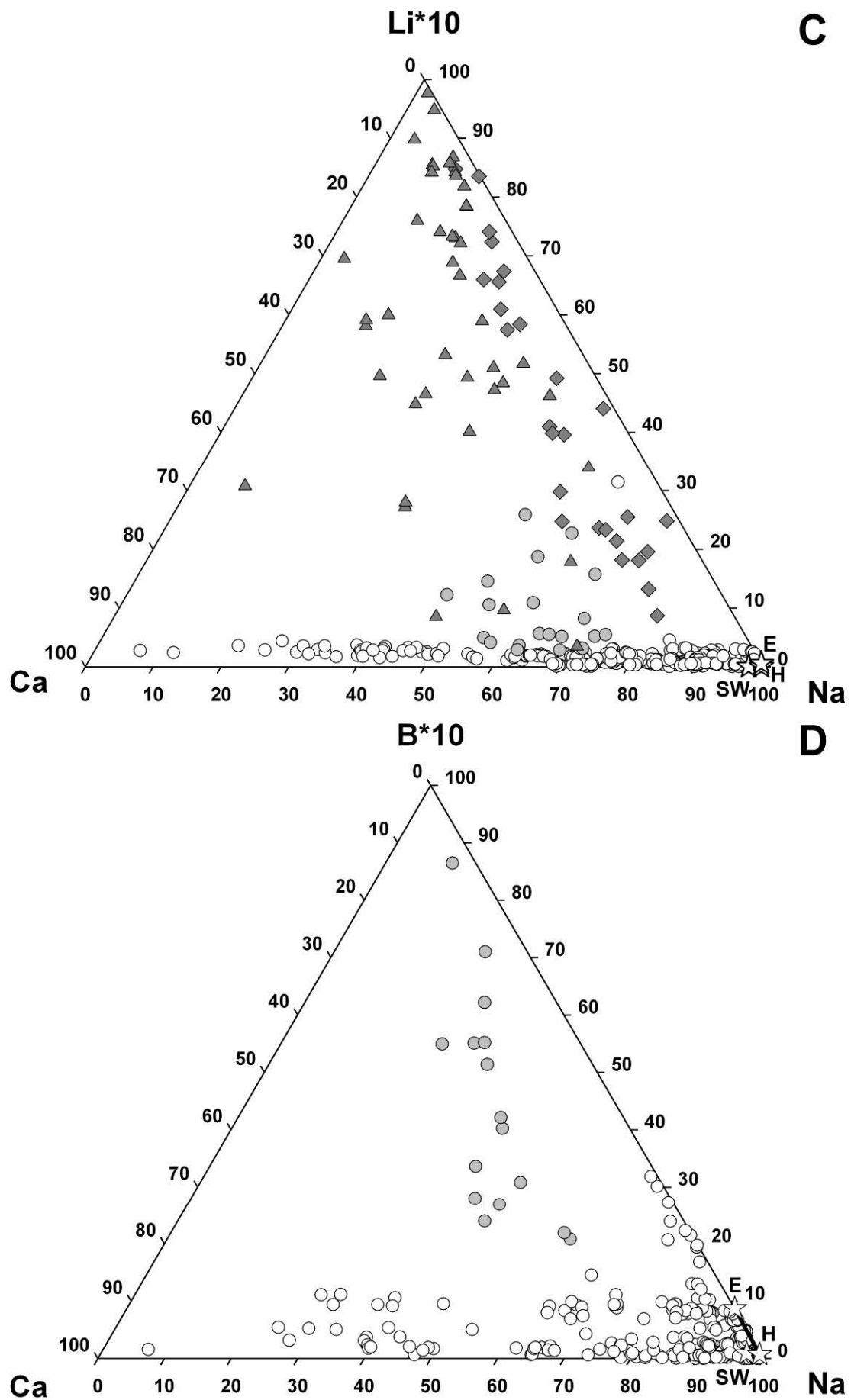
Table 7.2 : Reconstitution of composition of bulk fluid inclusion population from crush-leach analysis. All concentrations in ppm. wt%: average salinity from microthermometry. Qz: quartz. Dol: dolomite. Cal: calcite. na: not analyzed. nd: not determined. bd: below detection limit.

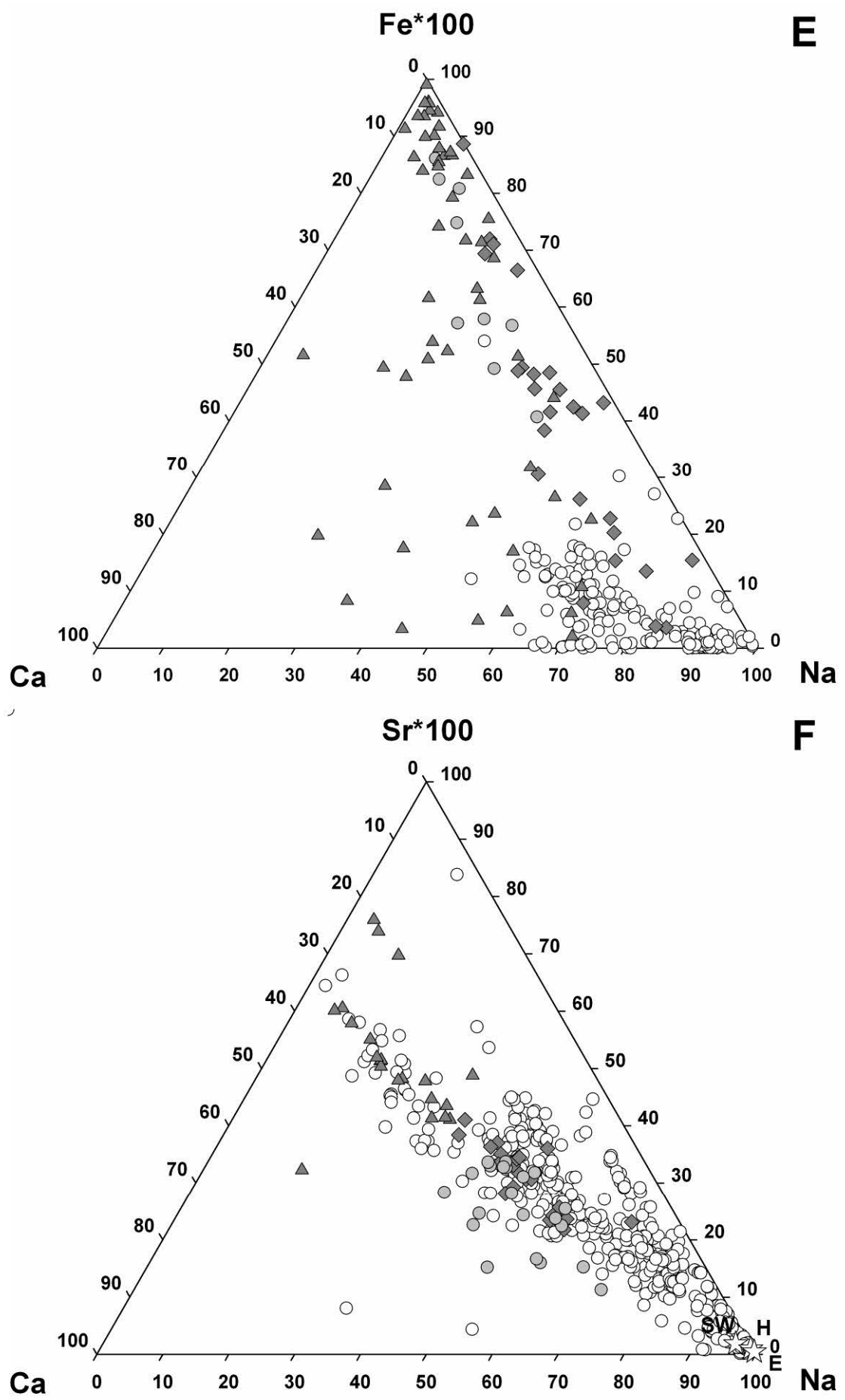
## 7.4. Comparison of brine compositions with basinal fluids

### 7.4.1. Cation concentrations

Data from basinal fluid database, LA-ICP-MS and crush-leach analyses were plotted in ternary (Na-Ca-X) diagrams for the following reasons ([Figure 7.1](#)): (1) Ternary diagrams allow the comparison of fluids regardless of their salinity. (2) Na and Ca are the two dominant cations in basinal brines and ternary (Na-Ca-X) diagrams could then allow the identification of unusual compositions. (3) The origin of compositional shift from Ca-rich composition to Ca-rich composition is the main topic of this paper and (Na-Ca-X) diagrams could help resolving this issue. Scaling problems were solved by multiplying molar elements concentration by 10 (K, Li, B), 100 (Fe, Sr), 1000 (Ba, Mn, Cu, Zn, Pb) or 10000 for Rb. Seawater evaporation trends were also plotted in ternary (Na-Ca-X) diagrams up to epsomite saturation when solutes concentrations in evaporated seawater are known. Indeed, epsomite saturation is thought to be the highest evaporation degree underwent by the Athabasca Basin brines ([Part 6](#)). Modern seawater evaporation trend, typical of that of  $MgCl_2$  seas ([Fontes and Matray, 1993a](#)), and Cretaceous seawater evaporation trend, typical of  $CaCl_2$  seas ([Timofeff et al., 2006; Lowenstein and Timofeff, 2008](#)) were plotted in ternary diagrams and illustrate of the potential variability of evaporated seawater composition.

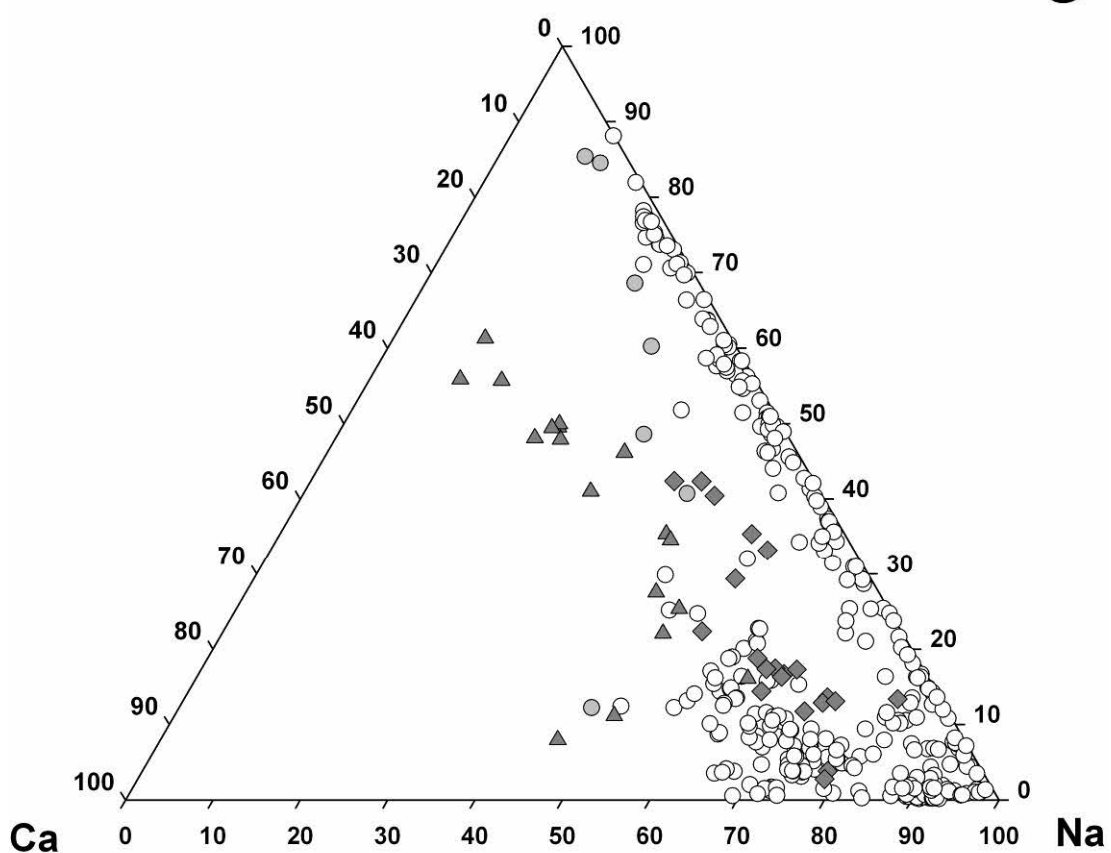






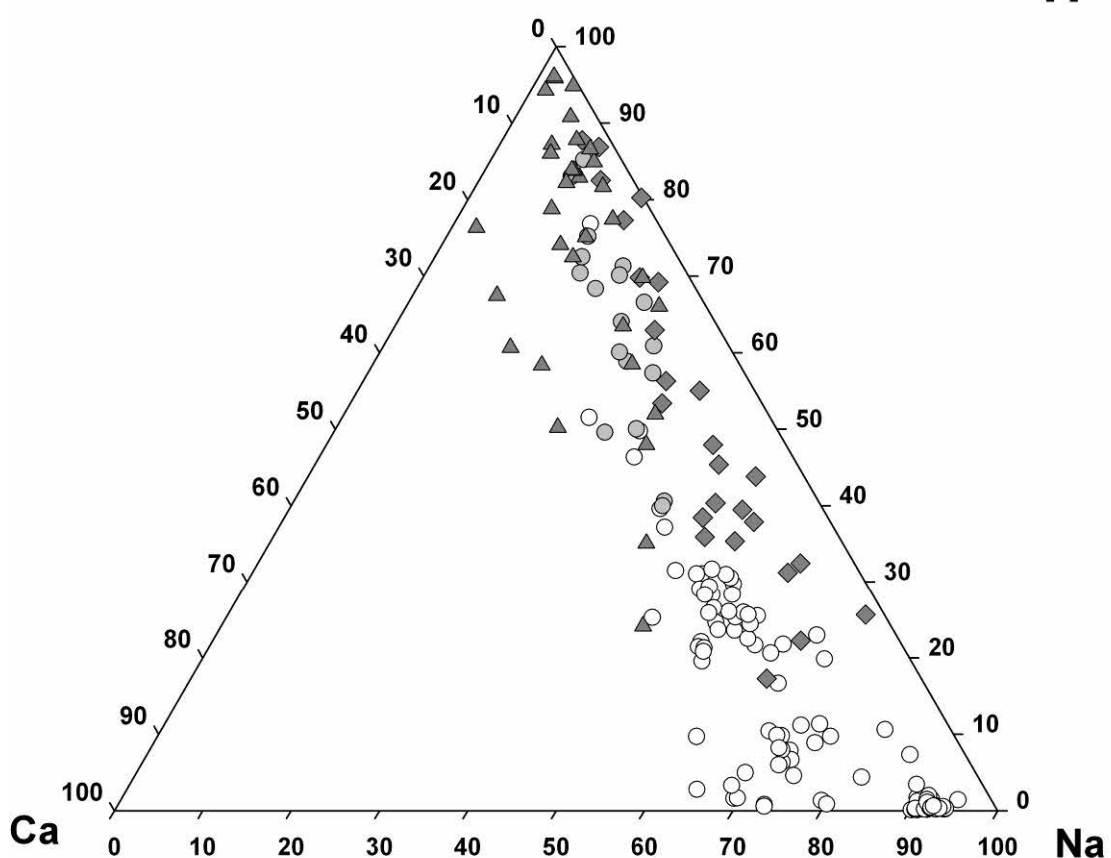
**Ba\*1000**

**G**

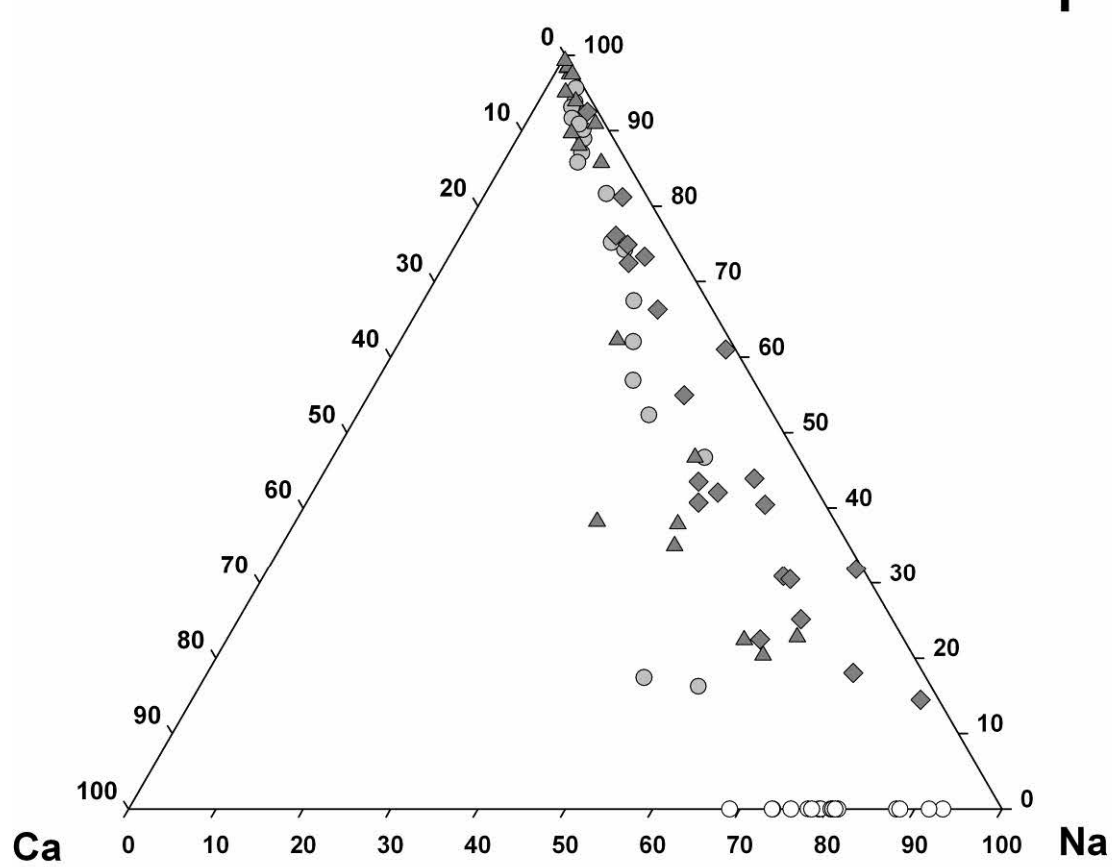


**Mn\*1000**

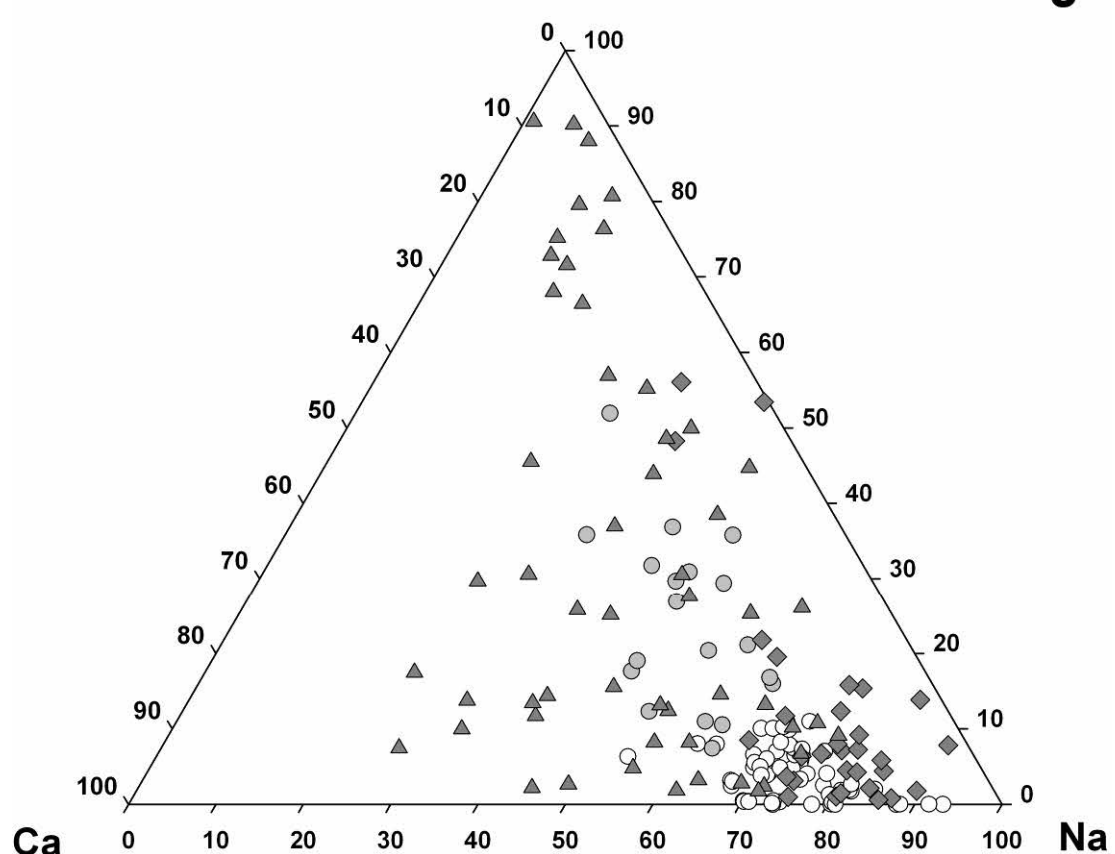
**H**



**Cu\*1000**



**Pb\*1000**



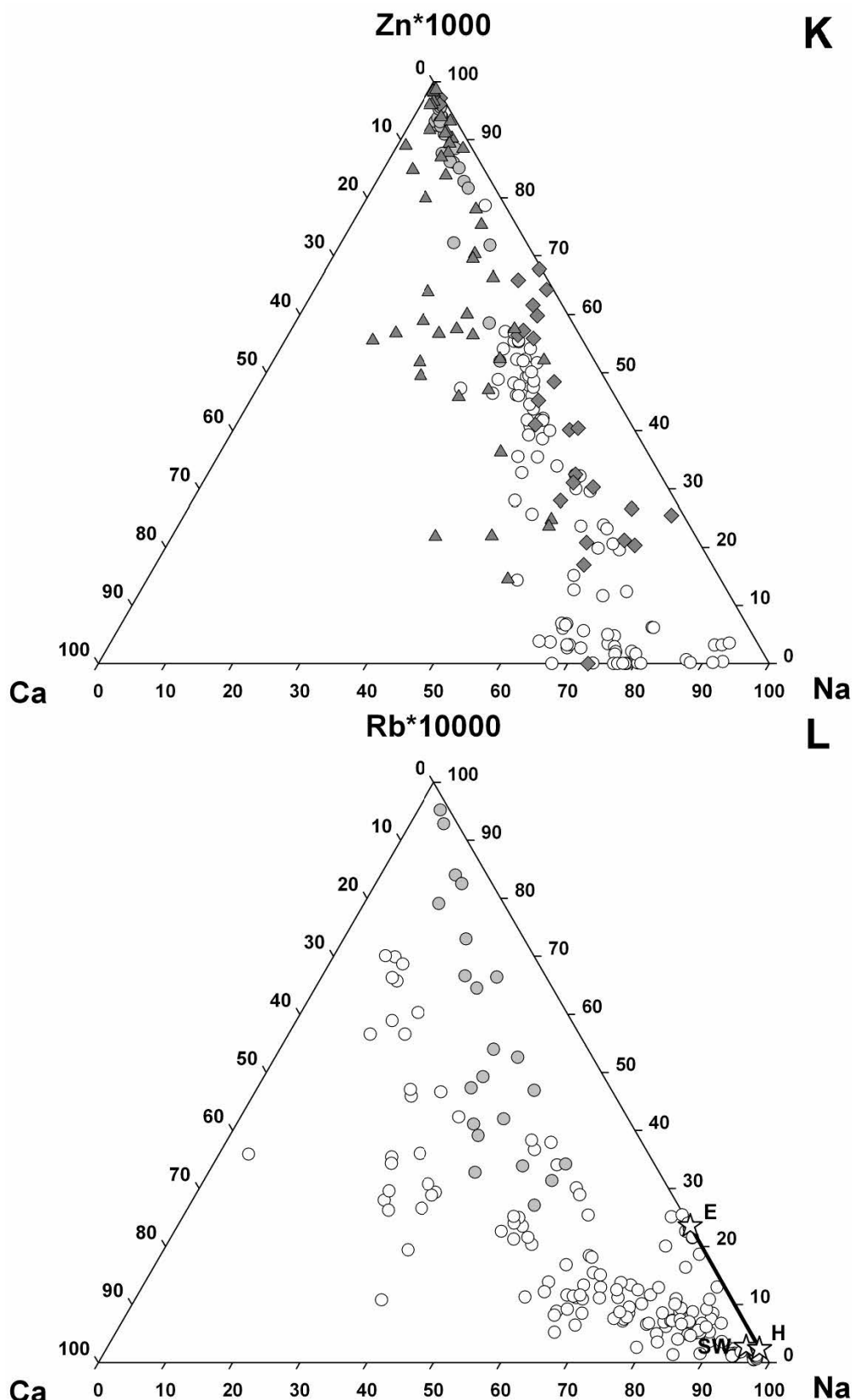


**Figure 7.1 : Comparison between chemistry of Athabasca NaCl-rich and CaCl<sub>2</sub>-rich brines with commonly sampled basinal fluids from basinal fluid database ([Table 7.1](#)), with emphasis on transition between Na-dominated fluids and Ca-dominated fluids. Ternary diagrams are built on molar element concentrations. SW: seawater. H: halite. E: epsomite. Modern seawater evaporation trend from [Fontes and Matray \(1993a\)](#). Cretaceous seawater evaporation trend from [Lowenstein and Timofeef \(2008\)](#).**

In the Na-Ca-Mg diagram ([Figure 7.1A](#)), LA-ICP-MS data show a trend from Na-rich composition to Ca-Mg-rich composition, which was interpreted as a mixing trend between the NaCl-rich brine and the CaCl<sub>2</sub>-rich brine ([Part 3](#)). Half of NaCl-rich brine inclusions have Na-Ca-Mg composition consistent with Na-rich and Mg-poor basinal fluids. The other half of NaCl-rich brine inclusions are enriched in Mg compared to basinal fluids. As discussed in [Part 3](#) these inclusions do not represent pure NaCl-rich brine end-member but rather a mixing term dominated by NaCl-rich brine. NaCl-rich brine inclusions are enriched in Ca and depleted in Mg compared to modern evaporated seawater, and have Ca content more compatible with Cretaceous evaporated seawater. CaCl<sub>2</sub>-rich brine inclusions have Na/Ca ratios compatible with CaCl<sub>2</sub>-rich basinal brines but most inclusions are enriched in Mg compared to basinal fluids. Mg content of CaCl<sub>2</sub>-rich brine inclusions is compatible with both modern and Cretaceous evaporated seawaters, and Ca content is higher than both modern and Cretaceous evaporated seawaters.

In the Na-Ca-K diagram ([Figure 7.1B](#)), LA-ICP-MS data show a mixing trend similar to that described for Na-Ca-Mg diagram, between Na-rich composition (NaCl-rich brine) and Ca-K-rich compositions (CaCl<sub>2</sub>-rich brine). Half of NaCl-rich brine inclusions have Na-Ca-K composition consistent with predominant Na-rich and K-poor basinal fluids and have low K and high Ca compared to evaporated seawaters, the other half being enriched in K and, together with CaCl<sub>2</sub>-rich brine inclusions, have K compatible with evaporated seawaters, and K-rich basinal fluids from Michigan Basin and Central Mississippi ([Carpenter 1974; Kharaka et al., 1987; Wilson and Long 1993a, 1993b](#)). LA-ICP-MS data show that NaCl-rich brine inclusions are predominantly relatively Li-poor and CaCl<sub>2</sub>-rich brine inclusions are predominantly relatively Li-rich ([Figure 7.1C](#)) as noted in [Part 4](#). LA-ICP-MS data for both brines plot in a Li-rich field, above basinal fluids and modern evaporated seawater. Surprisingly, crush-leach data plot in an intermediate field between LA-ICP-MS data and basinal fluids. Despite inconsistencies between LA-ICP-MS and crush-leach analyses, these results indicate that both brines have Li content higher than basinal fluids.

[Figure 7.1D](#) shows that crush-leach data plot in a B-rich field in a Na-Ca-B diagram. Considering that crush-leach data represent mixing terms between the NaCl-rich brine and the CaCl<sub>2</sub>-rich brine and that the B seems to be positively correlated to Ca, the NaCl-rich brine is likely to have B content compatible with basinal fluids and modern evaporated seawaters, while the CaCl<sub>2</sub>-rich brine has probable B content well higher than basinal fluids. In a Na-Ca-Rb diagram ([Figure 7.1L](#)), some crush-leach data are compatible with observed compositions in basinal fluids, while some other data plot in a Rb-rich field. As for B, the most B-enriched samples are linked to high Ca content. These data suggest that the NaCl-rich brine could have Na-Ca-Rb composition compatible with basinal fluids and modern evaporated seawater, while the CaCl<sub>2</sub>-rich brine could have Rb content higher than commonly sampled basinal fluids.

Not surprisingly, due to their similar geochemical behaviour, Ca and Sr concentrations are highly correlated in basinal fluids as well as in Athabasca brines ([Figure 7.1F](#)). Both NaCl-rich brine and CaCl<sub>2</sub>-rich brine inclusions are enriched in Sr compared to modern evaporated seawater. NaCl-rich brine inclusions have Na-Ca-Sr composition Sr-rich basinal fluids ([Carpenter 1974; Kharaka et al., 1987; Wilson and Long 1993a, 1993b](#)).

Ba content of basinal brines is highly variable and is compatible with all LA-ICP-MS data. High Ba in crush-leach data, if reliable, would indicate a Ba-rich fluid with Ba content well above that of basinal fluids ([Figure 7.1G](#)). In a Na-Ca-Cu diagram ([Figure 7.1I](#)), LA-ICP-MS data show that NaCl-rich brine inclusions are predominantly relatively Cu-poor and CaCl<sub>2</sub>-rich brine inclusions are predominantly relatively Cu-rich as noted in [Part 4](#). Very few data are available for Cu concentrations in basinal fluids. Data plotted here suggest that the brines studied here have Cu content well higher than basinal brines. Part of data for NaCl-rich brine show Fe, Mn, Pb, Zn content compatible with basinal fluids, while a majority of data for CaCl<sub>2</sub>-rich brine show Fe, Mn, Pb, Zn content higher than basinal fluids ([Figure 7.1E-H-J-K](#)).

#### 7.4.2. Anion concentrations

Br is conservative in solution and could hardly be affected by fluid-rock interactions. The significance of Cl/Br ratios is discussed in [Part 6](#). F and SO<sub>4</sub> concentrations from crush-leach analyses and basinal fluid database were plotted as a function of Cl concentration ([Figure 7.2](#)).

[Figure 7.2A](#) shows that SO<sub>4</sub> concentration rarely exceeds 1000 ppm in basinal fluids and is comprised between 100 and 1000 ppm in crush-leach data. Thus, there is some evidence for anomalously high SO<sub>4</sub> concentrations probably in both NaCl-rich and CaCl<sub>2</sub>-rich brines, close to or higher than concentrations found in modern evaporated seawater.

[Figure 7.2B](#) shows that F concentration is always lower than 100 ppm and predominantly below 10 ppm in basinal brines. Few data are available for F concentration in our basinal fluid database, but compilation of literature data from [Worden \(1996\)](#) confirms that F in basinal fluids generally does not exceed 20 ppm. No data are available for F concentration in evaporated seawater, but following the hypothesis of [Worden \(1996\)](#) assuming evaporative concentration of F at the same rate as Cl up to halite precipitation, a maximum of ca. 10 ppm should be expected for F in evaporated seawater. Crush-leach data plot up to two orders of magnitude above basinal brines and evaporated seawater. As for SO<sub>4</sub>, there is some evidence for anomalously high F concentrations probably in both NaCl-rich and CaCl<sub>2</sub>-rich brines. Note that a majority of samples have F concentrations below LOD and that F concentrations are thus highly heterogeneous among samples and brines.

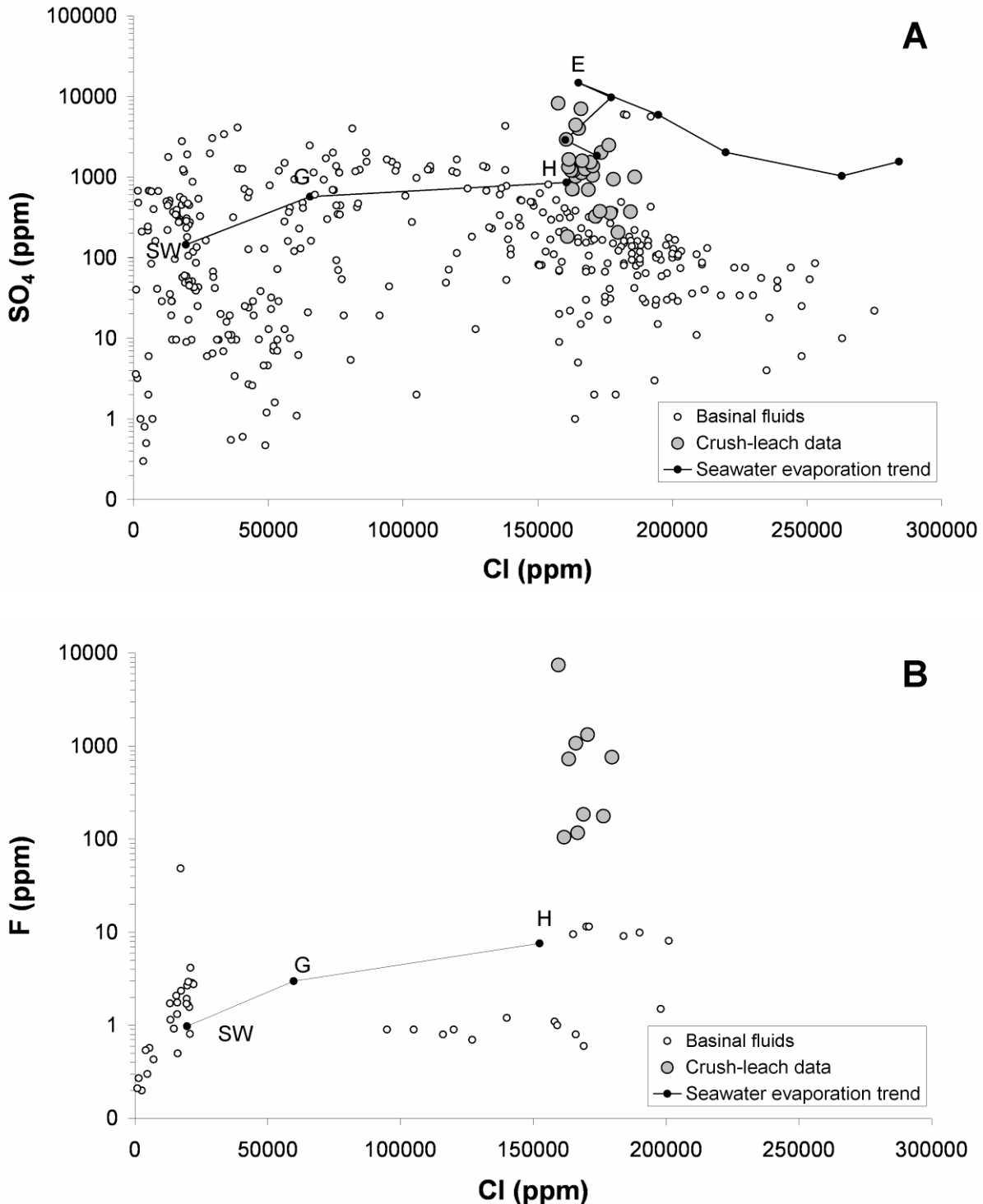


**Figure 7.2 : Comparison between  $\text{SO}_4$  and F concentrations in Athabasca NaCl-rich and  $\text{CaCl}_2$ -rich brines with commonly sampled basinal fluids. SW: seawater. H: halite. E: epsomite. (A) Modern seawater evaporation trend from [Fontes and Matray \(1993a\)](#). (B) Seawater evaporation trend from [Worden \(1996\)](#).**

## 7.5. Discussion

### 7.5.1. Origin of solutes in the NaCl-rich brine

From direct comparison with basinal fluid database ([Figure 7.1](#)), NaCl-rich brine inclusions have Na-Ca-Mg-K-Sr compositions clearly compatible with commonly sampled basinal fluids. This suggests that the major element chemistry of the NaCl-rich brine was partly to completely controlled by evaporation of seawater, mixing with halite-dissolution fluid and diagenetic reactions. An argument in favour of an homogeneous NaCl-rich brine aquifer throughout the base of the Athabasca Basin is the ubiquitous and widespread presence of NaCl-rich brine fluid inclusions with restricted salinity range (generally 25-30 eq. wt% NaCl) and Na/Ca atomic ratios (generally 3-5) corresponding to the Lw2 microthermometric type fluid inclusions in [Derome et al., \(2005\)](#) and [Part 4](#). For Zn, Pb, Fe, Mn and Rb, comparison with basinal fluids do not allow to clearly point out a basement origin for these elements in the NaCl-rich brine. However, if some of the NaCl-rich brine inclusions are compatible with basinal fluid, a significant number are in the highest range or even in concentrations higher than in basinal fluids. This suggests that these elements at least partly originate from basement lithologies. For Ba, simple comparison with basinal fluids does not allow to speculate on its origin. Cu, is anomalously high in NaCl-rich brine inclusions and, despite the very few data for basinal fluids suggest that it was partly leached by the NaCl-rich brine in the basement.

Ca. 60% of measured Na/K ratios lie in the 20-200 range and are thus compatible with temperatures of 100-200°C following the Na/K geothermometer from [Verma and Santoyo \(1997\)](#) ([Figure 7.3](#)). This temperature range corresponds to that estimated for NaCl-rich brine inclusions ([Derome et al., 2005; Part 4](#)). Ca. 40% of NaCl-rich brine inclusions show Na/K ratios below 20 which would indicate temperatures up to 350°C which is incompatible with PT reconstructions from microthermometric measurements. Because NaCl-rich brine inclusions with low Na/K ratios may not represent pure NaCl-rich brine end-

member but rather a NaCl-rich brine-dominated mixing term with CaCl<sub>2</sub>-rich brine, we consider that the NaCl-rich brine has Na/K ratios compatible equilibrium with feldspars at 100-200°C. The case of Li is complicated by contradictory results from crush-leach and LA-ICP-MS analyses. Crush-leach analyses suggest that Li in the NaCl-rich brine is potentially compatible with basinal fluids, while LA-ICP-MS results indicate anomalously high Li content. Na/Li geothermometer indicates temperatures well above 200°C for LA-ICP-MS analyses, while crush-leach analyses indicate temperatures compatible with 100-200°C range but predominantly above 200°C. Thus, from Li/Na geothermometer, both techniques suggest that Li is anomalously high in the NaCl-rich brine, which could have inherited Li from interaction with basement rocks.

[Figure 7.4](#) shows that NaCl-rich brine inclusions plot above the basinal fluid line defined by [Davisson and Criss, \(1996\)](#) in a Na excess vs. Ca deficit diagram. As, shown by these authors, the vast majority of basinal fluids plot along the basinal fluid line, defined by 2:1 exchange reaction between Na and Ca from a seawater-like parent fluid. A common interpretation for Ca excess at constant Na deficit in basinal brines is dolomitisation processes. Therefore, these results suggest that the Ca and Mg concentrations in the NaCl-rich brine were partly controlled by dolomitization in the basin.

### 7.5.2. Origin of solutes in the CaCl<sub>2</sub>-rich brine

From comparison with basinal fluids, CaCl<sub>2</sub>-rich brine inclusions are highly enriched in Mg. Such high Mg concentrations are also found in evaporated seawaters but Mg is generally removed from basinal fluids by dolomitization ([Hanor, 1994](#)). Thus, we strongly suggest that the CaCl<sub>2</sub>-rich brine has inherited the majority of its Mg from fluid-rock interactions in the basement. Ca, K and Sr in the CaCl<sub>2</sub>-rich brine inclusions are compatible with Ca-K-Sr-rich formation waters typically found in Central Mississippi and Michigan Basins ([Carpenter et al., 1974](#), [Kharaka et al., 1987](#); [Wilson and Long, 1993a, 1993b](#)). However, as mentioned above, the presence of ubiquitous NaCl-rich brine at the base of the Athabasca

Basin is the most reasonable hypothesis. In addition positive correlation between Mg-Ca-K-Sr and Ba concentrations ([Part 3](#)) suggest that these elements have the same origin. Because a basement origin for Mg in CaCl<sub>2</sub>-rich brine is strongly suspected, Ca, K, Sr and Ba in the CaCl<sub>2</sub>-rich brine probably originates from the basement

[Figure 7.3](#) shows that CaCl<sub>2</sub>-rich brine inclusions plot above the basinal fluid line, with comparable Ca excess compared to NaCl-rich brine inclusions. However CaCl<sub>2</sub>-rich brine inclusions define a compositional trend parallel to the basinal fluid line. Because NaCl-rich brine and CaCl<sub>2</sub>-rich brine inclusions show a continuum, the composition of the CaCl<sub>2</sub>-rich brine can partly be explained by conversion of NaCl-rich brine to CaCl<sub>2</sub>-rich brine through 2Na :1Ca exchange reactions.

Na/K ratios predominantly below 20 and Na/Li ratios below 300 indicate temperatures well above 200°C which is not consistent with 150 ± 30°C estimated from microthermometry ([Part 7.4](#)). Thus, Na/K ratios indicate that the CaCl<sub>2</sub>-rich brine was in strong disequilibrium with K-feldspars which is consistent with partial-to-complete dissolution of K-feldspars in alteration haloes ([Mercadier et al., in prep](#)). Alternatively, the CaCl<sub>2</sub>-rich brine could have been heated at depth in basement rocks and acquired low Na/K and Na/Li ratios before ascending along faults and being trapped as fluid inclusions.

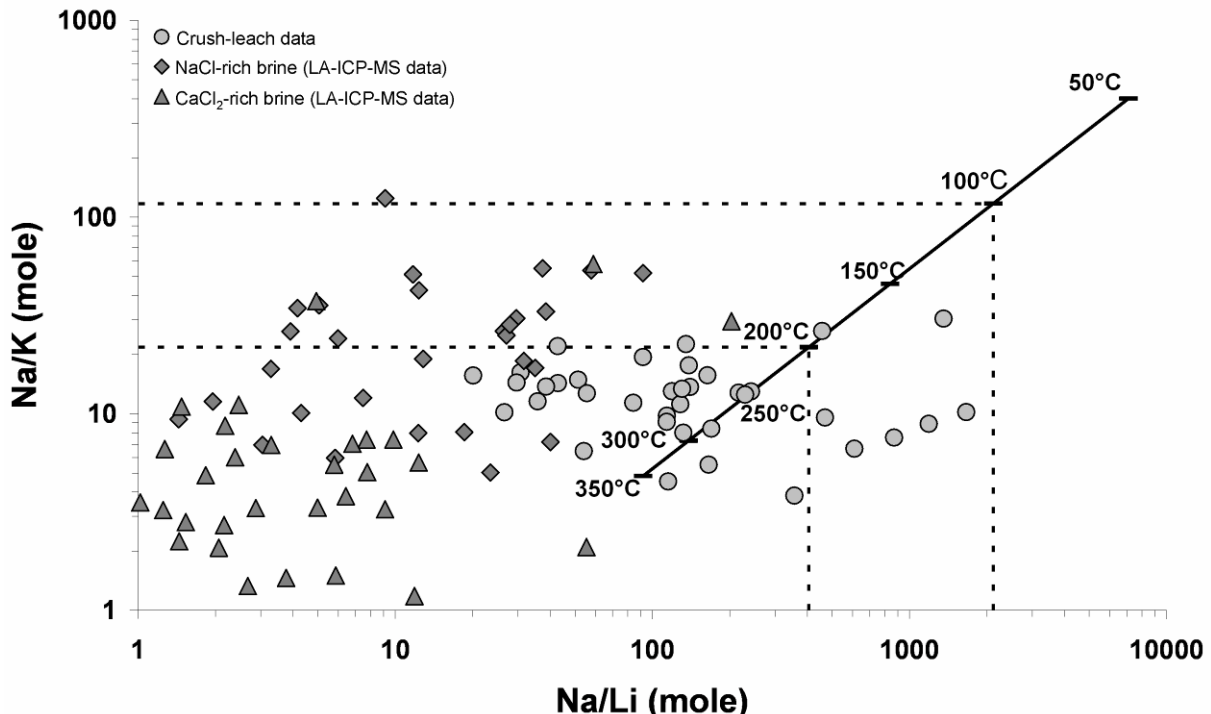


Figure 7.3 : Na/K – Na/Li molar ratios of Athabasca NaCl-rich and CaCl<sub>2</sub>-rich brines determined from crush-leach and LA-ICP-MS analyses. Full line: temperature estimation deduced from the geothermometric cation relationships (Verma and Santoyo, 1997). Dotted lines: expected ranges of Na/K and Na/Li ratios in Athabasca brines, from temperatures deduced from fluid inclusions (Part 4), if geothermometric relationships are respected.

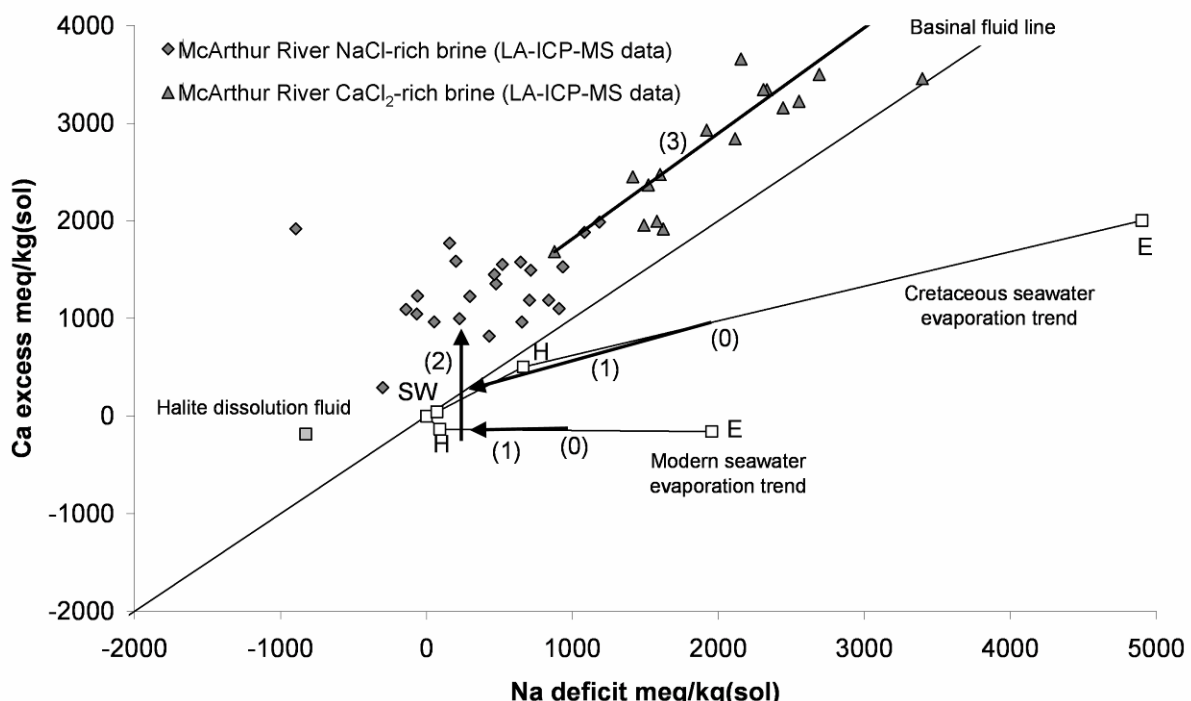
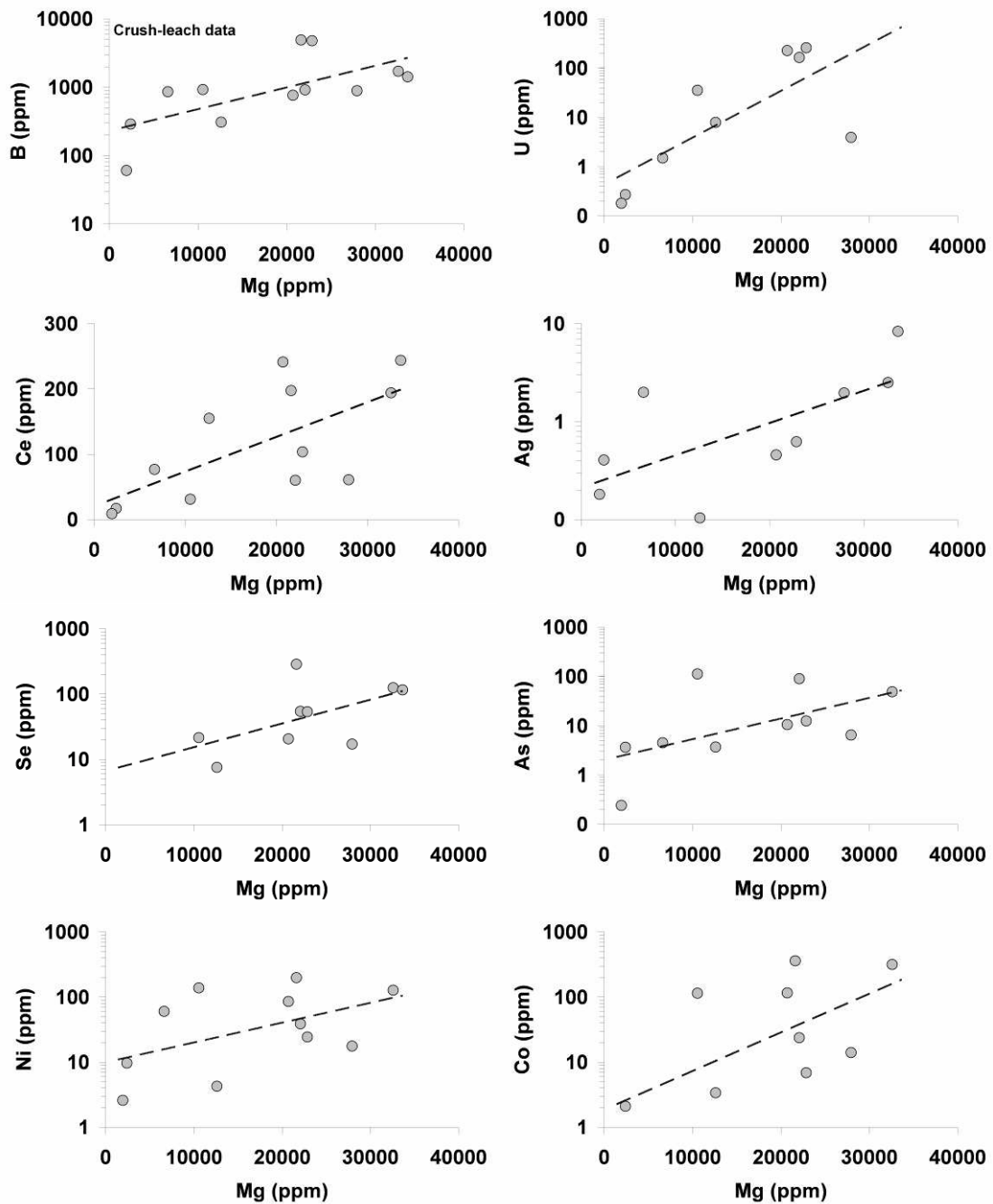


Figure 7.4 : Ca excess vs. Na deficit diagram for fluid inclusions analyzed by LA-ICP-MS. (0) Seawater evaporation. Proposed scenario for acquisition of fluids chemistry: (1) Mixing with halite-dissolution fluid (composition from Chi and Savard, 1997). (2) Ca gain by dolomitization. (3) 2Na : 1Ca exchange and conversion of NaCl-rich brine to CaCl<sub>2</sub>-rich brine. Basinal fluid line from Davisson and Criss (1996). SW: seawater. H: halite. E: epsomite. Modern seawater evaporation trend from Fontes and Matray (1993a). Cretaceous seawater evaporation trend from Lowenstein and Timofeev (2008).

### 7.5.3. Metal transport

High Mg concentrations are typical of CaCl<sub>2</sub>-rich brine inclusions. As discussed above, basement is the dominant source for Mg in the CaCl<sub>2</sub>-rich brine. In order to further investigate sources minor elements U, B, Ce, As, Ni, Co, Se, Ag concentrations from crush-leach analyses were plotted as a function of Mg concentration ([Figure 7.5](#)). High Mg concentrations in fluid inclusion leachates indicate that bulk fluid inclusion populations are dominated by CaCl<sub>2</sub>-rich brine inclusions. A slight positive correlation is observed between Mg and the plotted elements, suggesting that these elements are predominantly concentrated in the CaCl<sub>2</sub>-rich brine. Also, these correlations could imply that Mg and these elements are leached together within basement rocks.

As shown in [Part 3 to 5](#), both NaCl-rich and CaCl<sub>2</sub>-rich brines display highly variable metal (U-Pb-Cu-Zn) concentrations with four orders of magnitudes of variations for each metal concentration. The CaCl<sub>2</sub>-rich brine is generally slightly enriched in U-Pb-Cu-Zn compared to the NaCl-rich brine, the magnitude of this enrichment being less than one order of magnitude. [Figure 7.6](#) shows that U-Pb-Cu-Zn concentrations in brines measured by LA-ICP-MS analysis are relatively well positively correlated. One way to explain such results is that the above mentioned metals could have been leached from a single dominant source or reservoir (i. e. basin or basement). To add, this source or reservoir should be quite close to the location of the studied samples, so that the studied fluids did not have the time to become homogeneous before trapping as fluid inclusions. Also, when comparing with literature data ([Kharaka et al., 1987; Yardley et al., 2005](#)), the metal concentrations above 100 ppm are relatively unexpected for basinal brines which points out either the exceptional solubility of metals in such brines or the availability of metals in a proximal environment. Provided that both NaCl-rich and CaCl<sub>2</sub>-rich brines have interacted at various degree with basement lithologies, all of these criteria support the idea that the basement is a significant and possibly a dominant metal source for the brines.



**Figure 7.5 : Bivariate plots of Mg vs. B, metals (U, Ag, Se, As, Ni, Co) and REE (Ce), determined from crush-leach analyses. All plots show possible positive correlation.**

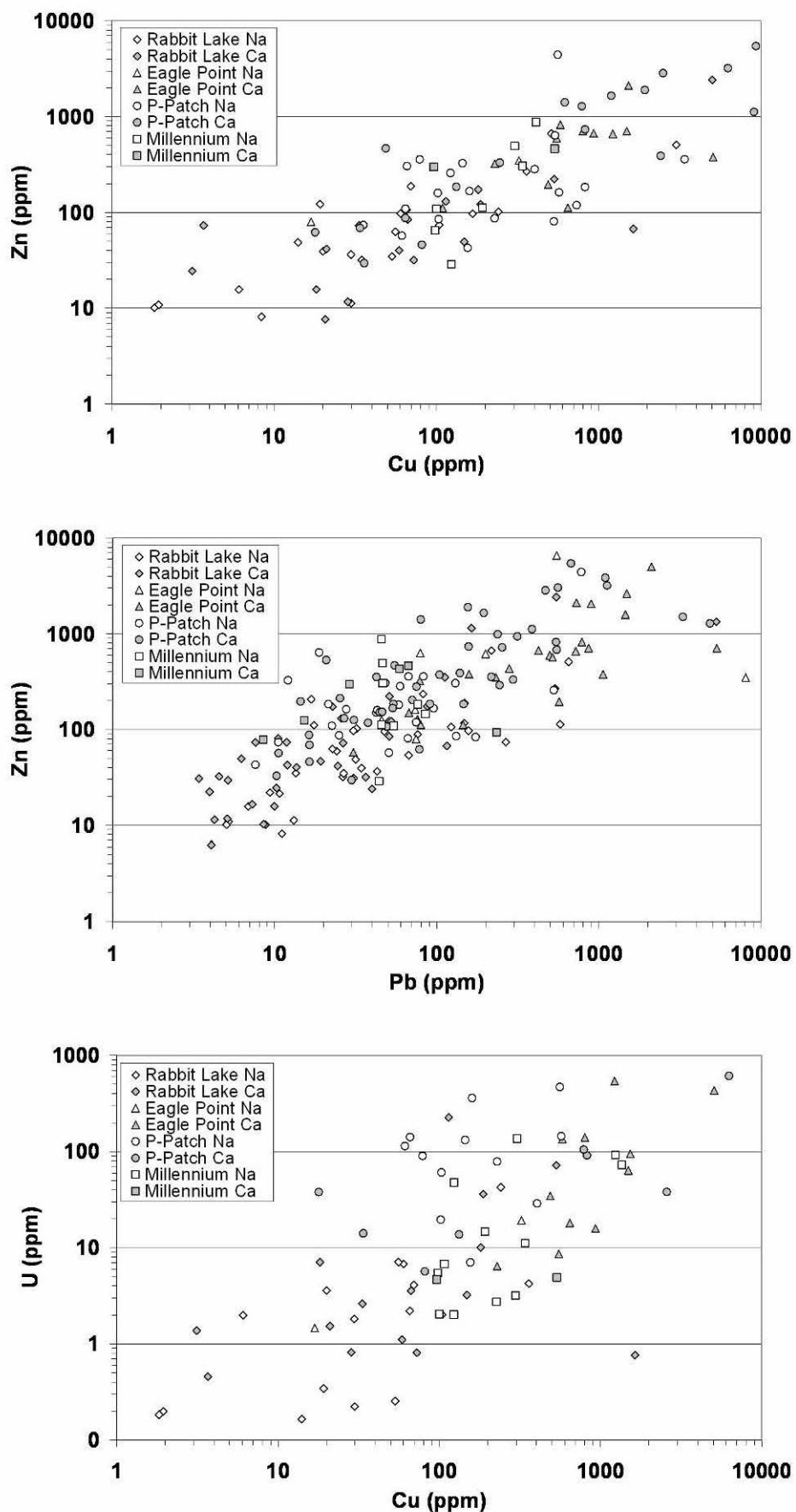


**Figure 7.6 :** Bivariate plots showing intercorrelation between metal (U, Cu, Zn, Pb) concentrations in fluid inclusions analyzed by LA-ICP-MS. Na: NaCl-rich brine inclusions; Ca: CaCl<sub>2</sub>-rich brine inclusions.

#### 7.5.4. Integration to geochemical budgets and fluid circulation models

[Figure 7.7](#) shows a summary of relative basin or basement origin of major and minor solutes in the studied brines. Relative abundances are not qualitative and deduced from element concentrations in brines discussed above. For the NaCl-rich brine, major elements Na, Ca, Mg, K and Sr were not shifted by percolation in the basement. Part of B was possibly leached in basement rocks. Ca. half of Fe, Ba, Pb and Zn concentration could be explained by basement leaching. The majority of Li, Cu and U originate from basement rocks. Thus, the NaCl-rich brine shows some evidence of interaction with basement-rocks although its major ions chemistry was not affected. Fe, Li, Ba, Cu, Pb, Zn, U, SO<sub>4</sub> and F could have been leached by the NaCl-rich brine in the basement. These elements were probably the most mobile elements in basement rocks. For the CaCl<sub>2</sub>-rich brine, the majority of major and trace elements were acquired by fluid-rock interaction in the basement. These compositions could only be explained by removal of Na from solution and exchange with Ca, Mg, K, Sr and other trace elements. Thus, the conversion of NaCl-rich brine to CaCl<sub>2</sub>-rich brine requires combined multiple reactions whose result is an exchange of Na for Ca, Mg, K, Sr and other traces. However, no Na-rich altered areas are known in the basement close to uranium deposits. Only discrete albitionization of plagioclases and K-feldspars is mentioned by [Mercadier \(2008\)](#).

		Na	Ca	Mg	K	Fe	Li	Sr	Ba	Cu	Pb	Zn	U	B	Ni	Co	Ce	Se	As	Ag	Cl	Br	SO <sub>4</sub>	F
NaCl-rich brine	Basin	+	+	+	+	+	+	+	+	+	+	+	+++	?	?	?	?	?	?	?	+++	+	+	+
	Basement												?	?	?	?	?	?	?	?	+	+	+	+
CaCl <sub>2</sub> -rich brine	Basin	+	+	+	+	+	+	+	+	+	+	+	+	?	?	?	?	?	?	?	+++	+	+	+
	Basement	+++	+++	+++	++	+++	++	+++	+	+	+++	+++	+	+	+	+	+	+	+	+	+	+	+	+

**Table 7.3 : Summary of relative contributions of basin and basement to element concentration in Athabasca NaCl-rich and CaCl<sub>2</sub>-rich brines.**

Geochemical budgets in basin and basement rocks showed that Mg, K and B were transferred from basement to basin altered areas. These elements are thought to have been removed from basement-rocks and redistributed among alteration minerals (illite, sudoite, dravite) ([Kister et al., 2005-2006; Laverret et al., 2006](#)). Altered areas in the basement are

depleted in K and enriched in Mg and B ([Mercadier et al., in prep](#)). Thus, an external source is needed for Mg and B. Mg-rich lithologies are not abundant in the vicinity of unconformity-related U deposits although some amphibolite sills (meta-gabbros and meta-diorites) are commonly found in the Wollaston Domain ([Annesley et al., 2005](#)). As for B, basement tourmalines are possible candidates. If Mg and B were provided to altered areas by the CaCl<sub>2</sub>-rich brine, these elements were necessarily leached in the basement remote from alteration haloes surrounding uranium deposits. Conversely, K could have been leached from K-feldspars closer to the deposits. Calc-silicate metasediments are described in the Wollaston Domain, and could have provided part of Ca to the CaCl<sub>2</sub>-rich brine ([Annesley et al., 2005](#)).

Sulphide and arsenide minerals containing Fe, Ni, Co, Cu, Pb, Zn, As, Mo and occasionally Au, Ag, Se and PGEs are well documented in ore mineralogy ([Ruzicka, 1989](#); [Thomas et al., 2000](#); [Jefferson et al., 2007](#)). Ni, Co, As are metals typical of mafic lithologies, which are not abundant close to the deposits. Metal concentrations in fluid inclusions suggest that metals precipitated in the form of sulphide and arsenide minerals (Fe, Ni, Co, Cu, Pb, Zn, As) share a basement-dominated origin and were preferentially transported by the CaCl<sub>2</sub>-rich brine. In addition, REE-bearing aluminium phosphate-sulfates and REE-rich pitchblades attest for intense REE mobilisation during hydrothermal events ([Fayek and Kyser, 1997](#); [Gaboreau et al., 2007](#)). As for metals, Ce concentrations in fluid inclusions suggest that REEs have a basement-dominated origin and were preferentially transported by the CaCl<sub>2</sub>-rich brine.

Finally, conversion of NaCl-rich brine to CaCl<sub>2</sub>-rich brine requires reactions with basement rocks that were not observed in the vicinity of uranium deposits. Large-scale circulation of brines in the Athabasca Basement is necessary to account for conversion of NaCl-rich basinal brines, to CaCl<sub>2</sub>-rich brines.

## **7.6. Conclusion**

Comparison between detailed chemistry of Athabasca NaCl-rich and CaCl<sub>2</sub>-rich brines, obtained from LA-ICP-MS and crush-leach analyses of fluid inclusions, with 520 analyses of basinal fluids representative of the variability of basinal fluid compositions led to the following conclusions:

- (1) The NaCl-rich brine has Na-Ca-Mg-K-Sr composition clearly compatible with commonly sampled basinal fluids, consistent with a low degree of interaction with basement rocks.
- (2) The CaCl<sub>2</sub>-rich brine shows Mg-K-Ca-Sr concentrations supporting a dominant basement origin for Mg, Ca, K and Sr, together with Na removal by fluid-rock interaction in the basement.
- (3) Compositional shift from NaCl-rich brine to CaCl<sub>2</sub>-rich brine results from multiple reactions with heterogeneous basement lithologies.
- (4) K, B and Mg were leached in the basement and redistributed by CaCl<sub>2</sub>-rich brine in illite-sudoite-dravite alteration haloes surrounding uranium deposits.
- (5) Percolation of NaCl-rich basinal brines in basement rocks and subsequent conversion to CaCl<sub>2</sub>-rich brines was accompanied by metal (U, Ag, Se, As, Ni, Co) and REEs (Ce) leaching in basement rocks, that were further deposited in association to uranium ores.
- (6) The compositional shift form NaCl-rich basinal brines to CaCl<sub>2</sub>-rich brines by fluid-rock interaction in basement rocks has necessitated large scale and possibly great depth percolation of basinal brines in basement rocks. Migration paths for brines were not restricted to alteration haloes around unconformity-related uranium deposits.

## Version abrégée

Des eaux de formation riches en Ca sont couramment échantillonnées dans les bassins sédimentaires et les socles cristallins. L'origine des fortes teneurs en Ca est souvent débattue. Les compositions riches en Ca sont souvent interprétées comme le résultat d'interactions fluides-roches dans les bassins ou les socles, ou bien comme le résultat de l'évaporation de l'eau de mer pendant les périodes durant lesquelles celle-ci a un rapport Ca/SO<sub>4</sub> supérieur à 1, ce qui implique une concentration du Ca près de la précipitation du gypse.

Dans le Bassin de l'Athabasca et son socle cristallin, les saumures sodiques et calciques partagent une origine commune, et les mécanismes de conversion de la saumure sodique en saumure calcique sont mal connus.

Les compositions détaillées des saumures (F, SO<sub>4</sub>, B, Na, Mg, K, Ca, Mn, Fe, Co, Ni, Cu, Zn, As, Se, Rb, Sr, Ag, Ba, Ce, Pb et U) obtenues en analyse par ablation laser couplée à la spectrométrie de masse (LA-ICP-MS), ainsi que celles obtenues par analyses en « écrasement lessivage » pour les six gisements étudiés, ont été comparées avec 520 analyses de fluides de bassins actuels, supposées représentatives de la diversité des compositions des fluides de bassin ([Table 7.1](#)).

La saumure sodique a des compositions en Na, Ca, Mg, K et Sr tout à fait comparables à celles de fluides de bassins actuels, ce qui va dans le sens d'un degré limité d'interaction entre la saumure sodique et le socle ([Figure 7.1](#)).

La saumure calcique a des compositions plus « exotiques », avec de fortes concentrations en Mg, K, Ca et Sr. Couplés avec des rapports Na/K anormalement bas selon les modèles géothermométriques, pour des températures de 150 ± 30°C, ces concentrations impliquent que Mg, Ca, K et Sr de la saumure calcique proviennent du socle ([Figure 7.1, 7.3](#)).

La conversion de la saumure sodique en saumure calcique ne peut pas être expliquée seulement par l'échange Na/Ca dans le socle (albitisation des plagioclases), mais

plutôt par un ensemble de réactions dont le bilan final est d'échanger le Na des saumures par Mg, Ca, K, Sr et autres traces.

Or, aucune roche altérée enrichie en Na n'est observée dans l'environnement des gisements. Ceci implique que les saumures aient circulé à grande échelle dans le socle avant de migrer vers les gisements.

Des études géochimiques précédentes ont montré que K, B et Mg sont enrichis dans les halos d'altération à illite-sudoite-dravite par des fluides ayant lessivé ces éléments dans le socle.

Les fortes concentrations en K, B et Mg de la saumure calcique sont compatibles avec un lessivage de ces éléments dans le socle. D'après les études géochimiques, le B et le Mg ne peuvent avoir une origine proximale ce qui favorise l'hypothèse de circulation de saumures à grande échelle dans le socle.

Une possible corrélation positive est observée entre le Mg et les métaux (U, Ag, Se, As, Ni, Co) et éléments des terres rares (Ce) ([Figures 7.5, 7.6](#)). Si le magnésium de la saumure calcique provient clairement du socle, ces corrélations indiquent que les métaux et les éléments des terres rares ont été également lessivés dans le socle, préférentiellement par la saumure calcique.

Ces métaux, ainsi que les éléments des terres rares ont été en partie précipités sous forme de sulfures et arséniures de Ag, Se, As, Ni, Co et sous forme d'alumino-phosphates-sulfates et de pechblendes riches en éléments des terres rares.

Ces saumures sont un exemple remarquable de conversion des saumures sodiques en saumures calciques par interactions fluides-roches dans les socles.

## **8. Stable isotope composition (O, H, C) of diagenetic brines in the Athabasca Basement, Canada**

Antonin Richard<sup>1</sup>, Philippe Boulvais<sup>2</sup>, Marie-Christine Boiron<sup>1</sup>, Michel Cathelineau<sup>1</sup>, Julien Mercadier<sup>1</sup>, Christian France-Lanord<sup>3</sup>, Michel Cuney<sup>1</sup>.

Article in preparation for *Chemical Geology*

<sup>1</sup>G2R, Nancy-Université, CNRS, CREGU, Boulevard des Aiguillettes B.P. 239, F-54506,  
Vandoeuvre-lès-Nancy, France

<sup>2</sup>UMR 6118, Université de Rennes 1, Campus de Beaulieu, 35042 Rennes Cedex, France.

<sup>3</sup>CRPG, Nancy-Université, CNRS/INSU, 15 rue Notre-Dame-des-Pauvres, F-54501  
Vandoeuvre-lès-Nancy, France

### **Abstract**

Diagenetic basinal brines have deeply penetrated and interacted with basement rocks of the Mesoproterozoic Athabasca Basin, Canada. Interaction with basement lithologies led to chemical differentiation between a NaCl-rich brine and a CaCl<sub>2</sub>-rich brine. The two brines show evidence of mixing in the basement in close temporal relation to the formation of giant unconformity-related uranium deposits. These brines are commonly sampled as fluid inclusions in quartz and carbonate veins associated to alteration haloes around uranium deposits. Stable isotope (O, H, C) composition of these brines was investigated in this paper. δ<sup>18</sup>O of host quartz, coupled with δ<sup>18</sup>O and δ<sup>13</sup>C analysis of host carbonates were carried out. By crushing of samples and release of bulk fluid inclusion populations, δD analysis of H<sub>2</sub>O and δ<sup>13</sup>C analysis of CO<sub>2</sub> dissolved in fluid inclusions were performed. δ<sup>18</sup>O of brines was calculated using fluid-mineral fractionation at 150 ± 30°C. The NaCl-rich brine has δ<sup>18</sup>O of ca.

0‰ while CaCl<sub>2</sub>-rich brine has  $\delta^{18}\text{O}$  of ca. 6‰ which supports the idea that the CaCl<sub>2</sub>-rich brine has more interacted with basement rocks than the NaCl-rich brine.  $\delta^{13}\text{C}$  of CO<sub>2</sub> dissolved in fluid inclusions and and  $\delta^{13}\text{C}$  of carbonates are consistent with interaction of brines with graphite-rich lithologies in the basement as origin for CO<sub>2</sub>.  $\delta\text{D}$  of both brines is highly variable and ranges from ca. -50 to ca. -150‰.  $\delta\text{D}$  below -80‰ are anomalously low for basinal brines and more compatible with organic waters, which suggests that part of H<sub>2</sub>O was produced by reaction with organic matter. We propose that production of low  $\delta\text{D}$  H<sub>2</sub> (ca. -500‰) from water radiolysis, combined with CO<sub>2</sub>, could have released low  $\delta\text{D}$  water, through Fischer-Tropsch-like reactions at the origin of abiogenic bitumen found in the vicinity of U ores. Finally, the results strongly support the presence of low  $\delta\text{D}$  brines responsible of alteration of the Athabasca basement rocks, as origin of the anomalously low  $\delta\text{D}$  alteration minerals commonly interpreted as resulting from retrograde H-isotopic exchange.

## 8.1. Introduction

Stable isotopic compositions of crustal fluids are particularly relevant tracers of fluid origin and fluid rock-interactions. In sedimentary basins the O and H isotopic compositions of formation waters result from various processes such as, seawater evaporation, mixing with meteoric water and interaction with sediments. Diagenetic reactions have very limited influence on H isotopic composition because most minerals in sedimentary basin have little to no H compounds. As a consequence, H is frequently considered to be a conservative tracer while O is more sensitive to fluid-rock interactions (Sheppard, 1986; Kyser and Kerrich, 1990).

In the case of unconformity-related U deposits from Athabasca Basin (Saskatchewan, Canada), diagenetic brines are widely recognized as a major fluid involved in the mineralizing process (e.g. Hoeve and Sibbald, 1978, Kotzer and Kyser, 1995, Derome et al., 2005, Part 4). A large amount of work was carried out on the O and H isotopic composition of the main alteration minerals (illite, sudoite, dravite, kaolinite) around the deposits in order to

reconstruct the isotopic composition of the fluids involved (Wilson and Kyser, 1987; Bray et al., 1988; Kotzer and Kyser, 1995; Alexandre et al., 2005; Alexandre et al., 2009b). In most works, O and H isotopic compositions were interpreted in terms of mixing between a basin-derived fluid and a basement-derived fluid. A controversy has emerged from some extremely low  $\delta D$  values which were alternatively explained by late reequilibration with meteoric waters (Wilson and Kyser, 1987; Wilson et al., 1987; Kyser and Kerrich, 1991; Kotzer and Kyser, 1991; Kotzer and Kyser; 1995; Alexandre et al., 2005; Alexandre et al., 2009b), radiation-induced catalysis (Halter et al., 1987) or the presence of low  $\delta D$  fluids (Pagel et al., 1980; Bray et al., 1988). Up to now, the first hypothesis has prevailed.

To date, few direct measurements of the hydrogen isotopic composition of the brines have been undertaken. Pagel et al., (1980) have found  $\delta D$  ranging from -63 to -94‰ in quartz and dolomite-hosted fluid inclusions from Rabbit Lake deposit. Although the highest  $\delta D$  values were compatible with basinal brines, the lowest values were considered by Bray et al., (1988) to be in favour of the presence of low  $\delta D$  fluids, whose origin could not be meteoric since  $\delta^{18}O$  of host minerals was pretty constant among all samples. Kotzer and Kyser (1995) have found  $\delta D$  of -53‰ for fluid inclusions in quartz (Q2) considered to be coeval with uranium deposition at McArthur River deposit. This value was consistent with  $\delta D$  of basinal fluids calculated from  $\delta D$  of alteration minerals. Thus, the authors have invoked late reequilibration with meteoric waters to account low  $\delta D$  values in alteration minerals.

In this paper, we propose to reconstruct the O, H, C isotopic composition of fluids trapped as fluid inclusions in quartz and carbonate veins from unconformity-related U deposits.  $\delta D$  was measured directly on fluid inclusions from crushed quartz and carbonate samples.  $\delta^{18}O$  of the fluids was calculated from the  $\delta^{18}O$  values of the host quartz and carbonates and their temperature of crystallisation given by fluid inclusions (Part 4).  $\delta^{13}C$  of carbonate samples was also measured and when the amount of CO<sub>2</sub> recovered from crushing was high enough,  $\delta^{13}C$  of CO<sub>2</sub> was measured.

## **8.2. Analytical methods**

### **8.2.1. $\delta^{18}\text{O}$ of quartz**

Analyses of the oxygen isotope composition of 49 quartz samples were carried out at the stable isotopes laboratory of Géosciences (University of Rennes 1, France). Pure quartz grains were separated by handpicking under binocular microscope and ground in a boron carbide mortar. In order to remove O<sub>2</sub> from quartz, about 7 mg of quartz powder were reacted overnight with BrF<sub>5</sub> at 670°C using the methodology of [Clayton and Mayeda \(1963\)](#). O<sub>2</sub> was then converted into CO<sub>2</sub> by reaction with hot graphite. CO<sub>2</sub> was analyzed isotopically using a VG SIRA 10 triple collector mass spectrometer. Values of  $\delta^{18}\text{O}$  for quartz are reported in standard per mil (‰) notation relative to SMOW (Standard Mean Ocean Water). During analyses, repeated measurements on NBS 28 quartz standard implied to increase  $\delta^{18}\text{O}$  values by 0.19 to 0.46‰ depending on the specific analytical session. Taking into account standard correction and internal reproducibility, analytical precision for  $\delta^{18}\text{O}$  values of quartz is estimated at 0.2‰.

### **8.2.2. $\delta^{18}\text{O}$ and $\delta^{13}\text{C}$ of carbonates**

Analyses of the oxygen and carbon isotope composition of 29 carbonate samples were carried out at the stable isotopes laboratory of Géosciences (University of Rennes 1, France). Besides sample RBL12 (calcite), samples consist of dolomite. Pure carbonate grains were separated by handpicking under binocular microscope and ground in a boron carbide mortar. CO<sub>2</sub> was extracted from about 10 mg of carbonate powders by reaction with anhydrous phosphoric acid (H<sub>3</sub>PO<sub>4</sub>) in vessels at 50°C for 12 hours using the methodology of [McCrea \(1950\)](#). CO<sub>2</sub> was then analyzed isotopically using a VG SIRA 10 triple collector mass spectrometer. Values of  $\delta^{13}\text{C}$  for carbonates are reported in standard per mil (‰) notation relative to PDB (Pee DEE Belemnite). The oxygen isotope composition of dolomites was

calculated assuming pure dolomitic or calcitic composition and experimental fractionation coefficients  $\alpha_{\text{Dol}-\text{CO}_2} = 1.01066$  and  $\alpha_{\text{Cal}-\text{CO}_2} = 1.009306$  at 50°C. During analyses, measurements on Prolabo Rennes intern-lab standard and NBS 19 limestone international standard allowed to correct  $\delta^{18}\text{O}$  and  $\delta^{13}\text{C}$  values by less than 0.1‰. Taking into account standard correction and internal reproducibility, the analytical precision is better than  $\pm 0.1\text{\AA}$  for  $\delta^{13}\text{C}$  and is about  $\pm 0.1\text{\AA}$  for  $\delta^{18}\text{O}$  values.

### **8.2.3. $\delta\text{D}$ of brines and $\delta^{13}\text{C}$ of $\text{CO}_2$**

Analyses of hydrogen and carbon isotope composition of bulk fluid inclusions populations were carried out on 43 and 14 samples respectively at the CRPG laboratory, Nancy, France. Quartz and carbonate veins were crushed to a grain size of 1-5mm and separated by handpicking under binocular microscope to avoid mineral impurities. Quartz and carbonate grains were then heated at 100°C over night to remove atmospheric water before analyses. 2-8g of quartz or carbonate grains were crushed in inox tubes under vacuum at 110°C. Liberated  $\text{H}_2\text{O}$  and  $\text{CO}_2$  were collected in a liquid nitrogen cold trap and non-condensable volatiles such as  $\text{H}_2$ ,  $\text{O}_2$ ,  $\text{CH}_4$ , and  $\text{N}_2$  were evacuated. In order to separate  $\text{CO}_2$  from  $\text{H}_2\text{O}$ , the liquid nitrogen trap was replaced by an alcohol and liquid nitrogen slush trap at -80°C. The liberated  $\text{CO}_2$  was trapped in a liquid nitrogen cold trap and the amount of recovered  $\text{CO}_2$  was measured in a calibrated volume using a Keller manometer. Then  $\text{CO}_2$  was extracted and analyzed isotopically using a VG Micromass 602D mass spectrometer. Values of  $\delta^{13}\text{C}$  for  $\text{CO}_2$  are reported in standard per mil (‰) notation relative to PDB. Although small quantities of  $\text{CO}_2$  were extracted from quartz samples, only carbonate samples contained sufficient quantities of  $\text{CO}_2$  to be analyzed isotopically. Standard  $\text{CO}_2$  samples reproduced to within  $\pm 0.1\text{\AA}$ . Owing to the small amounts of recovered  $\text{CO}_2$  (typically 1 µmole),  $\delta^{13}\text{C}$  values are given with an uncertainty of  $\pm 5\text{\AA}$ . Water was liberated from the -80°C trap and passed through a uranium furnace at 800°C where  $\text{H}_2\text{O}$  was reduced to  $\text{H}_2$ .  $\text{H}_2$  was then pumped using a Toepler pump. The recovery of  $\text{H}_2$  from  $\text{H}_2\text{O}$  is

assumed to be of 100%. The amount of H<sub>2</sub> was measured in a calibrated volume using a Keller manometer. Then H<sub>2</sub> was then extracted and analyzed isotopically using a VG Micromass 602D mass spectrometer. Values of δD for H<sub>2</sub> and thus for H<sub>2</sub>O are reported in standard per mil (‰) notation relative to SMOW. When introduced into the same vacuum line the standards reproduced to within ± 2‰. The heterogeneity of samples was tested by repeated measurements on individual quartz and carbonate veins. Although some samples have reproducible δD values (± 5‰) other samples display larger variability and a preservative maximum uncertainty of ± 10‰ was applied to all samples.

## 8.3. Results

### 8.3.1. Oxygen isotopes

δ<sup>18</sup>O values of quartz range from 11.9 to 17.4‰ most values being comprised between 14.5 and 16.5‰ ([Table 8.1](#)). For comparison, [Wilson and Kyser, \(1987\)](#) found δ<sup>18</sup>O values ranging from 14 to 16‰ and [Kotzer and Kyser \(1995\)](#) found δ<sup>18</sup>O values from 10.3 to 16.3‰ with a maximum values between 13 and 15‰ in paragenetically similar quartz (secondary quartz from Key Lake in [Wilson and Kyser, \(1987\)](#) and Q2 from McArthur River in [Kotzer and Kyser, \(1995\)](#)). Thus, δ<sup>18</sup>O values of quartz presented here are broadly consistent with previously published data. [Figure 8.1A](#) shows that δ<sup>18</sup>O values for quartz are not homogeneously distributed among studied deposits. δ<sup>18</sup>O values for quartz show a mode at 16-17‰ at Eagle Point and P-Patch, 15-17‰ at Millennium, 15-16‰ at Rabbit Lake and Shea Creek and 13-14‰ at McArthur River. δ<sup>18</sup>O values of quartz show a positive relationship with depth below unconformity at Shea Creek (4 data) while a negative relationship is observed at P-Patch (3 data). There is no relationship between δ<sup>18</sup>O values of quartz and depth below unconformity.

δ<sup>18</sup>O of dolomites and a calcite sample were measured only for Rabbit Lake, Eagle Point, P-Patch and McArthur River deposit (1 sample) due to the lack of available carbonate

samples from Shea Creek and Millennium.  $\delta^{18}\text{O}$  range from 13.1 to 23.8‰ for dolomite and is of 13.6‰ for the calcite sample from Rabbit Lake (Table 8.1). The only published isotopic data on carbonates in the Athabasca Basin are from Pagel et al., (1980) who found  $\delta^{18}\text{O}$  values ranging from 14.4 to 15.4‰ on four dolomite samples and 16.7‰ for one calcite sample at Rabbit Lake. Here,  $\delta^{18}\text{O}$  of Rabbit Lake dolomites range from 13.1‰ to 16.6‰ with one value of 20.5‰, which is broadly consistent with data from Pagel et al., (1980). A relatively wide range of  $\delta^{18}\text{O}$  values for dolomites is found in all studied deposits (Figure 8.1B).  $\delta^{18}\text{O}$  values for dolomites show a mode at 13-17‰ at Rabbit Lake and 19-21‰ at P-Patch.  $\delta^{18}\text{O}$  Values for Eagle Point are homogeneously distributed in the 13.4-21.1‰ range. There is no observed relation between  $\delta^{18}\text{O}$  values of carbonates and depth below unconformity.

### 8.3.2. Hydrogen isotopes

$\delta\text{D}$  values of brines display great variability among samples and sometimes among duplicates of individual samples. As noted by Pagel et al., (1980) for comparable measurements on Rabbit Lake samples, some duplicate analyses agree with  $\pm 5\text{\textperthousand}$  while for some other samples, variability is closer to  $\pm 10\text{\textperthousand}$ . This relatively high internal variability is well beyond analytical uncertainty (ca. 2‰) and is attributed to heterogeneities at the scale of individual veins.  $\delta\text{D}$  values range from -46.3 to -147.2‰, predominantly above -70‰, for carbonate-hosted fluid inclusions, and from -51.5 to -109.9‰, predominantly below -70‰, for quartz-hosted fluid inclusions (Table 8.1). Although the distribution of  $\delta\text{D}$  values among quartz and carbonate samples appears to be different, brines in both host minerals cover comparable  $\delta\text{D}$  range with one extremely low  $\delta\text{D}$  of -147.2‰ for one carbonate sample (MAC005Carb, McArthur River). Thus, given the relatively small number of carbonate samples compared to quartz samples, it is difficult to identify clear differences between  $\delta\text{D}$  values of carbonate-hosted and quartz-hosted brines.  $\delta\text{D}$  values of brines in both quartz and

carbonate samples do not show relationship to depth below unconformity. Relationship between  $\delta D$ ,  $\delta^{18}O$  values and  $\delta^{13}C$  of  $CO_2$  will be discussed below.

### 8.3.3. Carbon isotopes

$\delta^{13}C$  of dolomites range from -23.5 to -3.5‰ with majority of values between -3.5 and -8‰. One calcite sample has  $\delta^{13}C$  of -5‰. There is no apparent difference between  $\delta^{13}C$  of carbonates among Rabbit Lake, Eagle Point and P-Patch deposits. The only analyzed McArthur River sample yields the lowest measured  $\delta^{13}C$  value of -23.5‰. [Pagel et al., \(1980\)](#) found  $\delta^{13}C$  values ranging from -6.2 to -6.5‰ on four dolomite samples and -7.6‰ for one calcite sample at Rabbit Lake, which is broadly comparable with our results.  $\delta^{13}C$  of  $CO_2$  dissolved in fluid inclusions, extracted from dolomite samples ranges from -30.1 to -3.8‰ with majority of values between -8 and -16‰.  $CO_2$  in the calcite sample has  $\delta^{13}C$  of -14.7‰.  $\delta^{13}C$  of carbonates and  $CO_2$  do not show relationship to depth below unconformity.

Deposit	Mineral	Sample	Depth below unconformity (m)	Brine content	$\delta^{18}\text{O}$ (mineral) ‰ (SMOW)	$\delta\text{D}$ ( $\text{H}_2\text{O}$ ) ‰ (SMOW)	$\delta^{13}\text{C}$ (mineral) ‰ (PDB)	$\delta^{13}\text{C}$ ( $\text{CO}_2$ ) ‰ (PDB)	$\delta^{18}\text{O}$ ( $\text{H}_2\text{O}$ ) ‰ (SMOW)	$\delta^{13}\text{C}$ ( $\text{CO}_2$ ) ‰ (PDB)
								Calculated at 150°C		
P-Patch	Dol	P49-4	149.3	Na+Ca	22.8		-5.1		9.4	-7.8
P-Patch	Dol	P63-7	106.4	Na+Ca	19.5		-3.6		6.1	-6.3
P-Patch	Dol	P63-4 (rose)	102.8	Na+Ca	23.8		-6.5		10.3	-9.2
P-Patch	Dol	P63-3	101.9	Na+Ca	19.3		-4.1		5.9	-6.8
P-Patch	Dol	P63-2	100.7	Na+Ca	18.2		-3.5		4.7	-6.2
P-Patch	Dol	P55-15	24.2	Na+Ca	23.5		-9.4		10.1	-12.0
P-Patch	Dol	P53-10	41.9	n.o.	15.6		-6.5		2.2	-9.2
P-Patch	Dol	P63-8 (rose)	106.8	Ca	21.2		-5.0		7.8	-7.7
P-Patch	Dol	P63-8 (blanche)	106.8	Ca	22.5		-4.5		9.1	-7.2
P-Patch	Dol	P63-6	103.7	Ca	19.2	-81.2	-4.0	-8.8	5.8	-6.6
P-Patch	Dol	P63-5	103.2	Ca	19.8	-85.9	-3.6	-15.4	6.4	-6.2
P-Patch	Dol	P63-4 (blanche)	102.8	Ca	19.3		-5.2		5.9	-7.9
P-Patch	Dol	P48-3Dol	40	Ca	19.4	-97.0	-5.6	-19.3	6.0	-8.2
P-Patch	Qz	P54-5	64	Na+Ca	16.3	-92.0			0.8	
P-Patch	Qz	P48-5	52	Na+Ca	16.1	-66.0			0.6	
P-Patch	Qz	P48-3Qz	40	Na+Ca	15.9	-76.6			0.4	
P-Patch	Qz	P48-2	39	Na+Ca	16.6	-79.4			1.1	
P-Patch	Qz	P48-1	29	Na+Ca	16.5	-78.6			1.0	
P-Patch	Qz	P70-1	122	Na	15.8	-88.5			0.4	
P-Patch	Qz	P57-2	104	Na	14.8	-104.2			-0.7	
P-Patch	Qz	P53-6	96	Na	15.6	-109.9			0.1	
P-Patch	Qz	P56-17	163.5	n.o.	13.9	-90.6			-1.6	
Rabbit Lake	Cal	RBL12Carb	-	Ca	13.6	-66.4	-5.0	-14.7	2.3	-6.5
Rabbit Lake	Dol	RLB9Carb	-	Na+Ca	13.7		-6.3		0.3	-9.0
Rabbit Lake	Dol	RBL14Carb	-	Na+Ca	20.5	-46.3	-4.5	-3.8	7.1	-7.1
Rabbit Lake	Dol	RBL011Carb	-	Na+Ca	16.1	-62.3	-5.1	-8.3	2.7	-7.8
Rabbit Lake	Dol	RBL7Carb	-	Na+Ca	15.9	-60.3	-5.0	-12.1	2.5	-7.6
Rabbit Lake	Dol	DDH197-5	-	Na+Ca	14.5	-65.8	-5.3	-14.0	1.1	-8.0
Rabbit Lake	Dol	RBL2Carb	-	Na	14.4	-64.3	-4.8	-8.7	1.0	-7.4
Rabbit Lake	Dol	RBL1Carb	-	Na	16.6	-47.3	-4.9	-8.4	3.1	-7.6
Rabbit Lake	Dol	RBL5Carb	-	Ca	13.1	-53.0	-6.6	-11.7	-0.3	-9.2
Rabbit Lake	Qz	RBL9Qz	-	Na+Ca	16.2	-83.2			0.7	
Rabbit Lake	Qz	RBL7Qz	-	Na+Ca	15.5	-103.3			0.0	
Rabbit Lake	Qz	RBL5Qz	-	Na+Ca	15.2	-98.4			-0.3	
Rabbit Lake	Qz	RBL4Qz	-	Na+Ca	16.5				1.0	
Rabbit Lake	Qz	RBL3Qz2	-	Na+Ca	15.5				0.0	
Rabbit Lake	Qz	RBL3Qz1	-	Na+Ca	14.7	-92.4			-0.8	
Rabbit Lake	Qz	RBL1Qz	-	Na+Ca	13.6				-1.9	
Rabbit Lake	Qz	DDH7-32-8	300.1	Na+Ca	15.0				-0.5	
Rabbit Lake	Qz	DDH7-1	125.5	Na+Ca	15.9				0.4	
Rabbit Lake	Qz	DDH197-2	21.6	Na+Ca	16.4	-81.9			1.0	
Rabbit Lake	Qz	RBL14Qz	-	Na	13.4	-79.2			-2.1	
Rabbit Lake	Qz	RBL2Qz	-	Na	13.0	-79.8			-2.5	

Deposit	Mineral	Sample	Depth below unconformity (m)	Brine content	$\delta^{18}\text{O}$ (mineral) ‰ (SMOW)	$\delta^{13}\text{C}$ (mineral) ‰ (PDB)	$\delta^{13}\text{C}$ ( $\text{CO}_2$ ) ‰ (PDB)	$\delta^{18}\text{O}$ ( $\text{H}_2\text{O}$ ) ‰ (SMOW)	$\delta^{13}\text{C}$ ( $\text{CO}_2$ ) ‰ (PDB)	$\delta^{18}\text{O}$ ( $\text{H}_2\text{O}$ ) ‰ (SMOW)	$\delta^{13}\text{C}$ ( $\text{CO}_2$ ) ‰ (PDB)
Eagle Point	Dol	EPE44-14	360.7	Na+Ca	20.5	-7.4	-5.4	-15.0	7.1	-10.1	-8.1
Eagle Point	Dol	H1935-8	177.9	Na+Ca	15.1	-61.6	-11.2	-11.2	1.7	-13.9	-13.9
Eagle Point	Dol	EPE44-11	263.4	n.o.	17.3	-54.8	-4.5	-13.4	3.8	-7.2	-7.2
Eagle Point	Dol	ES287-1	39.9	n.o.	23.3	n.o.	-5.3	9.9	9.9	-8.0	-8.0
Eagle Point	Dol	H1935-4	29.3	n.o.	21.1	n.o.	-5.3	7.7	7.7	-13.9	-13.9
Eagle Point	Dol	H1935-2	23.1	n.o.	13.4	n.o.	-5.3	0.0	0.0	-8.0	-8.0
Eagle Point	Qz	H3042-1	263.5	Na+Ca	16.3	-72.4	n.o.	n.o.	0.8	0.6	-7.2
Eagle Point	Qz	ES287-8	253.2	Na+Ca	16.1	n.o.	n.o.	n.o.	0.6	-13.9	-13.9
Eagle Point	Qz	ES287-14	248.4	Na+Ca	15.3	n.o.	n.o.	n.o.	-0.2	-0.2	-7.2
Eagle Point	Qz	EPE44-4	211.4	Na+Ca	16.0	n.o.	n.o.	n.o.	0.5	0.5	-7.2
Eagle Point	Qz	DDH2306-2	135.3	Na+Ca	16.8	n.o.	n.o.	n.o.	1.3	1.3	-7.2
Eagle Point	Qz	EPE44-17	131.2	Na+Ca	16.2	n.o.	n.o.	n.o.	0.7	0.7	-7.2
Eagle Point	Qz	DDH2306-1	130	Na+Ca	16.0	-67.2	n.o.	n.o.	0.5	0.5	-7.2
Eagle Point	Qz	H1935-5	29.8	Na+Ca	16.4	n.o.	n.o.	n.o.	0.9	0.9	-7.2
Eagle Point	Qz	ES287-10	259	Na	16.3	-89.3	n.o.	n.o.	0.9	0.9	-7.2
Eagle Point	Qz	DDH1733-14	178.5	Na	16.3	n.o.	n.o.	n.o.	0.8	0.8	-7.2
Eagle Point	Qz	ES287-23	-	n.o.	16.5	-90.8	n.o.	n.o.	1.0	1.0	-7.2
Eagle Point	Qz	ES287-13	272.1	n.o.	16.8	n.o.	n.o.	n.o.	1.3	1.3	-7.2
McArthur River	Dol	MAC5Carb	25	n.o.	19.7	-147.2	-23.5	-30.1	6.3	-26.2	-26.2
McArthur River	Qz	MAC13Qz	sandstones	Na+Ca	12.6	-102.4	n.o.	n.o.	-2.9	-2.9	-2.9
McArthur River	Qz	MAC8Qz	sandstones	Na+Ca	16.0	-68.3	n.o.	n.o.	0.5	0.5	-2.9
McArthur River	Qz	MAC48	-	Na+Ca	16.3	n.o.	n.o.	n.o.	-3.6	-3.6	-3.6
McArthur River	Qz	MAC5Qz	25	Na+Ca	11.9	-58.0	-147.2	-23.5	6.3	-26.2	-26.2
McArthur River	Qz	MAC54Qz	50	Na	14.6	-107.9	n.o.	n.o.	-0.9	-0.9	-0.9
McArthur River	Qz	CX51	-	Na+Ca	16.3	n.o.	n.o.	n.o.	0.8	0.8	-0.9
Millennium	Qz	CX48-01-12a	265	Na+Ca	17.4	n.o.	n.o.	n.o.	-1.3	-1.3	-1.3
Millennium	Qz	CX44-2	213	Na+Ca	15.9	-82.7	-23.5	-30.1	6.3	-26.2	-26.2
Millennium	Qz	CX48-03	130	Na+Ca	15.6	-100.9	n.o.	n.o.	0.1	0.1	-0.9
Millennium	Qz	CX52-1	99	Na+Ca	16.6	-106.6	n.o.	n.o.	1.1	1.1	-0.9
Shea Creek	Qz	ERC5922-0	195.8	Na+Ca	16.9	-51.5	n.o.	n.o.	1.4	1.4	-0.9
Shea Creek	Qz	SHE123-9/H506	75.8	Na+Ca	15.8	-93.7	n.o.	n.o.	0.3	0.3	-0.9
Shea Creek	Qz	SHE 123-9/H503	49.1	Na+Ca	12.9	n.o.	n.o.	n.o.	-2.6	-2.6	-2.6
Shea Creek	Qz	SHE03 externe	sandstones	n.o.	16.7	n.o.	n.o.	n.o.	1.3	1.3	-0.9
Shea Creek	Qz	IF74	sandstones	n.o.	14.1	n.o.	n.o.	n.o.	-1.3	-1.3	-0.9
Shea Creek	Qz	SH-E38a	63	n.o.	15.4	n.o.	n.o.	n.o.	-0.1	-0.1	-0.9

Table 8.1 : Table 1: Analytical results. Mineral: Dol : dolomite ; Qz : Quartz ; Cal : calcite. Brine content : Na : NaCl-rich brine ; Ca : CaCl<sub>2</sub>-rich brine ; n.o.: not observed.

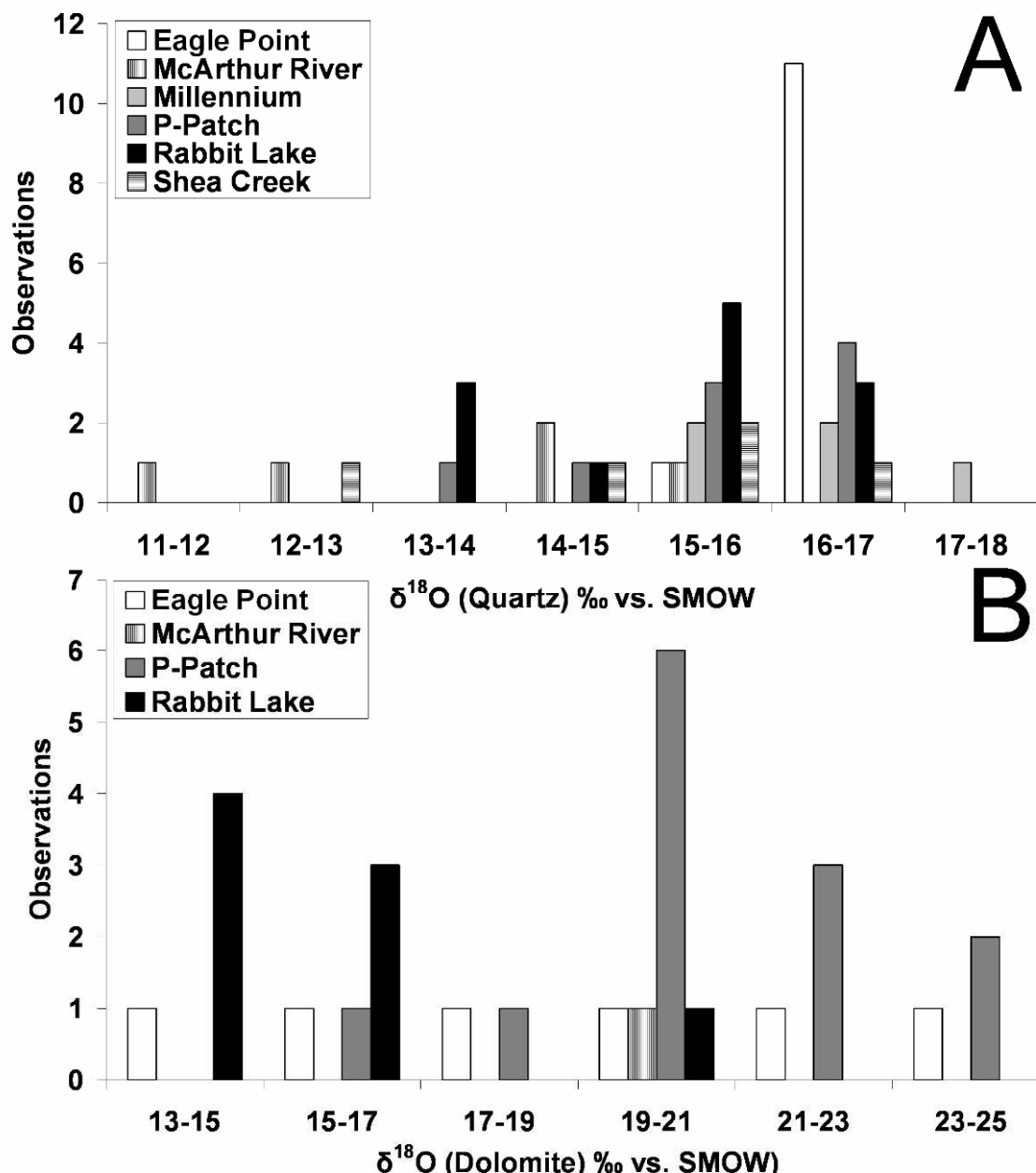


Figure 8.1 : Frequency histogram for  $\delta^{18}\text{O}$  values of hydrothermal quartz (A) and dolomites (B) veins in all studied deposits.

## 8.4. Discussion

### 8.4.1. $\delta^{18}\text{O}$ ( $\text{H}_2\text{O}$ ) shift during basement alteration

Calculating  $\delta^{18}\text{O}$  values of brines is possible only if the temperature of quartz and carbonates precipitation is known. The temperature derived from microthermometry of fluid inclusions was estimated at  $150 \pm 30^\circ\text{C}$  ([Part 4](#)). The fractionation factors of [Zheng \(1993\)](#) and [Zheng \(1999\)](#) were used for carbonate-water and quartz-water pairs, respectively.  $\delta^{18}\text{O}$  value of quartz-hosted, dolomite-hosted and calcite-hosted fluids were obtained by correcting  $\delta^{18}\text{O}$  value of host minerals by  $-15.47\text{\textperthousand}$ ,  $-13.41\text{\textperthousand}$ , and  $-11.33\text{\textperthousand}$  respectively, which corresponds to mineral- $\text{H}_2\text{O}$  fractionation at isotopic equilibrium at  $150^\circ\text{C}$ . A bulk uncertainty, taking into account analytical precision and an uncertainty of  $\pm 30^\circ\text{C}$  for temperature, is estimated at  $\pm 2.5\text{\textperthousand}$  for the  $\delta^{18}\text{O}$  values of brines.

The distribution  $\delta^{18}\text{O}$  of quartz and dolomites ([Figure 8.2A-B](#)) and of calculated  $\delta^{18}\text{O}$  ( $\text{H}_2\text{O}$ ) at  $150^\circ\text{C}$  ([Figure 8.2C](#)) differs as a function of the brine content. Samples containing dominantly  $\text{NaCl}$ -rich brine inclusions show calculated  $\delta^{18}\text{O}$  ( $\text{H}_2\text{O}$ ) ranging from  $-2$  to  $4\text{\textperthousand}$  while samples containing dominantly  $\text{CaCl}_2$ -rich brine inclusions display calculated  $\delta^{18}\text{O}$  ( $\text{H}_2\text{O}$ ) ranging from  $0$  to  $10\text{\textperthousand}$  with most values around  $10\text{\textperthousand}$ . Samples containing variable proportions of  $\text{NaCl}$ -rich and  $\text{CaCl}_2$ -rich brine inclusions, show intermediate calculated  $\delta^{18}\text{O}$  ( $\text{H}_2\text{O}$ ) values that cover the whole range of values for  $\delta^{18}\text{O}$  ( $\text{H}_2\text{O}$ ). Thus, if the  $\text{CaCl}_2$ -rich brine was ca.  $50^\circ\text{C}$  cooler than the  $\text{NaCl}$ -rich brine as proposed by [Derome et al., \(2005\)](#), then our  $\delta^{18}\text{O}$  data on host minerals would suggest that both brines have comparable  $\delta^{18}\text{O}$  ( $\text{H}_2\text{O}$ ). Alternatively, if both brines have circulated at the same temperature of  $150 \pm 30^\circ\text{C}$  as suggested in [Part 4](#), then the  $\text{CaCl}_2$ -rich brine was isotopically heavier than the  $\text{NaCl}$ -rich brine.

$\text{NaCl}$ -rich and  $\text{CaCl}_2$ -rich brines share a common basinal origin. Cl/Br ratios and stable chlorine isotope composition have shown the parent brine originated from seawater evaporation beyond halite saturation and mixing with halite-dissolution brines, and slight

dilution by low-latitude meteoric waters ([Part 6](#)). Little is known about diagenetic reactions involving the parent brine and basin lithologies as only basal sandstones have been preserved from erosion. Seawater evaporation beyond halite saturation would lead to residual brines with  $\delta^{18}\text{O}$  close to -3‰ ([Holser, 1979](#), [Knauth and Beeunas, 1986](#)). Further mixing with halite-dissolution fluid would shift  $\delta^{18}\text{O}$  to a minimum of ca. -5‰ if halite was dissolved by low-latitude meteoric water and to a maximum of ca. 0‰ if halite was dissolved by seawater. Slight dilution of brines by low-latitude meteoric waters would then lower  $\delta^{18}\text{O}$  values to a minimum of -5‰. Finally,  $\delta^{18}\text{O}$  values for parent brine, was probably of  $-3 \pm 2\text{\textperthousand}$  ([Figure 8.3](#)) if diagenetic reactions are considered to have negligible impact on the  $\delta^{18}\text{O}$  of parent brines.

$\delta^{18}\text{O}$  shift from ca. -3‰ (parent brine) to ca. 0‰ (NaCl-rich brine) could alternatively account for diagenetic processes in the Athabasca Basin or result from fluid-rock interactions in the basement. As major element chemistry of NaCl-rich brine is broadly compatible with commonly sampled basinal fluids ([Part 7](#)), we support the idea that the NaCl-rich brine was not equilibrated isotopically with basement rocks and that the observed shift could be attributed to diagenetic reactions.  $\delta^{18}\text{O}$  shift from ca. -3‰ (NaCl-rich brine) to ca. 6‰ (CaCl<sub>2</sub>-rich brine) is consistent with the idea that the CaCl<sub>2</sub>-rich brine results from protracted interaction between the NaCl-rich brine and basement rocks ([Part 4](#)). This is also consistent with observed  $\delta^{18}\text{O}$  (H<sub>2</sub>O) shifts toward high values observed in geothermal systems as a result of fluid-rock interaction ([Williams and McKibben, 1989](#)). Therefore, our data probably indicate local control of  $\delta^{18}\text{O}$  (H<sub>2</sub>O) by fluid-rock interactions in the basement. Finally,  $\delta^{18}\text{O}$  variations among samples with comparable brine content could be due to a combination of the following factors: (i) temperature variation in the  $150 \pm 30^\circ\text{C}$  range (ii) equilibration with heterogeneous basement lithologies.

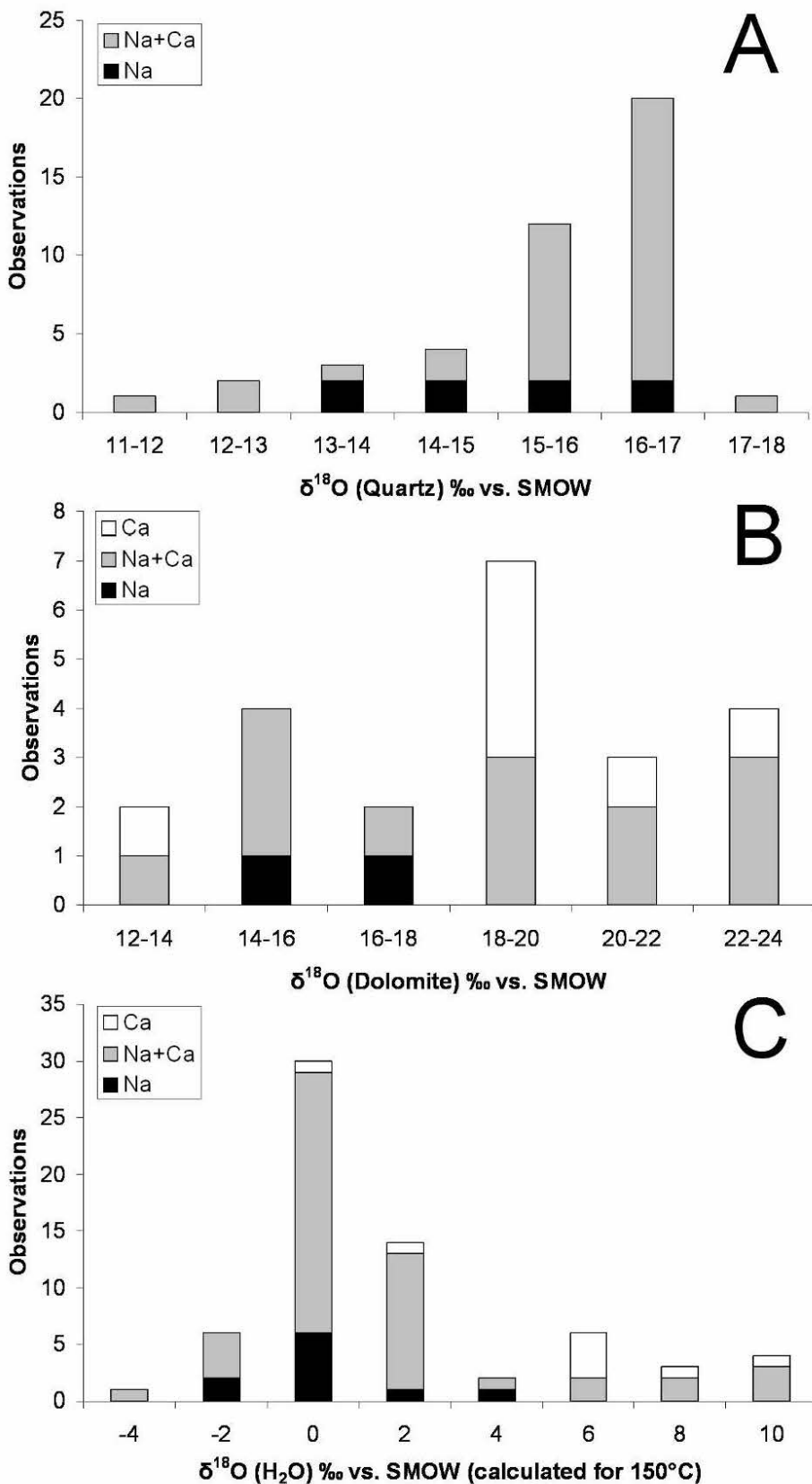


**Figure 8.2 :** Frequency histogram for hydrothermal  $\delta^{18}\text{O}$  values of quartz (A) and dolomite (B) veins as a function of their fluid inclusion content. Na : NaCl-rich brine ; Ca : CaCl<sub>2</sub>-rich brine. (C) Frequency histogram of  $\delta^{18}\text{O}$  values for H<sub>2</sub>O calculated from fractionation factors between quartz, dolomite, calcite and water at 150°C as a function of fluid inclusion content.

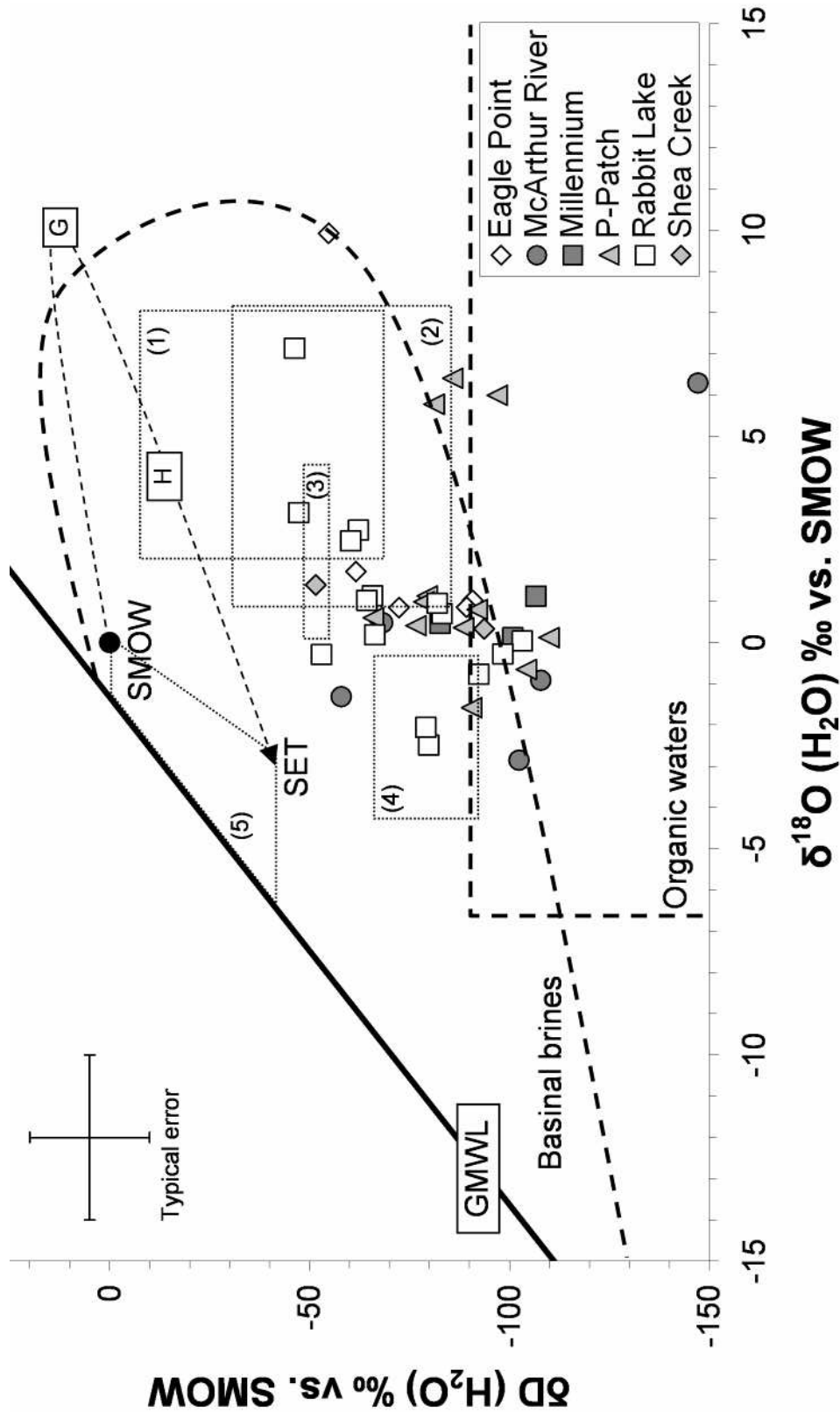


**Figure 8.3 :  $\delta D$  for water recovered from crushing vs.  $\delta^{18}\text{O}$  for water calculated from fluid-mineral equilibria at  $150 \pm 30^\circ\text{C}$ . *SET*: Seawater evaporation trend (Hoiser, 1979; Knauth and Beeunas, 1986). *G*: onset of gypsum precipitation. *H*: onset of halite precipitation. *SET* ends at late stage of halite precipitation. Dotted contours: (1) basement fluids in equilibrium with alteration minerals (Kotzer and Kyser, 1995), (2) basin fluids in equilibrium with alteration minerals (Kotzer and Kyser, 1995), (3) fluid inclusions from McArthur River quartz (Kotzer and Kyser, 1995), (4) fluid inclusions from Rabbit Lake quartz and dolomites (Pagel et al., 1980). (5) Hypothetical field for parent brine to NaCl-rich and  $\text{CaCl}_2$ -rich brines before diagenetic reactions: mixing of evaporated seawater and halite-dissolution fluids and low latitude meteoric water (Part 6). Fields for basinal brines and organic waters after Sheppard (1986). *GMWL*: Standard modern ocean water.**

#### 8.4.2. Production of CO<sub>2</sub> during fluid-graphite interaction

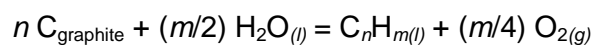
$\delta^{13}\text{C}$  of CO<sub>2</sub> recovered by crushing and  $\delta^{13}\text{C}$  of host carbonates could help to ascertain the origin of CO<sub>2</sub>.  $\delta^{13}\text{C}$  of recovered CO<sub>2</sub> ranges from -30.1 to -3.8‰ with a majority of values between ca. -15 and -5‰.  $\delta^{13}\text{C}$  of carbonates range from -23.5 to -3.5‰ ([Table 8.1](#)). If carbon isotopic equilibrium was respected during precipitation of dolomites, then  $\delta^{13}\text{C}(\text{dolomite})$ - $\delta^{13}\text{C}(\text{CO}_2)$  pairs should indicate the temperature of vein formation. Here, [Figure 8.4A](#) shows that given the uncertainty on  $\delta^{13}\text{C}$  values of extracted CO<sub>2</sub>, a majority of (dolomite)- $\delta^{13}\text{C}(\text{CO}_2)$  pairs are compatible with temperatures of  $150 \pm 30^\circ\text{C}$  estimated from fluid inclusions ([Part 4; Ohmoto and Rye, 1979](#)).  $\delta^{13}\text{C}$  of CO<sub>2</sub> can also be deduced using fractionation factors for dolomite-CO<sub>2</sub> and calcite-CO<sub>2</sub> pairs from [Ohmoto and Rye \(1979\)](#) at  $150 \pm 30^\circ\text{C}$ , by adding -2.68 and -1.5 to  $\delta^{13}\text{C}$  values for dolomites and calcite respectively. A bulk uncertainty, taking into account analytical precision and an uncertainty of  $\pm 30^\circ\text{C}$  for temperature, is estimated at  $\pm 2\text{‰}$  for the calculated  $\delta^{13}\text{C}$  of CO<sub>2</sub>. Calculated  $\delta^{13}\text{C}$  values of CO<sub>2</sub> in isotopic equilibrium at  $150 \pm 30^\circ\text{C}$  with the studied carbonates range from -26.2 to -6.2‰ with a majority of values between ca. -15 and -5‰ ([Table 8.1](#)). Thus, we consider that measured  $\delta^{13}\text{C}(\text{CO}_2)$  were not significantly affected by isotopic disequilibrium during dolomite precipitation or post-trapping reequilibration within fluid inclusions, or reequilibration at  $110^\circ\text{C}$  during crushing experiments.

[Figure 8.4B](#) shows that the majority of  $\delta^{13}\text{C}$  values of dolomites lie in the lower range for Proterozoic marine carbonates ([Shield and Veizer, 2002](#)), while other values tend to that of graphite and bitumen found in the vicinity of the U-ores. This suggests that  $\delta^{13}\text{C}$  of CO<sub>2</sub> was partly controlled by interaction with graphite and/or bitumen. To add, a possible relationship is observed between  $\delta^{13}\text{C}$  of CO<sub>2</sub> and  $\delta\text{D}$  of brines ([Figure 8.4C](#)) which suggests a possible common process controlling C and H isotopic compositions.

Alteration of graphite from metasediments is widespread in the vicinity of uranium deposits of the Athabasca Basin ([Kyser et al., 1989](#)). This alteration is mainly attributed to the percolation of diagenetic brines and results in partial to complete dissolution and

remobilization of graphite along faults (Wang et al., 1989). Alteration of graphite is spatially related to major faults where brine circulations were the most intense. Considering  $\delta^{13}\text{C}$  of graphite ranging from -30 to -20‰ (Kyser et al., 1989), and by using fractionation factors for graphite-CO<sub>2</sub> isotopic equilibrium (Ohmoto and Rye, 1979), CO<sub>2</sub> in equilibrium with graphite resulting from brine-graphite interaction at 150 ± 30°C would have  $\delta^{13}\text{C}$  value of ca. -15 to -5‰ (Figure 8.4C). Thus,  $\delta^{13}\text{C}$  values of carbonates and CO<sub>2</sub> dissolved in fluid inclusions are consistent with brine-graphite interaction at 150 ± 30°C as origin of CO<sub>2</sub> in the studied brines.

Bray et al., (1988) proposed that interaction of brines with graphitic metasediments could have produced CO<sub>2</sub>±CH<sub>4</sub>±H<sub>2</sub>S±H<sub>2</sub> gases. They suggested that CO<sub>2</sub> was the dominant product of graphite alteration based on gas chromatographic analysis of heated illitic and chloritic material. Based on  $\delta^{13}\text{C}$  measurements on fresh to altered graphite, Kyser et al., (1989) concluded that CO<sub>2</sub> was also the dominant product of brine-graphite interaction. Thermodynamic calculations have been carried out by Richard and Sangély (2004) to evaluate the importance of hydrocarbon generation by hydrothermal alteration of graphite, for which a general reaction can be written as:



where H<sub>2</sub>O<sub>(l)</sub>, C<sub>n</sub>H<sub>m(l)</sub> and O<sub>2(g)</sub> represent liquid water, a given liquid hydrocarbon species and oxygen gas, respectively. After Richard and Sangély (2004), hydrocarbon liquids cannot be produced by hydrothermal alteration of graphite under at P-T-fO<sub>2</sub> conditions prevailing around unconformity-related uranium deposits. These authors support the idea that CO<sub>2</sub> is the dominant product of graphite alteration and also that bitumen found in unconformity-related deposits do no originate from brine-graphite interaction.

Therefore, carbon isotopic composition of hydrothermal carbonates and CO<sub>2</sub> released from fluid inclusions for the four studied deposits are in good agreement with previous studies concerning the origin of CO<sub>2</sub> and carbonates in the vicinity of unconformity-related uranium deposits.

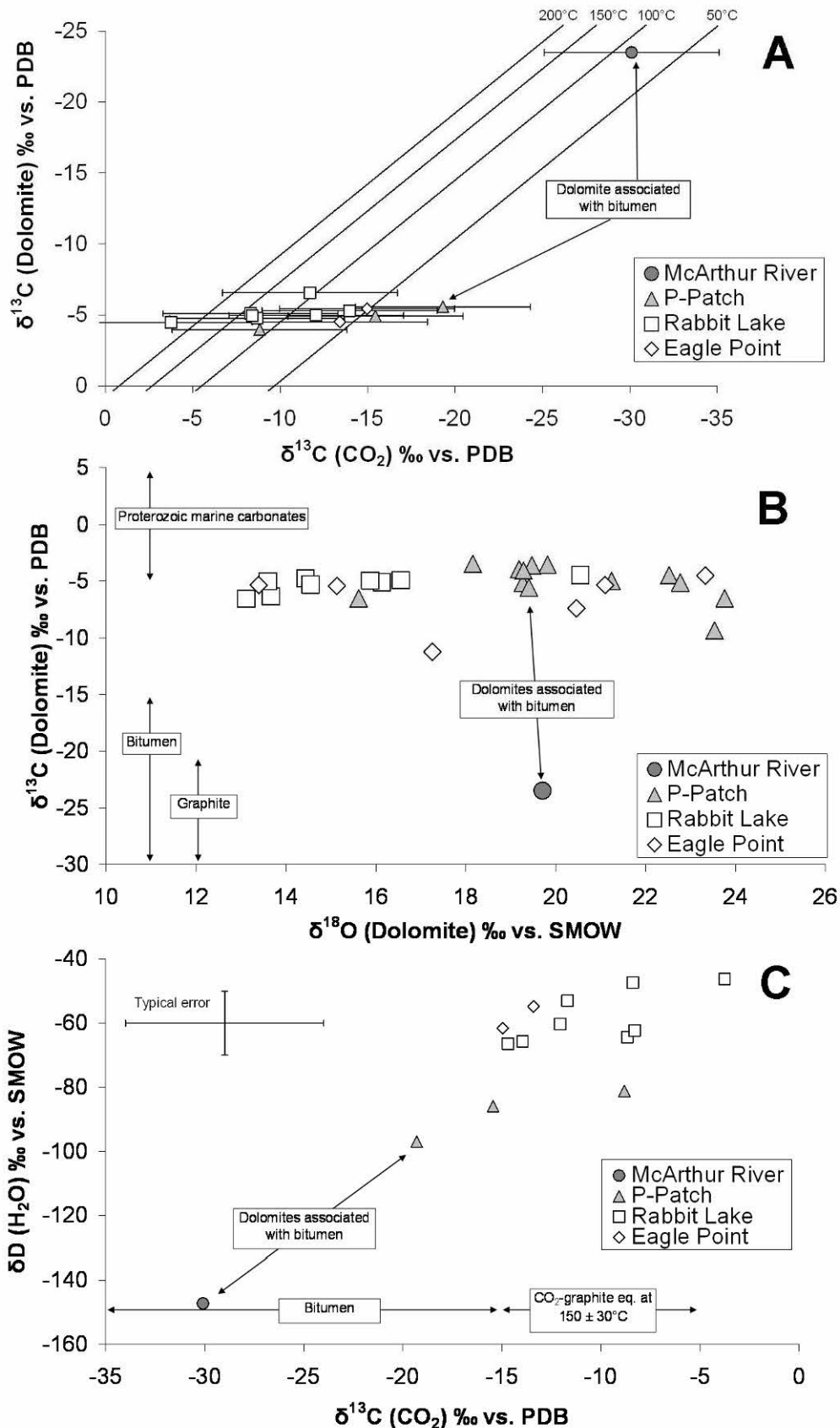


**Figure 8.4 :** (A)  $\delta^{13}\text{C}$  (dolomite) vs.  $\delta^{13}\text{C}$  of  $\text{CO}_2$  recovered from crushing. Straight lines indicate compositions at isotopic equilibrium between  $\text{CO}_2$  and dolomite between 50 and 200°C. (B)  $\delta^{18}\text{O}$  vs.  $\delta^{13}\text{C}$  diagram for dolomites. Field for Proterozoic marine carbonates after [Shields and Veizer \(2002\)](#).  $\delta^{13}\text{C}$  for graphite after [Kyser et al., \(1989\)](#).  $\delta^{13}\text{C}$  for bitumen after [Sangély et al., \(2007\)](#). (C)  $\delta\text{D}$  for water recovered from crushing vs.  $\delta^{13}\text{C}$  of  $\text{CO}_2$  recovered from crushing.

### 8.4.3. Production of low $\delta$ D H<sub>2</sub> during water radiolysis

As for  $\delta^{18}\text{O}$ , the  $\delta\text{D}$  value of parent brine was controlled by seawater evaporation, mixing with halite-dissolution fluid and mixing with low-latitude meteoric water (Part 6). Figure 8.3 shows that  $\delta\text{D}$  of parent brine was probably comprised between -40 and 0‰. Thus, the vast majority of measured  $\delta\text{D}$  were shifted towards lower values, some of them being still compatible with basinal brines, and others being more compatible with organic waters with  $\delta\text{D}$  below -90‰.

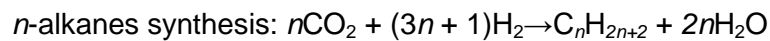
Anomalously low  $\delta\text{D}$  fluids have been reported in a variety of geological environments (Gleeson et al., 1999 and references therein) and controversy has emerged on the significance of low  $\delta\text{D}$  values measured on bulk fluid inclusion populations, alternatively interpreted as reflecting geological processes, or experimental artefacts (i.e. mixing between fluid inclusion water and structurally bound water) (Simon et al., 2001; Gleeson et al., 2008). However, mechanical crushing at temperature below 200°C appears to be a reliable method for  $\delta\text{D}$  analysis of bulk fluid inclusion population which supports that  $\delta\text{D}$  values presented here reflect the original  $\delta\text{D}$  of brines.

The unusually low  $\delta\text{D}$  values of brines require reaction with low  $\delta\text{D}$  component. A good candidate for low  $\delta\text{D}$  component is H<sub>2</sub> which was detected in variable amounts in fluid inclusions from McArthur River deposits by Derome et al., (2003b, 2005) and mineralized areas from Australian unconformity-related uranium deposits Derome et al., (2003a). In the latter studies H<sub>2</sub> was sometimes associated to O<sub>2</sub> within fluid inclusions and was interpreted as resulting from water radiolysis. Indeed, water radiolysis is a common phenomenon in the environment of uranium deposits (Dubessy et al., 1988; Savary and Pagel., 1997). H<sub>2</sub> produced by water radiolysis has  $\delta\text{D}$  of ca. -500‰ (Lin et al., 2005). According to Dubessy et al., (1988), water radiolysis could either occur in the U-bearing mineralizing brines, or in any fluid in contact with uranium minerals, or within U-bearing fluid inclusions. In the first two cases, buoyant H<sub>2</sub> could have migrated through basin and

basement rocks prior or during first stages of uranium deposition. This hypothesis is supported by observation of H<sub>2</sub>-rich primary fluid inclusions in quartz veins ([Part 2](#)).

#### **8.4.4. Production of low δD water during abiogenic bitumen synthesis**

Reactions involving low δD radiolytic H<sub>2</sub> and producing low δD water could potentially account for the observed low δD of brines. In this paragraph, we evaluate the possibility of production of low δD water from low δD H<sub>2</sub> and CO<sub>2</sub>, during abiogenic bitumen synthesis, proposed by [Sangely et al., \(2007\)](#) to be a possible origin for bitumen associated to uranium deposits in the Athabasca Basin. Indeed, solid bitumen are widespread in the environment of unconformity-related uranium deposits ([Landais and Dereppe, 1985; Leventhal et al., 1987; Landais et al., 1990 ; Landais et al., 1993; Landais, 1996 ; McCready et al., 1999 ; Alexandre and Kyser, 2006; McCready et al., 2007 ; Wilson et al., 2007](#)). Petrographic analysis show that they formed during the late-ore to post-ore stage. Based on ion microprobe δ<sup>13</sup>C measurements on bitumen, [Sangély et al., \(2007\)](#) proposed that CO<sub>2</sub>, originating from brine-graphite interaction, was combined with radiolytic H<sub>2</sub> to form hydrocarbons through Fischer-Tropsch-like reactions such as illustrated in the following equations:



Such reaction should produce low δD H<sub>2</sub>O from low δD H<sub>2</sub>, although δD value of produced H<sub>2</sub>O is difficult to estimate due to uncertainties in hydrogen isotopic fractionation between hydrocarbons and H<sub>2</sub>O. In addition, δD of Athabasca bitumen is unknown. Low δD waters produced during abiogenic bitumen synthesis should then dilute brines and shift their δD. If δD of produced waters is similar to that of radiolytic H<sub>2</sub> (ca. -500‰), only a 10% dilution could account for a δD shift of brines from -50‰ to ca. -95‰. Salinity of Na-Ca brines from the Athabasca basin range from 25 to 40 eq. wt% NaCl ([Part 4](#)) and part of this high variability could be attributed to dilution by low δD water issued from abiogenic bitumen synthesis. The heterogeneity of measured δD from one sample to another and even at the scale of

individual quartz or carbonate veins, as previously shown by Pagel et al., (1980), probably reflects that abiogenic bitumen synthesis occurred at restricted periods and in restricted areas. The relative timing of successive events leading to the production of low  $\delta D$  waters and then low  $\delta D$  brines is shown in Figure 8.5.

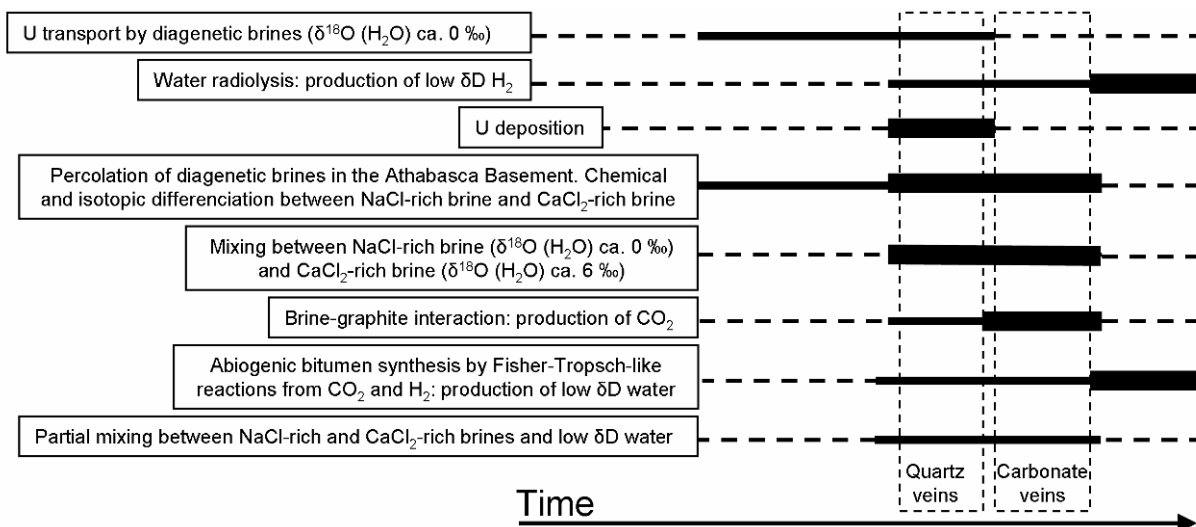


**Figure 8.5 : Summary and relative timing of successive events controlling stable isotope (C, O, H) composition of NaCl-rich and CaCl<sub>2</sub>-rich brines in the Athabasca Basement. Relative importance of each event is indicated as follows: *dotted lines*: possible or not effective; *solid line*: effective; *thick solid lines*: highly effective.**

#### 8.4.5. Implication for interpretation of low $\delta D$ of alteration minerals

Wilson et al., (1987) and Kotzer and Kyser (1995) have interpreted  $\delta D$  values of alteration minerals (Illite-sudoite-dravite-kaolinite) as resulting from mixing between a basement-derived fluid ( $\delta D$  between 0 and -70‰) and a basin-derived fluid ( $\delta D$  between -40 and -70‰) (Figure 8.3). Calculated  $\delta D$  of fluids in equilibrium with alteration minerals below -80‰ were considered as not reflecting hydrogen isotope composition of the fluids but rather retrograde low temperature exchange between alteration minerals and meteoric fluids.

Here, this study shows that  $\delta D$  values of brines, thought to be responsible for the formation of alteration minerals, are highly variable and cover the whole range for calculated values for fluids in equilibrium with alteration minerals except for the highest values (-50 to 0‰) (Figure 8.3).  $\delta D$  values of brines above -80‰ are compatible with calculated  $\delta D$  of fluids

in equilibrium with alteration minerals (Wilson et al., 1987; Bray et al., 1988; Kotzer and Kyser 1995; Alexandre et al., 2005) (Figure 8.3). However,  $\delta D$  values below -80‰ are clearly indicative of low  $\delta D$  for brines. Thus, we strongly support the hypothesis of Bray et al., (1988) that the low  $\delta D$  values of alteration minerals are inherited from isotopic equilibrium with low  $\delta D$  brines. Bray et al., (1988) proposed that low  $\delta D$  of brines was resulting from equilibrium with low  $\delta D$   $\text{CO}_2 \pm \text{CH}_4 \pm \text{H}_2\text{S} \pm \text{H}_2$  gases resulting from interaction between brines and graphitic metasediments. As discussed above, we propose an alternative origin for low  $\delta D$  values of brines, which could result from heterogeneous dilution of brines by low  $\delta D$  waters produced during abiogenic bitumen synthesis (Figure 8.5). Finally, low temperature exchange with meteoric waters and radiation-catalyzed hydrogen exchange (Halter et al., 1987) are not incompatible with low  $\delta D$  brines but their relative importance for  $\delta D$  values of alteration minerals is questionable.

## **8.5. Conclusion**

Oxygen, hydrogen and carbon isotopic analyses of fluid inclusions and host minerals in five unconformity-related uranium deposits from the Athabasca Basement led to the following conclusions:

- (1) Oxygen isotopic composition of both NaCl-rich and CaCl<sub>2</sub> rich brines were controlled by fluid-rock interaction with basin and mostly basement lithologies. δ<sup>18</sup>O shift from ca. -3‰ for the NaCl-rich brine basin to ca. 6‰ for the CaCl<sub>2</sub>-rich brine, accounts for the conversion of the NaCl-rich brine to CaCl<sub>2</sub>-rich brine by fluid-rock interactions within basement rocks.
- (2) CO<sub>2</sub> dissolved in both brines was produced by interaction between brines and graphite-rich lithologies in the basement.
- (3) The observed anomalously low δD of brines are attributed to input of low δD water resulting from (i) water radiolysis producing low δD H<sub>2</sub> during uranium transport and/or after uranium precipitation (ii) Fischer-Tropsch-like reactions involving low δD H<sub>2</sub> produced by water radiolysis and CO<sub>2</sub> produced by brine graphite-interaction. These reactions lead to the production of abiogenic bitumen and low δD water that was heterogeneously mixed with brines.
- (4) Our data demonstrate the existence of low δD fluids in the environment of Athabasca uranium deposits, and could be an alternative or supplementary explanation to previously published anomalously low δD values for alteration minerals interpreted as resulting from retrograde hydrogen isotope exchanges.

## Version abrégée

La composition isotopique en oxygène ( $\delta^{18}\text{O}$ ), hydrogène ( $\delta\text{D}$ ) et carbone ( $\delta^{13}\text{C}$ ) des saumures a été reconstituée en analysant le  $\delta^{18}\text{O}$  et le  $\delta^{13}\text{C}$  des veines de quartz et carbonates, et en analysant directement le  $\delta\text{D}$  de l'eau des saumures, et le  $\delta^{13}\text{C}$  du  $\text{CO}_2$  dissous dans les saumures, par écrasement sous vide.

Le  $\delta^{18}\text{O}$  des saumures a ensuite été calculé pour des fractionnements isotopiques fluide-quartz et fluide-carbonate à  $150 \pm 30^\circ\text{C}$ .

La saumure sodique a un  $\delta^{18}\text{O}$  calculé proche de  $0 \pm 2\text{\textperthousand}$  alors que la saumure calcique a un  $\delta^{18}\text{O}$  calculé proche de  $6 \pm 3\text{\textperthousand}$  ([Figure 8.2](#)). Cette différence de  $\delta^{18}\text{O}$  calculé va dans le sens d'un plus haut degré d'interaction entre la saumure calcique et le socle, par rapport à la saumure sodique.

Les valeurs de  $\delta\text{D}$  sont très hétérogènes à l'échelle de l'échantillon et peuvent varier de  $\pm 10\text{\textperthousand}$  entre les duplicitats. Les valeurs de  $\delta\text{D}$  sont également très hétérogènes pour chacune des deux saumures, et sont comprises entre  $-50$  et  $-150\text{\textperthousand}$ . Les valeurs supérieures à  $-80\text{\textperthousand}$  sont compatibles avec des saumures de bassin. En revanche, les valeurs inférieures à  $-80\text{\textperthousand}$  sont plutôt compatibles avec celles des eaux dites « organiques » c'est-à-dire résultant de réactions impliquant de la matière organique ([Figure 8.3](#)).

Les valeurs de  $\delta^{13}\text{C}$  du  $\text{CO}_2$  dissous dans les inclusions et des veines de carbonates sont compatibles avec l'interaction entre les saumures et le graphite du socle à  $150 \pm 30^\circ\text{C}$ , comme origine du  $\text{CO}_2$  dissous ([Figure 8.4](#)).

Les variations du  $\delta^{13}\text{C}$  du  $\text{CO}_2$  dissous dans les inclusions semblent corrélées avec les variations du  $\delta\text{D}$  des saumures, ce qui suggère qu'ils sont contrôlés par une réaction commune, ou plusieurs réactions associées ([Figure 8.4C](#)).

Les valeurs de  $\delta\text{D}$  très basses pour les saumures nécessitent l'implication de composés à  $\delta\text{D}$  très bas. L'hydrogène issu de la radiolyse de l'eau est fréquemment détecté dans les fluides associés aux gisements d'uranium, et en particulier dans les gisements de

type discordance. L'hydrogène issu de la radiolyse de l'eau peut avoir des  $\delta D$  très bas, jusqu'à -500‰.

Des bitumes sont très fréquemment associés aux minéralisations uranifères. L'hypothèse la plus récente concernant leur origine, est la synthèse abiogénique par des réactions de type Fischer-Tropsch, impliquant du CO<sub>2</sub> issu des interactions saumures-graphite, et du H<sub>2</sub> issu de la radiolyse de l'eau. Ces réactions produisent des bitumes et de l'eau.

Si le H<sub>2</sub> impliqué dans la réaction a un  $\delta D$  de -500‰, alors l'eau produite par la réaction aura un  $\delta D$  également très bas. Il est proposé que l'eau issue de la synthèse abiogénique des bitumes se soit mélangée en faible proportion avec les saumures, et a pu abaisser considérablement leurs  $\delta D$ , sans pour autant les diluer significativement ([Figure 8.5](#)).

L'implication de ces résultats va au-delà de la compréhension de l'origine des  $\delta D$  très bas des saumures. En effet, les minéraux d'altération (illite-sudoite-dravite-kaolinite) montrent fréquemment des  $\delta D$  anormalement bas. Ceci est le plus souvent interprété comme le résultat d'échanges d'hydrogène entre les minéraux d'altération et des fluides météoriques après leur cristallisation.

Les saumures, qui sont responsables de la formation de ces halos d'altérations, ont des  $\delta D$  anormalement bas. Il est donc proposé que les minéraux présentant des  $\delta D$  anormalement bas aient cristallisé en équilibre isotopique avec ces saumures.

Bien que ceci ne remette pas en cause l'existence d'échanges ultérieurs, ceci peut constituer une explication alternative pour les  $\delta D$  anormalement bas des minéraux d'altération.



## **9. Conclusion générale**

Cette partie synthétise les conclusions majeures de ce travail, et les apports au modèle de circulation des saumures liées à la formation des gisements d'uranium du Bassin de l'Athabasca. Les détails des résultats et des discussions des [Parties 3 à 8](#) ne sont volontairement pas à nouveau exposés, et seules les conclusions majeures sont proposées. Les perspectives de travail ayant émergé pendant cette thèse sont présentées en conclusion.

### **9.1. Synthèse des résultats et apports au modèle de circulations de fluides**

#### **9.1.1. Homogénéité des fluides à l'échelle du bassin**

Deux saumures de salinité équivalente à 10 fois celle de l'eau de mer avaient été décrites par [Derome et al., \(2003, 2007\)](#) pour les gisements australiens, et par [Derome et al., \(2005\)](#) pour le gisement de McArthur River dans le Bassin de l'Athabasca : une saumure sodique (25 pd. % NaCl, jusqu'à 14 pd. % CaCl<sub>2</sub>, et jusqu'à 1 pd. % MgCl<sub>2</sub>) et une saumure calcique (5–8 pd. % NaCl, 20 pd. % CaCl<sub>2</sub>, et jusqu'à 11 pd. % MgCl<sub>2</sub>).

Dans ce travail, ces deux saumures ont été reconnues dans les cinq nouveaux gisements étudiés du Bassin de l'Athabasca, grâce à l'analyse systématique des échantillons en microthermométrie. Les types d'inclusions fluides déterminés par des caractéristiques microthermométriques distinctes par [Derome et al., \(2005\)](#) (Lw1, Lw2, Lwh pour la saumure sodique, Lw' et Lwh' pour la saumure calcique) ont été reconnus dans tous les gisements. Les compositions détaillées en éléments majeurs et traces, obtenues en LA-ICP-MS, montrent que les deux saumures ont des compositions similaires dans tous les gisements.

Les deux saumures sodique et calcique sont donc décrites dans tous les gisements canadiens et australiens et semblent être une caractéristique majeure des gisements d'uranium de type discordance. En outre, il ne semble pas que les gisements montrent des variations significatives d'abondance relative des deux saumures.

A la différence des gisements australiens, les saumures du Bassin de l'Athabasca ne montrent pas de trace de dilution par un fluide de recharge. Un fluide peu salé a bien été identifié (inclusions type Lw") mais représente un nombre très limité d'inclusions. Selon Boiron et al., (submitted), la dilution des saumures de fond de bassin par des fluides de recharge est pourtant un phénomène observé dans de nombreux contextes tels que les gisements d'uranium australiens de type discordance (Derome et al., 2003, 2007), les gisements d'uranium du Bassin de Franceville, Gabon, (Mathieu et al., 2000), les gisements de F-Pb-Zn-Ba liés à l'ouverture de l'Océan Atlantique et au rifting du Golfe de Gascogne (Boiron et al., 2002) ou encore le Graben du Rhin (Dubois et al., 1996 ; Cathelineau and Boiron, in press). Il semble donc que le cas des gisements canadiens soit assez original. Le fait que les saumures qui ont circulé à proximité des gisements n'aient pas été diluées par des fluides de recharge pourrait impliquer que les gisements se sont formés trop loin des zones de recharge du socle en bordure de bassin. Si certains gisements sont actuellement situés en bordure de bassin (Eagle Point, Rabbit Lake), ceci implique que l'étendue passée du bassin de l'Athabasca a pu être bien plus grande que l'étendue actuelle.

### **9.1.2. Identification des processus de mélange de saumures**

Le mélange entre les deux saumures peut s'identifier par un continuum de compositions et de salinités entre le pôle riche en sodium et le pôle riche en calcium. Ce continuum s'observe dans tous les gisements, aussi bien par la microthermométrie (continuité des températures de fusion de la glace entre -60 et -15°C et des rapports molaires Na/Ca entre 0.3 et 50), que par les compositions obtenues en LA-ICP-MS (continuité entre les compositions riches en Na et les compositions riches en Ca-Mg-K).

Si ces mélanges sont bien identifiés dans les inclusions fluides considérées comme contemporaines des minéralisations, le rôle exact de ce mélange pour le dépôt de l'uranium reste à déterminer. Il reste également à déterminer si ces mélanges ont lieu uniquement dans les fractures majeures, matérialisées par les veines de quartz et carbonates, ou également dans la porosité et/ou la microfracturation. Les travaux de Mercadier et al., (*in press*) montrent que les microfractures dans les quartz métamorphiques et magmatiques des gneiss et pegmatoïdes du socle, dans le gisement de P-Patch, ont été cimentés par les deux saumures. Ceci suggère que les saumures ont pu se mélanger loin des drains majeurs, et à la faveur d'une perméabilité microfissurale importante, et de microfractures matérialisées par les plans d'inclusions fluides.

#### **9.1.3. Conditions de température et de pression**

Le modèle de circulation de saumures autour du gisement de McArthur River impliquait le mélange anisotherme entre la saumure sodique (env. 200°C) et la saumure calcique (env. 140°C) ([Derome et al., 2005](#)). Ces températures ont été révisées à la vue des résultats en microthermométrie sur les cinq nouveaux gisements étudiés.

Il semble que le contraste de température apparent (Th) entre les deux saumures soit beaucoup moins marqué dans les nouveaux gisements étudiés que dans le gisement de McArthur River. Ceci pose la question du caractère exceptionnel de ce dernier en termes de température des saumures, potentiellement lié au caractère exceptionnellement élevé du tonnage et de la teneur en U de ce gisement.

La contamination des fluides ayant circulé à proximité des minéralisations par de l'hydrogène issu de la radiolyse avait été notée par [Derome et al., \(2003, 2005\)](#). Un effet attendu de la contamination des fluides par le H<sub>2</sub> est l'augmentation artificielle des Th. Le modèle ne tenait pas compte de l'effet des potentielles contaminations en H<sub>2</sub> à plus faibles concentrations des inclusions fluides pour l'interprétation des Th, qui se révèlent plus élevées pour la saumure sodique à McArthur River que partout ailleurs.

Il est donc proposé qu'à McArthur River, les inclusions fluides ont été significativement plus contaminées par l'hydrogène que dans les autres gisements, même de manière indiscernable optiquement, ce qui est probable compte tenu de sa teneur exceptionnelle en uranium. Ceci amène à réviser la température des saumures à la baisse et à considérer que les deux saumures ont circulé et se sont mélangées à une température de  $150 \pm 30^\circ\text{C}$ .

Les variations apparentes de températures d'homogénéisations s'intègrent dans le modèle par des fluctuations de pression dans le temps et dans l'espace à l'échelle du gisement, entre des conditions lithostatiques (800-1500 bars) et hydrostatiques (300-500 bars). Ces variations de régime de pression sont attendues à de telles profondeurs (3-6 km) et à la vue des nombreux épisodes de fracturation et de bréchification qui accompagnent la formation des gisements ([Lorilleux et al., 2002](#)).

Il semble que la température de formation des gisements d'uranium du Bassin de l'Athabasca soit significativement plus basse que celle couramment admise (env.  $200^\circ\text{C}$ ) et basée sur les Th les plus élevées ([e.g. Kotzer and Kyser, 1995](#)). Les implications, en ce qui concerne la reconstitution des compositions isotopiques en oxygène et hydrogène des saumures, à partir de l'analyse des minéraux d'altération équilibrés avec celles-ci (Illite-chlorite-dravite-kaolinite), restent à évaluer ([Wilson and Kyser, 1987 ; Kotzer and Kyser, 1995](#), [Alexandre et al., 2005, 2009b](#)).

#### **9.1.4. Source et transport de l'uranium**

Les deux saumures transportent de l'uranium dans des gammes de concentrations comparables (de 0.2 à plusieurs centaines de ppm), avec un enrichissement préférentiel dans la saumure calcique de moins d'un ordre de grandeur en moyenne. Les teneurs en uranium mesurées, en particulier celles au-delà du ppm, sont parmi les plus hautes jamais mesurées dans des fluides crustaux, et sont du même ordre de grandeur que celles décrites

dans des fluides de haute température liés à l'activité magmatique-hydrothermale d'intrusions granitiques.

En particulier, les teneurs en uranium sont anormalement hautes pour des fluides de bassin, ce qui indique que l'uranium a probablement été lessivé préférentiellement dans le socle, dans lequel les sources potentielles sont multiples. Si cette idée a déjà été évoquée (Hecht and Cuney, 2000 ; Derome et al., 2005), de nombreux auteurs évoquent toujours le bassin comme source majeure, voire unique, de l'uranium pour ces gisements (e.g. Fayek and Kyser, 1997). Ce travail apporte un poids supplémentaire à l'idée que la source de l'uranium de ces gisements est bien le socle, ce qui montre l'importance de la compréhension des circulations de fluides entre bassins et socles pour ces systèmes minéralisateurs.

D'une façon plus générale, ces résultats supportent l'idée que les gisements métalliques se forment à partir de fluides dont les concentrations en métaux sont exceptionnelles (Wilkinson et al., 2008).

#### **9.1.5. Lessivage du socle**

Les deux saumures montrent des compositions chimiques qui témoignent d'interactions avec les lithologies du socle.

La saumure sodique semble la moins affectée par ces interactions. Sa composition en éléments majeurs Na-Ca-K-Mg-Sr est globalement compatible avec celles des saumures de bassin actuelles. En revanche, ses teneurs très élevées en éléments mineurs et traces, comme Fe, Li, Ba, Cu, Pb, Zn, U, B et en anions F et SO<sub>4</sub>, indiquent que la saumure sodique s'est partiellement équilibrée avec certains minéraux du socle.

La saumure calcique a une composition totalement exotique par rapport à des fluides de bassin actuels. Sa teneur élevée en Mg, K et B est probablement à l'origine des enrichissements en ces éléments dans les halos d'altération (Kister et al., 2005 ; Laverret et al., 2006 ; Mercadier et al., in prep). Le lessivage du socle en ces trois éléments est la seule

explication possible pour justifier ces enrichissements. Les zones proximales ne montrent pas de lithologies basiques donc riches en Mg, ce qui implique que les saumures ont extrait ces éléments dans des zones du socle éloignées des minéralisations, et donc rarement échantillonnées.

Les implications de ces résultats sont donc importantes en ce qui concerne les échelles de circulation de ces saumures dans le socle, qui ne semblent alors pas limitées aux seules zones altérées liées aux minéralisations. De plus, l'enrichissement en Mg des saumures s'accompagne d'un enrichissement en Se, Ce, Ni, Co, As, Ag qui s'exprime sous forme de sulfures ou séléniures associés aux minéralisations en uranium ([Ruzicka, 1989](#)).

Il est proposé que la plus grande partie des métaux, dont l'uranium, associés à ces gisements, a été lessivé dans le socle. Ceci constitue une explication alternative à l'idée que les métaux sont lessivés dans des niveaux de « red beds » dans le bassin ([Quirt, 1989](#)).

#### **9.1.6. Conversion saumure sodique – saumure calcique**

Les rapports Cl/Br, ainsi que la composition isotopique du chlore, ont permis de montrer que les deux saumures ont une origine commune. [Derome et al., \(2005 ; 2007\)](#) ont proposé que la saumure calcique dérive de la saumure sodique par échange Na/Ca dans le socle. Les nouvelles données sur les compositions d'inclusions fluides montrent qu'un simple échange Na/Ca entre saumure sodique et socle ne suffit donc pas à rendre compte de la composition de la saumure calcique, mais que du Na est également échangé pour du Mg, K, et Sr. La conversion d'une saumure à l'autre nécessite un piège pour le sodium dans le socle. L'albitisation des plagioclases et des feldspaths-K est une réaction possible pour piéger du sodium et libérer du calcium et du potassium. Ces réactions sont observées mais restent assez discrètes autour des gisements ([Mercadier, 2008](#)).

Le manque de piège pour le sodium ainsi que le manque de source pour le magnésium et le bore à proximité des gisements, impliquent que ces saumures ont circulé à grande échelle dans le socle pour acquérir leur composition calcique.

Les  $\delta^{18}\text{O}$  des saumures indiquent un plus fort degré d'interaction entre la saumure calcique ( $\delta^{18}\text{O}$  d'environ 6‰) et le socle, par rapport à la saumure sodique ( $\delta^{18}\text{O}$  d'environ 0‰), ce qui conforte l'idée de la nécessité d'une interaction de la saumure sodique avec le socle comme origine de la saumure calcique.

Si ce travail n'a pas permis d'identifier les réactions expliquant la conversion de la saumure sodique en saumure calcique, il semble que celle-ci s'opère par de multiples réactions avec des lithologies chimiquement hétérogènes du socle, dont le bilan final est d'échanger le Na des saumures principalement par du Ca, Mg, K et Sr.

#### **9.1.7. Origine du chlore**

Le chlore est probablement le principal complexant pour l'uranium dans ces saumures (Raffensperger and Garven, 1995a, 1995b ; Rozsypal, 2009). L'origine des fortes chlorinités des saumures du Bassin de l'Athabasca a été très discutée depuis trente ans. Les origines proposées ont été, successivement, la dissolution d'évaporites par des fluides météoriques (saumure dite « secondaire ») (Pagel et al., 1980 ; Bray et al., 1988) ou l'évaporation de l'eau de mer en surface (saumure dite « primaire ») (Derome et al., 2005 ; 2007), les deux processus pouvant conduire à des saumures de chlorinités équivalentes.

Dans ce travail, une étude systématique des traceurs conservatifs (Cl/Br et  $\delta^{37}\text{Cl}$ ) ainsi que l'analyse des teneurs en chlore dans les roches fraîches et altérées du socle, a permis de montrer l'origine multiple du chlore dans ces saumures. Les deux saumures résultent d'un mélange entre une eau de mer fortement évaporée, au-delà de la saturation vis-à-vis de la halite (Cl/Br d'environ 150 et  $\delta^{37}\text{Cl}$  d'environ -0.5‰), et un fluide issu de la dissolution d'évaporites (Cl/Br compris en 1000 et 10000 et  $\delta^{37}\text{Cl}$  compris entre -0.5 et 0.5‰). Si les proportions de ce mélange sont difficiles à évaluer de part la difficulté de définir un rapport Cl/Br type pour une saumure secondaire, un mélange à part égale entre une saumure primaire et une saumure secondaire avec un rapport Cl/Br d'environ 4000 peut rendre compte de la majorité des rapports Cl/Br mesurés.

L'évaporation de l'eau de mer a été favorisée par la situation géographique du Bassin de l'Athabasca, sous des latitudes basses pendant cette période. La dissolution d'évaporites est un processus très fréquent dans les bassins renfermant des formations évaporitiques. Le mélange entre ces deux types de saumures est fréquent dans les bassins associés aux gisements de type MVT ([Chi and Savard, 1997](#)). De plus, il semble que le chlore soit enrichi dans les saumures par altération des minéraux porteurs du socle, notamment les biotites.

[Derome et al., \(2005\)](#) ont proposé que les saumures dérivées de l'évaporation de l'eau de mer avaient été dans un premier temps piégées dans des formations évaporitiques, puis expulsées par compaction pendant la diagenèse d'enfouissement. Dans ce travail, il est proposé que cette dernière hypothèse permette difficilement de rendre compte des volumes importants de fluides ayant envahi la base du bassin. Les saumures dérivées de l'évaporation de l'eau de mer ont plus probablement percolé depuis la surface, grâce à leur densité élevée et/ou le long de failles extensives.

#### **9.1.8. Origine du CO<sub>2</sub> dissous**

Les inclusions fluides analysées contiennent des quantités très faibles de CO<sub>2</sub> dissous. Dans le cas des inclusions fluides piégées dans les quartz, le CO<sub>2</sub> dissous extrait par écrasement sous vide était en trop faible quantité pour être analysé isotopiquement. En revanche, pour les inclusions fluides piégées dans les carbonates, les quantité de CO<sub>2</sub> dissous, même faibles, ont permis la mesure direct du  $\delta^{13}\text{C}$  du CO<sub>2</sub>.

Les résultats montrent que le CO<sub>2</sub> est à l'équilibre isotopique à  $150 \pm 30^\circ\text{C}$  avec un CO<sub>2</sub> supposé produit par l'interaction saumure-graphite dans le socle. Le graphite est fortement présent dans les lithologies du socle et montre des traces de dissolution. Ceci confirme l'hypothèse de [Kyser et al., \(1989\)](#), qui suppose que le CO<sub>2</sub> est le produit dominant résultant des interactions saumures-graphite dans ces environnements.

### 9.1.9. Composition isotopique de l'hydrogène des saumures

Les deux saumures présentent des  $\delta D$  qui varient entre des valeurs habituelles pour des fluides de bassin (-50 à -80‰) et des valeurs anormalement basses (entre -80 et -150‰). Le  $\delta D$  des saumures semble hétérogène à l'échelle de l'échantillon, ce qui pourrait impliquer un contrôle local  $\delta D$  ou des piégeages successifs de fluides de  $\delta D$  contrastés.

Les valeurs de  $\delta D$  les plus basses sont similaires à celles des eaux organiques, c'est-à-dire issues d'interactions entre fluides et molécules organiques. Dans ce travail, un modèle est proposé faisant intervenir la radiolyse de l'eau et la synthèse abiogénique de bitumes comme principaux contrôles sur le  $\delta D$  des saumures.

La radiolyse de l'eau peut avoir lieu pendant le transport, le dépôt et/ou après le dépôt de l'uranium. La radiolyse produit de l'oxygène et de l'hydrogène avec des  $\delta D$  extrêmement bas (proches de -500‰). Selon le modèle de [Sangély et al., \(2007\)](#) cet hydrogène peut se combiner avec le CO<sub>2</sub> produit par interaction saumure-graphite pour former des bitumes par des réactions de type Fischer-Tropsch. Les bitumes sont très fréquemment associés aux minéralisations d'uranium dans tout le bassin. Ces réactions produisent de l'eau à partir de l'hydrogène issu de la radiolyse. Dans ce travail, il est proposé que les  $\delta D$  anormalement bas mesurés dans ces saumures s'expliquent par un léger mélange entre les saumures et l'eau produite par la synthèse abiogénique des bitumes.

Les implications de ces résultats sont très importantes en ce qui concerne l'interprétation des  $\delta D$  sur les minéraux d'altération (illite-sudoite-dravite-kaolinite). Ceux-ci montrent fréquemment des  $\delta D$  anormalement bas qui sont le plus souvent interprétés comme le résultat d'échanges avec des fluides météoriques, postérieurement à leur cristallisation ([Halter et al., 1987](#) ; [Wilson and Kyser, 1987](#) ; [Kotzer and Kyser, 1995](#), [Alexandre et al., 2005, 2009b](#)). Il semble bien que des fluides à  $\delta D$  anormalement bas aient circulé dans l'environnement des gisements et aient pu s'équilibrer isotopiquement avec les minéraux d'altération. Ceci n'invalider pas pour autant les hypothèses invoquant les

échanges ultérieurs mais peut constituer une explication complémentaire aux compositions isotopiques anormales des minéraux d'altération.

#### **9.1.10. Echelles des migrations de fluides**

Il apparaît que la saumure sodique a entièrement envahi la base du bassin et que celle-ci peut-être considérée comme un aquifère géant. Cette saumure a donc migré sur plusieurs centaines de kilomètres latéralement. Ce phénomène de migration de saumures de bassins à très grande échelle est décrit dans de nombreux contextes ([Garven, 1995](#)).

La saumure calcique s'est probablement formée par interaction entre la saumure sodique et les lithologies du socle. Il semble que sa présence ne soit pas uniquement restreinte aux zones minéralisées puisqu'une réinterprétation des données d'inclusions fluides du sondage de Rumple Lake (centre géographique du bassin) obtenues par [Pagel et al., \(1975\)](#) indique que la saumure calcique a pu être présente à la base des grès, ceci loin de tout gisement connu.

Ce travail montre que les deux saumures sont reconnues dans le socle jusqu'à près de 400 m de profondeur, ce qui correspond aux profondeurs maximales connues pour les minéralisations (Eagle Point). Cette limite de 400 m correspond à un minimum de profondeur possible car très peu de sondages plus profonds sont disponibles.

Les échelles latérales de circulation des saumures dans le socle sont également difficiles à appréhender faute d'échantillonnage conséquent loin des gisements. Il semble que la saumure sodique soit présente dans des zones du socle non altérées à plusieurs kilomètres du gisement de Shea Creek ([Freiburger and Cuney, 2003](#)).

De plus, ce travail a montré que la conversion de la saumure sodique en saumure calcique nécessite des interactions fluide-roches à grande échelle dans le socle loin des zones altérées liées aux minéralisations.

Le travail de [Mercadier et al., \(submitted\)](#) montre enfin que les deux saumures circulent grâce à une intense microfracturation du socle, en partie liée à la microfracturation

tardi-hudsonienne qui est réactivée pendant la période de formation des gisements. Cette infiltration n'est pas démontrée à grande échelle par manque d'échantillon, mais il semble raisonnable de penser que toute zone du socle sismiquement active à cette période a vu s'infiltarer verticalement, des fluides provenant du bassin, et latéralement, des fluides provenant du socle.

En résumé, il ne semble pas exister de barrière à la percolation des saumures du bassin vers le socle. En revanche, celle-ci est probablement limitée par l'intensité de la marco et micofracturation au moment de la formation des gisements. Il est donc logique que les gisements se forment dans des zones où la fracturation préexistante du socle est importante comme la Wollaston Mudjatik transition zone.

#### **9.1.11. Comparaison gisements type socle et type discordance**

Ce travail a mis en évidence une grande similarité des compositions chimiques et isotopiques des phases fluides impliquées dans les gisements strictement encaissés dans les socles (Eagle Point, P-Patch, Millennium) et les gisements montrant des minéralisations à la discordance (McArthur River, Rabbit Lake, Shea Creek).

Plusieurs études récentes ont tenté de démontrer les différences génétiques entre gisements de socle et gisements à la discordance ([Quirt, 2003](#) ; [Alexandre and Kyser, 2005](#)). Outre les difficultés rencontrées pour classer ces gisements (Rabbit Lake et McArthur River sont considérés comme des gisements de socle par [Alexandre and Kyser, 2005](#)), certains gisements renferment des minéralisations à la discordance, très profondes dans le socle, voire perchées dans les grès ([Shea Creek, Key Lake](#)).

La distribution spatiale des minéralisations est plus probablement contrôlée par le contexte tectonique, et cette classification semble purement géométrique et peu utile à la compréhension de la genèse de ces gisements.

### 9.1.12. Dépôt de l'uranium

Les mécanismes pour la précipitation de la pechblende, qui impliquent une réduction de l' $\text{U}^{\text{VI}}$  en solution en  $\text{U}^{\text{IV}}$ , sont encore mal connus pour les gisements de type discordance. Dans les gisements australiens, les saumures sodique et calcique sont systématiquement diluées par un fluide de recharge peu salé et enrichi en  $\text{CH}_4$  ([Derome et al., 2003, 2007](#)). Cependant, le rôle de la dilution et/ou du  $\text{CH}_4$  pour le dépôt de l'uranium est peu évident. Ce travail montre que, dans le Bassin de l'Athabasca, les saumures n'ont pas été diluées et que les fluides peu salés sont très rares. Il semble donc que la dilution des saumures ne soit pas une condition nécessaire pour le dépôt de l'uranium dans ces environnements. L'absence de dilution peut également expliquer la rareté relative des minéraux de Pb, Zn et Cu (qui précipitent par dilution des fluides et déstabilisation des complexes chlorurés) par rapport à la pechblende dans ces environnements, malgré les fortes concentrations en ces métaux dans les saumures.

Malgré de nombreuses études d'inclusions fluides dans le Bassin de l'Athabasca, dont ce travail, aucun fluide réducteur n'a été identifié. Bien que l'hypothèse d'un fluide réducteur ne puisse être écartée, un tel fluide aurait probablement dû être piégé sous forme d'inclusions fluides. S'il est certain qu'aucun fluide réducteur n'est présent dans les veines de quartz et carbonates, et dans les zones silicifiées des grès, l'étude de [Mercadier et al., \(in press\)](#) montre également qu'il est absent des plans d'inclusions fluides secondaires dans les quartz magmatiques et métamorphiques des gneiss et pegmatoïdes de P-Patch.

En l'absence de preuve directe par les inclusions fluides, ce travail soutient l'idée qu'aucun fluide réducteur n'est impliqué dans les minéralisations. Ceci renforce l'hypothèse selon laquelle les réactions redox entre les minéraux, c'est-à-dire avec certaines lithologies, du bassin et du socle contrôlent le processus minéralisateur.

## 9.2. Perspectives

Ce travail apporte des résultats qui, à leur tour, posent de nouvelles questions qui sont autant de pistes de travail futures, et dont les axes principaux sont : la composition des phases fluides, les interactions fluides-roches, et la modélisation.

### 9.2.1. La phase fluide

#### 9.2.1.1. Spéciation de l'uranium

Ce travail a permis de connaître les gammes de concentrations en uranium dans les saumures sodiques et calciques, qui se sont révélées exceptionnellement hautes en comparaison avec d'autres fluides géologiques de température et salinité équivalentes. Ceci pose la question de la spéciation de l'uranium dans ces solutions.

Il apparaît que ces solutions sont essentiellement chlorurées, ce qui laisse à penser que l'uranium est solubilisé sous forme de complexes chlorurés. Les travaux expérimentaux de [Rozsypal \(2009\)](#) montrent que la solubilité de l'uraninite dans des solutions à 5-6 moles de NaCl, à 155°C et pH < 4, implique des concentrations en uranium comparables à celles mesurées dans les inclusions fluides.

Le chlore est donc probablement un élément essentiel pour le transport de l'uranium. Un moyen de le montrer définitivement serait de déterminer la spéciation de l'uranium dans les inclusions fluides, à la température de piégeage, par analyse XAS (X-ray Absorption Spectroscopy) sous rayonnement synchrotron. Une expérience similaire a déjà été réalisée avec succès pour le Cu, sur des inclusions fluides provenant d'un gisement de Yankee Lode (Australie) par [Cauzid et al., \(2007\)](#).

#### *9.2.1.2. Concentrations des saumures en éléments des terres rares*

Le lessivage des éléments des terres rares dans les zones d'altération, ainsi que leurs fortes concentrations en substitution de l'uranium dans les pechblendes et d'alumino-phosphates-sulfates (APS), sont une caractéristique marquante de ces gisements ([Fayek and Kyser, 1997](#) ; [Gaboreau et al., 2007](#)).

Ce travail a permis de montrer la présence de Ce dans les saumures par analyse en écrasement-lessivage. En revanche, ces analyses n'ont pas permis de détecter d'autres éléments des terres rares. Une étude systématique des inclusions fluides par LA-ICP-MS serait actuellement le meilleur moyen de déterminer les teneurs en éléments des terres rares dans ces saumures, si ces teneurs sont supérieures à 1 ppm (limite de détection).

De plus, les pechblendes des gisements d'uranium du Bassin de l'Athabasca montrent des spectres d'éléments des terres rares d'une forme particulière dite « en cloche » ([Bonhoure, 2007](#)). L'incorporation des éléments des terres rares dans les pechblendes pourrait dépendre soit de la composition du fluide à partir duquel elles précipitent, soit d'un contrôle cristallo-chimique. L'analyse des éléments des terres rares dans des minéraux qui ont précipité à partir des mêmes fluides que les pechblendes pourrait permettre d'avancer sur cette question. Les dolomites hydrothermales étudiées dans ce travail seraient un excellent candidat pour ce type d'analyses.

#### *9.2.1.3. Analyse des gaz et de l'uranium par spectroscopie Raman*

Ce travail a permis de mieux comprendre l'origine du CO<sub>2</sub> piégé dans les inclusions fluides. Les espèces gazeuses suivantes ont été détectées dans les inclusions fluides près des gisements de type discordance par spectrométrie Raman: CO<sub>2</sub>, CH<sub>4</sub>, N<sub>2</sub>, C<sub>2</sub>H<sub>6</sub>, H<sub>2</sub> et O<sub>2</sub> ([Derome et al., 2003b](#)). Ces auteurs ont montré que les proportions relatives en H<sub>2</sub> et O<sub>2</sub> sont liées à la distance par rapport aux corps minéralisés, ce qui pourrait être un outil pour l'exploration minière.

Une étude plus systématique des inclusions fluides dans différents gisements pourrait permettre de confirmer cette hypothèse. De plus, la connaissance de la distribution des espèces gazeuses (notamment l'hydrogène produit par radiolyse) entre saumures sodiques et saumures calciques pourraient apporter des informations importantes en termes de chronologies relatives des phases fluides.

$\text{UO}_2^{2+}$  est potentiellement détectable dans des inclusions fluides par spectroscopie Raman à des concentrations élevées mais déjà mesurées dans ces environnements par LA-ICP-MS (100-1000 ppm). Une calibration des mesures par spectrométrie Raman des concentrations en  $\text{UO}_2^{2+}$  dans la phase aqueuse des inclusions fluides permettrait de mesurer les concentrations en uranium des inclusions fluides de manière non destructive.

### **9.2.2. Les interactions fluides-roches**

#### *9.2.2.1. Origine du bore dans les dravites*

Les zones altérées montrent d'importantes anomalies en K, B et Mg. Ce travail a permis de mettre en évidence le rôle du lessivage du socle par les saumures pour les apports en ces éléments dans les zones altérées.

Les dravites sont les principaux porteurs de B dans ces environnements. La composition isotopique du B, déterminée à la microsonde ionique dans les minéraux de la famille des tourmalines (dont fait partie la dravite), est couramment utilisée pour déterminer l'origine du B et plus largement des fluides dans les systèmes hydrothermaux ([Xavier et al., 2008 ; Garda et al., 2009](#)).

L'analyse isotopique du B sur ces dravites pourrait permettre d'établir une balance entre le B contenu dans les saumures de type primaire et le B lessivé par les saumures dans les roches du socle.

#### *9.2.2.2. Analyse des gaz rares et des halogènes*

L'extension de la méthode Ar-Ar permet l'analyse combinée des halogènes (Cl, Br, I) et des gaz rares (He, Ne, Ar, Kr et Xe), par spectrométrie des gaz rares sur population d'inclusions fluides. Cette technique a déjà été appliquée avec succès dans de nombreux contextes minéralisés, notamment des gisements de type Mississippi Valley ([Kendrick et al., 2002](#)).

Ce type d'analyses pourrait apporter des informations complémentaires à ce travail concernant l'origine des fluides, leur degré d'interaction avec les différents réservoirs (socle, bassin) et l'identification d'éventuels flux de gaz profonds le long des grandes structures contrôlant les minéralisations.

#### *9.2.2.3. Isotopie du strontium et du néodyme sur les carbonates*

Les compositions isotopiques du Sr et du Nd des minéraux sont de bons traceurs des sources pour les fluides à partir desquels ils précipitent. L'analyse isotopique du Sr et du Nd sur les minéraux d'altérations et les pechblendes a permis de mettre en évidence le mélange des fluides équilibrés isotopiquement avec le bassin ou avec le socle ([Kotzer and Kyser, 1995](#)).

Les dolomites hydrothermales, telles que celles étudiées dans ce travail, sont d'excellents candidats pour ce type d'analyses sont réalisables par MC-ICP-MS. De plus, la connaissance des inclusions fluides qu'elles renferment permettrait d'interpréter finement les résultats en termes de compositions chimique et isotopique et d'origine des fluides.

#### **9.2.2.4. Altération des monazites et sources de l'uranium**

Les monazites du socle sont considérées comme une source potentielle de l'uranium pour les gisements du Bassin de l'Athabasca ([Hecht and Cuney, 2000](#)). Si l'altération des monazites dans ces environnements est bien démontrée par la pétrographie, on connaît très mal, du point de vue expérimental, le comportement de la monazite en condition hydrothermale.

Ce travail a permis de connaître la composition détaillée des saumures sodiques et calciques, ainsi que les conditions de température et de pression dans lesquelles elles ont été piégées sous forme d'inclusions fluides. Ceci ouvre la voie à des travaux d'expérimentation sur la stabilité des monazites en présence de telles saumures.

L'analyse des fluides équilibrés avec la monazite en conditions hydrothermales pourrait apporter de précieuses informations sur les sources d'uranium de ces gisements ainsi que sur le comportement des éléments des terres rares et du thorium dans ces saumures.

### **9.2.3. La modélisation**

#### **9.2.3.1. Modélisation thermodynamique des interactions fluides-roches**

Les travaux de [Kister et al., \(2005\)](#) constituent une avancée importante dans la compréhension des équilibres thermodynamiques entre les saumures sodiques et calciques, et les minéraux d'altération associés aux gisements d'uranium du Bassin de l'Athabasca. Ces auteurs ont montré que les saumures sont responsables du transfert de K, Mg et B du socle vers les zones altérées des gisements.

Jusqu'à récemment, une telle approche était difficilement envisageable en ce qui concerne les minéraux d'altération du socle. Les travaux de [Mercadier \(2008\)](#) ont clairement mis en évidence la succession des différents stades d'altération, notamment sur les roches

magmatiques du socle. La composition des fluides étant maintenant connue, ces travaux ouvrent la voie à la modélisation thermodynamique des équilibres fluides-minéraux dans le socle.

#### *9.2.3.2. Moteurs des circulations de fluides*

Les moteurs des circulations de fluides aux interfaces socle – couverture ont été largement discutés dans des travaux de modélisations par [Oliver et al., \(2006\)](#), d'un point de vue général, et dans le cas du bassin de l'Athabasca, par [Raffensperger and Garven \(1995a, 1995b\)](#). Il apparaît que la convection de saumures en base d'un bassin gréseux comme celui de l'Athabasca et au toit du socle est possible même si les granites qui constituent le toit du socle ont une perméabilité très faible.

De récents travaux de modélisation numérique couplant flux de chaleur, déformation, et migrations de fluides avec le programme FLAC2D, ont permis d'associer différents épisodes de migrations de fluides des bassins vers les socles, à des stades de convection puis d'extension dans l'histoire du bassin. La présence dans le socle de sources de chaleur radiogéniques favorise la convection à petite échelle et le mélange localisé de fluides, conduisant à un enrichissement des saumures de bassin en métaux ([McLellan et al., 2006](#)).

Ce type d'approche est primordial pour la compréhension des styles de migration de fluides et l'établissement de modèles conceptuels pour la genèse des concentrations métalliques. Entre autres, les données d'entrée dans ces modèles sont la pression, la température et la composition des fluides, ainsi que les chemins potentiels et les échelles de migrations. Les données acquises pendant ce travail peuvent permettre de rendre plus pertinentes de telles simulations pour le Bassin de l'Athabasca.

## Références

- Alexandre P., Kyser K., Polito P. and Thomas D. (2005) Alteration mineralogy and stable isotope geochemistry of Paleoproterozoic basement-hosted unconformity-type uranium deposits in the Athabasca Basin, Canada. *Economic Geology*, 100, 1547-1563.
- Alexandre P. and Kyser T.K. (2006) Geochemistry of uraniferous bitumen in the Southwest Athabasca basin, Saskatchewan, Canada. *Economic Geology*, 101, 1605-1612.
- Alexandre P., Kyser K., Thomas D., Polito P. and Marlat J., (2009a) Geochronology of unconformity-related uranium deposits in the Athabasca Basin, Saskatchewan, Canada and their integration in the evolution of the basin. *Mineralium Deposita*, 44, 41-59.
- Alexandre P., Kyser K. and Jiricka D. (2009b) Critical Geochemical and Mineralogical Factors for the Formation of Unconformity-Related Uranium Deposits: Comparison between Barren and Mineralized Systems in the Athabasca Basin, Canada. *Economic Geology*, 104, 413-435.
- Allan M.M., Yardley B.W.D., Forbes L.J., Shmulovich K.I., Banks D.A. and Shepherd T.J. (2005) Validation of LA-ICP-MS fluid inclusion analysis with synthetic fluid inclusions. *American Mineralogist*, 90(11-12), 1767-1775.
- Annesley I.R. and Madore C. (1999) Leucogranites and pegmatites of the sub-Athabasca basement, Saskatchewan: U protore? In: Stanley, C.J. et al. (eds): *Mineral Deposits: Processes to Processing*. Balkema, Rotterdam, 297-300.
- Annesley I.R., Madore C. and Portella P. (2005) Geology and thermotectonic evolution of the western margin of the Trans-Hudson Orogen: Evidence from the eastern sub-Athabasca basement, Saskatchewan. *Canadian Journal of Earth Sciences*, 42(4), 573-597.
- Annesley I.R., McCready A.J., Madore C., Kamo S.L. and Kwok K.K. (2007) U-Pb age of overthrusting and reactivation at Cree Extension: structural preparation to the Millennium U deposit, Saskatchewan. In Andrew C.J. (ed.) *Proceedings of the Ninth Biennial SGA Meeting, Digging Deeper*, Dublin, Ireland, 1209-1212.
- Aquilina L., Ladouce B., Doerfliger N., Seidel J.L., Bakalowicz M., Dupuy C. and Le Strat P. (2002) Origin, evolution and residence time of saline thermal fluids (Balaruc springs, southern France): implications for fluid transfer across the continental shelf. *Chemical Geology*, 192, 1-21.
- Armstrong R.L. and Ramaekers P. (1985) Sr isotopic study of Helikian sediment and diabase dikes in the Athabasca Basin, Northern Saskatchewan. *Canadian Journal of Earth Sciences*, 22(3), 399-407.
- Audétat A., Günther D. and Heinrich C.A. (2000) Magmatic-hydrothermal evolution in a fractionating granite: a microchemical study of the Sn-W-F-mineralized mole granite (Australia). *Geochimica et Cosmochimica Acta*, 64, 3373-3393.
- Audétat A. and Pettke T. (2003) The magmatic-hydrothermal evolution of two barren granites: A melt and fluid inclusion study of the Rito del Medio and Canada Pinabete plutons in Northern New Mexico (USA). *Geochimica et Cosmochimica Acta*, 67, 97-121.
- Bakker R.L. (2003) Package FLUIDS 1. Computer programs for analysis of fluid inclusion data and for modelling bulk fluid properties. *Chemical Geology*, 194(1-3), 3-23.
- Banks D.A. and Yardley B.W.D. (1992) Crush-leach analysis of fluid inclusions in small natural and synthetic samples. *Geochimica et Cosmochimica Acta*, 56, 245-248.
- Banks D.A., Green R., Cliff R.A. and Yardley B.W.D. (2000a) Chlorine isotopes in fluid inclusions: determination of the origins of salinity in magmatic fluids. *Geochimica et Cosmochimica Acta*, 64, 1785-1789.

- Banks D.A., Giuliani G. and Yardley B.W.D. (2000b) Emerald mineralization in Colombia: fluid chemistry and the role of brine mixing. *Mineralium Deposita*, 35, 699-713.
- Banks D.A., Boyce A.J. and Samson I.M. (2002) Constraints on the origins of fluids forming Irish Zn-Pb-Ba deposits: evidence from the composition of fluid inclusions. *Economic Geology*, 97, 471-480.
- Banner J.L., Wasserburg G.J., Chen J.H. and Moore C.H. (1990)  $^{234}\text{U}$ - $^{238}\text{U}$ - $^{230}\text{Th}$ - $^{232}\text{Th}$  systematics in saline groundwaters from central Missouri. *Earth and Planetary Science Letters*, 101, 296-312.
- Beaucaire C., Gassam N., Tresonne N. and Louvat D. (1999) Saline groundwaters in the hercynian granites (Chardon Mine, France): geochemical evidence for the salinity origin. *Applied Geochemistry*, 14, 67-84.
- Beshears C., Fayek M., Camacho A., Thomas D., Sopuck V. and Halaburda J. (2008) The geology and geochemistry of the Millennium deposit, Athabasca Basin, Saskatchewan, Canada. *GAC-MAC meeting*, Québec.
- Bodnar R.J. (1994) Synthetic fluid inclusions: XII. The system  $\text{H}_2\text{O}$ -NaCl. Experimental determination of the halite liquidus and isochores for a 40 wt% NaCl solution. *Geochimica et Cosmochimica Acta*, 58, 1053-1063.
- Bodnar R.J. and Vityck, M.O. (1994) Interpretation of microthermometric data for  $\text{H}_2\text{O}$ -NaCl fluid inclusions. In De Vivo B. and Frezzotti M.L. (eds.) *Fluid Inclusions in Minerals: Methods and Applications*. Blacksburg, VA, Virginia Tech, 117-130.
- Böhlke J.K. and Irwin J.J. (1992) Laser microprobe analyses of Cl, Br, I and K in fluid inclusions: Implications for sources of salinity in some ancient hydrothermal fluids. *Geochimica et Cosmochimica Acta*, 56, 203-225.
- Boiron M.C., Cathelineau M., Banks D.A., Buschaert S., Fourcade S., Coulibaly Y., Michelot J.L. and Boyce A. (2002) Fluid transfers at a basement/cover interface: Part II. Large-scale introduction of chlorine into the basement by Mesozoic basinal brines. *Chemical Geology*, 192, 121-140.
- Boiron M.C., Cathelineau M. and Richard A. Fluid mixing at the sedimentary basin/basement unconformity: Role on metal transfer and deposition, *Geofluids*, submitted.
- Bonhoure J. (2007) Géochimie des éléments de terres rares et du plomb dans les oxydes d'uranium naturels. *Unpublished PhD thesis*, Institut National Polytechnique de Lorraine, Nancy, France, 394 p.
- Boulvais P., de Parseval P., D'Hulst A. and Paris P. (2006) Carbonate alteration associated with talc-chlorite mineralization in the eastern Pyrenees, with emphasis on the St. Barthelemy Massif. *Mineralogy and Petrology*, 88, 499-526.
- Boudreau A.E., Stewart M.A. and Spivack A.J. (1997) Stable Cl isotopes and origin of high-Cl magmas of the Stillwater Complex, Montana. *Geology*, 25, 791-794.
- Bray C.J., Spooner T.C. and Longstaffe F.J. (1988) Unconformity-related uranium mineralization, McClean deposits, North Saskatchewan, Canada: hydrogen and oxygen isotope geochemistry. *Canadian Mineralogist*, 26, 249-268.
- Brugger J., Long N., McPhail D.C. and Plimer I. (2005) An active amagmatic hydrothermal system: The Paralana hot springs, Northern Flinders Ranges, South Australia. *Chemical Geology*, 222, 35-64.
- Buchan K.L., Mertanen S., Park R.G., Pesonen L.J., Elming S.Å., Abrahamsen N. and Bylund G. (2000) Comparing the drift of Laurentia and Baltica in the Proterozoic: the importance of key palaeomagnetic poles. *Tectonophysics*, 319, 167-198.
- Bühn B. and Rankin A.H. (1999) Composition of natural, volatile-rich Na-Ca-REE-Sr carbonatitic fluids trapped in fluid inclusions. *Geochimica et Cosmochimica Acta*, 63, 3781-3797.
- Card C.D. (2002) New investigations of basement to the Western Athabasca Basin. *Summary of investigations 2002, Volume 2, Saskatchewan Geological Survey, Saskatchewan Industry Resources, Micellaneous Report 2002-4.2*.
- Card C.D., Campbell J.E. and Slimmon W.L. (2003) Basement lithologic framework and structural features of the Western Athabasca Basin. *Summary of investigations 2003,*

*Volume 2, Saskatchewan Geological Survey, Saskatchewan Industry Resources, Micellaneous Report 2003-4.2.*

- Card C.D., Pana D., Portella P., Thomas D.J., Annesley I.R. (2007) Basement rocks to the Athabasca Basin, Saskatchewan and Alberta, in C.W. Jefferson and G. Delaney (eds.) EXTECH IV: Geology and Uranium EXploration TECHnology of the Proterozoic Athabasca Basin, Saskatchewan and Alberta. *Geological Survey of Canada Bulletin*, 588, 69-87.
- Carpenter A.B., Trout M.L. and Pickett E.E. (1974) Preliminary report on the origin and chemical evolution of lead- and zinc-rich brines in central Mississipi. *Economic Geology*, 69, 1191-1206.
- Cathelineau M. and Boiron M.C. (2009) Downward penetration and mixing of sedimentary brines and dilute hot waters at 5 km depth in the granite basement at Soultz-sous-Forêts (Rhine graben, France). *Comptes Rendus Geoscience*, in press.
- Cauzid J., Philippot P., Martinez-Criado G., Menez B. and Laboure S. (2007) Contrasting Cu-complexing behaviour in vapour and liquid fluid inclusions from the Yankee Lode tin deposit, Mole Granite, Australia. *Chemical Geology*, 246, 39-54.
- Chen J.H., Wasserburg G.J., von Damm K.L. and Edmond J.M. (1986) The U-Th-Pb systematics in hot springs on the East Pacific Rise at 21°N and Guaymas Basin. *Geochimica et Cosmochimica Acta*, 50, 2467-2479.
- Chi G. and Savard M.M. (1997) Sources of basinal and Mississippi Valley-type mineralising brines: mixing of evaporated seawater and halite-dissolution brine. *Chemical Geology*, 143, 121-125.
- Chiarenzelli J., Aspler L., Villeneuve M. and Lewry J. (1998) Early Proterozoic evolution of the Saskatchewan craton and its allochthonous cover, Trans-Hudson orogen. *Journal of Geology*, 106, 247-267.
- Clayton R.N. and Mayeda T.K. (1963) The use of bromine pentafluoride in the extraction of oxygen from oxides and silicates for isotopic analysis. *Geochimica et Cosmochimica Acta*, 27, 43-52.
- Cloutier J., Kyser K., Olivo G.R. and Alexandre P. (2008) The Millennium uranium deposit, Athabasca Basin, Saskatchewan, Canada: Insights into an atypical basement-hosted uranium deposit, GAC-MAC meeting, Québec.
- Connolly C.A., Walter L.M., Baadsgaard H. and Longstaffe F. (1990) Origin and evolution of formation waters, Alberta Basin, Western Canada Sedimentary Basin. 1. Isotope systematics and water mixing. *Applied Geochemistry*, 5, 397-413.
- Creaser R.A. and Stasiuk L.D. (2007) Depositional age of the Douglas Formation, Northern Saskatchewan, determined by Re-Os geochronology. In C.W. Jefferson and G. Delaney (eds.) EXTECH IV: Geology and Uranium EXploration TECHnology of the Proterozoic Athabasca Basin, Saskatchewan and Alberta. *Geological Survey of Canada Bulletin*, 588, 341-346.
- Cumming G.L. and Rimsaite J. (1979) Isotopic studies of lead-depleted pitchblende, secondary radioactive minerals, and sulphides from the Rabbit Lake uranium deposit, Saskatchewan. *Canadian Journal of Earth Sciences* 16(9), 1702-1715.
- Cumming G.L. and Krstic D. (1992) The age of unconformity-related uranium mineralization in the Athabasca Basin, Northern Saskatchewan. *Canadian Journal of Earth Sciences*, 29, 1623-1639.
- Cuney M., Chabiron A., Kister P., Golubev V. and Deloule E. (2002) Chemical versus ion microprobe isotopic dating (CAMECA IMS 3F) of the Shea Creek unconformity-type uranium deposit (west athabasca, Saskatchewan, Canada). *GAC-MAC Meeting*, Saskatoon.
- Cuney M., Brouard M., Cathelineau M., Derome D., Freiberger R., Hecht L., Kister P., Lobaev V., Lorilleux G., Peiffert C. and Bastoul A.M. (2003) What parameter control high grade - large tonnage of the Proterozoic unconformity-related uranium deposits? *Proceedings of International Conference Uranium Geochemistry 2003*, Nancy, France, 123-126.

- Cuney M. (2005) World-class unconformity-related uranium deposits: Key factors for their genesis. *Proceedings of the Eighth Biennial SGA Meeting, Mineral Deposit Research: Meeting the Global Challenge*, Beijing, China, 245-248.
- Davis D.W., Lowenstein T.K. and Spencer R.J. (1990) Melting behavior of fluid inclusions in laboratory-grown halite crystals in the systems NaCl-H<sub>2</sub>O, NaCl-KCl-H<sub>2</sub>O, NaCl-MgCl<sub>2</sub>-H<sub>2</sub>O, and NaCl-CaCl<sub>2</sub>-H<sub>2</sub>O. *Geochimica et Cosmochimica Acta*, 54, 591-601.
- Davisson M.L. and Criss R.E. (1996) Na-Ca-Cl relations in basinal fluids. *Geochimica et Cosmochimica Acta*, 60, 2743-2752.
- Derome D., Cuney M., Cathelineau M., Fabre C., Dubessy J., Bruneton P. and Hubert A. (2003a) A detailed fluid inclusion study in silicified breccias from the Kombolgie sandstones (Northern Territory, Australia): inferences for the genesis of middle-Proterozoic unconformity-type uranium deposits. *Journal of Geochemical Exploration*, 80(2-3), 259-275.
- Derome D., Cathelineau M., Lhomme T. and Cuney M. (2003b) Fluid inclusion evidence of the differential migration of H<sub>2</sub> and O<sub>2</sub> in the McArthur River unconformity-type uranium deposit (Saskatchewan, Canada). Possible role on post-ore modifications of the host rocks. *Journal of Geochemical Exploration*, 78-79, 525-530.
- Derome D., Cathelineau M., Cuney M., Fabre C., Lhomme T. and Banks D.A. (2005) Mixing of sodic and calcic brines and uranium deposition at McArthur River, Saskatchewan, Canada: A Raman and laser-induced breakdown spectroscopic study of fluid inclusions. *Economic Geology*, 100(8), 1529-1545.
- Derome D., Cathelineau M., Fabre C., Boiron M.C., Banks D., Lhomme T. and Cuney M. (2007) Paleo-fluid composition determined from individual fluid inclusions by Raman and LIBS: Application to mid-proterozoic evaporitic Na-Ca brines (Alligator Rivers Uranium Field, Northern territories Australia). *Chemical Geology*, 237(3-4), 240-254.
- Desaulniers D.E., Kaufmann R.S., Cherry J.A. and Bentley H.W. (1986) <sup>37</sup>Cl-<sup>35</sup>Cl variations in a diffusion-controlled groundwater system. *Geochimica et Cosmochimica Acta*, 50, 1757-1764.
- Dubessy J., Pagel M., Beny J.M., Christensen H., Hickel B., Kosztolanyi C. and Poty B. (1988) Radiolysis evidenced by H<sub>2</sub>-O<sub>2</sub> and H<sub>2</sub>-bearing fluid inclusions in three uranium deposits. *Geochimica et Cosmochimica Acta*, 52, 1155-1167.
- Dubessy J., Derome D. and Sausse J. (2003) Numerical modelling of fluid mixings in the H<sub>2</sub>O-NaCl system. Applications to the North Caramal uranium prospect (Australia). *Chemical Geology*, 14102, 1-15.
- Dubois M., Ougougdal M.A., Meere P., Royer J.J., Boiron, M.C. and Cathelineau, M. (1996) Temperature of paleo- to modern self-sealing within a continental rift basin : The fluid inclusion data (Soultz-sous-Forêts, Rhine graben, France). *European Journal of Mineralogy*, 8, 1065-1080.
- Earle S.A.M. and Drever G.L. (1983) Hydrogeochemical exploration for uranium within the Athabasca basin, Northern Saskatchewan. *Journal of Geochemical Exploration*, 19, 57-73.
- Eastoe C.J., Guilbert J.M. and Kaufmann R.S. (1989) Preliminary evidence for fractionation of stable chlorine isotopes in ore-forming hydrothermal systems. *Geology*, 17, 285-288.
- Eastoe C.J. and Guilbert J.M. (1992) Stable chlorine isotopes in hydrothermal processes. *Geochimica et Cosmochimica Acta*, 56, 4247-4255.
- Eastoe C.J. and Peryt T. (1999) Stable chlorine isotope evidence for non-marine chloride in Badenian evaporites, Carpathian mountain region. *Terra Nova*, 11, 118-123.
- Eastoe C.J., Long A. and Knauth L.P. (1999) Stable chlorine isotopes in the Palo Duro Basin, Texas: evidence for preservation of Permian evaporite brines. *Geochimica et Cosmochimica Acta*, 63, 1375-1382.
- Eastoe C.J., Peryt T.M., Petrychenko O.Y. and Geisler-Cussey D. (2007) Stable chlorine isotopes in Phanerozoic evaporites. *Applied Geochemistry*, 22, 575-588.
- Edmunds W.M., Kay R.L.F., Miles D.L. and Cook J.M. (1987) The origin of saline groundwaters in the Carnmenellis Granite, Cornwall (U.K): Further evidence from

- minor and trace elements. *Geological Association of Canada Special Paper*, 33, 127-143.
- Egeberg P.K. and Aagaard P. (1989) Origin and evolution of formation waters from oil fields on the Norwegian shelf. *Applied Geochemistry*, 4, 131-142.
- Eggenkamp H.G.M., Middelburg J.J. and Kreulen R. (1994) Preferential diffusion of  $^{35}\text{Cl}$  relative to  $^{37}\text{Cl}$  in sediments of Kau Bay, Halmahera, Indonesia. *Chemical Geology*, 116, 317-325.
- Eggenkamp H.G.M. and Schuiling R.D. (1995)  $\delta^{37}\text{Cl}$  variations in selected minerals: a possible tool for exploration. *Journal of Geochemical Exploration*, 55, 249-255.
- Eggenkamp H.G.M., Kreulen R. and Koster Van Groos A.F. (1995) Chlorine stable isotope fractionation in evaporites. *Geochimica et Cosmochimica Acta*, 59, 5169-5175.
- Eggenkamp H.G.M. and Coleman M.L. (2009) The effect of aqueous diffusion on the fractionation of chlorine and bromine stable isotopes. *Geochimica et Cosmochimica Acta*, 73, 3539-3548.
- Eseme E., Abanda P.A., Agyingi C.M., Foba-Tendo J. and Hannigan R.E. (2006) Composition and applied sedimentology of salt from brines of the Mamfe Basin, Cameroon. *Journal of Geochemical Exploration*, 91, 41-55.
- Essarraj S., Boiron M.C., Cathelineau M., Banks D.A. and Benharref M. (2005) Penetration of surface-evaporated brines into the Proterozoic basement and deposition of Co and Ag at Bou Azzer (Morocco): Evidence from fluid inclusions. *Journal of African Earth Sciences*, 41, 25-39.
- Evans D.G., Nunn J.A. and Hanor J.S. (1991) Mechanisms driving groundwater flow near salt domes. *Geophysical Research Letters*, 18, 927-930.
- Fayek M. and Kyser T.K. (1997) Characterization of multiple fluid-flow events and rare-earth-element mobility associated with formation of unconformity-type uranium deposits in the Athabasca Basin, Saskatchewan. *Canadian Mineralogist*, 35, 627-658.
- Fayek M., Kyser T.K. and Ricuputi L.R. (2002) U and Pb isotope analysis of uranium minerals by ion microprobe and the geochronology of McArthur River and Sue zone uranium deposits, Saskatchewan, Canada. *Canadian Mineralogist* 40(6), 1553-1569.
- Feltrin L., Oliver N.H.S., Kelso I.J. and King S. (2003) Basement metal scavenging during basin evolution: Cambrian and Proterozoic interaction at the Century Zn-Pb-Ag Deposit, Northern Australia. *Journal of Geochemical Exploration*, 78-79, 159-162.
- Fisher R.S. and Kreitler C.W. (1987) Geochemistry and hydrodynamics of deep-basin brines, Palo Duro Basin, Texas, U.S.A. *Applied Geochemistry*, 2, 459-476.
- Fontes J.C. and Matray J.M. (1993a) Geochemistry and origin of formation brines from the Paris Basin, France 1. Brines associated with Triassic salts. *Chemical Geology*, 109, 149-175.
- Fontes J.C. and Matray J.M. (1993b) Geochemistry and origin of formation brines from the Paris Basin, France 2. Saline solutions associated with oil fields. *Chemical Geology*, 109, 177-200.
- Frape S. and Fritz P. (1987) Geochemical trends for groundwaters from the Canadian Shield. In Fritz P. and Frape, S.K. (eds.) *Saline Water and Gases in Crystalline Rocks*. *Geological Association of Canada Special Paper*, 33, 19-38.
- Freiberger R. and Cuney M. (2003) New evidence for extensive fluid-circulations within the basement in relation to unconformity type uranium deposit genesis in the Athabasca basin, Saskatchewan, Canada. *Proceedings of International Conference Uranium Geochemistry 2003*, 151-154.
- Fuge R. (1974) Chapter. 17 and 35. In Wedepohl K.H. (ed.) *Handbook of Geochemistry*, Springer, Berlin.
- Gaboreau S., Cuney M., Quirt D., Beaufort D., Patrier P. and Mathieu R. (2007) Significance of aluminium phosphate-sulfate minerals associated with U unconformity-type deposits: The Athabasca basin, Canada. *American Mineralogist*, 92, 267-280.
- Gagnon J.E., Samson I.M., Fryer B.J. and Williams-Jones A.E. (2004) The composition and origin of hydrothermal fluids in a NYF-type granitic pegmatite, South Platte District,

- Colorado: Evidence from LA-ICP-MS analysis of fluorite- and quartz-hosted fluid inclusions. *Canadian Mineralogist*, 42, 1331-1355.
- Garda G.M., Trumbull R.B., Beljavskis P. and Wiedenbeck M. (2009) Boron isotope composition of tourmalinite and vein tourmalines associated with gold mineralization, Serra do Itaberaba Group, central Ribeira Belt, SE Brazil. *Chemical Geology*, 264, 207-220.
- Garven G. (1995) Continental-scale groundwater flow and geologic processes. *Annual Review of Earth & Planetary Sciences*, 23, 89-117.
- Gascoyne M. (2004) Hydrogeochemistry, groundwater ages and sources of salts in a granitic batholith on the Canadian Shield, southeastern Manitoba. *Applied Geochemistry*, 19, 519-560.
- Gleeson S.A., Wilkinson J.J., Boyce A.J., Fallick A.E. and Stuart F.M. (1999) On the occurrence and wider implications of anomalously low  $\delta D$  fluids in quartz veins, South Cornwall, England. *Chemical Geology*, 160, 161-173.
- Gleeson S.A., Wilkinson J.J., Stuart F.M. and Banks D.A. (2001) The origin and evolution of base metal mineralising brines and hydrothermal fluids, South Cornwall, UK. *Geochimica et Cosmochimica Acta*, 65, 2067-2079.
- Gleeson S.A. (2003) Bulk analysis of electrolytes in fluid inclusions. In Samsom I., Anderson A. and Marshall D. (eds.), Fluid inclusions: Analysis and Interpretation. *Mineralogical Association of Canada Short Course Series*, 32, 233-246.
- Gleeson S.A., Yardley B.W.D., Boyce A.J., Fallick A.E. and Munz I.A. (2003) Infiltration of basinal fluids into high-grade basement South Norway: sources and behaviour of waters and brines. *Geofluids*, 3, 33-48.
- Gleeson S.A. and Turner W.A. (2007) Fluid inclusion constraints on the origin of the brines responsible for Pb-Zn mineralization at Pine Point and coarse non-saddle and saddle dolomite formation in southern Northwest Territories. *Geofluids*, 7, 51-68.
- Gleeson S.A., Roberts S., Fallick A.E. and Boyce A.J. (2008) Micro-Fourier Transform Infrared (FT-IR) and  $\delta D$  value investigation of hydrothermal vein quartz: Interpretation of fluid inclusion  $\delta D$  values in hydrothermal systems. *Geochimica et Cosmochimica Acta*, 72, 4595-4606.
- Goldstein R.H. and Reynolds T.J. (1994) Systematics of fluid inclusions in diagenetic minerals. *Society of Economic Paleontologists and Mineralogists (SEPM) Short Course* 31, 198 p.
- Godon A.R., Jendrejewski N., Eggenkamp H.G.M., Banks D.A., Ader M., Coleman M.L. and Pineau F. (2004) A cross-calibration of chlorine isotopic measurements and suitability of seawater as the international reference material. *Chemical Geology*, 207, 1-12.
- Grandia F., Canals A., Cardellach E., Banks D.A. and Perona J. (2003a) Origin of ore-forming brines in sediment hosted Zn-Pb deposits of the Basque-Cantabrian Basin, Northern Spain. *Economic Geology*, 98, 1397-1411.
- Grandia F., Cardellach E., Canals A. and Banks D.A. (2003b) Geochemistry of the fluids related to epigenetic carbonate-hosted Zn-Pb deposits in the Maestrat Basin, Eastern Spain: fluid inclusion and isotope (Cl, C, O, S, Sr) evidence. *Economic Geology*, 98, 933-954.
- Grenthe I., Fuger J., Konings R.J.M., Lemire R.J., Muller A.B., Nguyen-Trung Ch. and Wanner H (1992). In Wanner H. and I. Forest, (eds.) *Chemical Thermodynamics of Uranium*, Nuclear Energy Agency, OECD, Amsterdam.
- Guillong M., Meier D.L., Allan M., Heinrich C.A. and Yardley B.W.D. (2008) SILLS: A Matlab-based program for the reduction of laser ablation ICP-MS data of homogeneous materials and inclusions. In Sylvester P. (ed.) *Laser Ablation ICP-MS in the Earth Sciences: Current Practices and Outstanding Issues*. *Mineralogical Association of Canada Short Course Series*, 40, 328-333.
- Günther D., Audétat A., Frischknecht R. and Heinrich C.A. (1998) Quantitative analysis of major, minor and trace elements in fluid inclusions using laser ablation-inductively coupled plasma mass spectrometry. *Journal of Analytical Atomic Spectrometry*, 13, 263-270.

- Halter G., Sheppard S.M.F., Weber F., Clauer N. and Pagel M. (1987) Radiation-related retrograde hydrogen isotope and K-Ar exchange in clay minerals. *Nature*, 330, 638-641.
- Hanor J.S. (1994) Origin of saline fluids in sedimentary basins. In Parnell J. (ed.) *Geofluids: Origin, Migration and Evolution of Fluids in Sedimentary Basins*. Geological Society Special Publication, 78, 151-174.
- Hanor J.S. and McIntosh J.C. (2006) Are secular variations in seawater chemistry reflected in the compositions of basinal brines? *Journal of Geochemical Exploration*, 89, 153-156.
- Hardie L.A. (1990) The roles of rifting and hydrothermal  $\text{CaCl}_2$  brines in the origin of potash evaporites: an hypothesis. *American Journal of Science*, 290, 43-106.
- Haynes F.M. (1985) Determination of fluid inclusion compositions by sequential freezing. *Economic Geology*, 80, 1436-1439.
- Hecht L. and Cuney M. (2000) Hydrothermal alteration of monazite in the Precambrian crystalline basement of the Athabasca Basin (Saskatchewan, Canada): Implications for the formation of unconformity-related uranium deposits. *Mineralium Deposita*, 35(8), 791-795.
- Heine T.H. (1986) The geology of the Rabbit Lake uranium deposit, Saskatchewan. In Evans E.L. (ed) *Uranium deposits of Canada*. Canadian Institute of Mining, Metallurgy and Petroleum Special Volume, 33 ,134-143.
- Heinrich C.A., Pettke T., Halter W.E., Aigner-Torres M., Audéat A., Günther D., Hattendorf B., Bleiner D., Guillong M. and Horn I. (2003) Quantitative multi-element analysis of minerals, fluid and melt inclusions by laser-ablation inductively-coupled-plasma mass-spectrometry. *Geochimica et Cosmochimica Acta*, 67, 3473-3497.
- Hendry H.E. and Weathley K.L. (1985) The Carswell Formation, Northern Saskatchewan: Stratigraphy, sedimentology, and structure. In Lainé R., Alonso D. and Svab M. (eds.) *The Carswell Structure Uranium Deposits, Saskatchewan*. Geological Association of Canada Special Paper, 29, 87-103.
- Hodge V.F., Johannesson K.H. and Stetzenbach K.J. (1996) Rhenium, molybdenum, and uranium in groundwater from the southern Great Basin, USA: Evidence for conservative behaviour. *Geochimica et Cosmochimica Acta*, 60, 3197-3214.
- Hoeve J. and Sibbald T.I.I. (1978) On the genesis of the Rabbit Lake and other unconformity-type uranium deposits in Northern Saskatchewan, Canada. *Economic Geology*, 73(8), 1450-1473.
- Hoeve J. and Quirt D. (1984) Mineralization and host rock alteration in relation to clay mineral diagenesis and evolution of the middle Proterozoic Athabasca basin, Northern Saskatchewan, Canada. *Saskatchewan Research Council Technical Report*, 187, 187 p.
- Hoffman P.F. (1990) Subdivision of the Churchill Province and extent of the Trans-Hudson Orogen. In Lewry J.F. and Stauffer M.R. (eds.) *The Early Proterozoic Trans-Hudson Orogen of North America*. Geological Association of Canada Special Paper, 37, 15-39.
- Holser W. (1979) Trace elements and isotopes in evaporites. In Burns R.G. (ed.) *Marine Minerals*. Mineralogical Society of America, *Reviews in Mineralogy*, 6, 295-346.
- Hyeong K. and Capuano R.M. (2001) Ca/Mg of brines in Miocene/Oligocene clastic sediments of the Texas Gulf Coast: buffering by calcite/disordered dolomite equilibria. *Geochimica et Cosmochimica Acta*, 65, 3065-3080.
- Irwin J.J. and Reynolds J.H. (1995) Multiple stages of fluid trapping in the Stripa granite indicated by laser microprobe analysis of Cl, Br, I, K, U, and nucleogenic plus radiogenic Ar, Kr, and Xe in fluid inclusions. *Geochimica et Cosmochimica Acta*, 59, 355-369.
- Irwin J.J. and Roedder E. (1995) Diverse origins of fluid in magmatic inclusions at Bingham (Utah, USA), Butte (Montana, USA), St. Austell (Cornwall, UK), and Ascension Island (mid-Atlantic, UK), indicated by laser microprobe analysis of Cl, K, Br, I, Ba + Te, U, Ar, Kr, and Xe. *Geochimica et Cosmochimica Acta*, 59, 295-312.

- Jefferson C.W., Thomas D.J., Gandhi S.S., Ramaekers P., Delaney G., Brisbin D., Cutts C., Portella P. and Olson R.A. (2007) Unconformity associated uranium deposits of the Athabasca Basin, Saskatchewan and Alberta. In Jefferson C.W. and Delaney G. (eds.) EXTECH IV: Geology and Uranium EXploration TECHnology of the Proterozoic Athabasca Basin, Saskatchewan and Alberta. *Geological Survey of Canada Bulletin*, 588, 23-67.
- Kamineni D.C. (1984) Halogen-bearing minerals in plutonic rocks: a possible source of chlorine in saline groundwater in the Canadian Shield. In Fritz P. and Frape S.K. (eds.) Saline water and gases in crystalline rocks. *Geological Association of Canada Special Paper*, 33, 69-79.
- Kaufmann R., Long A., Bentley H. and Davis S. (1984a) Natural chlorine isotope variations. *Nature*, 309, 338-340.
- Kaufmann R., Frape S.K., Fritz P. and Bentley H. (1984b) Chlorine stable isotope composition of Canadian Shield brines. In Fritz P. and Frape S.K. Saline water and gases in crystalline rocks. *Geological Association of Canada Special Paper*, 33, 89-93.
- Kaufmann R., Long A. and Campbell D.J. (1988) Chlorine isotope distribution in formation waters, Texas and Louisiana. *American Association of Petroleum Geologists Bulletin*, 72, 839-844.
- Kendrick M.A., Burgess R., Pattrick R.A.D. and Turner G. (2002) Hydrothermal fluid origins in a fluorite-rich Mississippi Valley-type district: Combined noble gas (He, Ar, Kr) and halogen (Cl, Br, I) analysis of fluid inclusions from the South Pennine ore field, United Kingdom. *Economic Geology*, 97, 435-451.
- Kendrick M.A., Burgess R., Harrison D. and Bjorlykke A. (2005) Noble gas and halogen evidence for the origin of Scandinavian sandstone-hosted Pb-Zn deposits. *Geochimica et Cosmochimica Acta*, 69, 109-129.
- Kesler S.E., Appold M.S., Martini A.M., Walter L.M., Huston T.J. and Kyle J.R. (1995) Na-Cl-Br systematics of mineralizing brines in Mississippi Valley-type deposits. *Geology*, 23, 641-644.
- Kharaka Y.K., Maest A.S., Carothers W.W., Law L.M., Lamothe P.J. and Fries T.L. (1987) Geochemistry of metal-rich brines from central Mississippi Salt Dome basin, U.S.A. *Applied Geochemistry*, 2, 543-561.
- Kister P., Vieillard P., Cuney M., Quirt D. and Laverret E. (2005) Thermodynamic constraints on the mineralogical and fluid composition evolution in a clastic sedimentary basin: The Athabasca Basin (Saskatchewan, Canada). *European Journal of Mineralogy*, 17(2), 325-342.
- Kister P., Laverret E., Quirt D., Cuney M., Patrier Mas P., Beaufort D. and Bruneton P. (2006) Mineralogy and geochemistry of the host-rock alterations associated with the Shea Creek unconformity-type uranium deposits (Athabasca basin, Saskatchewan, Canada). Part 2. Regional-scale spatial distribution of the Athabasca Group sandstone matrix minerals. *Clays and Clay minerals*, 54(3), 295-313.
- Klemm L.M., Pettke T. and Heinrich C.A. (2007) Hydrothermal Evolution of the El Teniente Deposit, Chile: Porphyry Cu-Mo Ore Deposition from Low-Salinity Magmatic Fluids. *Economic Geology*, 102, 2021-1045.
- Kloppmann W., Negrel P., Casanova J., Klinge H., Schelkes K. and Guerrot C. (2001) Halite dissolution derived brines in the vicinity of a Permian salt dome (N German Basin). Evidence from boron, strontium, oxygen, and hydrogen isotopes. *Geochimica et Cosmochimica Acta*, 65, 4087-4101.
- Kloppmann W., Girard J.-P. and Negrel P. (2002) Exotic stable isotope compositions of saline waters and brines from the crystalline basement. *Chemical Geology*, 184, 49-70.
- Knauth L.P. and Beeunas M.A. (1986) Isotope geochemistry of fluid inclusions in Permian halite with implications for the isotopic history of ocean water and the origin of saline formation waters. *Geochimica et Cosmochimica Acta*, 50, 419-433.

- Komninou A. and Sverjensky D.A. (1996) Geochemical modeling on the formation of an unconformity-type uranium deposit. *Economic Geology*, 91, 590-606.
- Kotzer T.G. and Kyser T.K. (1991) Retrograde alteration of clay minerals in uranium deposits: Radiation catalyzed or simply low-temperature exchange? *Chemical Geology: Isotope Geoscience Section*, 86, 307-321.
- Kotzer T.G., Kyser T.K. and Irving E. (1992) Paleomagnetism and the evolution of fluids in the Proterozoic Athabasca Basin, Northern Saskatchewan, Canada. *Canadian Journal of Earth Sciences*, 29, 1474-1491.
- Kotzer T.G. and Kyser T.K. (1993) O, U, and Pb isotopic and chemical variations in uraninite: implications for determining the temporal and fluid history of ancient terrains. *American Mineralogist*, 78(11-12), 1262-1274.
- Kotzer T.G. and Kyser T.K. (1995) Petrogenesis of the Proterozoic Athabasca Basin, Northern Saskatchewan, Canada, and its relation to diagenesis, hydrothermal uranium mineralization and paleohydrogeology. *Chemical Geology*, 120, 45-89.
- Kraemer T.F. and Kharaka Y.K. (1986) Uranium geochemistry in geopressured-geothermal aquifers of the U.S. Gulf Coast. *Geochimica et Cosmochimica Acta*, 50, 1233-1238.
- Ku T.L., Knauss K.G. and Mathieu G.G. (1977) Uranium in open ocean: concentration and isotopic composition. *Deep-Sea Research*, 24, 1005-1017.
- Kyser T.K., Wilson M.R. and Ruhrmann G. (1989) Stable isotope constraints on the role of graphite in the genesis of unconformity-type uranium deposits. *Canadian Journal of Earth Sciences*, 26, 490-498.
- Kyser T.K. and Kerrich R. (1990) Geochemistry of fluids in tectonically active crustal regions. In Nesbitt N.E. (ed.) Fluids in Tectonically Active Regimes of the Continental Crust. *Mineralogical Association of Canada Short Course Series*, 18, 133-230.
- Kyser K. and Kerrich R. (1991) Retrograde exchange of hydrogen isotopes between hydrous minerals and water at low temperatures. In Taylor H.P., O'Neil J.R. and Kaplan I. (eds.) Stable Isotope Geochemistry: A Tribute to Samuel Epstein. *Geochemical Society Special Publication*, 3, 409-424.
- Kyser T.K., Hiatt E., Renac C., Durocher K., Holk G. and Deckart K. (2000) Diagenetic fluids in paleo- and meso-proterozoic sedimentary basins and their implications for long protracted fluid histories. In Kyser K. (ed.) Fluids and basin evolution. *Mineralogical Association of Canada Short Course Series*, 28, 225-262.
- Landais P. and Dereppe J.M. (1985) A chemical study of the carbonaceous material from the Carswell Structure. In Lainé R., Alonso D. and Svab M. (eds.) The Carswell Structure Uranium Deposits, Saskatchewan. *Geological Association of Canada Special Paper*, 29, 165-174.
- Landais P., Dubessy J., Poty B. and Robb L.J. (1990) Three examples illustrating the analysis of organic matter associated with uranium ores. *Organic Geochemistry*, 16, 601-608.
- Landais P., Dubessy J., Dereppe J. M., and Philp R.P. (1993) Characterization of graphite alteration and bitumen genesis in the Cigar Lake deposit (Saskatchewan, Canada). *Canadian Journal of Earth Sciences*, 30(4), 743-753.
- Landais P. (1996) Organic geochemistry of sedimentary uranium ore deposits. *Ore Geology Reviews*, 11, 33-51.
- Langmuir D. (1978) Uranium solution-mineral equilibria at low temperatures with applications to sedimentary ore deposits. *Geochimica et Cosmochimica Acta*, 42, 547-569.
- Laverret E., Patrier Mas P., Beaufort D., Kister P., Quirt D., Bruneton P. and Clauer N. (2006) Mineralogy and geochemistry of the host-rock alterations associated with the Shea Creek unconformity-type uranium deposits (Athabasca Basin, Saskatchewan, Canada). Part 1. Spatial variation of illite properties. *Clays and Clay Minerals*, 54(3), 275-294.
- Lawler J.P. and Crawford M.L. (1982) Fluid inclusions in the Midwest Lake Uranium deposit. *Geological Society of America, Abstracts with Programs*, 14, 542.
- Le Carlier de Veslud C., Cuney M., Lorilieur G., Royer J.-J. and Jébrak M. (2009) 3D modeling of uranium-bearing solution-collapse breccias in Proterozoic sandstones

- (Athabasca Basin, Canada) - Metallogenic interpretations. *Computers & Geosciences*, 35(1), 92-107.
- Leventhal J.S., Grauch R.I., Threlkeld C.N., Lichte F.E. and Harper C.T. (1987) Unusual organic matter associated with uranium from the Claude deposit, Cluff Lake, Canada. *Economic Geology*, 82, 1169-1176.
- Lin L.H., Slater G.F., Sherwood Lollar B., Lacrampe-Couloume G. and Onstott T.C. (2005) The yield and isotopic composition of radiolytic H<sub>2</sub>, a potential energy source for the deep subsurface biosphere. *Geochimica et Cosmochimica Acta*, 69, 893-903.
- Liu W.G., Xiao Y.K., Wang Q.Z., Qi H.P., Wang Y.H., Zhou Y.M. and Shirodkar P.V. (1997) Chlorine isotopic geochemistry of salt lakes in the Qaidam Basin, China. *Chemical Geology*, 136, 271-279.
- Lodemann M., Fritz P., Wolf M., Ivanovitch M., Hansen B.T. and Nolte E. (1998) On the origin of saline fluids in the KTB (continental deep drilling project of Germany). *Applied Geochemistry*, 13, 653-671.
- Longerich H.P., Jackson S.E. and Günther D. (1996) Laser ablation inductively coupled plasma mass spectrometric transient signal data acquisition and analyte concentration calculation. *Journal of Analytical Atomic Spectrometry*, 11(9), 899-904.
- Lorillex G., Jébrak M., Cuney M. and Baudemont D. (2002) Polyphase hydrothermal breccia associated with unconformity-related uranium mineralizations (Canada). From fractal analysis to structural significance. *Journal of structural geology*, 24, 223-238.
- Lowenstein T.K., Timofeeff M.N., Brennan S.T., Hardie L.A. and Demicco R.V. (2001) Oscillations in Phanerozoic seawater chemistry: Evidence from fluid Inclusions. *Science*, 294, 1086-1088.
- Lowenstein T.K., Hardie L.A., Timofeeff M.N. and Demicco R.V. (2003) Secular variation in seawater chemistry and the origin of calcium chloride basinal brines. *Geology*, 31, 857-860.
- Lowenstein T.K. and Timofeeff M.N. (2008) Secular variations in seawater chemistry as a control on the chemistry of basinal brines: test of the hypothesis. *Geofluids*, 8, 77-92.
- Macdonald C. (1985) Mineralogy and Geochemistry of the sub-Athabasca regolith near Wollaston Lake. In Sibbald T.I.I. and Petruk W. (eds.) *Geology of uranium deposits. The Canadian Institute of Mining and Metallurgy Special volume*, 32, 155-158.
- Madore C., Annesley I.R. and Wheatley K. (2000) Petrogenesis, age and uranium fertility of peraluminous leucogranites and pegmatites of the McClean Lake / Sue and Key Lake / P-Patch deposits area, Saskatchewan. *Geocanada 2000. The Millennium Geoscience Summit*, Calgary, Program with Abstracts, 1041-1044.
- Magenheim A.J., Spivack A.J., Michael P.J. and Gieskes J.M. (1995) Chlorine stable isotope composition of the oceanic crust: Implications for Earth's distribution of chlorine. *Earth and Planetary Science Letters*, 131, 427-432.
- Markl G., Musashi M. and Bucher K. (1997) Chlorine stable isotope composition of granulites from Lofoten, Norway: Implications for the Cl isotopic composition and for the source of Cl enrichment in the lower crust. *Earth and Planetary Science Letters*, 150, 95-102.
- Mathieu R., Cuney M. and Cathelineau M. (2000) Geochemistry of paleofluids circulation in the Franceville basin and around Oklo natural nuclear reaction zones (Gabon). *Journal of Geochemical Exploration*, 69-70, 245-249.
- Matthews R., Koch R. and Leppin, M. (1997) Advances in integrated exploration for unconformity uranium deposits in western Canada. *Exploration 97, International Conference on Mineral Exploration, 4th Decennial*, Toronto, Canada, Proceedings, 993–1024.
- McCrea J.M. (1950) On the isotope chemistry of carbonates and a paleotemperature scale. *Journal of Chemical Physics*, 18, 849–857.
- McCready A.J., Annesley I.R., Parnell J. and Richardson L.C. (1999) Uranium-bearing carbonaceous matter, McArthur River uranium ore-deposit, Saskatchewan. *Saskatchewan Geological Survey, Saskatchewan Energy and Mines, Summary of Investigations 1999*, 2, 110-120.

- McCready A.J., Annesley I.R., Rickers K. and Cavell R.G. (2007) First insights into the inorganic chemistry of 'carbon phases' from basement rocks to uranium deposits in the Athabasca Basin, Canada. *Proceedings of the Ninth Biennial SGA Meeting, Digging Deeper*, Dublin, Ireland, 1145-1148.
- McGill B.D., Marlatt R.B., Matthews R.B., Sopuck V.J. and Homeniuk L.A. (1993) The P2 North Uranium deposit, Saskatchewan, Canada. *Exploration and Mining geology*, 2(4), 321-331.
- McGowan R.R., Roberts S. and Boyce A.J. (2006) Origin of the Nchanga copper-cobalt deposits of the Zambian Copperbelt. *Mineralium Deposita*, 40, 617-638.
- McLellan J.G., Oliver N.H.S. and Hobbs B.E. (2006) The relative effects of deformation and thermal advection on fluid pathways in basin-related mineralization. *Journal of Geochemical Exploration*, 89, 271-275.
- Meert J.G. (2002) Paleomagnetic Evidence for a Paleo-Mesoproterozoic Supercontinent Columbia. *Gondwana Research*, 5, 207-215.
- Mercadier J. (2008) Conditions de genèse des gisements d'uranium associés aux discordances protérozoïques et localisés dans les socles. Exemple du socle du bassin d'Athabasca (Saskatchewan, Canada). *Unpublished PhD thesis*, Institut National Polytechnique de Lorraine, Nancy, France, 362 p.
- Mercadier J., Richard A., Boiron M.C., Cathelineau M. and Cuney M., Brine migration in the basement rocks of the Athabasca Basin through microfracture networks (P-Patch U deposit, Canada), *Lithos*, in press.
- Merino E. (1975) Diagenesis in tertiary sandstones from Kettleman North Dome, California - II. Interstitial solutions: Distribution of aqueous species at 100°C and chemical relation to the diagenetic mineralogy. *Geochimica et Cosmochimica Acta*, 39, 1629-1645.
- Michard A., Albarède F., Michard G., Minster J.F. and Charlou J.L. (1983) Rare-earth elements and uranium in high-temperature solutions from East Pacific Rise hydrothermal vent field (13°N). *Nature*, 303, 795-797.
- Möller P., Woith H., Dulski P., Lüders V., Erzinger J., Kämpf H., Pekdeger A., Hansen B., Lodemann M. and Banks D.A. (2005) Main and trace elements in KTB-VB fluid: composition and hints to its origin. *Geofluids*, 5, 28-41.
- Muchez P., Heijlen W., Banks D.A., Blundell D., Boni M. and Grandia F. (2005) Extensional tectonics and the timing and formation of basin-hosted deposits in Europe. *Ore Geology Reviews*, 27.
- Munoz M., Boyce A.J., Courjault-Rade P., Fallick A.E. and Tollon F. (1999) Continental basinal origin of ore fluids from southwestern Massif central fluorite veins (Albigeois, France): evidence from fluid inclusion and stable isotope analyses. *Applied Geochemistry*, 14, 447-458.
- Munz I.A., Yardley B.W.D., Banks D.A. and Wayne D.W. (1995) Deep penetration of sedimentary fluids in basement rocks from southern Norway: Evidence from hydrocarbon and brine inclusions. *Geochimica et Cosmochimica Acta*, 59, 239-254.
- Musashi M., Markl G. and Kreulen R. (1998) Stable chlorine-isotope analysis of rock samples: New aspects of chlorine extraction. *Analytica Chimica Acta*, 362, 261-269.
- Naden J. (1996), CalcicBrine: a Microsoft Excel 5.0 add-in for calculating salinities from microthermometric data in the system NaCl-CaCl<sub>2</sub>-H<sub>2</sub>O. *PACROFI VI*, Madison, WI.
- Nahnybida T., Gleeson S.A., Rusk B.G. and Wassenaar L.I. (2009) Cl/Br ratios and stable chlorine isotope analysis of magmatic-hydrothermal fluid inclusions from Butte, Montana and Bingham Canyon, Utah. *Mineralium Deposita*, 1-12.
- Oakes C.S., Bodnar R.J. and Simonson J. M. (1990) The system NaCl-CaCl<sub>2</sub>-H<sub>2</sub>O: I. The ice liquidus at 1 atm total pressure. *Geochimica et Cosmochimica Acta*, 54(3), 603-610.
- Ohmoto H. and Rye R.O. (1979) Isotope of sulfur and carbon. In Barnes H.L. (ed.) *Geochemistry of Hydrothermal deposits*, John Wiley & Sons, 509-567.
- Oliver N.H.S., McLellan J.G., Hobbs B.E., Cleverly J.S., Ord A. and Feltrin L. (2006) Numerical models of extensional deformation, heat transfer, and fluid flow across

- basement-cover interfaces during basin-related mineralization. *Economic Geology*, 101, 1-31.
- Pagel M. (1975) Détermination des conditions physico-chimiques de la silicification diagénétique des grès Athabasca (Canada) au moyen des inclusions fluides. *Comptes Rendus de l'Académie des Sciences de Paris*, 280(D), 2301-2304.
- Pagel M. and Jaffrezic H. (1977) Analyses chimiques des saumures des inclusions du quartz et de la dolomite du gisement d'uranium de Rabbit Lake (Canada). Aspect méthodologique et importance génétique. *Comptes Rendus de l'Académie des Sciences de Paris*, 284(D), 113-116.
- Pagel M., Poty B. and Sheppard S.M.F. (1980) Contribution to some Saskatchewan uranium deposits mainly from fluid inclusion and isotopic data. In IAEA (ed.) *International Uranium Symposium on the Pine Creek Geosyncline*, Vienna, 639-654.
- Pagel M., Wheatley K. and Ey F. (1985) The Origin of the Carswell circular structure. A summary of data for geological interpretation of its formation. In Lainé R, Alonso D and Svab M. (eds.) *The Carswell Structure Uranium Deposits Saskatchewan. Geological Association of Canada, Special Paper*, 29, 213-223.
- Pagel M. (1991) Lateritization and paleogeomorphology: Their roles in the genesis of unconformity-type uranium deposits in Saskatchewan, Canada. In Pagel M. and Leroy J. (eds.) *Source, transport and deposition of metals*, Rotterdam, Balkema, 331-332.
- Pagel M. and Ahmdach N. (1995) Etude des inclusions fluides dans les quartz des gisements d'uranium de l'Athabasca et du Thelon (Canada). *CREGU internal report*, 9 p.
- Palmer M.R. and Edmond J.M. (1993) Uranium in river water. *Geochimica et Cosmochimica Acta*, 57, 4947-4955.
- Parslow G.R. and Thomas D.J. (1982) Uranium Occurrences in the Cree Lake Zone, Saskatchewan, Canada. *Mineralogical Magazine*, 46, 63-171.
- Pesonen L.J., Elming S.Å., Mertanen S., Pisarevsky S., D'Agrella-Filho M.S., Meert J.G., Schmidt P.W., Abrahamsen N. and Bylund G. (2003) Palaeomagnetic configuration of continents during the Proterozoic. *Tectonophysics*, 375, 289-324.
- Pettke T., Halter W.E., Webster J.D., Aigner-Torres M. and Heinrich C.A. (2004) Accurate quantification of melt inclusion chemistry by LA-ICPMS: a comparison with EMP and SIMS and advantages and possible limitations of these methods. *Lithos*, 78, 333-361.
- Philippot P., Ménez B., Simionovici A., Chabiron A., Cuney M., Snigirev A. and Snigireva I. (2000) X-ray imaging of uranium in individual fluid inclusions. *Terra Nova*, 12, 84-89.
- Piqué À., Canals À., Grandia F. and Banks D.A. (2008) Mesozoic fluorite veins in NE Spain record regional base metal-rich brine circulation through basin and basement during extensional events. *Chemical Geology*, 257, 139-152.
- Pluta I. and Zuber A. (1995) Origin of brines in the Upper Silesian Coal Basin (Poland) inferred from stable isotope and chemical data. *Applied Geochemistry*, 10, 447-460.
- Polito P.A., Kyser T.K., Marlatt J., Alexandre P., Bajwah Z. and Drever G. (2004) Significance of alteration assemblages for the origin and evolution of the Proterozoic Nabarlek unconformity-related uranium deposit, Northern Territory, Australia. *Economic Geology*, 99, 113-139.
- Polito P.A., Kyser T.K., Thomas D., Marlatt J. and Drever G. (2005) Re-evaluation of the petrogenesis of the Proterozoic Jabiluka unconformity-related uranium deposit, Northern Territory, Australia. *Mineralium Deposita*, 40, 257-288.
- Poty B. and Pagel M. (1988) Fluid inclusions related to uranium deposits: a review. *Journal of Geological Society*, 145, 157-162.
- Quirt D. (1989) Host-rock alteration at Eagle Point South. *Saskatchewan Research Council Publication*, R-855-1-E-89, 72p.
- Quirt D. (2003) Athabasca unconformity-type uranium deposits: one type of deposit with many variations. *Proceedings of International Conference Uranium Geochemistry 2003*, Nancy, France, 309-312.

- Raffensperger J.P. and Garven G. (1995a) The formation of unconformity-type uranium ore deposits 1. Coupled groundwater flow and heat transport modeling. *American Journal of Science*, 295, 581-636.
- Raffensperger J.P. and Garven G. (1995b) The formation of unconformity-type uranium ore deposits 2. Coupled hydrochemical modelling. *American Journal of Science*, 295, 639-696.
- Rainbird R., Stern R.A., Rayner N. and Jefferson, C.W. (2007) Age, provenance, and regional correlation of the Athabasca Group, Saskatchewan and Alberta constrained by igneous and detrital zircon geochronology. In Jefferson C.W. and Delaney G. (eds.) EXTECH IV: Geology and EXploration TECHnology of the Proterozoic Athabasca basin, Saskatchewan and Alberta. *Geological Survey of Canada Bulletin*, 588, 193-209.
- Ramaekers P., Jefferson C.W., Yeo G.M., Collier B., Long D.G., Catuneanu O., Bernier S., Kupsch B., Post R., Drever G., McHardy S., Jircka D., Cutts C. and Wheatley K. (2007) Revised geological map and stratigraphy of the Athabasca Group, Saskatchewan and Alberta. In Jefferson C.W. and Delaney G. (eds.) EXTECH IV: Geology and Exploration Technology of the Proterozoic Athabasca basin, Saskatchewan and Alberta. *Geological Survey of Canada Bulletin*, 588, 155-578.
- Rawlings D.J. (1999) Stratigraphic resolution of a multiphase intracratonic basin system: the McArthur Basin, Northern Australia. *Australian Journal of Earth Sciences*, 46, 703–723.
- Richard L. (2000), A dual origin for the chloride ions of saline waters from crystalline rocks: Sur l'origine des ions chlorure dans les eaux salines des massifs granitiques. *Comptes-rendus de l'Académie des Sciences de Paris*, 331, 783-788.
- Richard L. and Sangély L. (2004) Thermodynamic and carbon isotopic constraints on the origin of unusual bitumens in the uranium deposits of Athabasca (Saskatchewan, Canada). *14<sup>th</sup> Annual Goldschmidt Conference 2004*, Copenhagen, Denmark, Abstract No. 3.2.24.
- Rippert J.C., Koning E., Robbins J., Koch R. and Baudemont D. (2000) The Shea Creek uranium project, West Athabasca Basin, Saskatchewan, Canada. *Geocanada 2000*, Calgary, Canada.
- Risacher F., Alonso H. and Salazar C. (2003) The origin of brines and salts in Chilean salars: a hydrochemical review. *Earth-Science Reviews*, 63, 249-293.
- Risacher F., Fritz B. and Alonso H. (2006) Non-conservative behavior of bromide in surface waters and brines of Central Andes: A release into the atmosphere? *Geochimica et Cosmochimica Acta*, 70, 2143-2152.
- Roy C., Halaburda D., Thomas D. and Hirsekorn D. (2005) Millenium deposit - basement-hosted derivative of the unconformity uranium model. *Symposium on Uranium Production and Raw Materials for the Nuclear Fuel Cycle - Supply and Demand, Economics, the Environment and Energy Security (IAEA-CN-128)*, Vienna, Extended synopsis.
- Rozsypal C. (2009) Modélisation du système binaire NaCl-H<sub>2</sub>O en fonction du pH, de la concentration en sodium, de la pression, et de la température. Etude expérimentale et modélisation, en fonction du pH et de la concentration en sodium, du système ternaire UVI-NaCl-H<sub>2</sub>O à T = 155°C et pression de vapeur saturante. *Unpublished PhD thesis*, Université Henri Poincaré, Nancy, France.
- Ruzicka V. (1989) Monometallic and polymetallic deposits associated with sub-Athabasca unconformity in Saskatchewan. *Geological Survey of Canada Paper*, 1-C, 67-79.
- Sangely L., Chaussidon M., Michels R., Brouard M., Cuney M., Huault V. and Landais P. (2007) Micrometer scale carbon isotopic study of bitumen associated with Athabasca uranium deposits: Constraints on the genetic relationship with petroleum source-rocks and the abiogenic origin hypothesis. *Earth and Planetary Science Letters*, 258, 378-396.

- Savary V. and Pagel M. (1997) The effects of water radiolysis on local redox conditions in the Oklo, Gabon, natural fission reactors 10 and 16. *Geochimica et Cosmochimica Acta*, 61(21), 4479-4494.
- Shelton K.L., Burstein I.B., Hagni R.D., Vierrether C.B., Grant S.K., Hennigh Q.T., Bradley M.F. and Brandom R.T. (1995) Sulfur isotope evidence for penetration of MVT fluids into igneous basement rocks, southeast Missouri, USA. *Mineralium Deposita*, 30, 339-350.
- Shepherd T.J., Bouch J.E., Gunn A.G., McKervey J.A., Naden J., Scrivener R.C., Styles M.T. and Large D.E. (2005) Permo-Triassic unconformity-related Au-Pd mineralisation, South Devon, UK: New insights and the European perspective. *Mineralium Deposita*, 40, 24-44.
- Sheppard S.M.F. (1986) Characterization and isotopic variations in natural waters. In Valley J.W., Taylor Jr., H.P. and O'Neil J. (eds.). *Stable Isotopes in High Temperature Geological Processes*. Mineralogical Society of America. *Reviews in Mineralogy*, 16, 165-183.
- Shields G. and Veizer J. (2002) Precambrian marine carbonate isotope database: Version 1.1. *Geochemistry, Geophysics, Geosystems*, 3, U1-U12.
- Shock E.L., Sassani D.C. and Betz H. (1997) Uranium in geologic fluids: Estimates of standard partial molal properties, oxidation potentials, and hydrolysis constants at high temperatures and pressures. *Geochimica et Cosmochimica Acta*, 61, 4245-4266.
- Sie P.M.J. and Frape S.K. (2002) Evaluation of the groundwaters from the Stripa mine using stable chlorine isotopes. *Chemical Geology*, 182, 565-582.
- Simon K. (2001) Does  $\delta D$  from fluid inclusion in quartz reflect the original hydrothermal fluid? *Chemical Geology*, 177, 483-495.
- Spencer R.J. (1987) Origin of Ca-Cl brines in Devonian formations, western Canada sedimentary basin. *Applied Geochemistry*, 2, 373-384.
- Stewart M.A. and Spivack A.J. (2004) The stable-chlorine isotope compositions of natural and anthropogenic materials. *Reviews in Mineralogy and Geochemistry*, 55, 231-254.
- Stueber A.M. and Walter L.M. (1991) Origin and chemical evolution of formation waters from Silurian-Devonian strata in the Illinois basin, USA. *Geochimica et Cosmochimica Acta*, 55, 309-325.
- Timofeeff M.N., Lowenstein T.K., da Silva M.A.M. and Harris N.B. (2006) Secular variation in the major-ion chemistry of seawater: Evidence from fluid inclusions in Cretaceous halites. *Geochimica et Cosmochimica Acta*, 70, 1977-1994.
- Thomas D., Matthews R.B. and Sopuck V. (2000) Athabasca basin (Canada) unconformity-type uranium deposits: Exploration model, current mine developments and exploration directions. *Geology and Ore deposits 2000: The Great Basin and Beyond: Geological Society of Nevada Symposium, Proceedings*, 1, 103-125.
- Thomas D. (2003) Preliminary Observations on the Structural Setting of Uranium Mineralization and Alteration – Eagle Point Deposit. *Cameco Corporation internal report*.
- Vanko D.A., Bodnar R.J. and Sterner S.M. (1988) Synthetic fluid inclusions: VIII. Vapor-saturated halite solubility in part of the system NaCl-CaCl<sub>2</sub>-H<sub>2</sub>O, with application to fluid inclusions from oceanic hydrothermal systems. *Geochimica et Cosmochimica Acta*, 52(10), 2451-2456.
- Verma S.P. and Santoyo E. (1997) New improved equations for Na/K, Na/Li and SiO<sub>2</sub> geothermometers by outlier detection and rejection. *Journal of Volcanology and Geothermal Research*, 79, 9-23.
- Walker R.N., Muir M.D., Diver W.L., Williams N. and Wilkins N. (1977) Evidence of major sulphate evaporite deposits in the Proterozoic McArthur Group, Northern Territory, Australia. *Nature*, 265, 526-529.
- Wang A., Dhamelincourt P., Dubessy J., Guerard D., Landais P. and Lelaurain M. (1989) Characterization of graphite alteration in an uranium deposit by micro-Raman

- spectroscopy, X-ray diffraction, transmission electron microscopy and scanning electron microscopy. *Carbon*, 27, 209-218.
- Warren, J.K. (2000) Evaporites, brines and base metals: Low-temperature ore emplacement controlled by evaporite diagenesis. *Australian Journal of Earth Sciences*, 47, 179-208.
- Wassenaar L.I. and Koehler G. (2004) On-line technique for the determination of the  $\delta^{37}\text{Cl}$  of inorganic and total organic Cl in environmental samples. *Analytical Chemistry*, 76, 6384-6388.
- Wheatley K. and Tan B. (1998) Discovery and geology of the P-Patch, Key Lake area, Canada. *Annual Exploration Report-Cree-Zimmer Project and Mineral Lease* (71-53, 71-62), Uranerz Exploration and Mining Ltd., Report #98-CND-110002-01, Saskatchewan Energy & Mines Assessment File no. 74H04-NE-0099.
- Wilde A.R., Mernagh T.P., Bloom M.S. and Hoffmann C.F. (1989) Fluid inclusion evidence on the origin of some Australian unconformity-related uranium deposits. *Economic Geology*, 84, 1627-1642.
- Wilkinson J.J., Stoffell B., Wilkinson C.C., Jeffries T.E. and Appold M.S. (2009) Anomalously Metal-Rich Fluids Form Hydrothermal Ore Deposits. *Science*, 323, 764-767.
- Williams A.E. and McKibben M.A. (1989) A brine interface in the Salton Sea Geothermal System, California: Fluid geochemical and isotopic characteristics. *Geochimica et Cosmochimica Acta*, 53, 1905-1920.
- Willmore C.C., Boudreau A.E., Spivack A. and Kruger F.J. (2002) Halogens of Bushveld Complex, South Africa:  $\delta^{37}\text{Cl}$  and Cl/F evidence for hydration melting of the source region in a back-arc setting. *Chemical Geology*, 182, 503-511.
- Wilson M.R. and Kyser T.K. (1987) Stable isotope geochemistry of alteration associated with the Key Lake uranium deposit, Canada. *Economic Geology*, 82, 1540-1557.
- Wilson M.R., Kyser T.K., Mehnert H.H. and Hoeve J. (1987) Changes in the H-O-Ar isotope composition of clays during retrograde alteration. *Geochimica et Cosmochimica Acta*, 51, 869-878.
- Wilson T.P. and Long D.T. (1993a) Geochemistry and isotope chemistry of Ca-Na-Cl brines in Silurian strata, Michigan Basin, U.S.A. *Applied Geochemistry*, 8, 507-524.
- Wilson T.P. and Long D.T. (1993b) Geochemistry and isotope chemistry of Michigan Basin brines: Devonian formations. *Applied Geochemistry*, 8, 81-100.
- Wilson N.S.F., Stasiuk L.D. and Fowler M.G. (2007) Origin of organic matter in the Proterozoic Athabasca Basin of Saskatchewan and Alberta, and significance to unconformity uranium deposits. In Jefferson C.W. and Delaney G. (eds.) EXTECH IV: Geology and Exploration Technology of the Proterozoic Athabasca basin, Saskatchewan and Alberta. *Geological Survey of Canada Bulletin*, 588, 325-339.
- Worden R.H. (1996) Controls on halogen concentrations in sedimentary formation waters. *Mineralogical Magazine*, 60, 259-274.
- Xavier R.P., Wiedenbeck M., Trumbull R.B., Dreher A.M., Monteiro L.V.S., Rhede D., de Araujo C.E.G. and Torresi I. (2008) Tourmaline B-isotopes fingerprint marine evaporites as the source of high-salinity ore fluids in iron oxide copper-gold deposits, Carajas Mineral Province (Brazil). *Geology*, 36, 743-746.
- Yardley B.W.D. (2005) 100th Anniversary Special Paper: Metal concentrations in crustal fluids and their relationship to ore formation. *Economic Geology*, 100, 613-632.
- Yardley B.W.D. (2009) The role of water in the evolution of the continental crust. *Journal of the Geological Society*, 166, 585-600.
- Ypma P.J.M. and Fuzikawa K. (1980) Fluid inclusion and stable isotope studies of the Nabarlek and Jabiluka uranium deposits, Northern Territory, Australia. In IAEA (ed.) *International Uranium Symposium on the Pine Creek Geosyncline*, Vienna, 375-395.
- Zajacz Z., Halter W.E., Pettke T. and Guillong M. (2008) Determination of fluid/melt partition coefficients by LA-ICPMS analysis of co-existing fluid and silicate melt inclusions: Controls on element partitioning. *Geochimica et Cosmochimica Acta*, 72, 2169-2197.

- Zhang Y.G. and Frantz J.D. (1987) Determination of the homogenization temperatures and densities of supercritical fluids in the system NaCl-KCl-CaCl<sub>2</sub>-H<sub>2</sub>O using synthetic fluid inclusions. *Chemical Geology*, 64, 335-350.
- Zhao G., Sun M., Wilde S.A. and Li S. (2004) A Paleo-Mesoproterozoic supercontinent: Assembly, growth and breakup. *Earth-Science Reviews*, 67, 91-123.
- Zheng Y.F. (1993) Calculation of oxygen isotope fractionation in anhydrous silicate minerals. *Geochimica et Cosmochimica Acta*, 57, 1079-1091.
- Zheng Y.F. (1999) Oxygen isotope fractionation in carbonate and sulfate minerals. *Geochemical Journal*, 33, 109–129.
- Zwart E.W. and Touret L.R. (1994) Melting behavior and composition of aqueous fluid inclusions in fluorite and calcite: applications within the system H<sub>2</sub>O-CaCl<sub>2</sub>-NaCl. *European Journal of Mineralogy*, 6, 773-786.

## Liste des figures

Figure 1.1 : Régimes hydrogéologiques et tectoniques pour les circulations de fluides de bassin à grandes échelles, d'après Garven, (1995). (A) Circulations induites par la topographie ou la gravité. (B) Convection thermique libre. (C) Circulations induites par la tectonique dans des ceintures de plis et chevauchements. (D) Surpression pendant la compaction d'une marge continentale. (E) Pompage sismique de fluides profonds dans un rift. (F) Compartimentation d'un bassin sans circulation de fluides à grande échelle. ....	12
Figure 1.2 : Schéma résumant la diversité des types de circulations de fluides impliqués dans des minéralisations dans les bassins sédimentaires, d'après Oliver et al., (2006). (1) Circulations induites par la topographie dans le bassin. (2) Circulations induites par la topographie dans le socle. (3) Convection dans le bassin. (4) Convection dans le socle. (5) Exhalation à l'aplomb de panaches convectifs. (6) Percolation de saumures par densité. (7) Convection localisée à l'interface socle-bassin. (8) Circulation induites par la déformation le long de failles extensives actives ou réactivées. (9) Convection autour des failles dans le socle. (10) Circulations induites par l'inversion d'anciennes failles extensives.....	13
Figure 1.3 : Concentrations en zinc dans les fluides crustaux en fonction de la température (g.) et de la concentration en chlore (dr.), d'après Yardley (2005). La température et la concentration en chlore sont les deux variables majeures contrôlant la concentration en métaux dans les fluides crustaux si leur composition est tamponnée par celle des roches encaissantes. ....	14
Figure 1.4 : Composition en Na-Cl-Br des fluides minéralisateurs en Pb-Zn dans les bassins sédimentaires européens, en contexte de tectonique extensive, d'après Muchez et al., (2005). Dans tous les districts, l'évaporation de l'eau de mer est la source principale des fortes salinités des saumures minéralisatrices. SW : eau de mer. SET : courbe d'évaporation de l'eau de mer.....	15
Figure 1.5 : Représentation schématique des circulations de fluides et des conditions P-T à la base du Bassin de l'Athabasca, à chaque étape des cimentations de quartz dans le gisement de McArthur River, et leur lien possible avec la genèse des minéralisations en uranium, d'après Derome et al., (2005). Qz : quartz. Dol : dolomite (1) Cimentation précoce à la base des grès. (B) Interactions entre la saumure sodique et les lithologies du socle, formation de la saumure calcique, et mélange entre ces deux saumures le long des failles pendant le dépôt de l'uranium. (C) Cimentation finale des brèches par la saumure sodique. ....	17

Figure 2.1 : (A) Lithostratigraphic cross-section of the Athabasca Basin (Jefferson et al., 2007). MF: Manitou Falls Formation. D: Douglas Formation. C: Carswell Formation. (B) Diagrammatic structural cross-section south of Key Lake, illustrates structural geometry of Wollaston-Mudjatik transition zone that underlies the most economically productive area of the Eastern Athabasca Basin (Jefferson et al., 2007). ....	24
Figure 2.2 : Simplified geological map of the Athabasca Basin and Basement, Canada. Basement domains are individualized. Modified from Jefferson et al., (2007). Circles indicate main uranium deposits. Large circles indicate uranium deposits studied in this work. TMZ: Thelon magmatic zone. WMTZ: Wollaston Mudjatik transition zone. VRSZ: Virgin River shear zone. BLSZ: Black Lake shear zone.....	25
Figure 2.3 : Simplified schematic representation of lithology, structure, clay mineral alteration halos, and orebodies of the McArthur River deposit (Alexandre et al., 2005).....	26
Figure 2.4 : Simplified schematic representation of lithology, structure, clay mineral alteration halos, and orebodies of the McArthur River deposit (Alexandre et al., 2005).....	27
Figure 2.5 : Simplified schematic representation of lithology, structure, clay mineral alteration halos, and orebodies of the Eagle Point deposit (Mercadier, 2008). .....	28
Figure 2.6 : Simplified schematic representation of lithology, structure, clay mineral alteration halos, and orebodies of the P-Patch deposit (Mercadier et al., in prep). .....	29

Figure 2.7 : Simplified schematic representation of lithology, structure, clay mineral alteration halos, and orebodies of the Millennium deposit (Mercadier, 2008) .....	30
Figure 2.8 : Cross-section displaying the relationship between faults, the breccia body, the unconformity and the mineralization at the Shea Creek deposit (Lorilleux et al., 2002).....	31
Figure 2.9 : Example of quartz and carbonate veins, hosting fluid inclusions studied in this work. (A) dravite+quartz vein cross-cutting graphite-rich pelitic gneiss (sample H3042-1, Eagle Point). (B) Quartz+dolomite vein, with small bitumen balls and pyrite (not shown) (sample P48-3, P-Patch). (C) Smoky quartz in open fracture cross-cutting illitized pegmatoid (sample P53-6, P-Patch). (D) Massive dolomite intercept, intergrown with hematite and chlorite (sample P63-6, P-Patch). (E) Hematite+dolomite vein in relatively unaltered fine grained gneiss (sample H-1935-8, Eagle Point). (F) Quartz+dolomite in open fracture cross-cutting bleached gneiss (sample CX52-1, Millennium).....	33
Figure 2.10 : Example of fluid inclusions and host minerals studied in this work. <i>Liq.</i> : liquid phase. <i>Vap.</i> : vapor phase. <i>Hal.</i> : halite solid. (A) Druzy quartz (sample RBL2Qz, Rabbit Lake), thick section, transmitted light. (B) Dolomite vein (sample RBL1Carb, Rabbit Lake) thick section, transmitted light. (C) Typical primary liquid-vapor fluid inclusion in quartz. (D). (C) Typical primary liquid-vapor fluid inclusion in dolomite. (F) Typical primary liquid-vapor-halite fluid inclusion in dolomite. (F) Typical fluid inclusions with anomalously large vapor phase, indicating contamination by $H_2$ .....	35
Figure 3.1 : Na-Ca-Mg-K-Sr-Ba-U relations in analyzed fluid inclusions. Black diamonds stand for NaCl-rich brine inclusions and grey diamonds stand for CaCl <sub>2</sub> -rich brine inclusions. Full circles represent the hypothetic composition of the common parent fluid for the NaCl and CaCl <sub>2</sub> -rich brines (halite-saturated evaporated seawater, data from Fontes and Matray, 1993). Dashed lines symbolize possible envelopes for mixing trends.....	47
Figure 3.2 : Range of minor and trace elements compositions for the NaCl-rich brine and for the CaCl <sub>2</sub> -rich brine fluid inclusions. ....	48
Figure 4.1 : Te vs. Tm ice diagram for studied fluid inclusions. Temperatures of phase changes: <i>Te</i> : eutectic melting, <i>Tm ice</i> : ice melting. <i>Te</i> indicate that low-salinity fluid is a nearly pure H <sub>2</sub> O-NaCl or H <sub>2</sub> O-NaCl-CaCl <sub>2</sub> fluid, while NaCl-rich and CaCl <sub>2</sub> -rich brines are either pure H <sub>2</sub> O-NaCl-CaCl <sub>2</sub> fluids or more complex fluids with additional salts.....	60
Figure 4.2: H <sub>2</sub> O-NaCl-CaCl <sub>2</sub> diagrams for studied fluid inclusions from microthermometry. (A) Data for the studied fluid inclusions. Data for McArthur River deposit are also plotted (Derome et al., 2005). (B) Interpretation of fluid inclusion data in terms of mixing between a NaCl-rich brine and a CaCl <sub>2</sub> -rich brine. Low-salinity fluid does not show clear evidence for mixing with brines.....	64
Figure 4.3 : Tm ice vs. Th diagram for studied fluid inclusions. Data for McArthur River are from Derome et al., (2005). Temperatures of phase changes: <i>Tm ice</i> : ice melting, <i>Th</i> : total homogenization. Note that a majority of Lw' and Lwh' inclusions failed to nucleate any ice upon cooling and could not be plotted in the CaCl <sub>2</sub> -rich brine field. Large variations of Tm ice suggest mixing between a NaCl-rich brine and a CaCl <sub>2</sub> -rich brine. Th mainly comprised between 100 and 150°C for both brines both brines suggest that mixing is isothermal.....	70
Figure 4.4 : Th histograms for the studied fluid inclusions. <i>Th</i> : temperature of total homogenization. Data for McArthur River are from Derome et al., (2005). Except for the McArthur River deposit, Th for NaCl-rich brine mostly range from 100 to 150°C with a mode at 135°C, and Th for CaCl <sub>2</sub> -rich brine mostly range from 80 to 130°C with a mode at 115°C. ....	74
Figure 4.5 : Box and whisker plots for element concentrations in the NaCl-rich and CaCl <sub>2</sub> -rich brines for studied deposits, from LA-ICP-MS analysis of individual fluid inclusions. Numbers of fluid inclusions above limits of detection are shown in italics. Whiskers indicate 10 <sup>th</sup> and 90 <sup>th</sup> deciles, and box indicate 25 <sup>th</sup> deciles, median and, 75 <sup>th</sup> deciles. Note that when the amount of data was less than 10 it was not possible to draw whiskers and only median values sometimes associated with 25 <sup>th</sup> and 75 <sup>th</sup> deciles were calculated. Outliers are not shown.....	78

Figure 4.6 : Na vs. Ca + Mg + K plot for the studied fluid inclusions from LA-ICP-MS analysis. A continuum is observed between a Na-rich compositions and Ca-Mg-K-rich compositions, which suggests mixing between a NaCl-rich brine end-member and a CaCl <sub>2</sub> -rich brine end-member.....	79
Figure 4.7 : Plots of microthermometric data in Th – T mice diagrams for isothermal fluid mixing between a fluid with a low salinity and a saline fluid (Dubessy et al., 2003). (a) Isobaric mixing. (f) Non-isobaric mixing. ....	82
Figure 4.8 : Th – Ts NaCl diagram for Lwh and Lwh' fluid inclusions. Temperatures of phase changes: <i>TsNaCl</i> : halite dissolution, <i>Th</i> : total homogenization. A majority of Lwh' inclusions plot below the 1:1 line, indicating that the CaCl <sub>2</sub> -rich brine was saturated with respect to halite at the time of trapping. ....	83
Figure 4.9 : P-T model for mixing conditions for the NaCl-rich and CaCl <sub>2</sub> -rich brines. Representative isochores have been drawn from the main range of Th (temperature of total homogenization) for the two brines. The hydrostatic and lithostatic pressures at 3 and 6 km depth are reported as well as the hydrostatic and lithostatic gradients calculated for thermal gradients of 30°, 35°, and 40°C/km. ....	86
Figure 5.1 : Time-resolved LA-ICP-MS response for Na, Ca, Mg, K and U in three quartz-hosted fluid inclusions showing Na, Ca, Mg, K and U signals. Dashed windows show quartz signal (Qz) during quartz ablation, and fluid inclusion signal and integration window (FI). These spectra suggest that U is nearly absent from quartz and entirely fluid inclusions-hosted, as no U signal is observed during quartz ablation prior Na-Ca-Mg-K shift (i.e. opening of fluid inclusion). Inclusion A returns 3.9 ppm U, inclusion B returns 35 ppm U, inclusions C returns 226 ppm U.....	97
Figure 5.2: Distribution of uranium concentration in fluid inclusions analyzed by LA-ICP-MS. Only orders of magnitude are indicated due to analytical uncertainties, and heterogeneous distributions.....	100
Figure 5.3 : Comparison of U concentrations in studied fluid inclusions with U concentrations in various crustal fluids. 1: Kraemer and Kharaka (1986). 2: Eseme et al., (2006). 3: Banner et al., (1990). 4: Pluta and Zuber (1995). 5: Hodge et al., (1996). 6: Palmer and Edmond (1993). 7: Ku et al., (1977). (*): Calculated U concentration in evaporated seawater assuming an evaporation ratio of 65x (halite facies, Knauth and Beeunas, 1986) and negligible incorporation of U in evaporitic minerals. Dashed line represents seawater evaporation trend. 8: Michard et al., (1983). 9-10: Chen et al., (1986). 11: Brugger et al., (2005). 12: Aquilina et al., (2002). 13: Edmunds et al., (1987). 14: Gascoyne (2004). 15: Audéat et al., (2000). 16: Audéat and Pettke (2003): 17: Zajacz et al., (2008). 18: Gagnon et al., (2004). 19: Bühn and Rankin (1999). 20: Irwin and Roedder (1995). 21: Irwin and Reynolds (1995). Grey bars refer to present-day fluids and black bars refer to paleofluids sampled as fluid inclusions.....	103
Figure 6.1 : Frequency histogram for δ <sup>37</sup> Cl observations in the Athabasca brines. (A) Data sorted by localities. (B) Data sorted by host minerals. (C) Data sorted by brine content. <i>n.o.</i> Not observed. <i>Na</i> : NaCl-rich brine. <i>Ca</i> : CaCl <sub>2</sub> -rich brine.....	118
Figure 6.2 : Cl/Br vs. Cl relationships in the Athabasca Brines. <i>SW</i> : seawater. Minerals precipitating during evaporation of seawater: <i>G</i> : gypsum; <i>H</i> : halite; <i>E</i> : epsomite; <i>S</i> : sylvite; <i>C</i> : carnallite. Also shown the ranges for Cl concentration in NaCl-rich and CaCl <sub>2</sub> -rich brines..	120
Figure 6.3 : δ <sup>37</sup> Cl-Cl/Br relationships in the Athabasca brines. Also shown the ranges for Cl concentration in NaCl-rich and CaCl <sub>2</sub> -rich brines Minerals precipitating during evaporation of seawater: <i>H</i> : halite; <i>E</i> : epsomite. δ <sup>37</sup> Cl-depth relationships in the Athabasca brines.....	121
Figure 6.4 : Mixing scenarios between evaporated seawater and halite dissolution fluid in equilibrium with halite at 100°C, and mixing between evaporated seawater and meteoric water or seawater. 0.5: equal mixing of the two end-members. <i>MW</i> : meteoric water. <i>SW</i> : seawater. Minerals precipitating during evaporation of seawater: <i>G</i> : gypsum; <i>H</i> : halite; <i>E</i> : epsomite; <i>S</i> : sylvite; <i>C</i> : carnallite. Also shown the ranges for Cl concentration in NaCl-rich and CaCl <sub>2</sub> -rich brines. ....	123

Figure 6.5 : Scenario for brine-halite reequilibration at 100, 150 and 200°C SW: seawater. Minerals precipitating during evaporation of seawater: G: gypsum; H: halite; E: epsomite; S: sylvite; C: carnallite. Also shown the ranges for Cl concentration in NaCl-rich and CaCl <sub>2</sub> -rich brines.....	125
Figure 6.6 : Loss on ignition (L.O.I.) vs. Cl content in fresh and altered porphyries and pegmatites of the Athabasca Basement .....	127
Figure 6.7 : Ranges of $\delta^{37}\text{Cl}$ of various fluids, rocks and minerals of interest for interpretation of $\delta^{37}\text{Cl}$ values of Athabasca brines. Numbers in parentheses indicate references as follows: (1) Kaufmann et al., (1984a); (2) Godon et al., (2004); (3) Eggenkamp et al., (1995); (4) Eastoe et al., (1999); (5) Eastoe et al., (2007); (6) Liu et al., (1997); (7) Stewart and Spivak (2004) and references therein; (8) Eastoe et al., (1989); (9) Eastoe and Guillet (1992); (10) Grandia et al., (2003b); (11) Möller et al., (2005); (12) Kaufmann et al., (1984b); (13) Sie & Frape (2002); (14) Musashi et al., (1998); (15) Marlé et al., (2007); (16) Eggenkamp & Schuiling (1995); (17) Magenheimer et al., (1995); (18) Boudreau et al., (1997); (19) Willmore et al., (2002).....	128
Figure 6.8 : $\delta^{37}\text{Cl}$ -depth relationships in the Athabasca brines. Possible $\delta^{37}\text{Cl}$ fractionation occurs during percolation of brines in the basement.....	130
 Figure 7.1 : Comparison between chemistry of Athabasca NaCl-rich and CaCl <sub>2</sub> -rich brines with commonly sampled basinal fluids from basinal fluid database (Table 7.1), with emphasis on transition between Na-dominated fluids and Ca-dominated fluids. Ternary diagrams are built on molar element concentrations. SW: seawater. H: halite. E: epsomite. Modern seawater evaporation trend from Fontes and Matray (1993a). Cretaceous seawater evaporation trend from Lowenstein and Timofeeff (2008).....	150
Figure 7.2 : Comparison between SO <sub>4</sub> and F concentrations in Athabasca NaCl-rich and CaCl <sub>2</sub> -rich brines with commonly sampled basinal fluids. SW: seawater. H: halite. E: epsomite. (A) Modern seawater evaporation trend from Fontes and Matray (1993a). (B) Seawater evaporation trend from Worden (1996).....	154
Figure 7.3 : Na/K – Na/Li molar ratios of Athabasca NaCl-rich and CaCl <sub>2</sub> -rich brines determined from crush-leach and LA-ICP-MS analyses. Full line: temperature estimation deduced from the geothermometric cation relationships (Verma and Santoyo, 1997). Dotted lines: expected ranges of Na/K and Na/Li ratios in Athabasca brines, from temperatures deduced from fluid inclusions (Part 4), if geothermometric relationships are respected.....	158
Figure 7.4 : Ca excess vs. Na deficit diagram for fluid inclusions analyzed by LA-ICP-MS. (0) Seawater evaporation. Proposed scenario for acquisition of fluids chemistry: (1) Mixing with halite-dissolution fluid (composition from Chi and Savard, 1997). (2) Ca gain by dolomitization. (3) 2Na : 1Ca exchange and conversion of NaCl-rich brine to CaCl <sub>2</sub> -rich brine. Basinal fluid line from Davisson and Criss (1996). SW: seawater. H: halite. E: epsomite. Modern seawater evaporation trend from Fontes and Matray (1993a). Cretaceous seawater evaporation trend from Lowenstein and Timofeeff (2008).....	158
Figure 7.5 : Bivariate plots of Mg vs. B, metals (U, Ag, Se, As, Ni, Co) and REE (Ce), determined from crush-leach analyses. All plots show possible positive correlation.....	160
Figure 7.6 : Bivariate plots showing intercorrelation between metal (U, Cu, Zn, Pb) concentrations in fluid inclusions analyzed by LA-ICP-MS. Na: NaCl-rich brine inclusions: Ca: CaCl <sub>2</sub> -rich brine inclusions.....	161
 Figure 8.1 : Frequency histogram for $\delta^{18}\text{O}$ values of hydrothermal quartz (A) and dolomites (B) veins in all studied deposits.....	177
Figure 8.2 : Frequency histogram for hydrothermal $\delta^{18}\text{O}$ values of quartz (A) and dolomite (B) veins as a function of their fluid inclusion content. Na : NaCl-rich brine ; Ca : CaCl <sub>2</sub> -rich brine. (C) Frequency histogram of $\delta^{18}\text{O}$ values for H <sub>2</sub> O calculated from fractionation factors between quartz, dolomite, calcite and water at 150°C as a function of fluid inclusion content.....	180
Figure 8.3 : $\delta\text{D}$ for water recovered from crushing vs. $\delta^{18}\text{O}$ for water calculated from fluid-mineral equilibria at 150 ± 30°C. SET: Seawater evaporation trend (Holser, 1979; Knauth	

and Beeunas, 1986). G: onset of gypsum precipitation. H: onset of halite precipitation. SET ends at late stage of halite precipitation. Dotted contours: (1) basement fluids in equilibrium with alteration minerals (Kotzer and Kyser, 1995), (2) basin fluids in equilibrium with alteration minerals (Kotzer and Kyser, 1995), (3) fluid inclusions from McArthur River quartz (Kotzer and Kyser, 1995), (4) fluid inclusions from Rabbit Lake quartz and dolomites (Pagel et al., 1980). (5) Hypothetic field for parent brine to NaCl-rich and CaCl<sub>2</sub>-rich brines before diagenetic reactions: mixing of evaporated seawater and halite-dissolution fluids and low latitude meteoric water (Part 6). Fields for basinal brines and organic waters after Sheppard (1986). GMWL: Global meteoric water line. SMOW: Standard modern ocean water. ....181  
 Figure 8.4 : (A)  $\delta^{13}\text{C}$  (dolomite) vs.  $\delta^{13}\text{C}$  of CO<sub>2</sub> recovered from crushing. Straight lines indicate compositions at isotopic equilibrium between CO<sub>2</sub> and dolomite between 50 and 200°C. (B)  $\delta^{18}\text{O}$  vs.  $\delta^{13}\text{C}$  diagram for dolomites. Field for Proterozoic marine carbonates after Shields and Veizer (2002).  $\delta^{13}\text{C}$  for graphite after Kyser et al., (1989).  $\delta^{13}\text{C}$  for bitumen after Sangély et al., (2007). (C)  $\delta\text{D}$  for water recovered from crushing vs.  $\delta^{13}\text{C}$  of CO<sub>2</sub> recovered from crushing. ....184  
 Figure 8.5 : Summary and relative timing of successive events controlling stable isotope (C, O, H) composition of NaCl-rich and CaCl<sub>2</sub>-rich brines in the Athabasca Basement. Relative importance of each event is indicated as follows: *dotted lines*: possible or not effective; *solid line*: effective; *thick solid lines*: highly effective. ....187



## Liste des tableaux

Table 1.1 : Résumé des techniques d'analyse d'inclusions fluides et minéraux hôtes utilisées dans ce travail, classées par gisements étudiés. <i>ifs</i> : inclusions fluides. <i>éch</i> : échantillons. <i>Qz</i> : quartz. <i>Carb</i> : carbonates. Les analyses en microthermométrie pour le gisement de McArthur River ont été réalisées par Derome et al., (2005). ....	20
Table 3.1 : Characteristics the Lw2, Lw' and Lwh' type fluid inclusions at McArthur River. All data are based on microthermometry, LIBS and Raman spectroscopy from Derome et al., (2005). <i>Te</i> : eutectic melting. <i>Tm ice</i> : final ice melting. <i>Tm hyd</i> : hydrohalite melting. <i>Ts NaCl</i> : halite dissolution. <i>Th</i> : total homogenization. Lw' and Lwh' frequently fail to nucleate any ice upon cooling and only observed <i>Tm ice</i> ranges are reported. Inclusions selected for LA-ICP-MS analyses were attributed to the Lw2, Lw' or Lwh' type, based on microthermometry. ....	42
Table 3.2 : Representative microthermometric and LA-ICP-MS analyses of selected fluid inclusions. <i>n.f.</i> : no freezing. <i>F.I.</i> : fluid inclusion. Value preceded by a < symbol stand for limit of detection (LOD). ....	43
Table 6.1 : Location, host minerals, brine content, depths (available data), and results from crush-leach analyses. <i>n.a.</i> : not analyzed (when ion chromatograph signal do not permit proper quantification). <i>b.d.</i> : bellow detection limit, <i>n.o.</i> : not observed. <i>Qz</i> : quartz. <i>Dol</i> : dolomite. <i>Cal</i> : calcite. <i>Depth</i> : estimated depth below unconformity. <i>Na</i> : NaCl-rich brine. <i>Ca</i> : CaCl <sub>2</sub> -rich brine. ....	117
Table 6.2 : Cl content and loss on ignition (L.O.I) of Athabasca Basement rocks and minerals. Numbers in parentheses are average Cl contents. <i>n</i> : number of measurements.	119
Table 7.1 : Sources of major and trace elements data for basinal fluids used in this study. <i>TDS</i> : total dissolved solids.....	141
Table 7.2 : Reconstitution of composition of bulk fluid inclusion population from crush-leach analysis. All concentrations in ppm. <i>wt%</i> : average salinity from microthermometry. <i>Qz</i> : quartz. <i>Dol</i> : dolomite. <i>Cal</i> : calcite. <i>na</i> : not analyzed. <i>nd</i> : not determined. <i>bd</i> : below detection limit.....	143
Table 7.3 : Summary of relative contributions of basin and basement to element concentration in Athabasca NaCl-rich and CaCl <sub>2</sub> -rich brines. ....	162
Table 8.1 : Table 1: Analytical results. Mineral: <i>Dol</i> : dolomite ; <i>Qz</i> : Quartz ; <i>Cal</i> : calcite. Brine content : <i>Na</i> : NaCl-rich brine ; <i>Ca</i> : CaCl <sub>2</sub> -rich brine ; <i>n.o.</i> : not observed.....	176

AUTORISATION DE SOUTENANCE DE THESE  
DU DOCTORAT DE L'INSTITUT NATIONAL  
POLYTECHNIQUE DE LORRAINE

000

VU LES RAPPORTS ETABLIS PAR :

**Monsieur Bruce W. D. YARDLEY, Professeur, School of Earth and Environment, Leeds, UK**

**Monsieur Philippe MUCHEZ, Professeur, Geo-Institut Celestijnenlaan, Heverlee, Belgique**

Le Président de l'Institut National Polytechnique de Lorraine, autorise :

**Monsieur RICHARD Antonin**

NANCY BRABOIS  
2, AVENUE DE LA  
FORET-DE-HAYE  
BOITE POSTALE 3  
F - 54501  
VANDOEUVRE CEDEX

à soutenir devant un jury de l'INSTITUT NATIONAL POLYTECHNIQUE DE LORRAINE, une thèse intitulée :

**« Circulation de saumures à la discordance socle / couverture sédimentaire et formation des concentrations uranifères protérozoïques (bassin de l'Athabasca, Canada) »**

en vue de l'obtention du titre de :

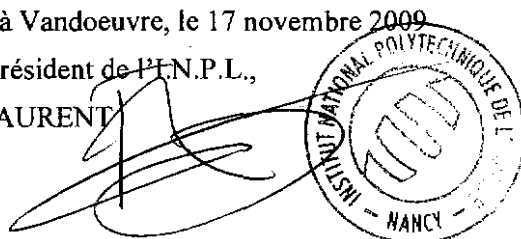
DOCTEUR DE L'INSTITUT NATIONAL POLYTECHNIQUE DE LORRAINE

Spécialité : « Géosciences »

Fait à Vandoeuvre, le 17 novembre 2009

Le Président de l'I.N.P.L.,

F. LAURENT



## **Circulation de saumures à la discordance socle / couverture sédimentaire et formation des concentrations uranifères protérozoïques (Bassin de l'Athabasca, Canada)**

### **Résumé :**

Les circulations de fluides aux interfaces entre les socles cristallins et leur couvertures sédimentaires sont des événements majeurs de transferts élémentaires dans la croûte. Dans de nombreux contextes, des fluides de bassins peuvent pénétrer dans les socles de faible perméabilité, interagir avec eux, y lessiver des métaux, et donner lieu à des concentrations métalliques, notamment en Pb, Zn, Cu, Ag et U. Les gisements d'uranium de type discordance du bassin d'âge protérozoïque de l'Athabasca (Canada), sont des témoins essentiels de ce type de circulations de fluides, et sont des objets modèles pour comprendre les mécanismes et les conséquences de tels événements.

Les inclusions fluides permettent d'échantillonner et d'analyser directement les paléofluides. Malgré les difficultés d'analyse, ces objets de taille micrométrique apportent des informations importantes sur les propriétés des fluides. Les techniques d'analyse disponibles (microthermométrie, LA-ICP-MS, écrasement-lessivage, écrasement sous vide) permettent de reconstituer la température, la pression, la composition chimique détaillée des fluides, dont les teneurs en métaux, ainsi que la composition isotopique de l'hydrogène de l'eau, du chlore et du carbone du CO<sub>2</sub> dissous. De plus, l'analyse de la composition isotopique de l'oxygène et du carbone des minéraux dans lesquels sont piégées les inclusions fluides apporte des informations complémentaires sur la température des fluides et les interactions fluides-roches.

Cette approche a été utilisée sur six gisements d'uranium du Bassin de l'Athabasca, et a permis d'apporter les résultats suivants, potentiellement généralisables à l'ensemble du bassin. (1) Deux saumures, une calcique et une sodique ont circulé et se sont mélangées à la base du bassin et dans le socle au cours de la formation des gisements à environ 150 ± 30°C. (2) Ces deux saumures ont transporté de l'uranium, dont les concentrations exceptionnelles et très hétérogènes (entre 0.2 et 600 ppm) indiquent qu'il a été lessivé dans le socle. (3) Ces saumures ont une origine commune et se sont formées essentiellement par évaporation en surface de l'eau de mer, et mélange avec des fluides issus de la dissolution de minéraux évaporitiques. (4) La saumure calcique s'est formée par interaction entre la saumure sodique et les roches du socle. (5) Les interactions des saumures avec les minéraux et le graphite du socle, la radiolyse de l'eau, et la synthèse de bitumes ont contrôlé la composition isotopique en oxygène, hydrogène et carbone de ces saumures.

**Mots-clef:** saumures, gisements d'uranium, discordance, Athabasca, inclusions fluides

## **Brine migration at the basement / sedimentary cover unconformity and formation of Proterozoic uranium mineralizations (Athabasca Basin, Canada)**

### **Abstract :**

Fluid circulations between crystalline basements and their sedimentary covers are major events for element transfer in the crust. In numerous settings, basinal fluids penetrate the low-permeability basement, interact with basement lithologies, leach metals, leading to metal concentrations, notably Pb, Zn, Cu, Ag and U. Unconformity-related uranium deposits from the Proterozoic Athabasca Basin (Canada) are crucial witnesses and useful tools for the understanding of mechanisms and consequences of such fluid events.

Fluid inclusions allow us to directly sample and analyze paleofluids. Despite analytical difficulties, these micrometer size objects provide key information on fluid properties. Available analytical techniques (microthermometry, LA-ICP-MS, crush-leach, in-vacuo crushing) provide reconstruction of temperature, pressure, detailed fluid chemistry, including metal concentrations, as well as isotopic composition of water hydrogen, chlorine and of dissolved CO<sub>2</sub> carbon. In addition, analysis of isotopic composition of oxygen and carbon from minerals in which fluid inclusions are trapped provide supplementary information on fluid temperatures and fluid-rock interactions.

This approach was used on six uranium deposits from the Athabasca Basin and provided the following results, which can be potentially generalized to the entire basin. (1) Two brines, a calcium-rich brine and a sodium-rich brine have circulated and mixed at the base of the basin and in the basement at the time of formation of uranium deposits, at temperature close to 150 ± 30°C. (2) Both brines have transported uranium, whose exceptional and highly heterogeneous concentrations (0.2 to 600 ppm) indicate that it was leached in the basement. (3) Both brines share a common origin and were formed mainly by surface evaporation of seawater and mixing with fluids originating from dissolution of evaporitic minerals. (4) The calcium-rich brine was formed by interaction between the sodium-rich brine and basement lithologies. (5) Interaction with basement minerals and graphite, water radiolysis, and bitumen synthesis were the main controls on the oxygen, hydrogen and carbon isotopic composition of brines.

**Keywords:** brines, uranium deposits, unconformity, Athabasca, fluid inclusions